

UNCLASSIFIED

AD NUMBER
AD916695
NEW LIMITATION CHANGE
TO Approved for public release, distribution unlimited
FROM Distribution authorized to U.S. Gov't. agencies only; Test and Evaluation; Aug 1973. Other requests shall be referred to AFFDL[FBA], Wright-Patterson AFB, OH 45433.
AUTHORITY
AFFDL, ltr, 28 May 1974

THIS PAGE IS UNCLASSIFIED

AD916695

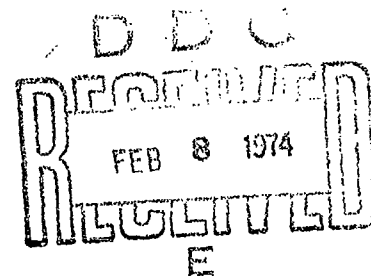
AFML-TR-73-204

CORROSION FATIGUE CRACK GROWTH IN AIRCRAFT STRUCTURAL MATERIALS

L. R. Hall, R. W. Finger and W. F. Spurr

BOEING AEROSPACE COMPANY
Seattle, Washington 98124

SEPTEMBER, 1973
FINAL TECHNICAL REPORT AFML-TR-73-204



DISTRIBUTION LIMITED TO U. S. GOVERNMENT AGENCIES AND
DESIGNATED RECIPIENTS ONLY SINCE THIS REPORT CONCERNS
THE TEST AND EVALUATION OF TECHNOLOGY DIRECTLY APPLICABLE
TO MILITARY HARDWARE (AUGUST 1973). ~~RECEIVED FOR ADDITIONAL~~
~~COPIES OR FOR FURTHER DISTRIBUTION OF THIS DOCUMENT MUST BE~~
REFERRED TO AFFDL (FBA), WPAFB, OH 46433.

AIR FORCE MATERIALS LABORATORY
AIR FORCE FLIGHT DYNAMICS LABORATORY
Air Force Systems Command
Wright-Patterson Air Force Base, Ohio

NOTICE

When Government drawings, specifications, or other data are used for any purpose other than in connection with a definitely related Government procurement operation, the United States Government thereby incurs no responsibility nor any obligation whatsoever; and the fact that the Government may have formulated, furnished, or in any way supplied the said drawings, specifications, or other data, is not to be regarded by implication or otherwise as in any manner licensing the holder or any other person or corporation, or conveying any rights or permission to manufacture, use, or sell any patented invention that may in any way be related thereto.

Copies of this report should not be returned unless return is required by security considerations, contractual obligations, or notice on a specific document.

UNCLASSIFIED

SECURITY CLASSIFICATION OF THIS PAGE (When Data Entered)

REPORT DOCUMENTATION PAGE		READ INSTRUCTIONS BEFORE COMPLETING FORM
1. REPORT NUMBER AFML-TR-73-204	2. GOVT ACCESSION NO.	3. RECIPIENT'S CATALOG NUMBER
4. TITLE (and Subtitle) CORROSION FATIGUE CRACK GROWTH IN AIRCRAFT STRUCTURAL MATERIALS		5. TYPE OF REPORT & PERIOD COVERED FINAL TECHNICAL REPORT JUNE 1971 THRU JUNE 1973
		6. PERFORMING ORG. REPORT NUMBER
7. AUTHOR(s) L. R. HALL, R. W. FINGER & W. F. SPURR		8. CONTRACT OR GRANT NUMBER(s) AF33615-71-C-1687
9. PERFORMING ORGANIZATION NAME AND ADDRESS BOEING AEROSPACE COMPANY SEATTLE, WASHINGTON 98124		10. PROGRAM ELEMENT, PROJECT, TASK AREA & WORK UNIT NUMBERS
11. CONTROLLING OFFICE NAME AND ADDRESS AIR FORCE MATERIALS LABORATORY AIR FORCE FLIGHT DYNAMICS LABORATORY AIR FORCE SYSTEMS COMMAND WRIGHT-PATTERSON AIR FORCE BASE, OHIO		12. REPORT DATE SEPTEMBER 1973
14. MONITORING AGENCY NAME & ADDRESS (if different from Controlling Office) SAME		13. NUMBER OF PAGES
		15. SECURITY CLASS. (of this report) UNCLASSIFIED
		15a. DECLASSIFICATION/DOWNGRADING SCHEDULE
16. DISTRIBUTION STATEMENT (of this Report) "DISTRIBUTION LIMITED TO U.S. GOVERNMENT AGENCIES AND DESIGNATED RECIPIENTS ONLY SINCE THIS REPORT CONCERNS THE TEST AND EVALUATION OF TECHNOLOGY DIRECTLY APPLI- CABLE TO MILITARY HARDWARE (AUGUST 1973). REQUESTS FOR ADDITIONAL COPIES OR FURTHER DISTRIBUTION OF THIS DOCUMENT MUST BE REFERRED TO AFFDL (FBA), WPAFB, OH 45433."		
17. DISTRIBUTION STATEMENT (of the abstract entered in Block 20, if different from Report)		
18. SUPPLEMENTARY NOTES		
19. KEY WORDS (Continue on reverse side if necessary and identify by block number) STRESS CORROSION CRACKING OVERLOAD FRACTURE TOUGHNESS 6Al-4V TITANIUM CORROSION FATIGUE 9Ni-4Co-0.3C STEEL CRACK GROWTH RATES 7075-T651 ALUMINUM 7475-T651 ALUMINUM		
20. ABSTRACT (Continue on reverse side if necessary and identify by block number) THIS EXPERIMENTAL PROGRAM WAS UNDERTAKEN TO OBTAIN INFORMATION ON STRESS CORROSION CRACKING AND CORROSION FATIGUE CRACK GROWTH IN HIGH STRENGTH METAL ALLOYS SUITABLE FOR AIRFRAME COMPONENTS. IN ADDITION, TESTS WERE CONDUCTED TO EVALUATE THE EFFECTS OF OVERLOADS AND METAL- LURGICAL FACTORS ON CORROSION FATIGUE CRACK GROWTH. THE TEST PROGRAM INVOLVED FIVE ALLOYS AND SEVEN TEST MEDIA. (CONTINUED ON NEXT PAGE)		

UNCLASSIFIED

SECURITY CLASSIFICATION OF THIS PAGE (When Data Entered)

UNCLASSIFIED

SECURITY CLASSIFICATION OF THIS PAGE(When Data Entered)

BLOCK 20 - ABSTRACT (CONTINUED)

THE FOUR PRINCIPAL ALLOYS WERE: 7075-T651 ALUMINUM, 6A1-4V(ELI) BETA ANNEALED (β A) TITANIUM, 6A1-4V RECRYSTALLIZE ANNEALED (RA) TITANIUM, AND 9Ni-4Co-0.3C STEEL (220-240 ksi); IN ADDITION THE 7475-T651 ALLOY WAS SUBJECTED TO A LIMITED NUMBER OF TESTS. ALL ALLOYS WERE TESTED IN THE FORM OF HOT ROLLED PLATE. TEST MEDIA INCLUDED: DESICCATED AIR, WATER SATURATED JP-4 FUEL, DISTILLED WATER, 3.5% NaCl SOLUTION, SUMP TANK WATER, ALTERNATING JP-4 FUEL AND DISTILLED WATER, AND DYE PENETRANT (TYPE ZL-2A). MOST TESTS WERE CONDUCTED AT 72F WITH A FEW TESTS BEING PERFORMED AT +175F AND -65F. DOUBLE CANTILEVER BEAM SPECIMENS WERE USED FOR ALL TESTS WITH THE EXCEPTION OF A LIMITED NUMBER OF SURFACE-FLAWED SPECIMEN TESTS. CORROSION FATIGUE TESTS WERE CONDUCTED USING TWO CYCLIC FREQUENCIES (6 AND 60 cpm) AND THREE RATIOS OF MINIMUM TO MAXIMUM STRESS (0.1, 0.5 AND 0.8). OVERLOAD EFFECTS WERE INVESTIGATED BY TESTING 7075-T651 ALUMINUM, Ti-6Al-4V AND Ti-6Al-4V RA TAPERED DOUBLE CANTILEVER BEAM SPECIMENS IN BOTH DESICCATED AIR AND 3.5% NaCl SOLUTION. FINALLY, A SERIES OF TESTS WAS UNDERTAKEN TO EVALUATE THE EFFECTS ON SCC AND CORROSION FATIGUE CRACKING OF VARIATIONS IN METALLURGICAL CHARACTERISTICS IMPARTED TO Ti-6Al-4V RA ALLOY PLATE BY VARIOUS THERMAL CYCLES.

UNCLASSIFIED

SECURITY CLASSIFICATION OF THIS PAGE(When Data Entered)

FOREWORD

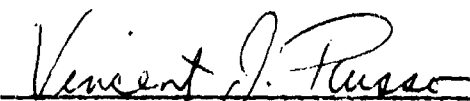
This report describes an investigation of corrosion fatigue crack growth in airframe structural materials performed by the Boeing Aerospace Company from 1 June 1971 through 30 June 1973 under Air Force Contract F33615-71-C-1687.

From 1 June 1971 through October 1972 the work was sponsored by the Air Force Materials Laboratory (AFML) with Mr. K. D. Shimmin as project engineer. Subsequent to October 1972, the effort was sponsored by the Advanced Metallic Structures - Advanced Development Program Office (AMS-ADPO), Air Force Flight Dynamics Laboratory (AFFDL), under the joint management and technical direction of AFFDL and AFML with Mr. N. G. Tupper as project engineer.

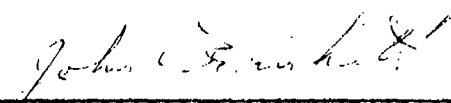
This program was conducted by the Research and Engineering Division of the Boeing Aerospace Company, Seattle, Washington under the supervision of H. W. Klopfenstein, Structures Research and Development Manager. The Program Leader was J. N. Masters, Supervisor, Failure Mechanisms Group. Technical Leader was L. R. Hall and program support was provided by R. W. Finger, test design and coordination, W. F. Spurr, metallurgical investigations, A. A. Ottlyk, test engineering, and D. G. Good, technical illustrations and art work.

This report was submitted by the authors on June 25, 1973.

This technical report has been reviewed and is approved.



Vincent J. Russo
Chief, NDT and Mechanics Branch
Metals and Ceramics Division
Air Force Materials Laboratory



John C. Frishett, Major, USAF
Program Manager, AMS Program Office
Structures Division
Air Force Flight Dynamics Laboratory

TABLE OF CONTENTS

	Page
SUMMARY	1
1.0 INTRODUCTION	5
2.0 MATERIALS AND PROCEDURES	9
2.1 Materials	9
2.1.1 Aluminum 7075-T651	9
2.1.2 Aluminum 7475-T651	15
2.1.3 Titanium 6Al-4V Beta Annealed	18
2.1.4 Titanium 6Al-4V Recrystallize Annealed	25
2.1.5 Steel Alloy 9Ni-4Co-0.3C	32
2.2 Selection of Environments	38
2.3 Procedures	43
2.3.1 Specimen Preparation	43
2.3.2 Testing	45
2.3.3 Evaluation of Results	49
2.3.4 Comments on Procedures	53
3.0 RESULTS AND DISCUSSION	57
3.1 Aluminum Alloy Test Results	57
3.1.1 Stress Corrosion Cracking Tests	57
3.1.2 Corrosion Fatigue Tests	65
3.1.2.1 Effect of Test Environment	65
3.1.2.2 Effect of Cyclic Frequency	72
3.1.2.3 Effect of Specimen Type	83
3.1.3 Aluminum Alloy 7475-T651 Results	85
3.1.3.1 Stress Corrosion Cracking Tests	85
3.1.3.2 Corrosion Fatigue Tests	85
3.2 Titanium Alloy 6Al-4V Beta Annealed Results	88
3.2.1 Stress Corrosion Cracking Tests	88
3.2.2 Corrosion Fatigue Tests	90
3.2.2.1 Effect of Test Environment	92
3.2.2.2 Effect of Cyclic Frequency	104
3.2.2.3 Effect of Specimen Type	104
3.2.2.4 Tests of Low O ₂ (Super ELI) Material	110

TABLE OF CONTENTS (Cont.)

	Page
3.3 Titanium Alloy 6Al-4V Recrystallize Annealed	112
3.3.1 Stress Corrosion Cracking Tests	112
3.3.2 Corrosion Fatigue Tests	112
3.3.2.1 Effect of Test Environment	115
3.3.2.2 Effect of Cyclic Frequency	126
3.3.2.3 Specimen Configuration Effect	126
3.3.2.4 Crack Closure Measurements	132
3.3.2.5 Thermal Processing Effects	142
3.4 Steel Alloy Test Results	158
3.4.1 Stress Corrosion Cracking Tests	158
3.4.2 Corrosion Fatigue Tests	162
3.4.2.1 Effect of Test Media and Cyclic Frequency	162
3.5 Overload Effect Tests	166
3.5.1 Test Procedures	166
3.5.2 Methods for Evaluating Results	168
3.5.3 Results and Discussion	170
3.5.4 Summary	178
3.6 Stress Ratio Effects	179
 4.0 OBSERVATIONS AND CONCLUSIONS	 187
4.1 Observations	187
4.2 Conclusions	191
REFERENCES	193
APPENDIX A - Test Data	195
APPENDIX B - Test Specimens	241
APPENDIX C - Compliance Measurements For Double Cantilever Beam Specimens	251
APPENDIX D - Crystallographic Texture Measured By X-Ray Pole Figures	257

LIST OF TABLES

<u>No.</u>	<u>Title</u>	<u>Page</u>
1	Test Program	6
2	Chemical Composition of Aluminum Alloy	11
3	Summary of Fracture Toughness Data for Plate Alloys	16
4	Mechanical Property Data for 7475-T651 Aluminum Alloy One Inch Thick Plate	19
5	Fracture Toughness (K_{Ic}) Data for 7475-T651 Aluminum Alloy One Inch Thick Plate	19
6	Chemical Composition of Titanium Alloys	20
7	Quantitative Texture Factors for Titanium Alloys	23
8	Chemical Composition of 9Ni-4Co-0.3C Steel (220-240 Ksi)	36
9	Chemical Content of Simulated Sump Tank Residue Water	39
10	Test Program for 7075-T651 Aluminum	58
11	Test Program for Ti-6Al-4V Beta Annealed	89
12	SCC Test Results for Ti-6Al-4V Beta Annealed Plate (WR Direction)	91
13	Test Program for Ti-6Al-4V Recrystallize Annealed	113
14	SCC Test Results for Ti-6Al-4V Recrystallize Annealed Plate (WR Direction)	114
15	Quantitative Texture Factors and Moduli for Ti-6Al-4V Alloy Subjected to Various Thermal Cycles	151
16	Mechanical Property Test Results at 72F for Ti-6Al-4V Plate Subjected to Various Thermal Cycles	151
17	Fracture Toughness Test Results for Ti-6Al-4V Subjected to Various Thermal Cycles (WR Orientation and CT specimens)	153
18	SCC Test Results in 72F/3.5% NaCl Solution for Ti-6Al-4V Subjected to Various Thermal Cycles	153

LIST OF TABLES (CONT'D)

<u>No.</u>	<u>Title</u>	<u>Page</u>
19	Test Program for 9Ni-4Co-0.3C (240 ksi) Steel Alloy Plate	
20	Overload Effects Test Program	
21	Results of Overload Effect Tests on 6Al-4V ELI Beta Annealed Titanium Alloy Plate	
22	Results of Overload Effect Tests on 6Al-4V Recrystallize Annealed Titanium Alloy Plate	
23	Results of Overload Effect Test on 7075-T651 Aluminum Alloy Plate	
24	Summary of Stress Ratio Effects Resulting from 6 CPM Tests	

LIST OF FIGURES

<u>No.</u>	<u>Title</u>	<u>Page</u>
1	7075-T651 Aluminum Alloy Microstructure Composite (200X, Kellers Etch)	12
2	Mechanical Properties for 7075-T651 Aluminum Alloy Plate (0.625-Inch Thick)	13
3	Fracture Toughness Data for All Test Alloys (CT Specimens)	14
4	7475-T651 Aluminum Alloy Microstructure Composite (200X, Kellers Etch)	17
5	6Al-4V Standard ELI Beta Annealed Titanium Alloy Microstructure Composite (500X)	21
6	Pole Figure for 6Al-4V Standard ELI Beta Annealed Titanium Alloy - Basal Plane (0002) _α	22
7	Mechanical Properties for 6Al-4V Standard ELI Beta Annealed Titanium Alloy Plate (1.0-Inch Thick)	24
8	6Al-4V "Super ELI" (O ₂ Content 0.06) Beta Annealed Titanium Alloy Microstructure Composite (500X)	26
9	Pole Figure for 6Al-4V "Super ELI" (O ₂ Content 0.06) Beta Annealed Titanium Alloy - Basal Plane (0002) _α	27
10	6Al-4V Recrystallize Annealed Titanium Alloy Microstructure (500X)	29
11	Pole Figure for 6Al-4V Recrystallize Annealed Titanium Alloy - Basal Planes (0002) _α	30
12	Mechanical Properties for 6Al-4V Recrystallize Annealed Titanium Alloy Plate (1.0-Inch Thick)	31
13	9Ni-4Co-0.3C Steel Alloy Microstructure Composite (500X)	33
14	Banding in 9Ni-4Co-0.3C Steel Alloy (200X)	34
15	Banding in 9Ni-4Co-0.3C Steel Alloy at High Magn- ification (1200X)	34
16	Mechanical Properties for 9Ni-4Co-0.3C Steel Alloy Plate (0.625-Inch Thick)	37

LIST OF FIGURES (CONT'D)

<u>No.</u>	<u>Title</u>	<u>Page</u>
17	Schematic Representation of Possible Effects of Mixing Environments A and B on Stress Corrosion Properties of an Alloy	41
18	Velocity of Stress Corrosion Cracks in a High Strength Aluminum Alloy as a Function of Water Content in Methanol	42
19	SCC Test Specimens for 7075-T651 Aluminum and 9Ni-4Co-0.3C Steel Alloys	47
20	SCC Test Specimen and Loading Method for 6Al-4V Titanium Alloys	48
21	Shape Parameter Curves for Surface and Internal Flaws	51
22	Estimated Elastic Stress Intensity Magnification Factors at Maximum Crack Depth for Surface Cracks in Tension (Reference 4)	52
23	Stress Corrosion Cracking Velocity Data for 7075-T651 Aluminum Alloy	60
24	SCC Test Results for 7075-T651 Aluminum Alloy, Crack Surface Sprayed with LPS-3 Prior to Immersion in Test Media	62
25	SCC Test Results for 7075-T651 Aluminum Alloy Crack Surface Sprayed with LPS-3 and Dried for 3.0 Hours Prior to Immersion in Test Media	63
26	Illustration of Fracture Face from 7075-T651 Aluminum Alloy Surface Flaw Specimen SCC Test in 3.5% NaCl Solution	64
27	Effect of Environment on Fatigue Crack Growth Rates at R=0.1 in 7075-T651 Aluminum Alloy (60 CPM)	66
28	Effect of Environment on Fatigue Crack Growth Rates at R=0.5 in 7075-T651 Aluminum Alloy (60 CPM)	67
29	Effect of Environment on Fatigue Crack Growth Rates at 6 CPM in 7075-T651 Aluminum Alloy	68

LIST OF FIGURES (CONT'D)

<u>No.</u>	<u>Title</u>	<u>Page</u>
30	Fatigue Crack Growth Rates for 7075-T651 Aluminum Alloy in Alternating JP-4 Fuel and Distilled Water (60 CPM)	70
31	Fatigue Crack Growth Rates for 7075-T651 Aluminum Alloy in Alternating JP-4 Fuel and Distilled Water (6 and 60 CPM)	71
32	Fatigue Crack Growth Rates for 7075-T651 Aluminum Alloy in Distilled Water, Crack Surface Sprayed with LPS-3 and Dried for 3.0 Hours Prior to Immersion in Test Media (60 CPM)	73
33	Fatigue Crack Growth Rates for 7075-T651 Aluminum Alloy in Dye Penetrant (60 CPM)	74
34	Fatigue Crack Growth Rates for 7075-T651 Aluminum Alloy in Dye Penetrant' (6 CPM)	75
35	Fatigue Crack Growth Rates for 7075-T651 Aluminum Alloy at -65F and +175F in Desiccated Air and 3.5% NaCl Solution (60 CPM)	76
36	Fatigue Crack Growth Rates for 7075-T651 Aluminum Alloy at 175F in JP-4 Fuel and Distilled Water (60 CPM)	77
37	Fatigue Crack Growth Rates for 7075-T651 Aluminum Alloy in Desiccated Air (6 CPM)	78
38	Fatigue Crack Growth Rates for 7075-T651 Aluminum Alloy in Distilled Water (6 CPM)	79
39	Fatigue Crack Growth Rates for 7075-T651 Aluminum Alloy in 3.5% NaCl Solution (6 CPM)	80
40	Fatigue Crack Growth Rates for 7075-T651 Aluminum Alloy in Water Saturated JP-4 Fuel (6 CPM)	81
41	Fatigue Crack Growth Rates for 7075-T651 Aluminum Alloy in Sump Tank Water (6 CPM)	82
42	Fatigue Crack Growth Rate Data for 7075-T651 Aluminum Alloy Surface Flawed Specimen (60 CPM)	84

LIST OF FIGURES (CONT'D)

<u>No.</u>	<u>Title</u>	<u>Page</u>
43	Stress Corrosion Cracking Velocity Data for 7475-T651 Aluminum Alloy	86
44	Fatigue Crack Growth Rates for 7475-T651 Aluminum Alloy in Desiccated Air and 3.5% NaCl Solution (60 CPM)	87
45	Effect of Environment on Fatigue Crack Growth Rates at $R=0.1$ for 6Al-4V Standard ELI Beta Annealed Titanium Alloy (60 CPM)	93
46	Effect of Environment on Fatigue Crack Growth Rates at $R=0.50$ in 6Al-4V Standard ELI Beta Annealed Titanium Alloy (60 CPM)	94
47	Effect of Environment on Fatigue Crack Growth Rates at $R=0.80$ in 6Al-4V Titanium Alloy (60 CPM)	95
48	Effect of Environment on Fatigue Crack Growth Rates at $R=0.10$ in 6Al-4V Standard ELI Beta Annealed Titanium Alloy (6 CPM)	96
49	Effect of Environment on Fatigue Crack Growth Rates at $R=0.50$ in 6Al-4V Standard ELI Beta Annealed Titanium Alloy (6 CPM)	97
50	Fatigue Crack Growth Rates for 6Al-4V Standard ELI Beta Annealed Titanium Alloy at $R=0.5$ in Alternating JP-4 Fuel and Distilled Water (60 CPM)	98
51	Fatigue Crack Growth Rates for 6Al-4V Standard ELI Beta Annealed Titanium Alloy at $R=0.1$ in Alternating JP-4 Fuel and Distilled Water (60 CPM)	99
52	Fatigue Crack Growth Rates for 6Al-4V Standard ELI Beta Annealed Titanium Alloy in Dye Penetrant (6 CPM)	101
53	Fatigue Crack Growth Rates for 6Al-4V Standard ELI Beta Annealed Titanium in Distilled Water, Crack Surface Sprayed with LPS-3 and Dried 3.0 Hours Prior to Immersion in Test Media (60 CPM)	102
54	Fatigue Crack Growth Rates for 6Al-4V Standard ELI Beta Annealed Titanium Alloy at -65F and 175F (60 CPM)	103

LIST OF FIGURES (CONT'D)

<u>No.</u>	<u>Title</u>	<u>Page</u>
55	Fatigue Crack Growth Rates for 6Al-4V Standard ELI Beta Annealed Titanium Alloy in Desiccated Air (6 CPM)	105
56	Fatigue Crack Growth Rates for 6Al-4V Standard ELI Beta Annealed Titanium Alloy in Distilled Water (6 CPM)	106
57	Fatigue Crack Growth Rates for 6Al-4V Standard ELI Beta Annealed Titanium Alloy in Water Saturated JP-4 Fuel (6 CPM)	107
58	Fatigue Crack Growth Rates for 6Al-4V Standard ELI Beta Annealed Titanium Alloy in 3.5% NaCl Solution (6 CPM)	108
59	Fatigue Crack Growth Rates for "Super Eli" 6Al-4V Beta Annealed Titanium Alloy in 3.5% NaCl Solution (60 CPM)	109
60	Fatigue Crack Growth Rates for 6Al-4V Standard ELI Beta Annealed Titanium Alloy Surface Flawed Specimen (60 CPM)	111
61	Effect of Environment on Fatigue Crack Growth Rates at $R=0.1$ for 6Al-4V Recrystallize Annealed Titanium Alloy (60 CPM)	116
62	Effect of Environment on Fatigue Crack Growth Rates at $R=0.5$ for 6Al-4V Recrystallize Annealed Titanium Alloy (60 CPM)	117
63	Effect of Environment on Fatigue Crack Growth Rates at $R=0.80$ for 6Al-4V Recrystallize Annealed Titanium Alloy (60 CPM)	118
64	Effect of Environment on Fatigue Crack Growth Rates at $R=0.10$ for 6Al-4V Recrystallize Annealed Titanium Alloy (6 CPM)	119
65	Effect of Environment on Fatigue Crack Growth Rates at $R=0.50$ for 6Al-4V Recrystallize Annealed Titanium Alloy (6 CPM)	120
66	Fatigue Crack Growth Rates for Recrystallize 6Al-4V Annealed Titanium Alloy in Alternating JP-4 Fuel and Distilled Water (60 CPM)	121

LIST OF FIGURES (CONT'D)

<u>No.</u>	<u>Title</u>	<u>Page</u>
67	Fatigue Crack Growth Rates for 6Al-4V Recrystallize Annealed Titanium Alloy in Dye Penetrant (60 CPM)	123
68	Fatigue Crack Growth Rates for 6Al-4V Recrystallize Annealed Titanium Alloy in Distilled Water, Crack Surfaces Sprayed with LPS-3 and Dried 3.0 Hours Prior to Immersion in Test Media (60 CPM)	124
69	Fatigue Crack Growth Rates for 6Al-4V Recrystallize Annealed Titanium Alloy at -65F and 175F (60 CPM)	125
70	Fatigue Crack Growth Rates for 6Al-4V Recrystallize Annealed Titanium Alloy in Desiccated Air (6 CPM)	127
71	Fatigue Crack Growth Rates for 6Al-4V Recrystallize Annealed Titanium Alloy in Water Saturated JP-4 Fuel (6 CPM)	128
72	Fatigue Crack Growth Rates for 6Al-4V Recrystallize Annealed Titanium Alloy in Distilled Water (6 CPM)	129
73	Fatigue Crack Growth Rates for 6Al-4V Recrystallize Annealed Titanium Alloy in 3.5% NaCl Solution (6 CPM)	130
74	Fatigue Crack Growth Rates for 6Al-4V Recrystallize Annealed Titanium Alloy in Sump Tank Water (6 CPM)	131
75	Fatigue Crack Growth Rates for 6Al-4V Recrystallize Annealed Titanium Alloy (obtained using NAR Specimen Design) (60 CPM)	133
76	Fatigue Crack Growth Rate Data for 6Al-4V Recrystallize Annealed Titanium Alloy Surface Flawed Specimen (60 CPM)	134
77	Clip Gage Location for Crack Closure Measurements	135
78	Loading Program Used for Crack Closure Measurements	137
79	Effect of Measurement Location on Apparent Stress Intensity Factor at Onset of Crack Closure	137
80	Examples of Crack Displacement vs Load Recording Obtained During Crack Closure Measurements	138
81	Effect of Peak Cyclic Stress Intensity Factor on Stress Intensity Factor at the Onset Crack Closure	140

LIST OF FIGURES (CONT'D)

<u>No.</u>	<u>Title</u>	<u>Page</u>
82	Effect of Crack Length and Load Increase on Stress Intensity Factor at Which Crack Closure Occurs	141
83	Cutting Diagram and Microstructural Variation for Thermally Cycled 6Al-4V Recrystallize Annealed Titanium Alloy Plates	145
84	Equiaxed Alpha-Beta Microstructure of Ti-6Al-4V Specimen 55K-1	147
85	Basketweave Microstructure of Ti-6Al-4V Specimen 44K-1	147
86	Microstructure of Fracture Toughness Specimen 66K-1 Showing Both the Equiaxed Alpha and Basketweave Grain Morphologies.	148
87	Basal Plane Pole Figure for Equiaxed Alpha-Beta Microstructure Resulting from Cyclic Heat Treatment of Plate 44	149
88	Basal Plane Pole Figure for Basketweave Microstructure Resulting from Cyclic Heat Treatment of Plate 44	150
89	Fracture Surface of Stress Corrosion Specimen from Plate 33	154
90	Corrosion Fatigue Crack Growth Rates for Thermal Processing Effects Tests	156
91	Stress Corrosion Cracking Velocity Data for 9Ni-4Co-0.3C Steel Alloy	160
92	Envelopes of Average Crack Growth Rate Data for 9Ni-4Co-0.3C Steel Alloy Plate in Six Environments	163
93	Effect of Environment on Fatigue Crack Growth Rates at R=0.10 for 9Ni-4Co-0.3C Steel Alloy Plate (6 CPM)	164
94	Effect of Environment on Fatigue Crack Growth Rates at R=0.5 for 9Ni-4Co-0.3C Steel Alloy Plate (6 CPM)	165
95	Example of Test Records Obtained from Overload Tests	169
96	Effect of Overload Ratio on Delay Cycles for Titanium Alloy Overload Tests	174

LIST OF FIGURES (CONT'D)

<u>No.</u>	<u>Title</u>	<u>Page</u>
97	Effect of Peak Overload Stress Intensity Factor on Change in Cyclic Life	177
98	Effect of Stress Ratio on Corrosion Fatigue Crack Growth Rate Behavior of Aluminum and Steel Alloy at at 60 CPM	180
99	Effect of Stress Ratio on Corrosion Fatigue Crack Growth Rate Behavior of Titanium Alloys at 60 CPM	181
100	Effect of Stress Ratio on Fatigue Crack Growth Rates for Steel and Titanium Alloys in Desiccated Air	182
101	Effect of Cyclic Frequency on Stress Ratio Effects in Titanium and Steel Alloys.	184

SUMMARY

This program was directed to a study of some of the factors affecting the growth of crack-like defects in aircraft structural materials. The objective was to study the characteristics of and the influence of metallurgical factors on corrosion fatigue crack growth in high strength metal alloys. Mechanical property, fracture toughness, stress corrosion cracking, and corrosion fatigue tests were conducted for five alloys in seven different environments. The four principal alloys included: 7075-T651 aluminum, 6Al-4V (ELI) beta annealed titanium, 6Al-4V recrystallized annealed (RA) titanium, and 9Ni-4Co-0.3C (220-240 ksi) steel, all in plate form. A limited number of tests were conducted on 7475-T651 aluminum alloy plate. Test environments included: desiccated air, distilled water, 3.5% NaCl solution, water saturated JP-4 fuel, sump tank water, alternating JP-4 fuel/distilled water, and dye penetrant. Most tests were conducted at 72F with a few tests being performed at +175F and -65F to evaluate the effects of temperature on material behavior. Double cantilever beam specimens were used for most stress corrosion cracking and corrosion fatigue tests; specimen thickness was sufficient to generate plane strain crack tip deformations. A limited number of surface-flawed specimens were tested for comparison. The majority of tests were undertaken to evaluate basic crack growth rates using cyclic frequencies of 6 and 60 cpm and ratios of minimum/maximum cyclic stress (R) of 0.1, 0.5, and 0.8. The effect of overloads on subsequent fatigue crack growth behavior was investigated by testing 7075-T651 aluminum, 6Al-4V (ELI) beta-annealed titanium and 6Al-4V RA titanium alloy tapered double cantilever beam specimens in both desiccated air and 3.5% NaCl solution. Finally, a series of tests was undertaken to evaluate the effect of both grain size and cooling rate on the crack growth resistance properties of Ti-6Al-4V RA plate.

A large body of crack growth rate data was generated in this program. These data are included in Appendix A to this report. The testing of double cantilever beam (DCB) specimens proved to be a very good method of generating large amounts of data. However, the DCB specimen is not suitable for testing the thickness direction of plate materials and hence, DCB specimen data are not always applicable to many practical cracking situations in airframe components

such as surface flaws and fastener hole flaws. The applicability of the DCB data to these problems must be checked by testing surface flawed or fastener hole flaw specimens.

A number of observations were made with respect to variations in resistance to stress corrosion and corrosion fatigue cracking among the alloys tested. For the Ti-6Al-4V alloy, beta annealing led to superior stress corrosion cracking and corrosion fatigue crack growth resistance than did recrystallize annealing. The 9Ni-4Co-0.3C steel alloy plate heat treated to the 240 ksi strength level was found to be very susceptible to stress corrosion cracking in aqueous environment. The 7475-T651 aluminum alloy plate had superior fracture toughness to the 7075-T651 aluminum alloy plate for the WR direction that was tested. Fatigue crack growth rates for the two aluminum alloys in 3.5% NaCl solution did not differ greatly.

A summary of some of the observations made during this program follows:

- The relative effects of potential models of the "worst" normal operating environment for airframe components, namely, 3.5% NaCl solution and sump tank water, was dependent on alloy.
- Changes in temperature from -65F to +175F had little or no effect on corrosion fatigue crack growth rates for the alloy/environment couples tested in this program.
- Spraying the crack surfaces of test specimens with the corrosion inhibitive compound LPS-3 prior to test had no significant effect on stress corrosion cracking and corrosion fatigue crack growth resistance.
- The effect of change in frequency from 60 to 6 cpm on corrosion fatigue crack growth rates was dependent on alloy/environment couple.
- The rate of increase of fatigue crack growth rates with increase in stress ratio varied considerably from one material/environment couple to another. In general, stress ratio effects were largest in material/environment combinations that were susceptible to SCC.

- Overloads increased cyclic life up to overload to fracture stress ratios of 0.9. For ratios greater than 0.9, the beneficial effect of crack growth rate retardation was more than offset by crack growth that occurred during the overload.

1.0 INTRODUCTION

Recent failures in first line military aircraft have demonstrated the need for additional and new design methods for airframe components. Some of the failures have been of the catastrophic variety and originated at crack-like defects that were previously undetected during production or in-service inspections. Since all aircraft structures contain defects that are either inherent in the materials or are introduced during production or service, it became evident that new design methods and criteria were required to minimize the detrimental effects of such defects.

In recent years, methods (1)* based on fracture mechanics have been successfully applied to the design of fracture resistant spacecraft and booster tanks. Hence, attempts were initiated to extend existing design methods to make them applicable to the complex geometries, environments, and loadings encountered during the operation of military aircraft. Specifically, design procedures are required to insure that the largest crack-like defect that would reasonably be expected to exist at the outset of service will not grow sufficiently to initiate a failure that could result in loss of aircraft. The design procedures require methods of: establishing the maximum possible initial defect size that could be expected to exist throughout the life of the structure; determining the critical defect sizes, i.e., sizes that would result in component failures; and calculating the number of aircraft missions that could grow the initial crack-like defect to critical sizes.

This program was directed to a study of some of the factors affecting the growth of crack-like defects in aircraft structural materials. The objective was to obtain information on load history and environmental effects and their interaction with metallurgical factors, on subcritical crack growth in high strength metal alloys. A summary of the overall test program is included in Table 1. Mechanical property, fracture toughness, stress corrosion cracking, and corrosion fatigue tests were conducted for five alloys in seven different environments. The four principal alloys (all in plate form) included: 7075-T651 aluminum, 6Al-4V (ELI) beta annealed titanium, 6Al-4V recrystallize

* Number in parentheses refer to references at end of report.

Table 1: Test Program

TEST TYPE	SPECIMEN TYPE	CYCLIC FREQUENCY	STRESS RATIO	ENVIRONMENT																				
				AIR			DISTILLED WATER			3.5% NaCl SOLUTION			JP-4			SUMP TANK			JP-4 + H ₂ O			DYE PEN		
				-65F	72F	175F	-65F	72F	175F	-65F	72F	175F	-65F	72F	175F	-65F	72F	175F	-65F	72F	175F			
MECHANICAL PROPERTY	TENS.	-	-	X	X	X	X	X	X	X	X	X	X	X	X	X	X	X	X	X	X	X	X	X
	CT SF	-	-	X	X	X	X	X	X	X	X	X	X	X	X	X	X	X	X	X	X	X	X	X
STRESS CORROSION CRACKING	DCB SF	-	-	X	X	X	X	X	X	X	X	X	X	X	X	X	X	X	X	X	X	X	X	X
	DCB	60	0.1 0.5 0.8	X	X	X	X	X	X	X	X	X	X	X	X	X	X	X	X	X	X	X	X	X
CORROSION FATIGUE	DCB	6	0.1 0.5	X	X	X	X	X	X	X	X	X	X	X	X	X	X	X	X	X	X	X	X	X
	SF	60	0.5	X	X	X	X	X	X	X	X	X	X	X	X	X	X	X	X	X	X	X	X	X
OVERLOAD	TDCB	60	0.5	X	X	X	X	X	X	X	X	X	X	X	X	X	X	X	X	X	X	X	X	X

X INDICATES CONDITIONS FOR WHICH TESTS WERE CONDUCTED

annealed (RA) titanium, and 9Ni-4Co-0.3C (220-240 ksi) steel. A limited number of tests were conducted on 7475-T651 aluminum alloy plate. Test environments included: desiccated air, distilled water, 3.5% NaCl solution, water saturated JP-4 fuel, sump tank water, alternating JP-4 fuel/distilled water, and dye penetrant (type Z1-2A). Most tests were conducted at 72F with a few tests being performed at +175F and -65F to evaluate the effects of temperature on material behavior. Double cantilever beam specimens were used for most stress corrosion cracking and corrosion fatigue tests; specimen thickness was sufficient to generate plane strain crack tip deformations. A limited number of surface-flawed specimens were tested for comparison. The majority of tests were undertaken to evaluate basic crack growth rates using cyclic frequencies of 6 and 60 cpm and ratios of minimum/maximum cyclic stress (R) of 0.1, 0.5, and 0.8. The effect of overloads on subsequent fatigue crack growth behavior was investigated by testing 7075-T651 aluminum, 6Al-4V (ELI) beta-annealed titanium and 6Al-4V RA titanium alloy tapered double cantilever beam specimens in both desiccated air and 3.5% NaCl solution. Finally, a series of tests was undertaken to evaluate the effect of both grain size and cooling rate on the crack growth resistance properties of Ti-6Al-4V RA plate.

2.0 MATERIALS AND PROCEDURES

Test materials and procedures are described in detail in this section. Results of mechanical property and metallurgical characterization tests of all test materials are described in Section 3.1. Bases for selection of test environments are discussed in Section 3.2, and procedures used for specimen preparation, testing and evaluation of results are included in Section 3.3.

2.1 Materials

Six different alloys were tested in this program. The four primary alloys were aluminum 7075-T651, steel 9Ni-4Co-0.3C, Ti-6Al-4V beta annealed, and Ti-6Al-4V recrystallize annealed (alpha-beta processed). The aluminum alloy 7475-T651 and "super ELI" Ti-6Al-4V were also tested to evaluate the effects of improved purity of composition. Various thermal cycles were applied to the Ti-6Al-4V recrystallize annealed (RA) material to assess the effects of microstructural changes on corrosion fatigue properties.

Each test material was characterized for mechanical properties, composition, microstructure and macrostructure. In addition, conductivity, hardness, and exfoliation corrosion testing were conducted for the aluminum alloys. The steel alloy, 9Ni-4Co-3.0C, was evaluated for inclusion content and alloy segregation. Crystallographic texture was determined for each titanium plate evaluated.

The material characterization data generated for the test materials of this program were evaluated and compared to other data for each alloy so that each test material could be rated against other material of the same alloy designation

2.1.1 Aluminum 7075-T651

The aluminum alloy, 7075 was procured from ALCOA in plate form, 0.625 x 48 x 72 inches per specification QQ-A-250/12d in the T651 condition. The alloy was selected for study since it is commonly used in existing aircraft structure

and no systematic study had been conducted on its corrosion fatigue characteristics, particularly for plane strain conditions.

The composition of the 7075-T651 plate as determined by Boeing is included in Table 2. "Wet" analytical techniques were utilized for each element. The test results indicate that the heat chemistry is representative of a typical 7075 composition.

The microstructure (Figure 1) and macrostructure were typical of 0.625 inch thick 7075-T651 plate. Plate hardness of 90.6 (Rockwell B) and conductivity of 31.6 (% IACS) also represented typical values.

The plate was characterized for exfoliation corrosion by the "Total Immersion Exfoliation Corrosion Test" (ASTM Task Group G01.05.02-T.6.8). The exfoliation characteristics were normal.

Mechanical properties were measured by The Boeing Company at temperatures of -65F, 72F and 175F. Detailed results are listed in Table A2 in Appendix A and are plotted against test temperature in Figure 2. The scatter bands in the upper part of Figure 2 enclose the ultimate strength and yield strength data. All mechanical properties are typical of 7075 alloy plate in the T651 condition.

Fracture toughness values were measured by The Boeing Company at temperatures of -65F, 72F, and 175F. Results are tabulated in Tables A3 and A4 in Appendix A and are plotted against test temperature in Figure 3. Fracture toughness values for the WR direction were measured using both compact tension and double cantilever beam specimens. Specimen configurations are detailed in Figures B2 and B10 in Appendix B. The compact tension data plotted in Figure 3 are typical of the 7075 aluminum alloy with the average value of K_{IC} at 72F being 22.7 ksi $\sqrt{\text{in}}$. Double cantilever beam specimens were tested only at 72F and yielded average K_{IC} values of 22.2 ksi $\sqrt{\text{in}}$ for the WR direction and 31.7 ksi $\sqrt{\text{in}}$ for the RW direction.

Six surface-flawed specimens were tested to measure fracture toughness at +175, +72, and -65F. The crack plan was parallel to the rolling direction in all

Table 2: Chemical Composition of Aluminum Alloys

MATERIAL	HEAT LOT	TEST LAB	Si	Fe	Cu	Mn	Mg	Cr	Zn	Ti
7075-T651	T713-143	SPEC LIMITS	0.40	0.50	1.2-2.0	0.30	2.1-2.9	0.18-	5.1-6.1	0.20
			MAX	MAX		MAX		0.35		MAX
		BOEING	0.07	0.23	1.55	0.06	2.15	0.20	5.52	0.03
7475-T651	S-395610	SPEC LIMITS	0.10	0.12	1.2-1.9	0.06	1.9-2.6	0.18-	5.2-6.2	0.06
			MAX	MAX		MAX		0.25		
		ALCOA	0.05	0.06	1.51	0.01	2.36	0.19	5.57	0.03
		BOEING	0.05	0.10	1.60	0.06	2.15	0.20	5.48	0.03

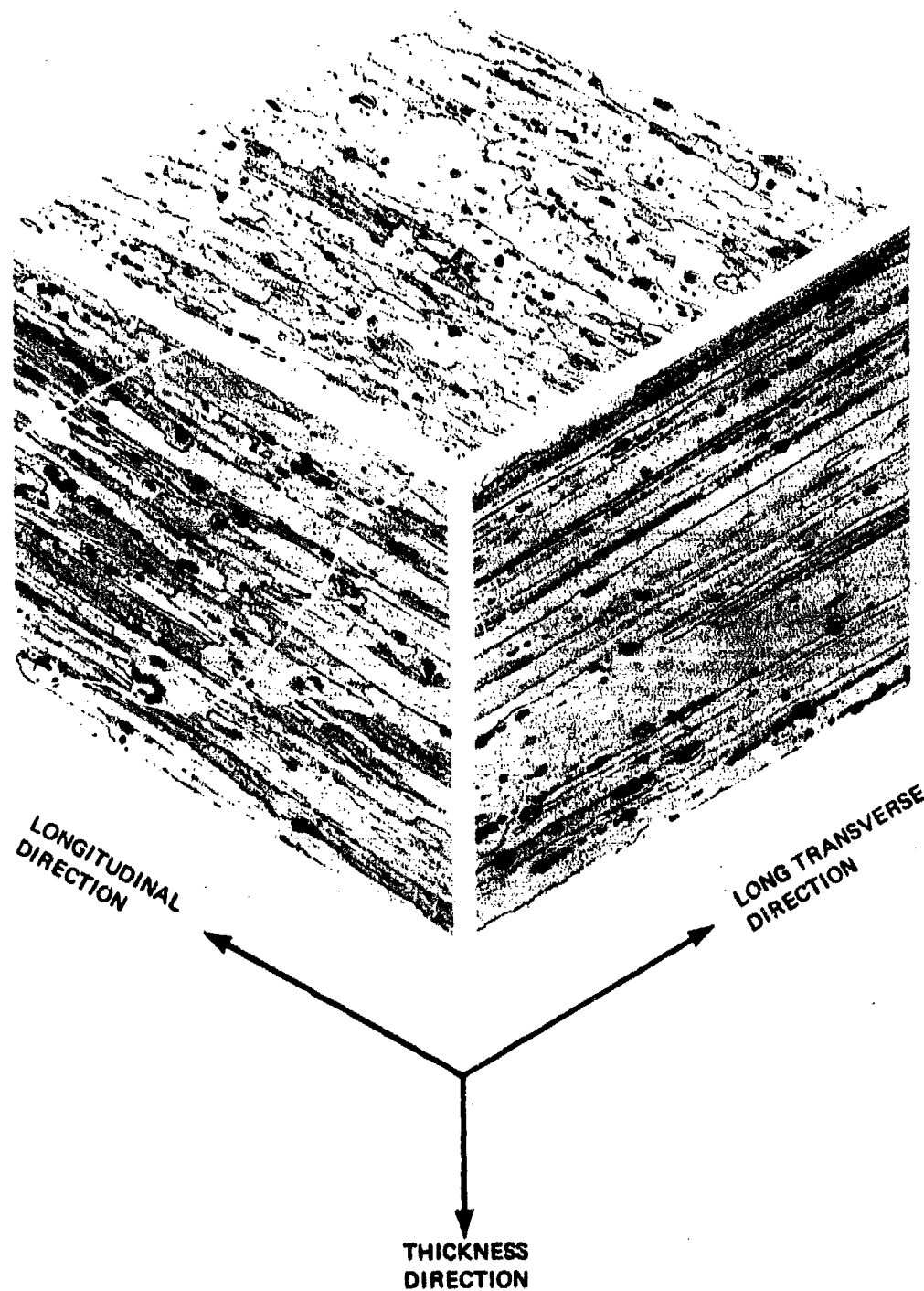


Figure 1: 7075-T651 Aluminum Alloy Microstructure Composite (200X, Kellers Etch)

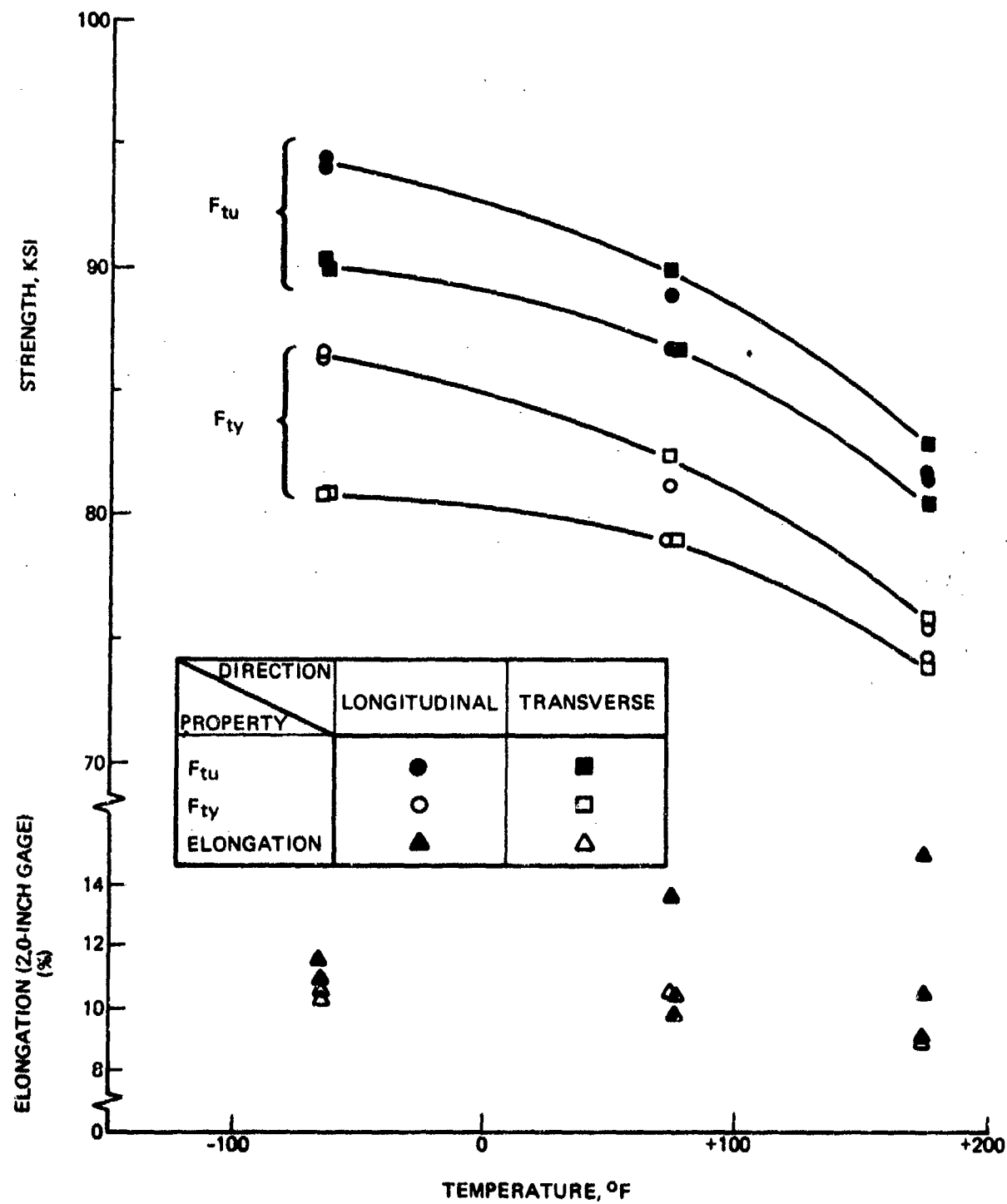


Figure 2: Mechanical Properties for 7075-T651 Aluminum Alloy Plate (0.625-Inch-Thick)

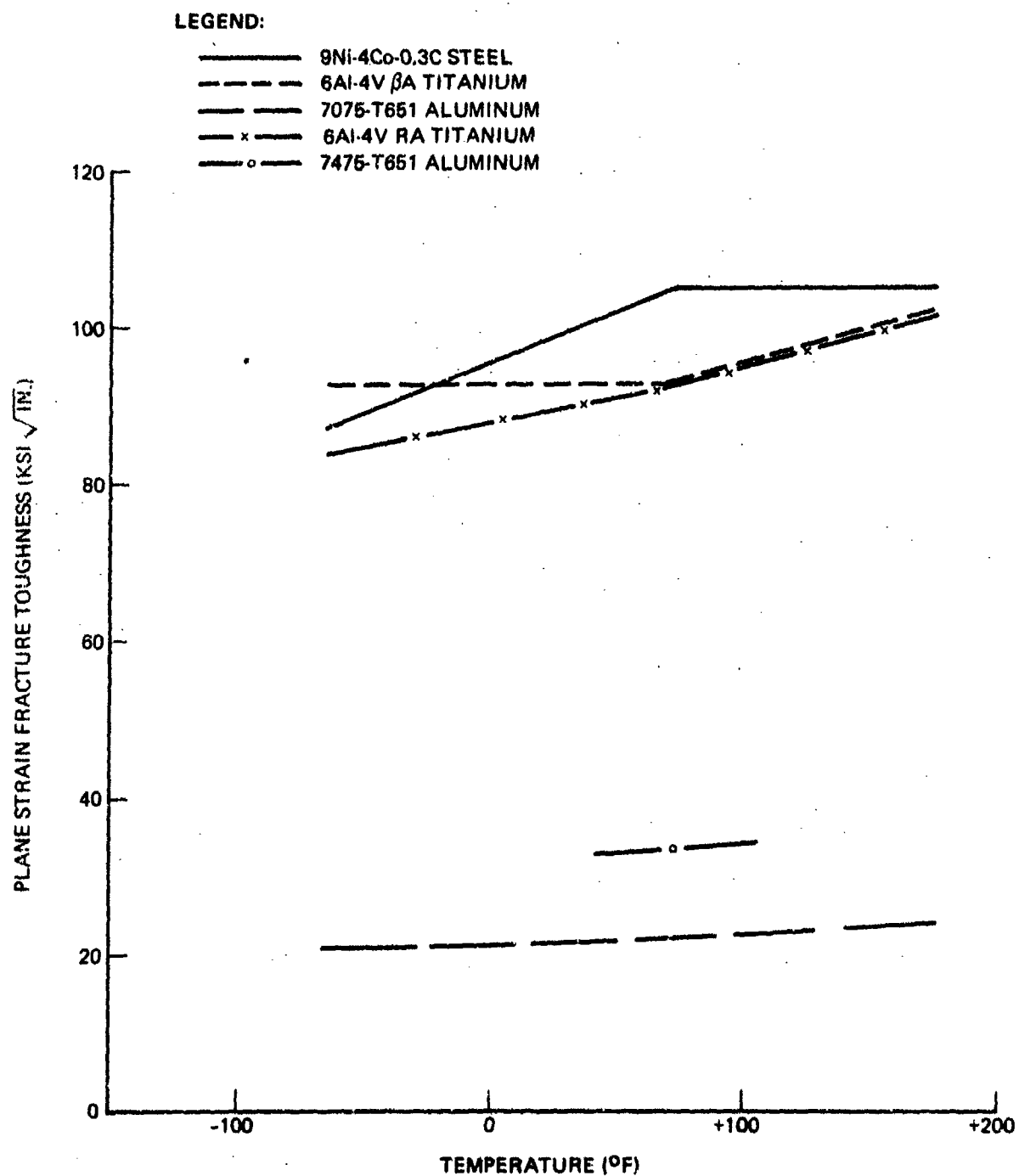


Figure 3: Fracture Toughness Data for All Test Alloys (CT Specimens)

specimens and two tests were conducted at each temperature. Results are summarized in Table 3. Detailed test data are included in Table A4 in Appendix A. For all specimens, records of crack displacement versus load showed that marked pop-ins occurred at loads less than the failure load. Previous testing has shown that pop-ins in 7075-T651 surface flawed specimens are common and result from bursts of crack growth in the lateral direction. Little or no growth occurs in the depthwise direction. This behavior is indicative of a higher resistance to crack propagation in the depthwise (WT) direction than in the lateral (WR) direction for the 7075-T651 plate material. Such behavior makes it difficult to calculate a value of stress intensity factor that equals the fracture toughness for a given direction of crack propagation. It is believed that stress intensity factors calculated using peak load and initial flaw dimensions are good approximations of the depthwise (WT) fracture toughness. The fracture toughness values for the WT direction listed in Table 3 are considerably greater than comparable values measured for the WR direction.

2.1.2 Aluminum 7475-T651

The 7475 alloy was tested so that the relative crack growth resistance of the 7075 and 7475 alloys could be compared. The 7475 alloy is a high purity 7075 alloy with lower specification limits on magnesium content. The 7475 alloy tested in this program was obtained from Alcoa in the form of a 1.0 x 18 x 12 inches plate in the T651 condition. The compositions as determined by both Boeing and Alcoa are listed in Table 2. The only significant difference in chemical composition between the 7475 and 7075 alloys was iron content which was significantly lower in the 7475 plate.

The microstructure (Figure 4) and macrostructure were typical of 1.0 inch thick 7475-T651 plate. Typical values were obtained for hardness (90.9 Rockwell B) and conductivity (32.9-% IACS).

The plate was characterized for exfoliation corrosion by the "Total Immersion Exfoliation Corrosion Test" (ASTM Task Group G01.05.02-T.6.8). Normal exfoliation characteristics were observed and negligible differences were noted compared to the corrosion characteristics of the 7075 plate.

Table 3: Summary of Fracture Toughness Data for Plate Alloys

ALLOY	TEMP (°F)	FRACTURE TOUGHNESS (KSI $\sqrt{IN.}$)	
		WR DIRECTION*	WT DIRECTION**
ALUMINUM 7075-T651	-65	21.4	30.7
	+72	22.7	32.6
	+175	24.2	34.7
STEEL 9Ni-4Co-0.3C (F _{tu} = 240)	-65	87.0	94.0
	+72	107.0	106.5
	+175	105.0	108.3
TITANIUM 6Al-4V BETA ANNEALED	-65	92.5	104.8
	+72	93.2	95.2 (a)
	+175	98.6	88.4 (a)
TITANIUM 6Al-4V RA	-65	84.0	103
	+72	92.5	93
	+175	102.5	90 (a)

* FROM COMPACT TENSION SPECIMENS

** FROM SURFACE FLAWED SPECIMENS

(a) FAILURE STRESSES $> 90\% \sigma_{ys}$

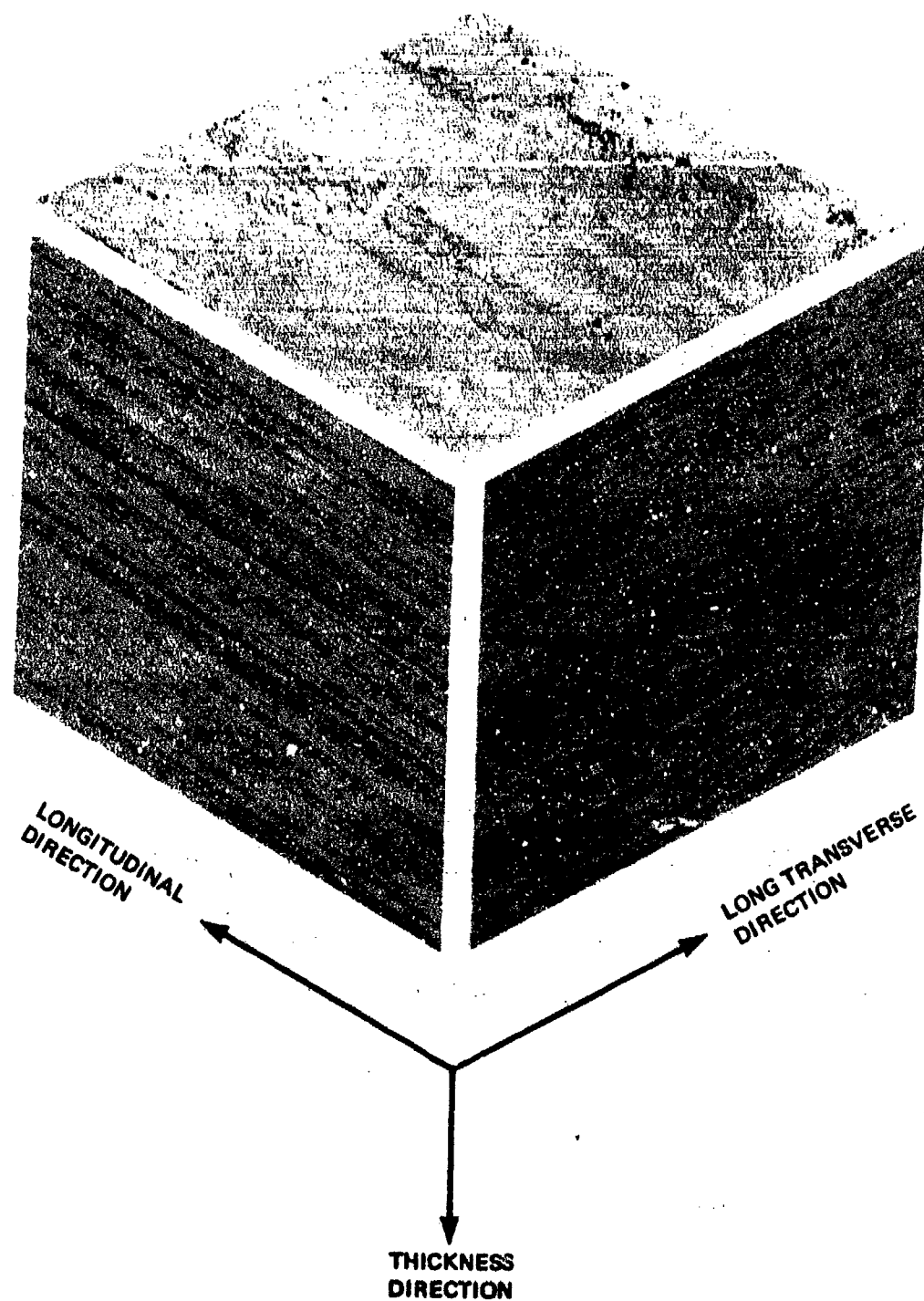


Figure 4: 7475-T651 Aluminum Alloy Microstructure Composite (200X, Kellers Etch)

Mechanical property and fracture toughness values were measured at 72F by The Boeing Company. Results are included in Tables 4 and 5. The ultimate and yield strength values were slightly lower than for the 7075 alloy. The plane strain fracture toughness for the WR direction of the 7475-T651 alloy ($31 \text{ ksi}\sqrt{\text{in}}$) was considerably greater than that for the 7075-T651 plate.

2.1.3 Titanium 6Al-4V Beta Annealed

The Ti-6Al-4V beta annealed alloy was purchased from RMI in the form of 1.0 x 48 x 84 inches plates per Boeing Material Specification XBMS7-174B. The B revision of the applicable specification requires an extra low interstitial grade and annealing above the beta transus to provide high toughness and resistance to stress corrosion cracking.

The plate composition as determined by the producer as verified by Boeing chemical analyses is shown in Table 6. The Boeing analysis yielded somewhat lower values for oxygen content. The microstructure, shown in Figure 5, is typical for beta annealed Ti-6Al-4V. Examination of the macrostructure revealed a uniform structure with only minor banding. The average prior beta grain size was approximately 10^{-4} square inches. Crystallographic average texture as determined by a computerized X-ray pole figure analysis (Figure 6 and Table 7) showed the material to have a generally random orientation of basal planes. The pole figure analysis method is described in Appendix D. A high intensity of basal planes normal to the maximum stress direction has been shown to degrade stress corrosion and corrosion fatigue characteristics. No significant effect of texture was expected in this material.

Mechanical properties were measured by The Boeing Company at temperatures of -65F, 72F and 175F. Mechanical property data are tabulated in Table A5 in Appendix A and plotted in Figure 7. The 72 F yield and ultimate strengths of 124 and 134 ksi exceed the corresponding minimum specification values of 115 and 127 ksi. The 72F elongation and reduction in area also meet specification values of ten and fifteen percent, respectively.

Fracture toughness values were measured using both compact tension and surface flawed specimens. The compact tension specimens were tested per ASTM E399-70T

Table 4 : Mechanical Property Data for 7475-T651 Aluminum Alloy One Inch Thick Plate

GRAIN DIRECTION	TEMP (°F)	ULTIMATE TENSILE STRENGTH (KSI)	0.2% OFFSET YIELD STRENGTH (KSI)	ELONGATION IN 2.0 INCHES (%)	REDUCTION IN AREA (%)
LONGITUDINAL	72	88.7 88.6	80.0 79.5	10 10	21 23
LONG TRANSVERSE	72	84.9 86.0	75.0 75.5	11 11	29 23

Table 5 : Fracture Toughness (K_{Ic}) Data for 7475-T651 Aluminum Alloy One Inch Thick Plate

PROPAGATION DIRECTION	TEMP (°F)	AVERAGE CRACK LENGTH (IN.)	MAXIMUM LOAD (K)	P_Q (K)	K_Q (KSI $\sqrt{IN.}$)
WR	72 72	0.74 0.73	2.74 2.74	2.49 2.74	30.0 32.1

Table 6: Chemical Composition of Titanium Alloys

MATERIAL	HEAT	TEST LAB	O ₂	Al	V	Fe	N ₂	C	H ₂
Ti6Al-4V BETA-ANNEALED	304623	SPEC LIMITS	.06-.13	5.5-6.3	3.5-4.5	0.25 MAX	.03 MAX	0.08 MAX	.0125 MAX
		RMI	.125	6.1	3.9	.17	.010	0.02	.0044
		BOEING	.103	6.07	3.8	.16		0.04	.0053
Ti6Al-4V BETA-ANNEALED SUPER ELI	G8200 (NO SPECIFICATION)								
		TIMET	.06	6.0	4.1	.05	.008	.023	.005
Ti-6Al-4V RECRYSTALLIZE ANNEALED		SPEC LIMITS	.09-.13	5.5-6.2	3.5-4.5	0.25 MAX	.03 MAX	0.08 MAX	.0125 MAX
		TIMET	.13	6.0	4.1	.11	.018	.026	.0050
		BOEING	.084	6.01	4.1	.15		.02	.0052

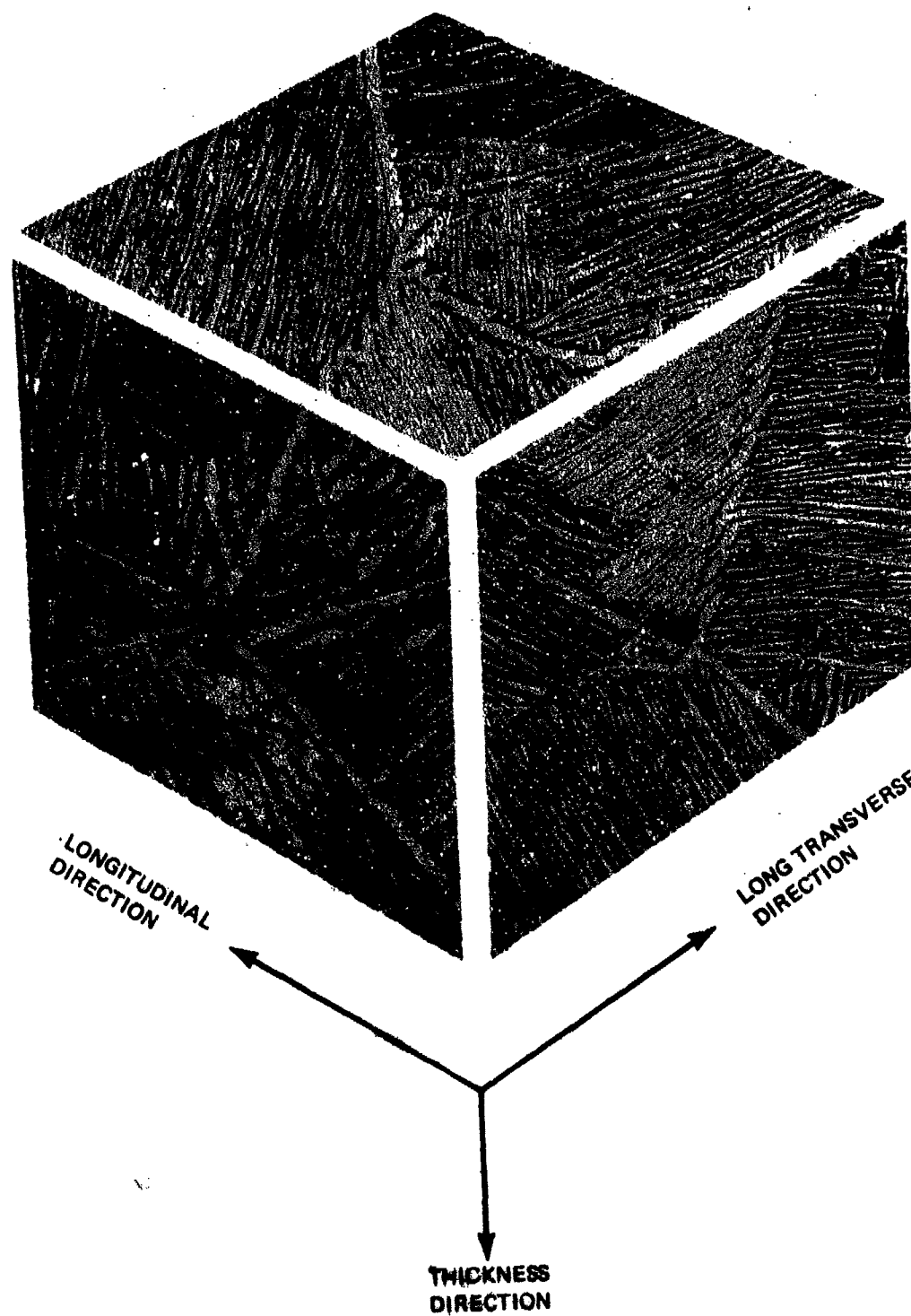
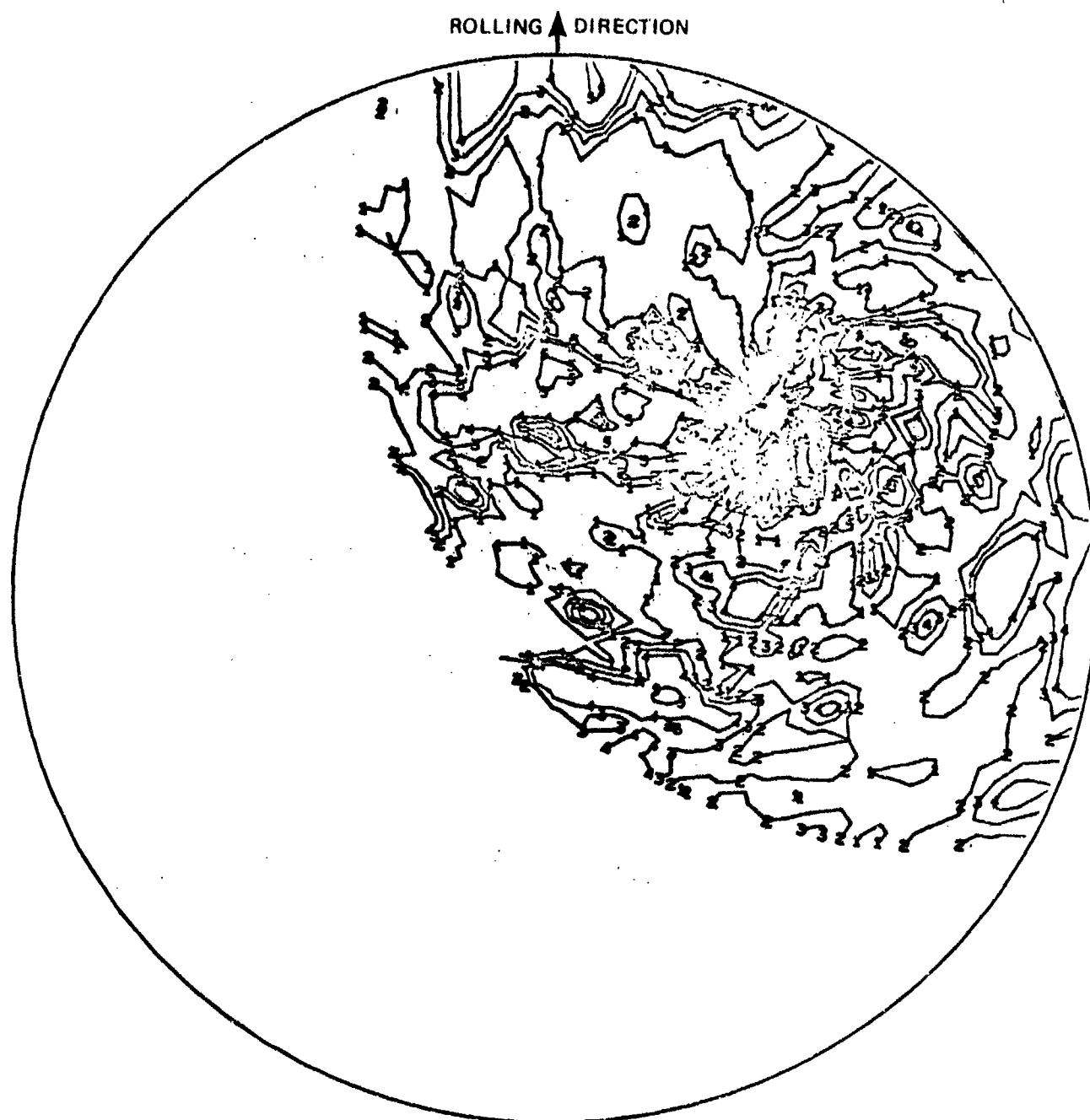


Figure 5: 6Al-4V Standard ELI Beta Annealed Titanium Alloy Microstructure Composite (500X)



CONTOUR LINES	1	2	3	4	5	6	7	8	9	0
TIMES RANDOM INTENSITY	0.5	1.0	1.5	2.0	4.0	8.0	14.0	20.0	25.0	30.0

Figure 6: Pole Figure for 6Al-4V Standard ELI Beta Annealed Titanium Alloy - Basal Plane (0002)

Table 7: Quantitative Texture Factors* for Titanium Alloys

MATERIAL	HEAT TREATMENT	TEXTURE FACTORS		
		% I _L	% I _T	% I _{ST}
Ti-6Al-4V SUPER ELI BETA ANNEALED	AS-RECEIVED	32.2	36.1	31.7
Ti-6Al-4V RECRYSTALLIZE ANNEALED	1900F/40 MIN/AC 1350F/2 HRS/AC	33.5	35.1	31.3
Ti-6Al-4V STANDARD ELI BETA ANNEALED	AS-RECEIVED	34.0	41.2	24.8

* QUANTITATIVE TEXTURE FACTOR DESCRIBES NUMERICALLY THE PERCENTAGE OF BASAL PLANES ORIENTED NORMAL TO A SPECIFIC GRAIN DIRECTION, I.E., LONGITUDINAL (L), TRANSVERSE (T), AND SHORT TRANSVERSE (ST). THE TEXTURE FACTOR IS CALCULATED FROM X-RAY POLE FIGURE INTENSITIES (SEE APPENDIX D) AS FOLLOWS:

$$\% I_L = \frac{\sum_{\phi=0}^{90^\circ} I_L \sin \phi \sin \alpha}{\text{TOTAL INTENSITY}}$$

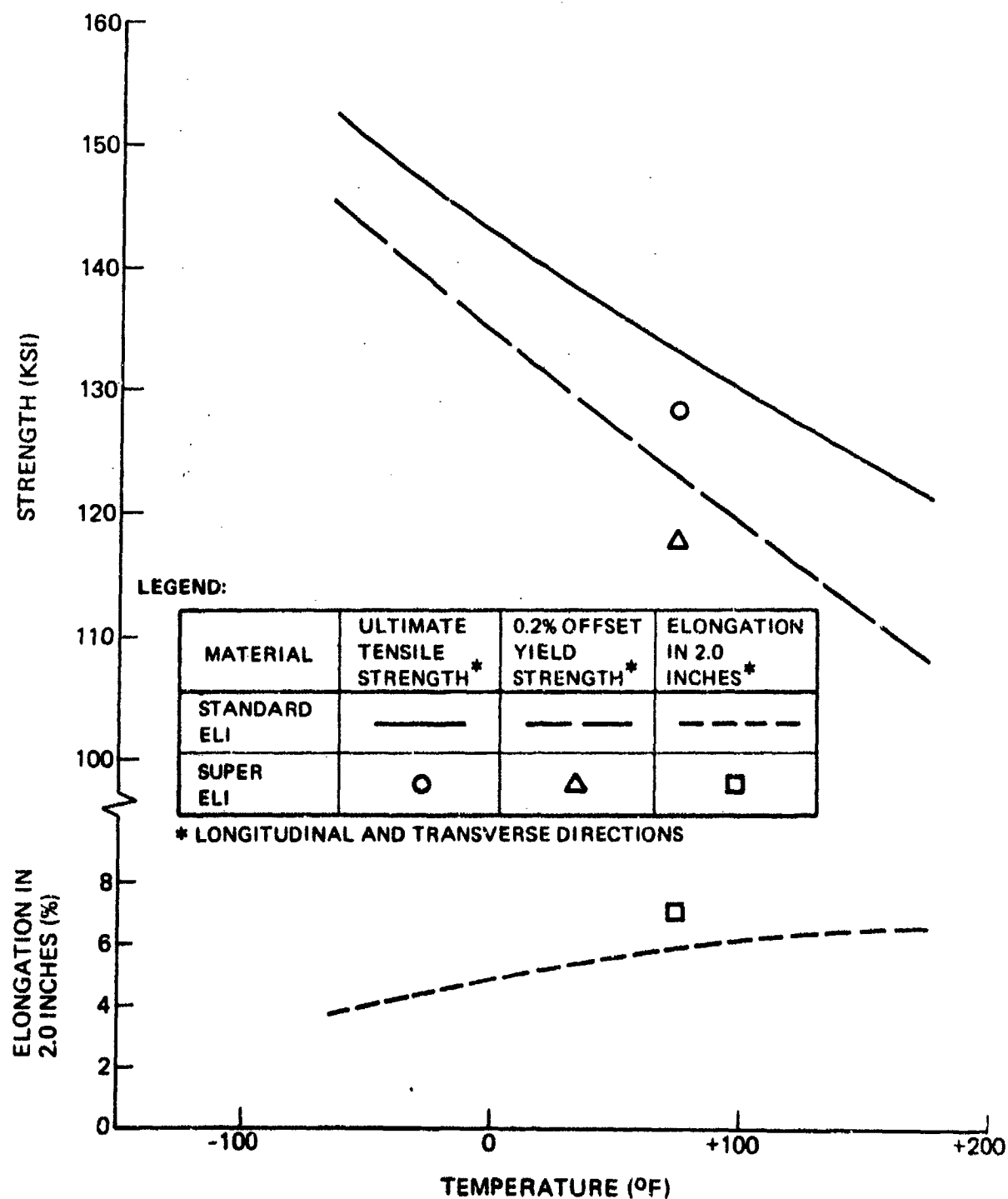


Figure 7: Mechanical Properties For 6Al-4V Beta Annealed Titanium Alloy Plate (1.0-Inch Thick)

except for specimen thickness requirements; detailed results are tabulated in Table A6 in Appendix A and fracture toughness are plotted as a function of test temperature in Figure 3. The average 72F fracture toughness value of $93 \text{ ksi}\sqrt{\text{in}}$ is believed to be a close approximation of the plane strain fracture toughness of the material since the specimen thickness of one inch was a high percentage of the minimum specimen thickness required for plane strain fracture toughness testing by E399-70T, namely, $2.5 (K_{IC}/\sigma_{ys})^2$ or about 1.4 inches. Six surface flawed specimens with crack planes perpendicular to the long transverse plate direction were tested to evaluate fracture toughness for the WT direction at -65F, 72F and 175F. Test details and results are tabulated in Table A7 in Appendix A and fracture toughness values are reported in Table 3 where they are compared to fracture toughness values obtained from the compact tension specimen tests. The trend of increasing toughness with increasing temperature for the WR direction is apparently reversed for the WT direction. However, the failure stresses for the surface-flawed specimens tested at 72F and 175F were greater than 90% of the corresponding uniaxial yield strengths and it is believed that the high failure stresses resulted in apparent fracture toughness values that are less than the actual values.

The Ti-6Al-4V beta annealed titanium plate having an oxygen content of 0.06% was obtained as a 1.0 x 8 x 11 inches plate from the Boeing Commercial Airplane Company. The plate was produced by TMCA per Boeing Material Specification BMS7-174B. The microstructure shown in Figure 8 was typical for beta annealed Ti-6Al-4V. Crystallographic average texture as determined by X-ray pole figure analysis (Figure 9 and Table 7) showed the material to have a nearly random orientation of basal planes. Chemical composition as determined by the vendor is included in Table 6 and mechanical properties measured by The Boeing Aerospace Company are shown in Figure 7. The K_{ISCC} for the WR direction of the plate was previously measured using a single edge notch tension specimen and found to be $87 \text{ ksi}\sqrt{\text{in}}$.

2.1.4 Ti-6Al-4V Recrystallized Annealed (RA)

Ti-6Al-4V RA plate, 1.0 inch thick, was fabricated to meet the requirements of the North American Rockwell Specification ST0170LB0032, Rev. B. The material was developed for use on the B-1 Bomber and was selected to meet high fracture

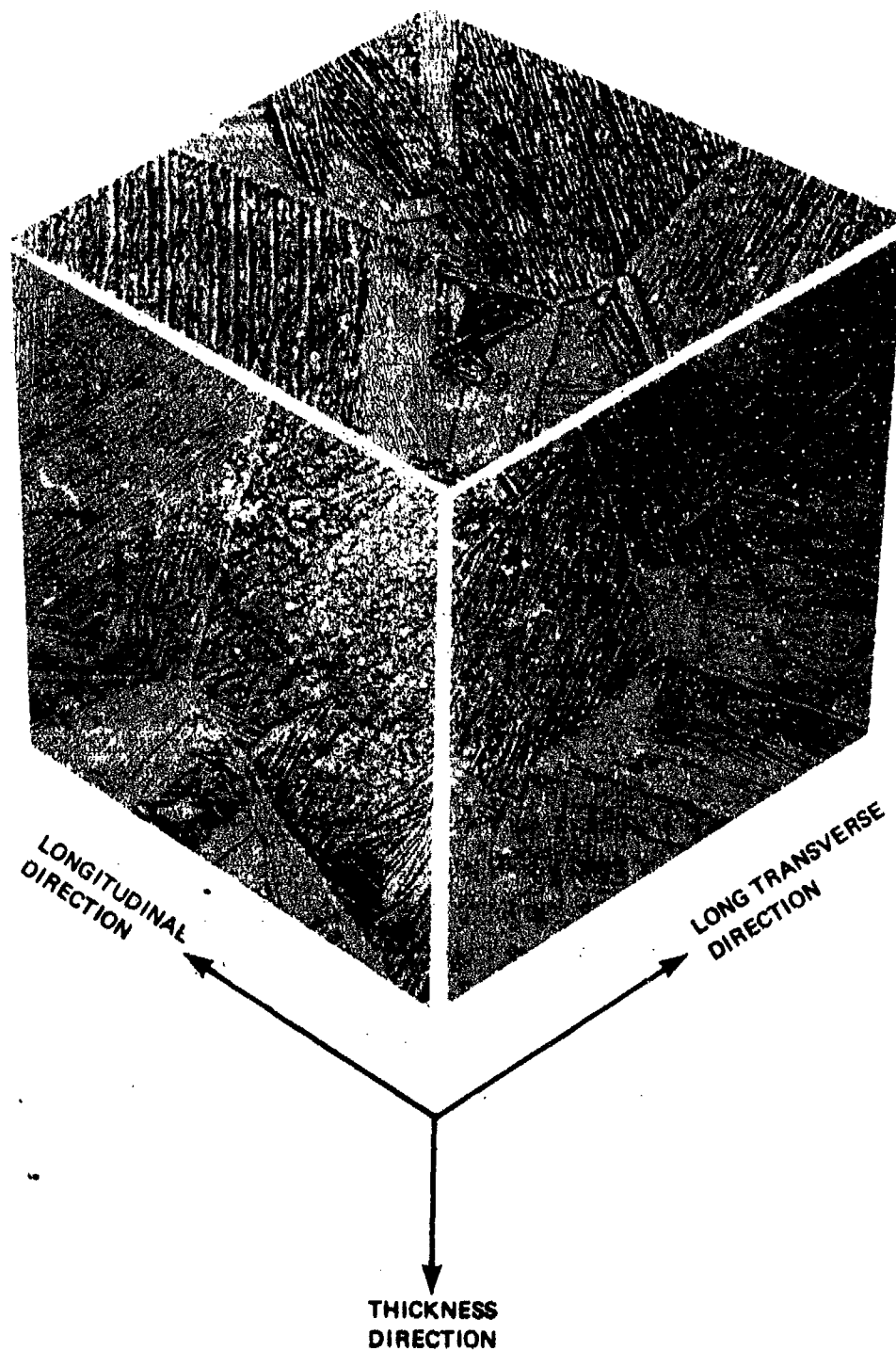
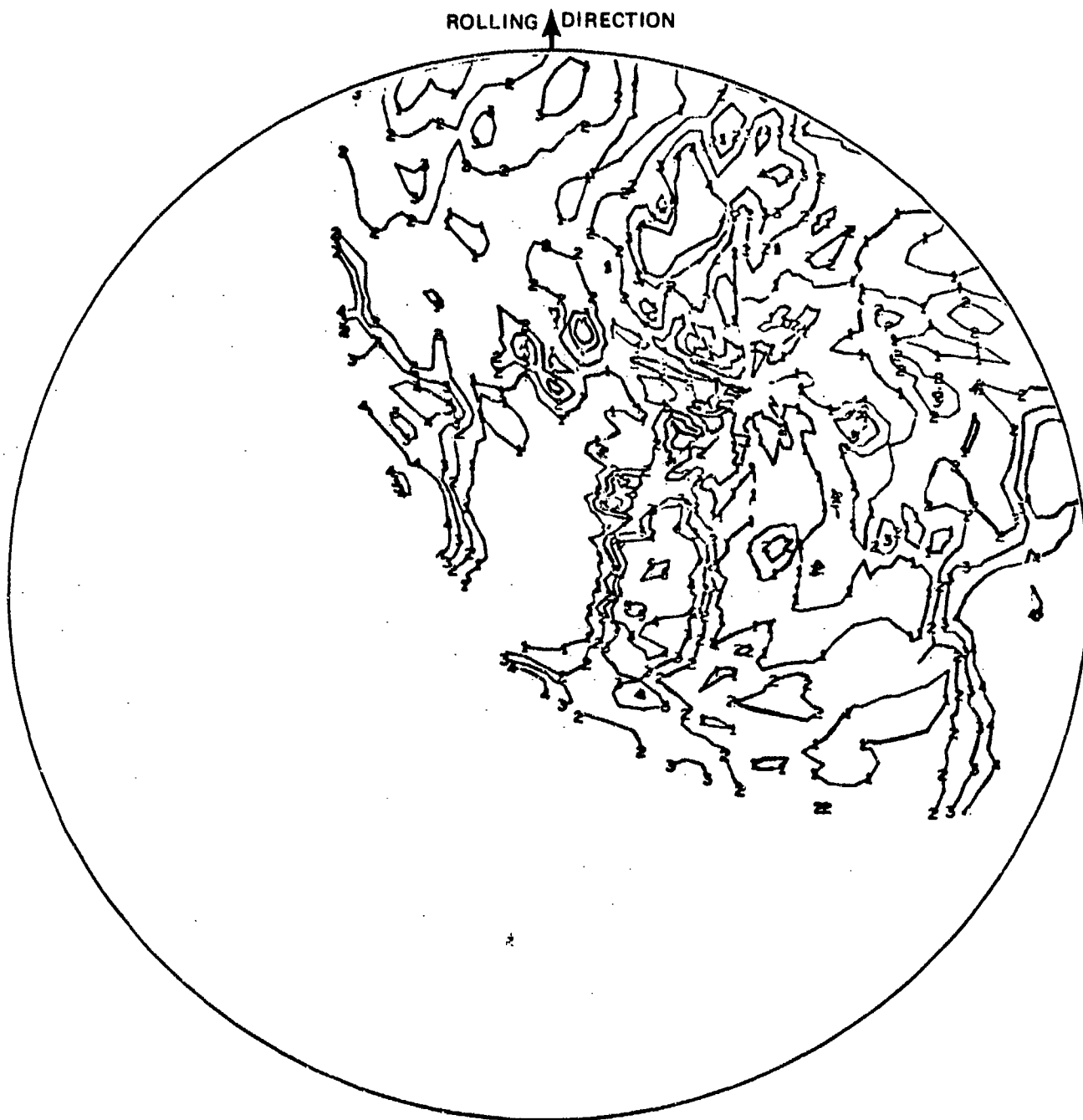


*Figure 8 : 6Al-4V "Super ELI" (O_2 Content = 0.06) Beta
Annealed Titanium Microstructure Composite (500X)*



CONTOUR LINES	1	2	3	4	5	6	7	8	9	0
TIMES RANDOM INTENSITY	0.5	1.0	1.5	2.0	4.0	8.0	14.0	20.0	25.0	30.0

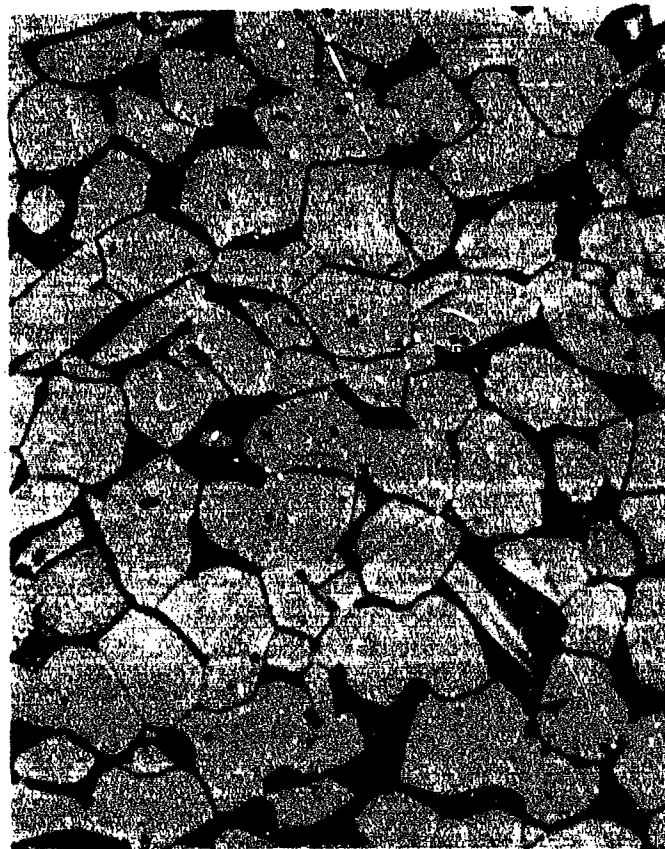
Figure 9: Pole Figures For 6Al-4V "Super ELI" (D_2 Content = 0.06) Beta Annealed Titanium Alloy-Basal Plane (0002) $_{\alpha}$

toughness criteria. The plate material was supplied to Boeing by North America Rockwell. The specification requirements include an ELI composition grade (0.13 wt. percent oxygen) and thermal processing near, but below the beta transus temperature to achieve a fully recrystallized alpha-beta microstructure. Both of these specification requirements provide improvements in the fracture characteristics compared to the conventional MIL-SPEC Ti-6Al-4V material. Following the RA processing, the material is annealed at 1400F and cooled relatively fast to 900F.

The plate composition as determined by the supplier and by Boeing is shown in Table 6. The Boeing analysis indicated a markedly lower oxygen content than that obtained by the supplier, TIMET. The plate microstructure, shown in Figure 10, was uniform and showed a high degree of alpha-beta recrystallization with equiaxed primary alpha grains in a retained beta matrix. The macrostructure revealed some variation in alpha grain size across the plate thickness. Basal plane pole figure (Figure 11) as determined by a computerized X-ray analysis technique indicated only moderate texturing with relatively balanced high intensity basal plane regions for both the transverse and longitudinal grain directions. The transverse direction, however, had a slightly higher intensity of basal planes (Table 7).

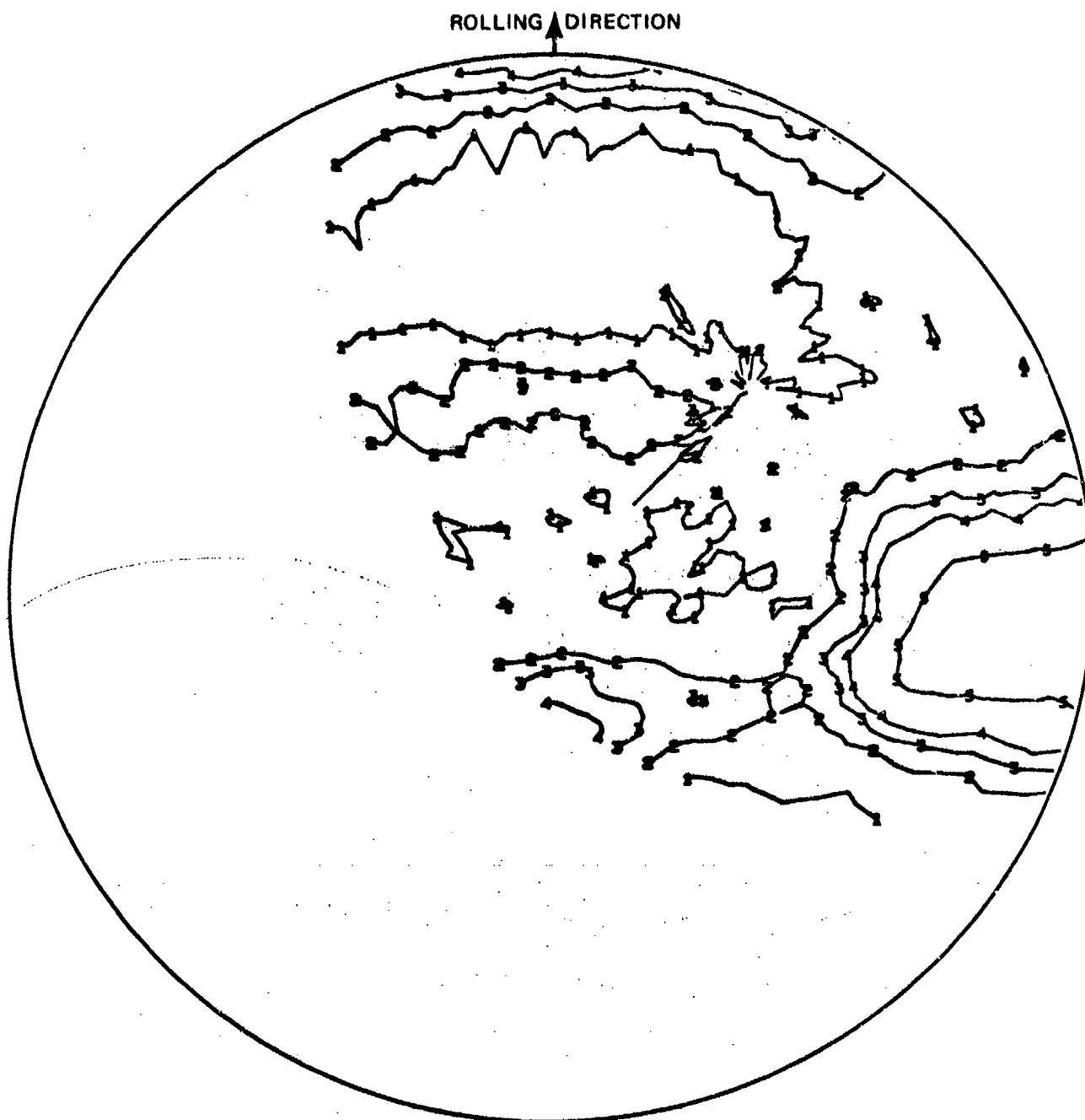
Mechanical properties were measured by The Boeing Company at temperatures of -65F, 72F and 175F. The resulting data are tabulated in Table A8 in Appendix A and are plotted against temperature in Figure 12. The 72F yield and ultimate strengths of 125 and 137 ksi exceed the specification minima of 120 and 130 ksi. The 72F elongation of 12 percent exceeds the specification requirement of 10 percent.

Fracture toughness values were measured using both compact tension and surface flawed specimens. The compact tension specimens were tested per ASTM E399-70T except for specimen thickness requirements; detailed results are tabulated in Table A9 in Appendix A and fracture toughness values are plotted against test temperature in Figure 3. The average 72F fracture toughness of $93 \text{ ksi}\sqrt{\text{in.}}$ is identical to that of the beta processed alloy and is well in excess of the specified minimum value of $75 \text{ ksi}\sqrt{\text{in.}}$ Six surface flawed specimens with crack



LONGITUDINAL VIEW

Figure 10: 6Al-4V Recrystallized Annealed Titanium Alloy Microstructure (500X)



CONTOUR LINES	1	2	3	4	5	6	7	8	9	0
TIMES RANDOM INTENSITY	0.5	1.0	1.5	2.0	4.0	8.0	14.0	20.0	25.0	30.0

Figure 11: Pole Figure For 6Al-4V Recrystallized Annealed Titanium Alloy – Basal Planes (0002)_c

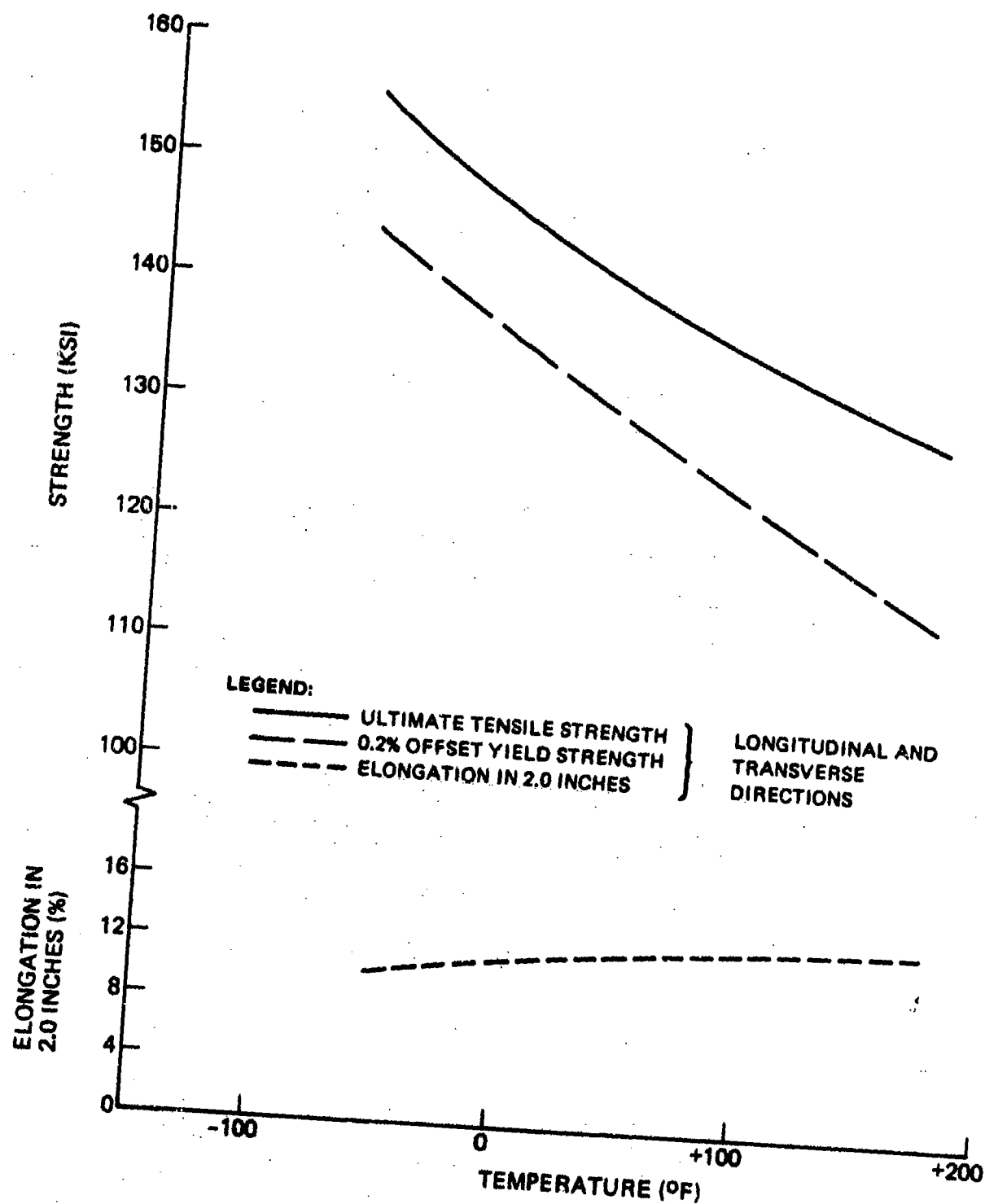


Figure 12: Mechanical Properties For 6Al-4V Recrystallized Annealed Titanium Alloy Plate (1.0-Inch Thick)

planes perpendicular to the long transverse plate direction were tested to evaluate fracture toughness for the WT direction at -65F, 72F and 175F. Test details and results are tabulated in Table A10 in Appendix A and fracture toughness values are summarized in Table 3 where they are compared to fracture toughness values obtained from the compact tension tests. Results are nearly identical to those for the Ti-6Al-4V beta annealed plate and again, the apparent trend of decreasing WT direction toughness with increasing temperature may have been influenced by the high failure stresses for the 175F tests.

2.1.5 Steel Alloy 9Ni-4Co-0.3C

The alloy steel, 9Ni-4Co-0.30C, was selected for evaluation since it is considered the leading candidate for aircraft applications in the 220-240 ksi strength range. The alloy is currently used in various primary structure applications as are similar alloys including D6AC and 4330V. The 9Ni-4Co alloy however has superior fracture toughness. The material for this study was purchased as annealed hot rolled plate per the Boeing specification BMS 7-182A. The plate size was 0.625 x 48 x 72 inches. The material was heat treated at Boeing to a strength range of 220-240 ksi using the following procedures:

- Normalize at 1650F, one hours, air cool
- Solution treat at 1550F, one hours, oil quench
- Refrigerate at -100F, two hours
- Double temper at 950F (2 + 2) hours, air cool.

The microstructure (Figure 13) is typical for the 9Ni-4Co-0.30 alloy. The macrostructure indicated evidence of banding (Figure 14). Microprobe analysis across the bands for Co, Ni and C showed no significant variation. Typical band thickness were approximately 0.0005 inch.

Delaminations were also observed on the fracture face of corrosion fatigue specimens used to test the WR direction. The average spacing of the delaminations was approximately 0.010 inch with the thicknesses ranging from 0.005 to 0.050 inch. Differences in microstructural features were not readily observable between the bands and adjacent regions even at magnifications of 1200X (Figure 15). The martensitic structure appeared to be slightly less predominant in the centers of the dark etching areas.

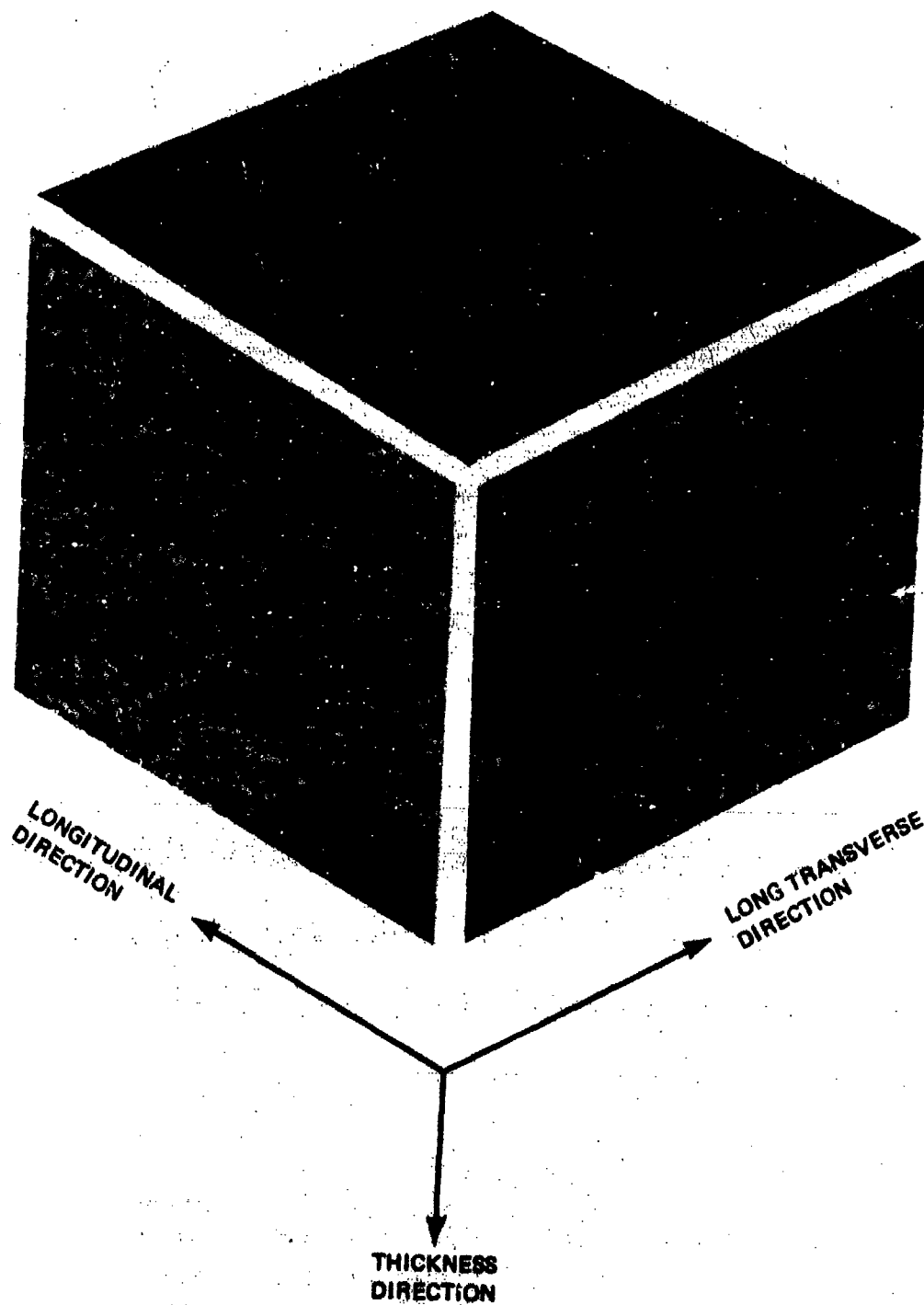


Figure 13: 9Ni-4Co-0.3C Steel Alloy Microstructure Composite (500X)

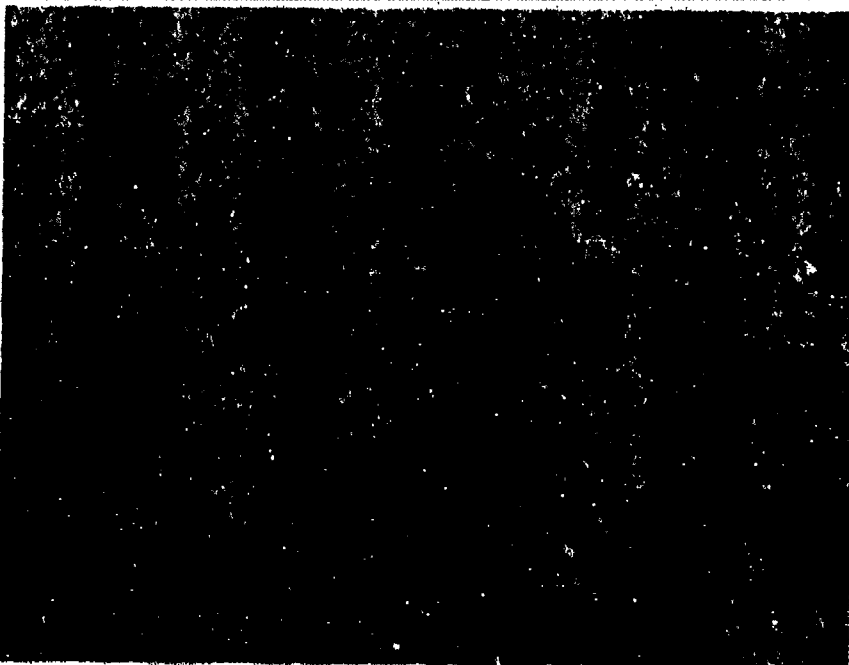
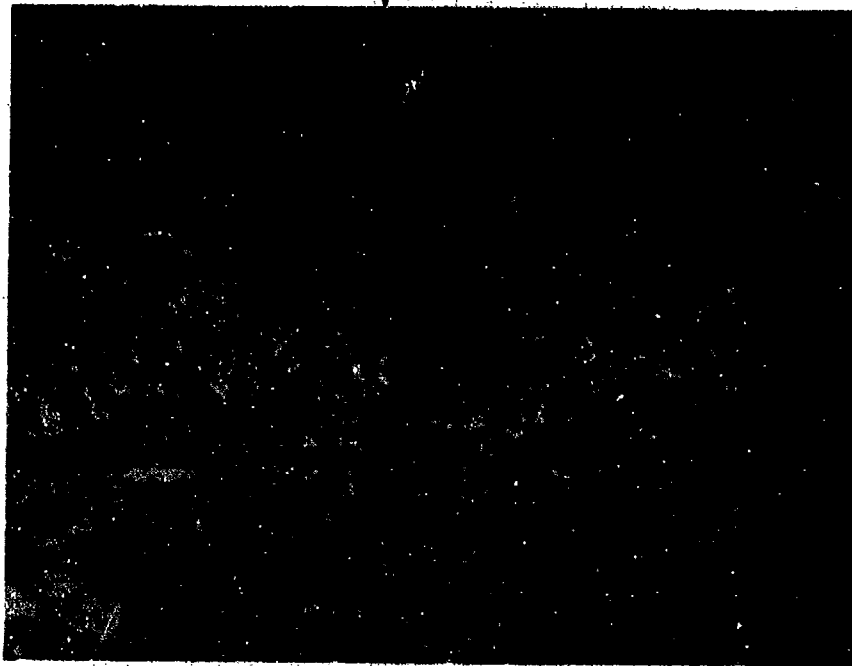


Figure 14: Banding in 9Ni-4Co-0.3C Steel Alloy (200X)



← BANDING

Figure 15: Banding in 9Ni-4Co-0.3C Steel Alloy at High Magnification, (1200X)

The alloy composition and specification limits are listed in Table 8. Except for the carbon content which was 0.34 wt %, the specification maximum, the plate composition was typical for the alloy. The inclusion content as determined per ASTM E-45 resulted in a D-2 rating which is considered relatively clean and typical of vacuum arc remelt steel.

The banding observed in the 9Ni-4Co-0.30C is not considered typical by the plate producer (Republic Steel) and was considered by Republic to be a hot working process problem. They considered the material to represent the "low end" with respect to other previous heats of the alloy. In previous limited experience at Boeing, deleterious banding in 9Ni-4Co alloys has not been observed.

Mechanical properties of the heat treated steel were measured at -65F, 72F and 175 by The Boeing Company. The resulting data are tabulated in Table A11 in Appendix A and mechanical properties are plotted against temperature in Figure 16. The 72F yield strengths of 204 to 209 ksi were within the desired yield strength range of 200-210 ksi. The corresponding ultimate strength values ranged from 240 to 245 ksi and exceeded the minimum specification value of 230 ksi.

Fracture toughness values were measured at -65F, 72F and 175F using compact tension, double cantilever beam, and surface flawed specimens. Compact tension specimens (Figure B2) were tested at -65F and 175F per ASTM E399-70T requirements. Double cantilever beam specimens (Figure B10) were tested at 72F per the ASTM requirements except for specimen length. The resulting data are tabulated in Table A12 in Appendix A and fracture toughness values are plotted against temperature in Figure 3. The 72F fracture toughness was $106 \text{ ksi}\sqrt{\text{in}}$. Six surface flawed specimens with crack planes perpendicular to the long transverse plate direction were tested to evaluate fracture toughness for the WT direction at -65F, 72F and 175F. Test details and results are tabulated in Table A13 in Appendix A, and fracture toughness values are summarized in Table 3 along with values obtained from the compact tension tests. The good agreement between all of the fracture toughness data is indicative of the homogeneity of the 9Ni-4Co-0.3C steel alloy plate.

Table 8: Chemical Composition of 9Ni-4Co-0.3C Steel (220-240 ksi)

HEAT LOT	TEST LAB	C	Mn	Si	P	S	Cr	Ni	Co	Mo	V	Fe
SPEC LIMITS		0.29 -0.34	0.10 -0.35	0.10 MAX	0.10 MAX	0.10 MAX	0.90 -1.10	7.00 -8.00	4.00 -5.00	0.90 -1.10	0.06 -0.12	BAL
		0.34	0.27	0.01	.004	.007	1.06	7.50	4.5	1.04	0.09	BAL
3830071	REPUBLIC											
	BOEING		0.28	0.05			1.0	7.6	4.7	1.0	0.10	

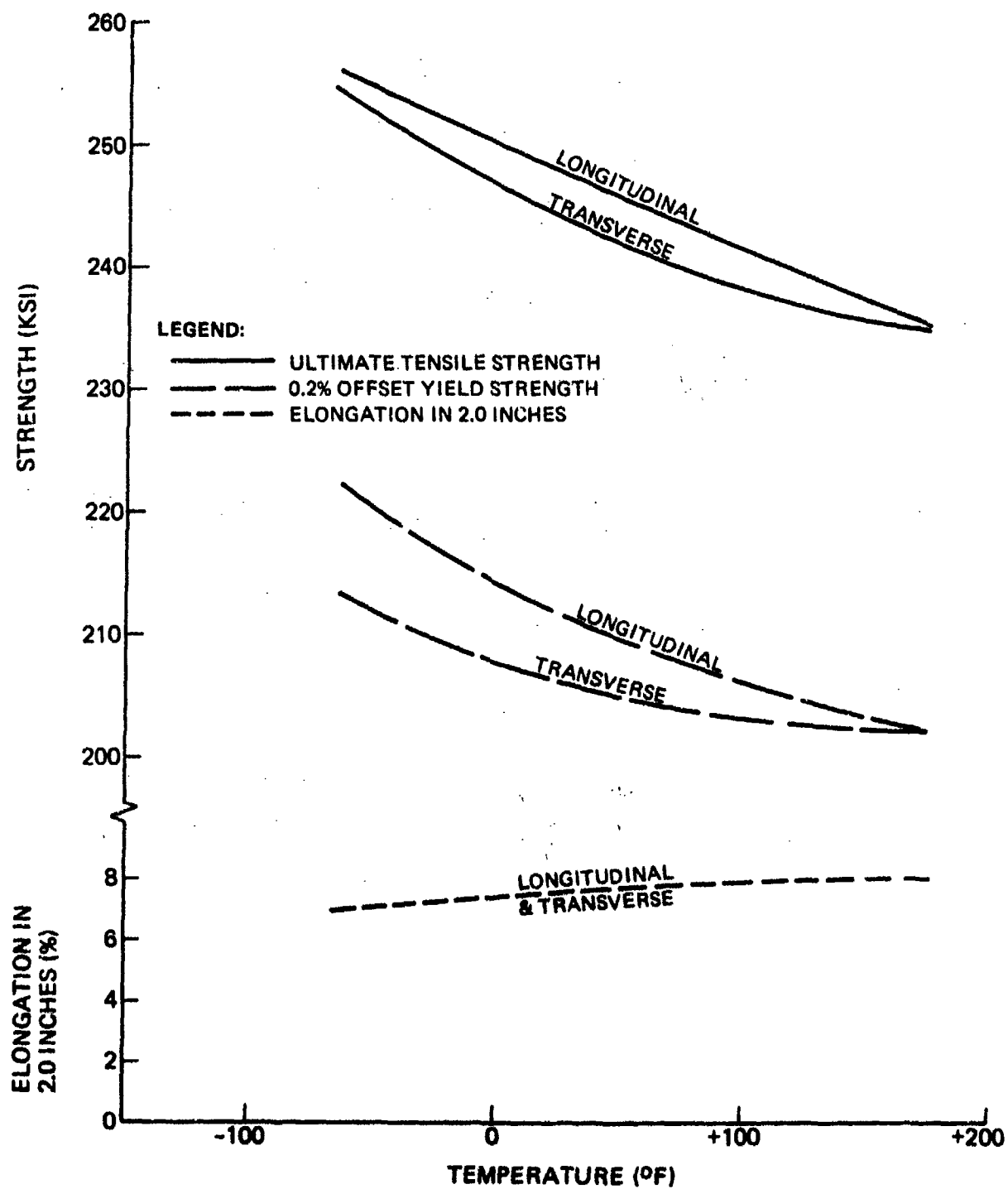


Figure 16: Mechanical Properties for 9Ni-4Co-0.3C Steel Alloy Plate (0.625-Inch Thick)

2.2 Selection of Environments

Stress corrosion cracking and corrosion fatigue tests were conducted in seven different environments as shown in Table 1. Five primary environments included desiccated air having a relative humidity of about 10 percent, distilled water, 3.5% NaCl solution, water saturated JP-4 fuel, and sump tank water. Two secondary environments included alternating JP-4 fuel and distilled water, and dye penetrant (type ZL-2A). The desiccated air was selected as a realistic reference environment. There was no intention of selecting a completely inert reference environment for the program since one of the primary objectives was to develop useable data. Distilled water was selected to determine the results of moisture and water on crack growth behavior in the absence of salts. The 3.5% NaCl solution was thought to be representative of the worst environments to which airframe components could be frequently exposed. Other investigators have concluded that 3.5% NaCl solution is an overly severe representative of the "worst" environment and have recommended sump tank water as an alternative test environment. Sump tank water is representative of solutions that are found in sump areas of aircraft and has the chemical content shown in Table 9. Since sump tank water has a smaller chloride ion content than does 3.5% NaCl solution, it should be less aggressive in promoting crack growth in titanium alloys. Since all of the materials tested could come in contact with JP-4 fuel, the fuel environment was selected as a primary test environment. Distilled water was added to the JP-4 fuel to saturate the fuel to the limit of approximately 50 ppm of water. Tests conducted in alternating JP-4 fuel and distilled water were representative of the environmental mix encountered in a "wet" wing. Finally, tests were conducted in dye penetrant after it was observed in previous work (2) that type ZL-2A dye penetrant promoted considerable stress corrosion cracking in Ti-4Al-2.5Sn (ELI) base metal and weld metal. Hence, the question arose as to whether poor inspection practice could have detrimental effects on aircraft components. Type ZL-2A dye penetrant was tested because of its applicability to the three alloy systems tested in this program.

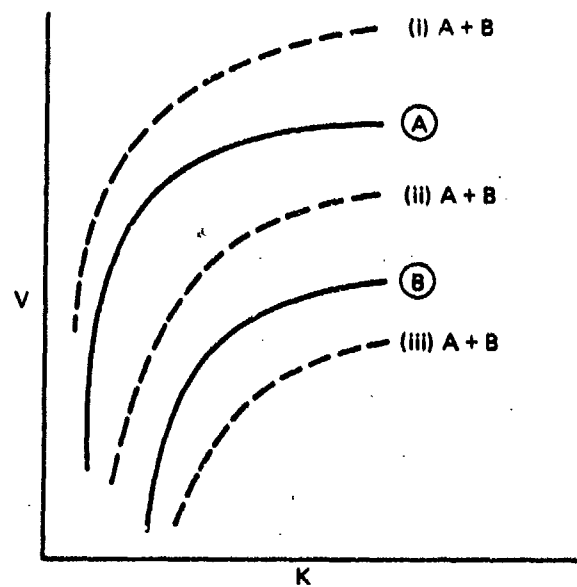
An attempt was made to identify environmental spectra that could be particularly detrimental to crack growth characteristics of airframe metal alloys. In particular, consideration was given to potential synergistic effects resulting from the concurrent action of two or more environments. There are a multitude of

Table 9: Chemical Content of Simulated Sump Tank Residue Water

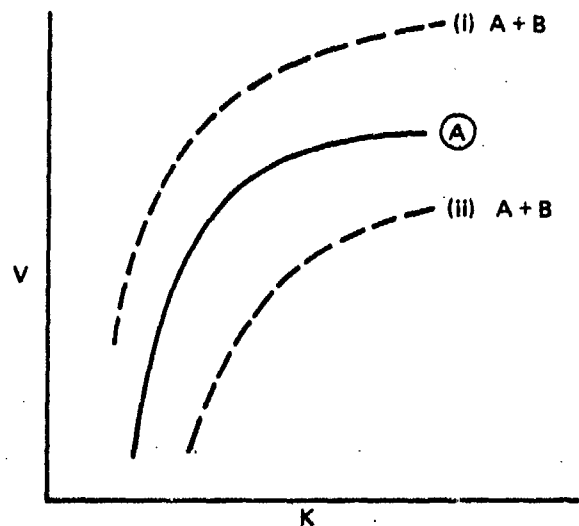
CONSTITUENT	CONCENTRATION (PPM)
CaCl_2	50
CdCl_2	1000
MgCl_2	50
NaCl	100
ZnCl_2	10
PbCl_2	1
$\text{CuCl}_3 \cdot 2\text{H}_2\text{O}$	1
$\text{CrCl}_3 \cdot 6\text{H}_2\text{O}$	1
FeCl_3	5
$\text{MnCl}_2 \cdot 4\text{H}_2\text{O}$	5
$\text{NiCl}_2 \cdot 6\text{H}_2\text{O}$	1
DISTILLED WATER	BAL

different operational fluids and manufacturing aids with which aircraft components can come in contact. However, no success was met in identifying particular combinations that would be expected to have a synergistic effect. Synergistic effects are not particularly common in subcritical crack growth tests and, in many cases, are difficult to define. For example, three cases observed in stress corrosion cracking tests are shown in Figure 17.

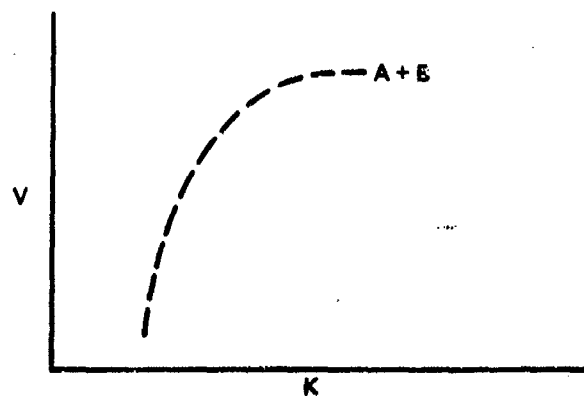
1. Alloy susceptible to SCC in both environments A and B; when the two environments are mixed, there are three possibilities.
 - a. Mixture produces more rapid crack propagation and possibly reduces K_{Isc} ; for example, $H_2O - CH_3OH - Cl^-$ on some titanium alloys.
 - b. Mixture produces intermediate crack growth rates and possibly increases K_{Isc} ; for example, H_2O -glycerine- Cl^- on some titanium alloys.
 - c. Mixture reduces crack growth rates and possibly varies K_{Isc} ; for example, H_2O -methylene chloride mixtures on some titanium alloys.
2. Alloy susceptible in only environment A: when B is added, there are two possibilities:
 - a. Mixture produces more rapid crack growth and possibly lowers K_{Isc} ; for example, H_2O -methanol mixtures on the aluminum alloy 7075-T651. (see Figure 18)
 - b. Mixture produces lower crack growth rates; for example, H_2O -methanol mixtures in the aluminum alloy 7075-T651 (see Figure 18) and H_2O -hydrogen mixtures on titanium alloys.
3. Alloy not susceptible in either component A or B but susceptible in mixture, possible examples:
 - a. Chemical reaction of components to produce damaging environment, e.g., hydrogen and oxygen to produce water inducing susceptibility of aluminum alloys.



(a): Both A & B Produce SCC



(b): Only Environment A Produces SCC



(c): Neither Environment Produces SCC

Figure 17: Schematic Representation of Possible Effect of Mixing Environments A & B on Stress Corrosion Properties of an Alloy

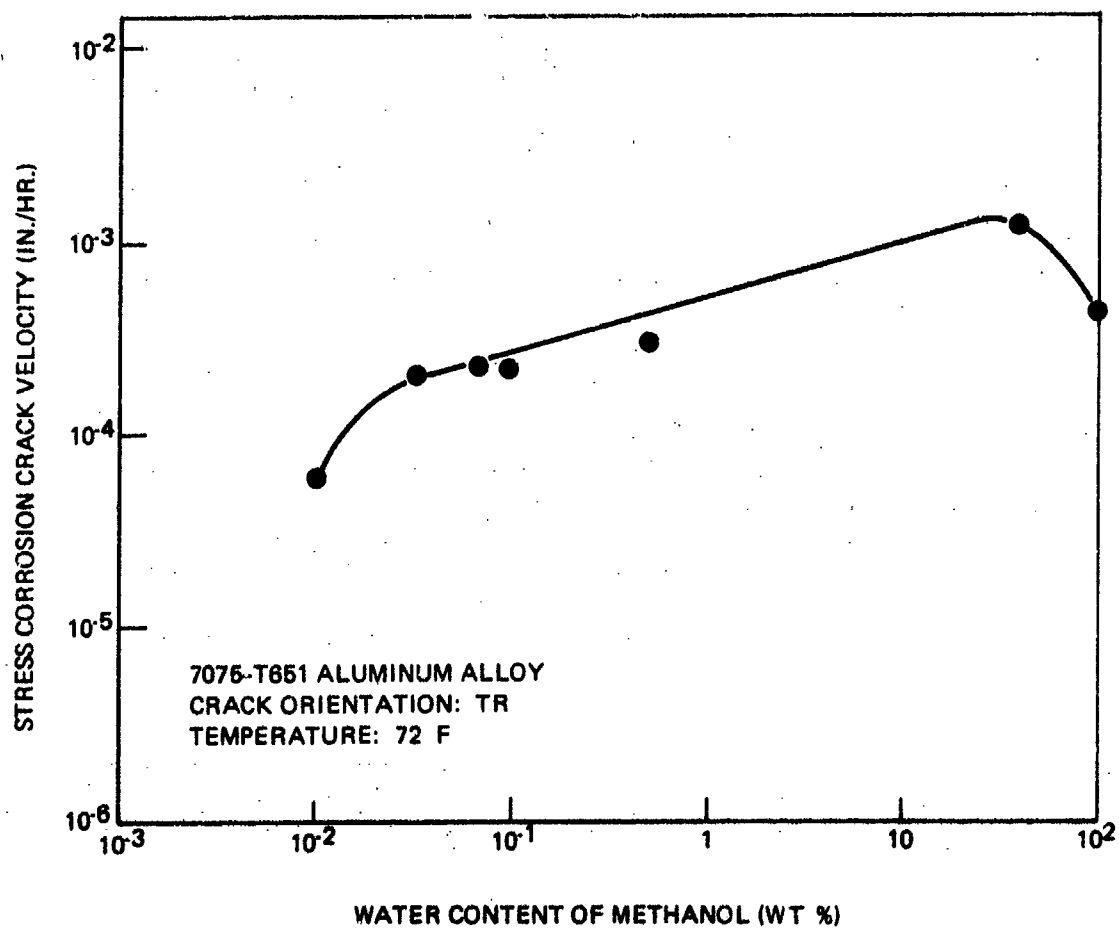


Figure 18: Velocity of Stress Corrosion Cracks in a High-Strength Aluminum Alloy as a Function of Water Content in Methanol

When the additional variable of composition, i.e., amount of A and B is introduced such as in the case of MeOH-H₂O mixture on 7075, one could conclude that both synergistic and retardation effects occur. For 7079 aluminum alloy, no synergistic effect is observed and thus, the extension of a result for one alloy to all alloys is also doubtful.

Rather than search for synergistic phenomena, it was decided to look at the effect of a corrosion inhibitive compound on crack growth behavior for several material/environment couples. The intent was to investigate whether or not corrosion inhibitive compounds had any beneficial effects on crack growth resistance at existing cracks. If such were the case, then such compounds could be useful in protecting inaccessible areas of airframe structure and as a temporary corrective action. The specific corrosion inhibitive compound used in these tests was LPS-3.

2.3 Procedures

Procedures used for specimen preparation, handling, testing, and evaluation of results are described in this section.

2.3.1 Specimen Preparation

Thirteen different specimen configurations were used to accomplish the tests reported herein. Specimen configurations are detailed in Figures B1 through B13 in Appendix B. A summary of specimen configurations used for each type of test is included in Table B1 in Appendix B.

Mechanical property tests were conducted using one smooth tensile specimen configuration as shown in Figure B1.

Static fracture toughness tests were conducted using compact tension (CT) and surface-flawed (SF) specimens. Specimen configurations for all CT specimens are included in Figure B2. Specimen configuration for aluminum alloy SF specimens is detailed in Figure B3; similar titanium and steel alloy specimens are shown in Figure B4.

Stress corrosion cracking tests were performed using double cantilever beam (DCB) and SF specimens. DCB specimen configurations are included in Figures B5 through B7. Specimens detailed in Figure B5 were used for testing the short transverse direction of the plate materials. Specimens in Figures B6 and B7 were used for testing either the WR or RW crack propagation directions. SF specimen configurations are detailed in Figures B3, B4, B8 and B9.

Corrosion fatigue tests were conducted using both DCB and SF specimens. Most tests were conducted using the DCB specimens. Grooves were vee shaped with a 60° included angle, 0.01 inch root radius, and depth equal to ten percent of the specimen thickness. SF specimen configurations are shown in Figures B3 and B4.

Overload tests were performed using tapered double cantilever beam specimens having the configurations shown in Figures B12 and B13. Specimens were linearly tapered to approximate the contour defined by the equation.

$$3 a^2/h^3 + 1/h = 4.0$$

where: a is crack length

h is one-half specimen height at the cross section through the crack tip.

The above equation defines the approximate contour required to make stress intensity factors independent of crack length for constant load (3). Since the equation is approximate and deviates only slightly from a straight line, a linear taper was used to fabricate the tapered double cantilever beam specimens. Compliance measurements on the linearly tapered specimens verified that stress intensity factor was independent of crack length within experimental accuracy. Results of compliance measurements for the tapered double cantilever beam specimens are summarized in Appendix C.

Crack starters in all CT and DCB specimens consisted of a 0.125 inch wide milled slot terminating in a chevron Vee notch. Precracking was accomplished using fatigue loadings having a stress ratio of 0.06 and a cyclic frequency of 1800

cpm. The 0.10 inch of precrack was grown using peak cyclic stress intensity to Young's modulus ratios less than $0.0012 \sqrt{\text{inch}}$. Crack starters in SF specimens were produced using an electrical discharge machine and 0.06 inch thick circular electrodes; electrode tips were machined to a radius of 0.003 inch and an included angle of less than 20 degrees. Fatigue cracks were grown from the starter slots using a stress ratio of 0.06, cyclic frequency of 1800 cpm, and peak cyclic stress of 10 ksi for the aluminum alloy specimens, and 25-30 ksi for the steel and titanium alloy specimens.

All specimens were cleaned by brushing with commercial grade naptha. Each specimen was then sealed in a plastic bag until tested.

2.3.2 Testing

Test procedures used for fracture toughness, stress corrosion cracking, corrosion fatigue, and overload tests are described in the following.

Fracture Toughness

All compact tensions tests were conducted per the ASTM method of tests for plane strain fracture toughness of metallic materials (E399-70T). Surface-flawed specimens were loaded to failure in standard tensile test machines at a rate required to precipitate failure in about one minute. All specimens were instrumented with clip gages spring loaded against knife edges integrally machined at the mouth of the flaw. The clip gage and load cell of the test machine were connected to an X-Y recorder to obtain records of load versus crack opening displacement for each specimen.

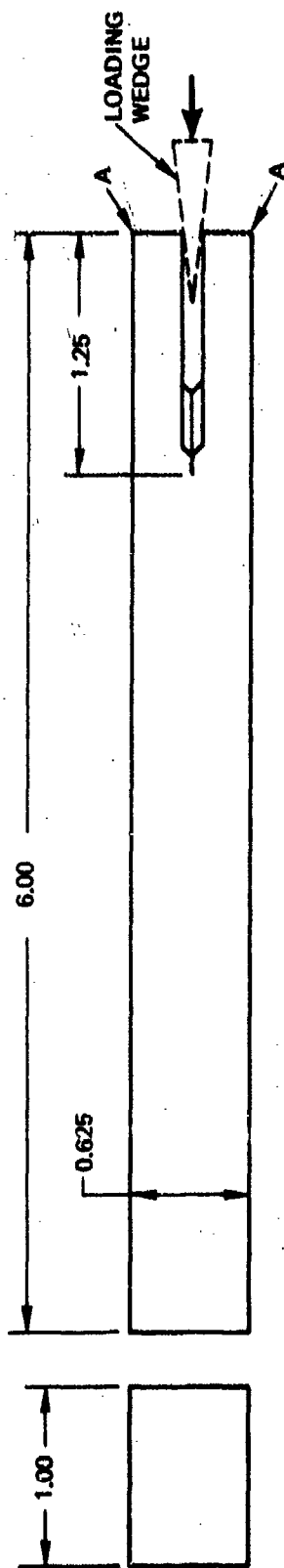
Temperature control was accomplished as follows. Tests at 72F were conducted within an enclosed environmentally controlled laboratory. Tests at -65F were conducted in a mixture of cold nitrogen gas and air, the temperature of which was controlled by a servo valve actuated by a thermocouple attached to the specimen. Tests at +175F were conducted with the specimen surrounded by a metallic jacket with heaters attached. Heaters and temperature were controlled by thermocouples attached to the specimen. All temperatures were controlled to within $\pm 2F$ of the nominal values.

Stress Corrosion Cracking

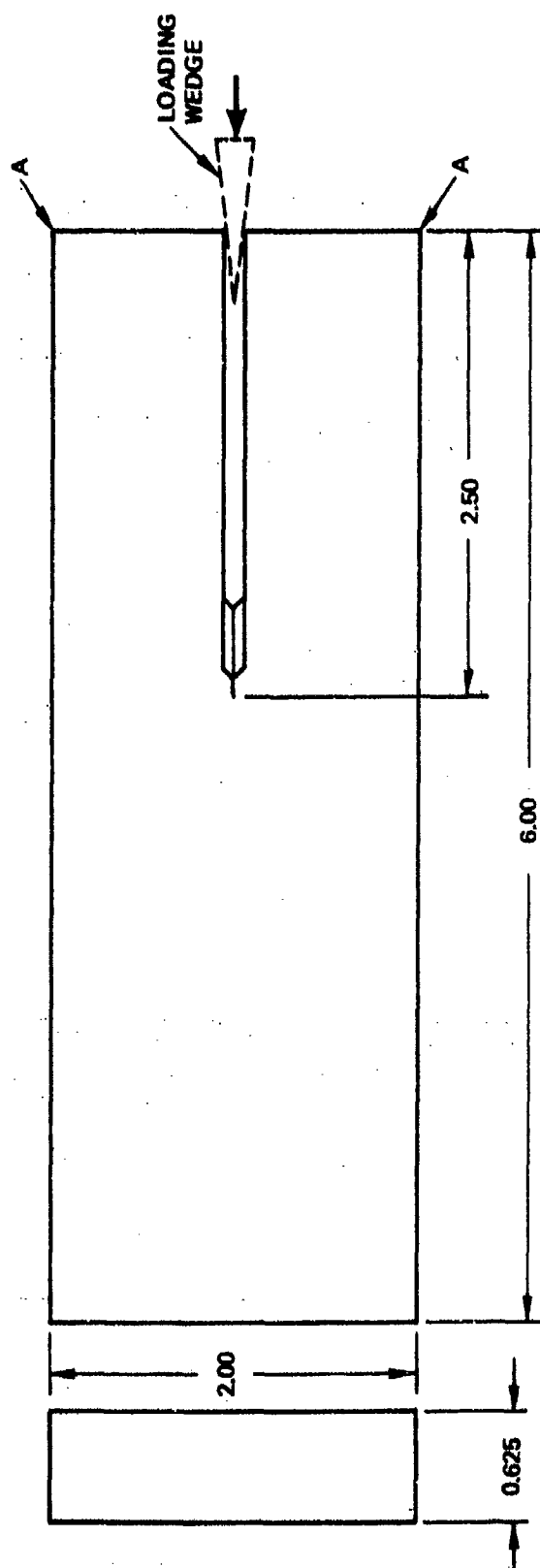
Stress corrosion cracking tests were conducted by subjecting DCB specimens to constant opening mode deflections at the mouth of the crack. All aluminum and steel alloy specimens, and titanium alloy short transverse specimens were loaded by driving a wedge into the end of the crack starter slot as illustrated in Figure 19. The crack tip was submerged in the test medium during the loading operations and the wedge was inserted until a small amount of crack extension occurred. Specimens were then placed in sealed glass containers filled with the test media. Periodic recording of crack length were taken by observing the specimens under a 30X microscope. Titanium alloy specimens used to test the WR crack propagation direction were loaded in a slightly different manner. With reference to Figure 20, specimens were pin loaded in a test machine with the crack tip submerged in the test medium. A clip gage was used to monitor crack opening displacement during the loading process. After the desired displacement was attained, a pair of circular wedges were inserted into the central hole to wedge open the crack. The load was then reduced by 1000 pounds and the wedges were driven in further to recover the crack displacement lost due to elastic deformations in the vicinity of the wedges. This incremental unloading procedure was repeated two or three times after which the applied load was reduced to zero and a final crack surface displacement reading was taken. The specimens were then transferred to enclosed test chambers filled with the test media. Periodic readings of crack length were made throughout each test.

Corrosion Fatigue

Corrosion fatigue tests were conducted by subjecting specimens to either constant load or constant deflection cycling. Tests designed to yield crack growth rates for intermediate and high ΔK values were conducted by subjecting specimens to constant peak cyclic loadings to grow the cracks over a series of predetermined increments of crack length in the required test media. The first increment of crack growth was induced using a constant peak cyclic load slightly greater than the load used to precrack the specimen. The peak cyclic load was then increased by 100 lb for the aluminum alloys and 500 lb for the steel and titanium alloys, and a second increment of crack growth was induced. This procedure was repeated until the stress intensity factor was at or near the critical value. Crack growth increments required to grow the cracks from initial to critical conditions



(a) Specimen for TR Tests



(b) Specimen for RW and WR Tests

Figure 19: SCC Test Specimens for 7075-T651 Aluminum and 9Ni-4Co-0.3C Steel Alloys

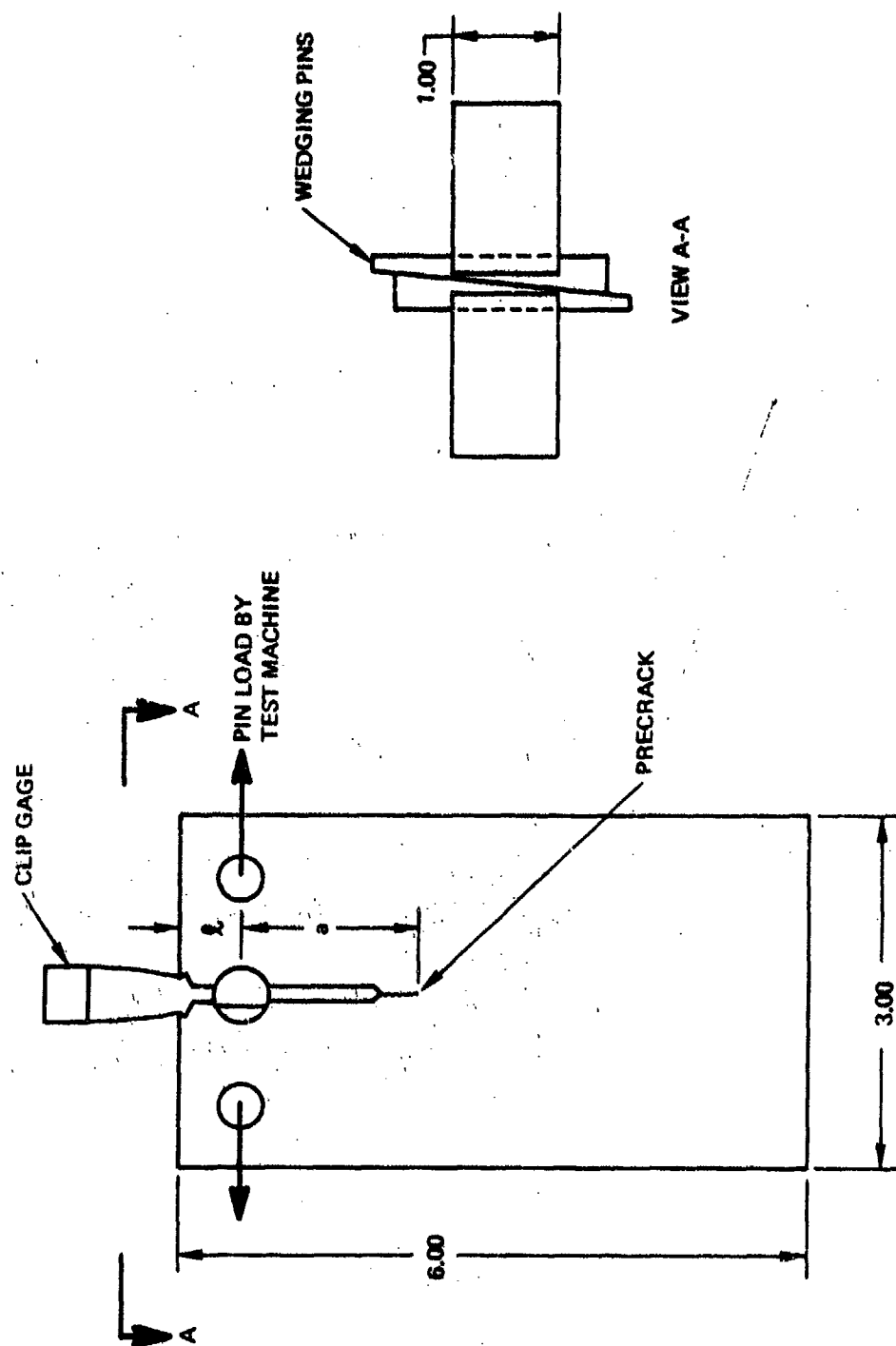


Figure 20: SCC Test Specimen and Loading Method for 6Al-4V Titanium Alloys

ranged from five to seven. The increments of crack growth could generally be identified on the fracture surface of the specimen and the known locations of the crack front after each crack growth increment provided a check of the instrumentation output used to evaluate crack growth rates.

Corrosion fatigue tests for the lower ΔK values were conducted by subjecting specimens to constant deflection loadings. The initial load was set equal to the load used to precrack the specimens. The load cell and clip gage were parts of a servo system that kept the peak cyclic crack displacement constant during the remainder of the test. Consequently, the cracks grew under gradually decreasing ΔK values until the test was terminated. The load decreased smoothly throughout each test and incremental load adjustments were not used. For alloy/environment couples where crack growth rate data obtained from both constant load and constant deflection tests overlapped, agreement between the data was good. For example, see Figure A19 in Appendix A.

All corrosion fatigue and fracture toughness specimens were instrumented with clip gages to obtain recordings of opening mode crack displacement versus cycles. Clip gages were spring loaded against integrally machined knife edges at the mouth of the crack starter. Knife edge details and locations are shown in Figure B10 in Appendix B. Gage output was recorded periodically to obtain relationships between specimen compliance and loading cycles.

2.3.3 Evaluation of Results

Static fracture toughness values were calculated from CT specimen results using ASTM recommended procedures (E399-70T). Fracture toughness values were calculated from DCB specimen results using ASTM recommended procedures for CT specimens with the exception that stress intensity factors were calculated using the following equation:

$$K_I = \frac{2P}{b} \left[\frac{b}{b_n} \right]^{1/2} \left[\frac{3(a + 0.6h)^2 + h^2}{(1 - \mu^2) h^3} \right]^{1/2} \quad (1)$$

where P is 5 percent secant offset load

" b is specimen width

b_n is crack width
 h is one-half the specimen height
 E is Young's modulus
 a is crack length
 μ is Poisson's ratio

Fracture toughness values for SF specimen tests were calculated using the equation

$$K_I = \sigma \sqrt{\pi a / Q} M_K \quad (2)$$

where σ is gross section failure stress

a is the crack depth

Q is the modified shape factor shown in Figure 21

M_K is shown in Figure 22 (Reference 4).

Stress corrosion cracking results were evaluated by plotting increase in crack length versus test duration using intermittent readings of crack length versus time. The slopes of the resultant curves were taken as the SCC velocities. Corresponding stress intensity factors were determined using the measured crack opening displacements at the end of the specimen. For specimens loaded as shown in Figure 19, deflections were measured between the outer corners of the test specimen designated by the letter A in Figure 19. For specimens loaded as shown in Figure 20, deflections measured with the clip gage were multiplied by the ratio of $a/(a + 1)$ to determine the displacement at the load line. Stress intensity factors were calculated by substituting measured displacements (δ) into the equation

$$K_I = \frac{\delta E h [3h(a + 0.6h)^2 + h^3]^{1/2}}{\sqrt{1 - \mu^2} 4 [(a + 0.6h)^3 h^2 a]} \left[\frac{b}{b_n} \right]^{1/2} \quad (3)$$

where the symbols represent the same measurements as in Equation 1.

Crack growth rates for corrosion fatigue tests were determined using crack displacement versus cycles records. Crack displacements were measured at

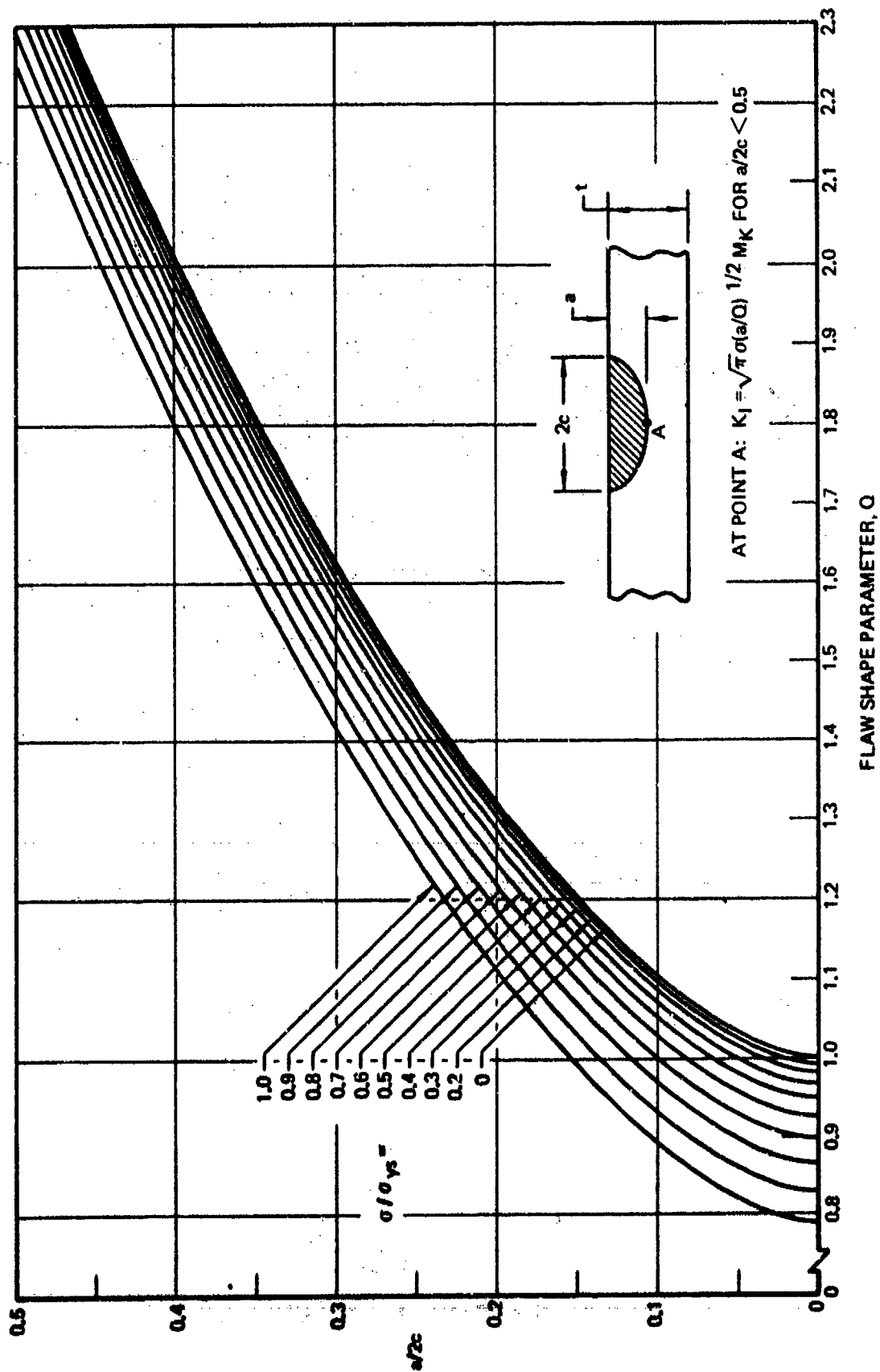


Figure 21: Shape Parameter Curves for Surface and Internal Flaws

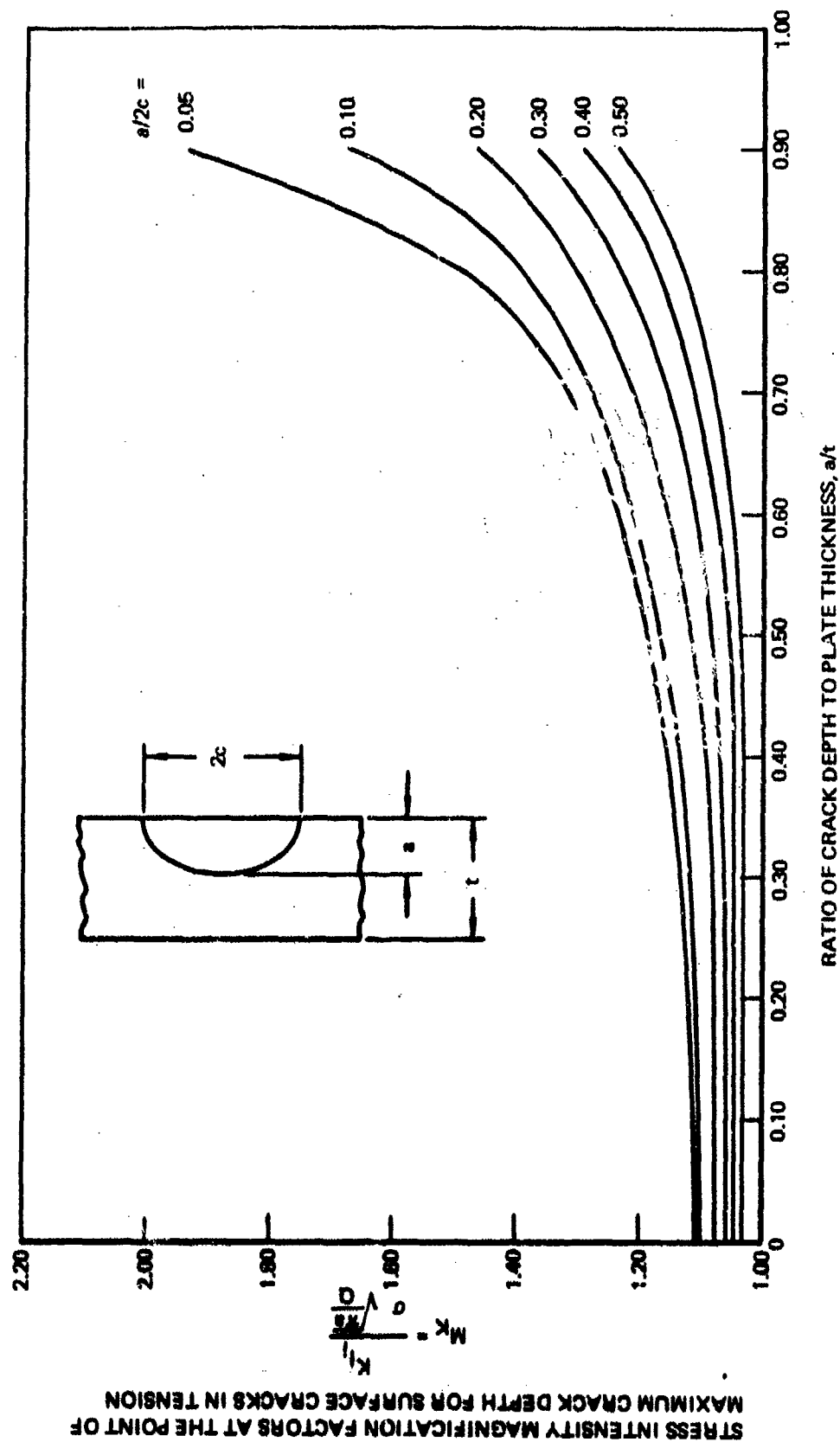


Figure 22: Estimated Elastic Stress Intensity Magnification Factors at Maximum Crack Depth for Surface Cracks in Tension (Reference 4)

predetermined cyclic intervals and corresponding compliance values were determined by dividing the measured displacements by the applied load. Crack lengths corresponding to the individual compliance values were determined from previously measured compliance/crack length calibrations. Increments of crack length were divided by the corresponding number of loading cycles to determine average crack growth rates over the cyclic intervals. Stress intensity factors at the beginning and end of each cyclic interval were averaged to determine the stress intensity factor against which average crack growth rates were plotted. Stress intensity factors for uniform height DCB specimens were calculated using either Equations 1 or 3. Stress intensity factors for tapered double cantilever beam specimens were calculated using the equation

$$K_I = \frac{P}{\sqrt{2b_n}} \cdot \left[\frac{E}{(1 - \mu^2)} \right]^{1/2} \cdot \sqrt{\partial c / \partial a} \quad (4)$$

where P is applied load

b_n is crack width

c is specimen compliance

a is crack length

Specimen compliance was measured experimentally and results are reported in Appendix C.

2.3.4 Comments on Procedures

A considerable amount of experience was obtained in applying the DCB specimen testing procedures used in this program. In light of this experience, the following evaluation of the procedures is made.

The data resulting from the DCB specimen tests was very consistent and repeatable. Hence, it is believed that the procedures were more than adequate for generating the type of corrosion fatigue data contained in this report. Some of the key features of the procedures were: (1) no periodic visual measurements of crack length were made; (2) the load was incrementally increased throughout each test; (3) side grooves were used to restrict the growing crack to its original plane.

The need for intermittent visual measurements of crack length was circumvented by periodically increasing the applied load after predetermined increments of crack growth. This procedure left marks on the fracture surface which periodically established the location of the crack front. Hence, a recurrent check of instrumentation output was available throughout each test. Comparisons between actual and calculated crack length based on the initial compliance tests never yielded differences greater than 0.03 inch. However, since each specimen was individually calibrated the actual location of the crack front was always known with accuracy much greater than 0.03 inch. Total crack length was used only to calculate stress intensity factor and was not used in crack growth rate calculations. Since total crack lengths varied from 1 to 3 inches, the accuracy of crack length determinations in these tests was more than adequate.

The amount of crack growth generated under constant test conditions influences the accuracy of crack growth rate calculations. In these tests, cracks were grown in 0.30 inch increments under constant test conditions. Increments of this size were required to yield readily interpretable test records, i.e. records having sufficient change in compliance to establish the proper curvature of the crack deflection versus cycles record. Smaller increments of crack growth would have required increased sensitivity for the strip chart recorders and would have taxed the accuracy of normal recording equipment. Hence, the size of increments in which the crack is grown has to be tailored to the available test equipment.

The use of side grooves to restrict the growing cracks to the original crack plane is believed to be an acceptable procedure as long as the groove depth is not an excessively large percentage of the specimen thickness. In these tests, groove depth was 10% of the specimen thickness. The resulting crack growth rates compared very well with large DCB specimens in which side grooves were not used and so it was concluded that 10 per cent deep grooves did not have a significant effect on crack growth rate behavior. The authors are not aware of any systematic study of the effects of side grooves on crack growth rate behavior.

Side grooving of DCB specimens has both advantages and disadvantages. The main advantage is that smaller specimens can be tested without encountering crack

rotation problems. Without grooves, the height of the specimen arms must be increased until the ratio of bending stress to applied load is sufficiently low to preclude crack rotation. This approach leads to larger specimens and test load capacities. One disadvantage of side grooves is that they made visual measurements of crack length very difficult. A second disadvantage is that systematic studies of the effects of side groove on fatigue crack growth rates are lacking. If side grooves deeper than about 10 per cent of the specimen thickness are required, the grooves could have influences on crack growth rate that cannot be accounted for using existing knowledge.

3.0 RESULTS AND DISCUSSION

Results of stress corrosion cracking and corrosion fatigue tests for each of the four major alloys are presented and discussed in separate sections. The effects of test environment, cycle frequency, and specimen type on results are treated individually for each alloy. A combined presentation of overload and stress ratio effects is included in the last two subsections. Test results for the 7475-T651 aluminum alloy are included in Section 4.1 along with the 7075-T651 aluminum alloy results. Results for the super ELI Ti-6Al-4V beta annealed plate are included in Section 4.2 along with results for the standard ELI Ti-6Al-4V beta annealed plate. Results of the thermal processing effect tests on Ti-6Al-4V recrystallized annealed alloy are included in Section 4.3.2.4.

3.1 Aluminum Alloy Test Results

The test program for 7075-T651 aluminum alloy plate is summarized in Table 10. Mechanical property and fracture toughness tests were conducted for both the longitudinal (RW) and long transverse (WR) directions. Stress corrosion cracking tests were conducted for the short transverse (TR), RW and WR crack propagation directions. Corrosion fatigue and overload tests were conducted for only the WR crack propagation direction. Results of mechanical property and fracture toughness tests were previously described in Section 2.1. Results of the stress corrosion cracking and corrosion fatigue tests are described in the following subsections 3.1.1 through 3.1.3

Two stress corrosion cracking (SCC) and four corrosion fatigue (CF) tests were conducted for 7475-T651 aluminum alloy plate. One SCC test was conducted in each of two environments of 3.5% NaCl solution and desiccated air; CF tests were performed in both 3.5% NaCl solution and desiccated air. Results are described and compared to comparable 7075-T651 results in Section 3.1.4.

3.1.1 Stress Corrosion Cracking Tests

Stress corrosion cracking tests were conducted in distilled water, 3.5% NaCl solution, and water-saturated JP-4 fuel. Three series of tests were undertaken.

Table 10: Test Program for 7075-T651 Aluminum

TEST TYPE	SPECIMEN TYPE	CYCLIC FREQUENCY	STRESS RATIO	ENVIRONMENT																				
				AIR			DISTILLED WATER			3.5% NaCl SOLUTION			JP-4			SUMP TANK			JP-4 + H ₂ O			DYE PEN		
				-65F	72F	175F	-65F	72F	175F	-65F	72F	175F	-65F	72F	175F	-65F	72F	175F	-65F	72F	175F			
MECHANICAL PROPERTY	TENS.			4	4	4																		
FRACT JRE TOUGHNESS	CT			2	4	2																		
	SF			2	2	2																		
STRESS CORROSION CRACKING	DCB			2			4			4						2				4		4		
	SF			1						1										1		1		
CORROSION FATIGUE	DCB	60	0.1	2	2	2	1			1			1			2			1	2		2		
			0.5	2	2	2	2	1		2	1		2	1		2	2		2	1		2		
			0.8	1						1			1											
CORROSION FATIGUE	DCB	6	0.1	1			1			1			1						1					
			0.5	2			2			2			2						2			2		
OVERLOAD	SF	60	0.5	2						2			2											
	TDCB	60	0.5	2																				

The first series involved tests for the RW, WR, and TR crack propagation directions using wedge loaded double cantilever beam specimens. For each of the RW and WR directions, two specimens were tested; one specimen was loaded with the crack tip submerged in the test medium, and the second specimen was loaded in laboratory air. For the TR direction, all specimens were loaded with the crack tip submerged in the test medium. No SCC was observed for either of the RW or WR directions. In the TR (short transverse) direction, SCC was observed in all three test media. Periodic measurements of crack length were used to obtain the SCC velocity vs. stress intensity factor (v - K) data plotted in Figure 23. The trend of the v - K data indicate the existence of a threshold stress intensity factor below which SCC would not occur. The authors are not aware of any data verifying the existence of a threshold stress intensity factor in aluminum alloys. Crack growth rates become very slow at K levels approaching the apparent threshold value and tests of very long duration would be required to explore crack growth behavior at very low K values. In this program, tests were terminated after nine months when the surface of the specimens became too corroded to permit further crack length readings.

A considerable amount of corrosion product buildup between the crack faces of the TR/3.5% NaCl DCB specimen was observed. After the surface of the specimen became too corroded to allow further crack length measurements, the wedge used to load the specimen was removed and the opening mode deflection at the end of the specimen was measured both before and after the removal of the wedge. The removal of the wedge results in only a slight relaxation of the crack surface displacement. This result indicates that the corrosion products were exerting a wedging action between the crack surfaces after the removal of the wedge. It is not possible to quantitatively assess the effect of corrosion product buildup on stress intensity factors at the crack tip during the nine month test duration. The possibility exists that actual stress intensity factors during the latter stages of the tests were higher than the calculated values due to corrosion product wedging action. Effects of corrosion product buildup have been previously observed during tests of aluminum alloy DCB specimens in 3.5% NaCl solution. The effect of wedging action on crack displacement at the ends of 7075-T651 aluminum alloy DCB specimens has been investigated⁽⁵⁾ by measuring the deflections on a number of specimens that were tested for up to a year. The

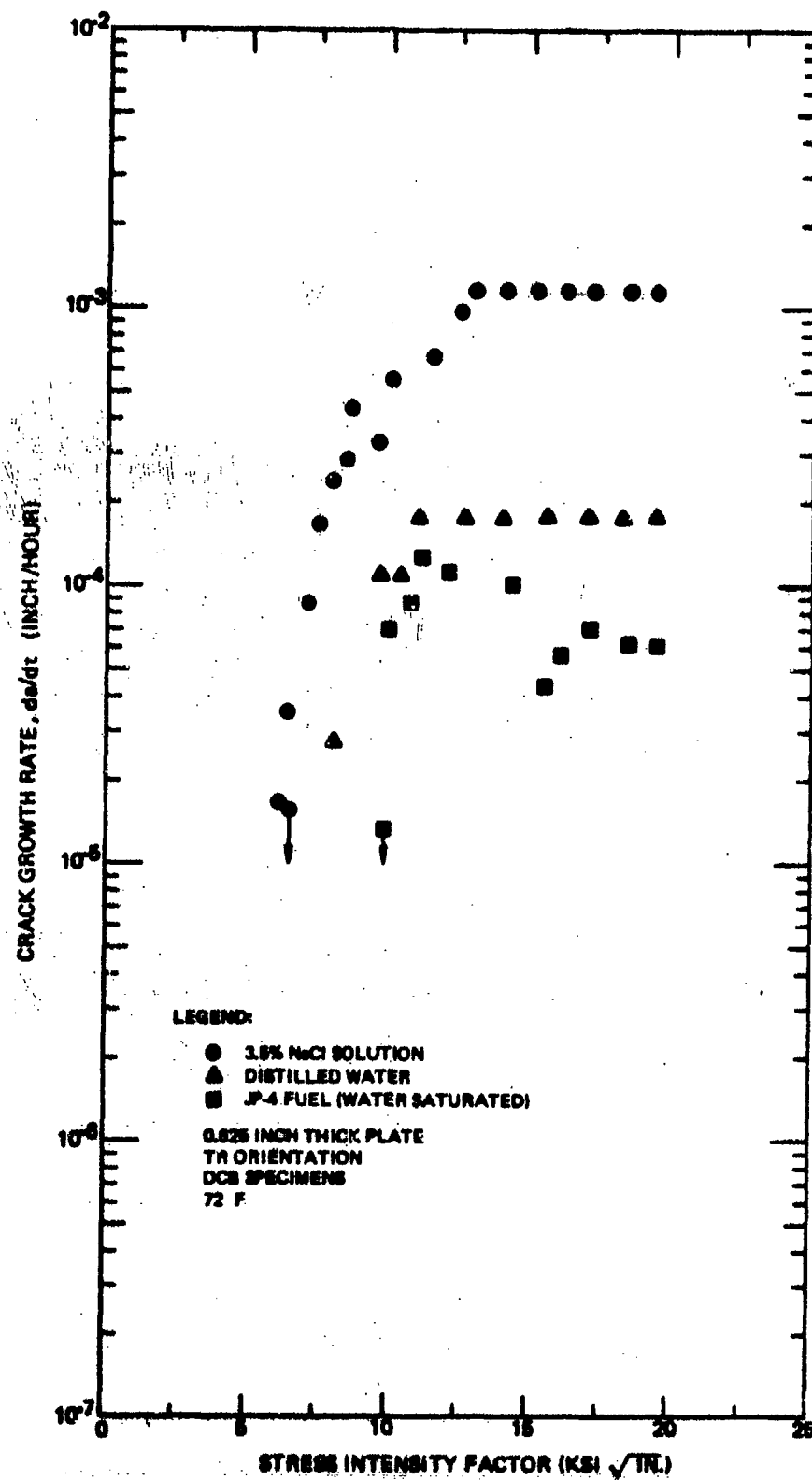


Figure 23: Stress Corrosion Cracking Velocity Data for 7075-T651 Aluminum Alloy

changes in deflection ranged from zero to +0.006 in. In one specimen tested for more than a year, the deflection increased by 0.015 inch. Hence, corrosion products do result in a wedging action that can increase crack opening displacement, hence, stress intensity factor.

A second series of tests was conducted for the TR crack propagation direction after the DCB specimens were wedge loaded with the crack tip submerged in the corrosion inhibitive compound LPS-3, then immediately placed in the test medium. Results are plotted in terms of crack length versus test duration in Figure 24. After a modest initial delay in SCC growth rate, cracking proceeded at rates comparable to those obtained from the initial series of test where LPS-3 was not used.

A third series of tests was conducted for the TR crack propagation direction after specimens were loaded with the crack tip submerged in LPS-3, dried for three hours, then immersed in the test medium. Increases in crack length versus test duration are plotted in Figure 25. In distilled water, crack growth initiated immediately upon contact with the test medium and proceeded at rates that were slightly less than the plateau velocity for distilled water in Figure 23. In 3.5% NaCl solution, 40 hours elapsed between immersion of the specimen and initiation of crack growth; cracking then proceeded at rates slightly less than the plateau velocity for 3.5% NaCl solution in Figure 23.

A sustained load test of a surface-flawed specimen was discontinued after 1100 hours of exposure to a 3.5% NaCl solution. The semi-minor axis of the flaw coincided with the WT crack propagation direction. The specimen was loaded in the test environment to generate a stress intensity factor at the crack tip of $28 \text{ ksi} \sqrt{\text{in}}$ (about 90% of K_{IC}). As illustrated in Figure 26, the fracture surface revealed that considerable splitting had taken place in the short transverse planes all around the periphery of the flaw. It appeared that SCC occurred in the WR direction along the individual laminates formed by the splitting. The corresponding average growth rate is 5×10^{-5} inches/hour. Depthwise growth was prevented by splits. A second essentially identical specimen was loaded to the same peak stress level as used in the SCC test and was then immediately unloaded, fatigue marked, and failed. The loading process induced about 0.005

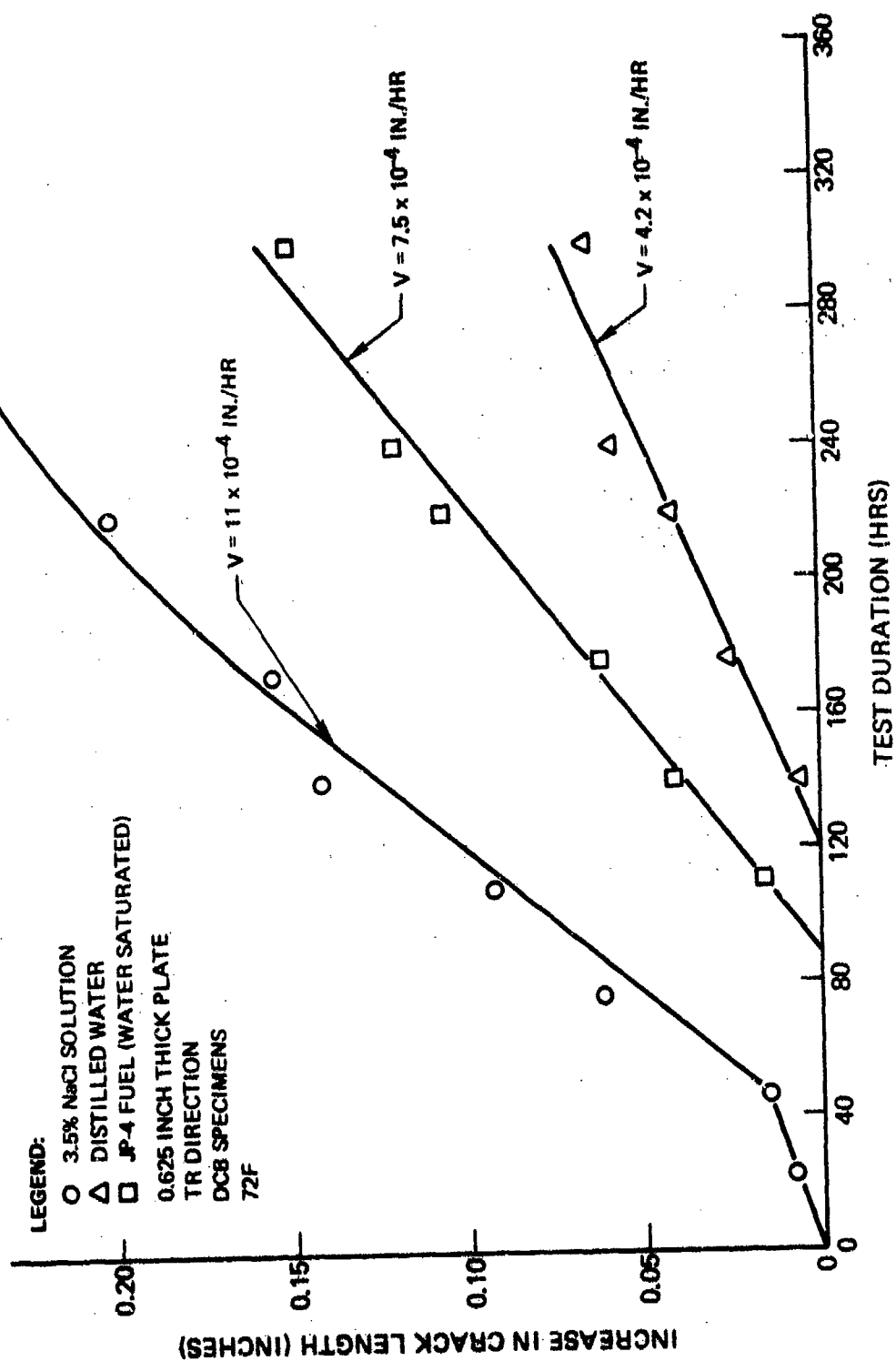


Figure 24: SCC Test Results for 7075-T651 Aluminum Alloy, Crack Surface Wet With LPS-3 Prior to Immersion in Test Medium

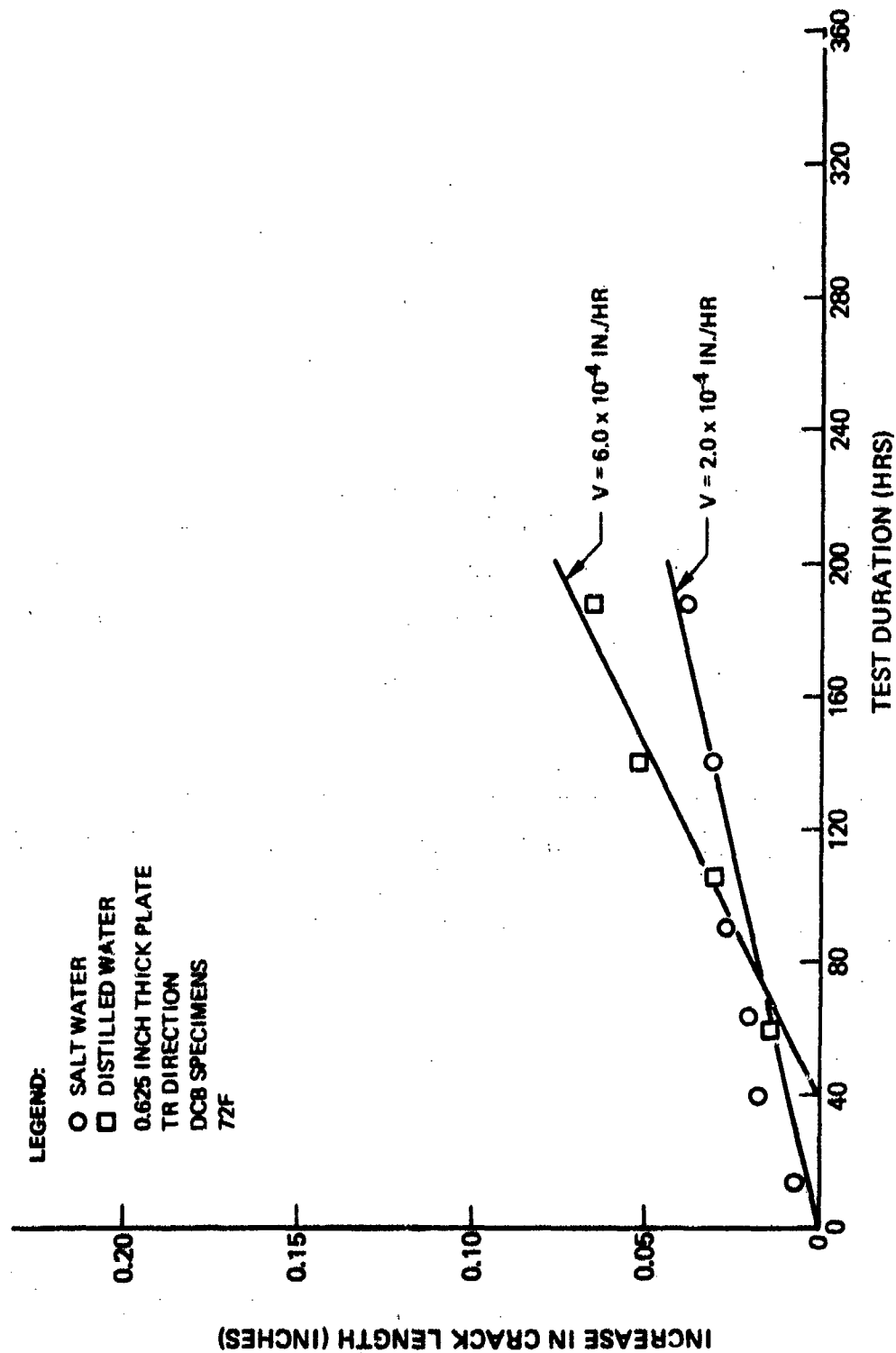
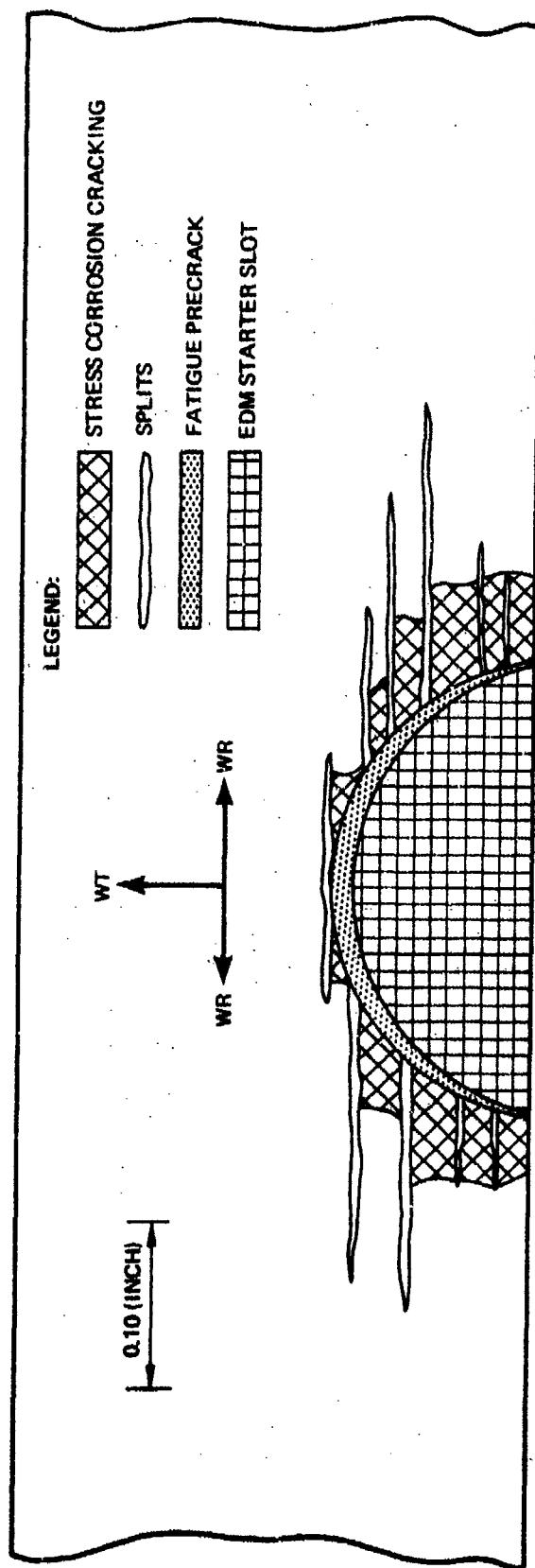


Figure 25: SCC Test Results for 7075-T651 Aluminum Alloy, Crack Surface Sprayed With LPS-3 and Dried for 3.0 Hours Prior to Immersion in Test Medium



APPLIED STRESS = 60 KSI
TEST DURATION = 1103 HRS

Figure 26: Illustration of Fracture Face From 7075-T651 Aluminum Alloy Surface Flow Specimen SCC Test in 3.5% NaCl Solution

inches of growth observed in the SCC test was due to SCC rather than pop-in or stable tear that occurred during the loading process.

The foregoing results indicate a difference between SCC test results obtained from DCB and SF specimens. In the DCB specimen tests, no SCC was observed for the WR direction at stress intensity factor values as high as $25 \text{ ksi}\sqrt{\text{in}}$. In the SF tests, SCC occurred in the WR direction at an estimated stress intensity factor of $16 \text{ ksi}\sqrt{\text{in}}$.

3.1.2 Corrosion Fatigue Tests

Variables involved in the corrosion fatigue tests were environment, cyclic frequency, specimen type, and stress ratio. The effects of environment, frequency, and specimen type on fatigue crack propagation behavior are described below. Stress ratio effects are described in Section 4.6.

All data collected from corrosion fatigue tests of the 7075-T651 aluminum alloy are included in Figures A1 through A15 in Appendix A. Only a limited amount of actual data are used in the body of the report. Rather, the effects of test variables are illustrated using average curves drawn through the data.

3.1.2.1 Effect of Test Environment

Test Media

Average crack growth rate curves for the five principal test media at 72F are summarized in Figures 27, 28 and 29. For all conditions tested, desiccated air and/or water saturated JP-4 fuel yielded the slowest crack growth rates at any given ΔK value; 3.5% NaCl solution and/or sump tanks water yielded the highest crack growth rates; distilled water yielded intermediate crack growth rates. At both 6 and 60 cpm, the maximum difference between the slowest and fastest crack growth rates at given ΔK values was about a factor of four. Hence, the effect of test media on fatigue crack growth behavior of 7075-T651 aluminum alloy plate was significant, but not sufficiently large to create unmanageable problems in the operation of airframe components manufactured therefrom.

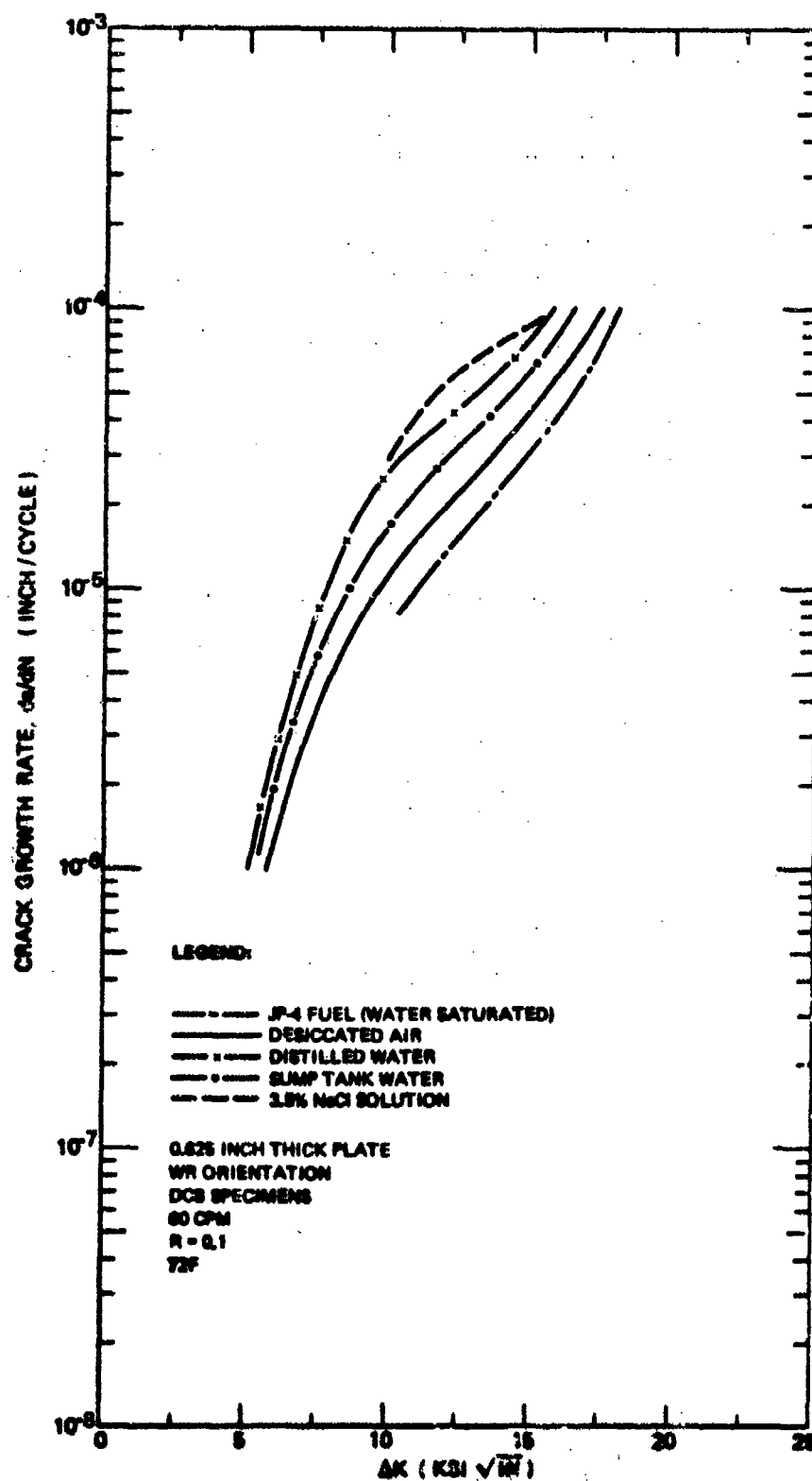


Figure 27: Effect of Environment on Fatigue Crack Growth Rates at $R=0.1$ in 7075-T651 Aluminum Alloy (60 CPM)

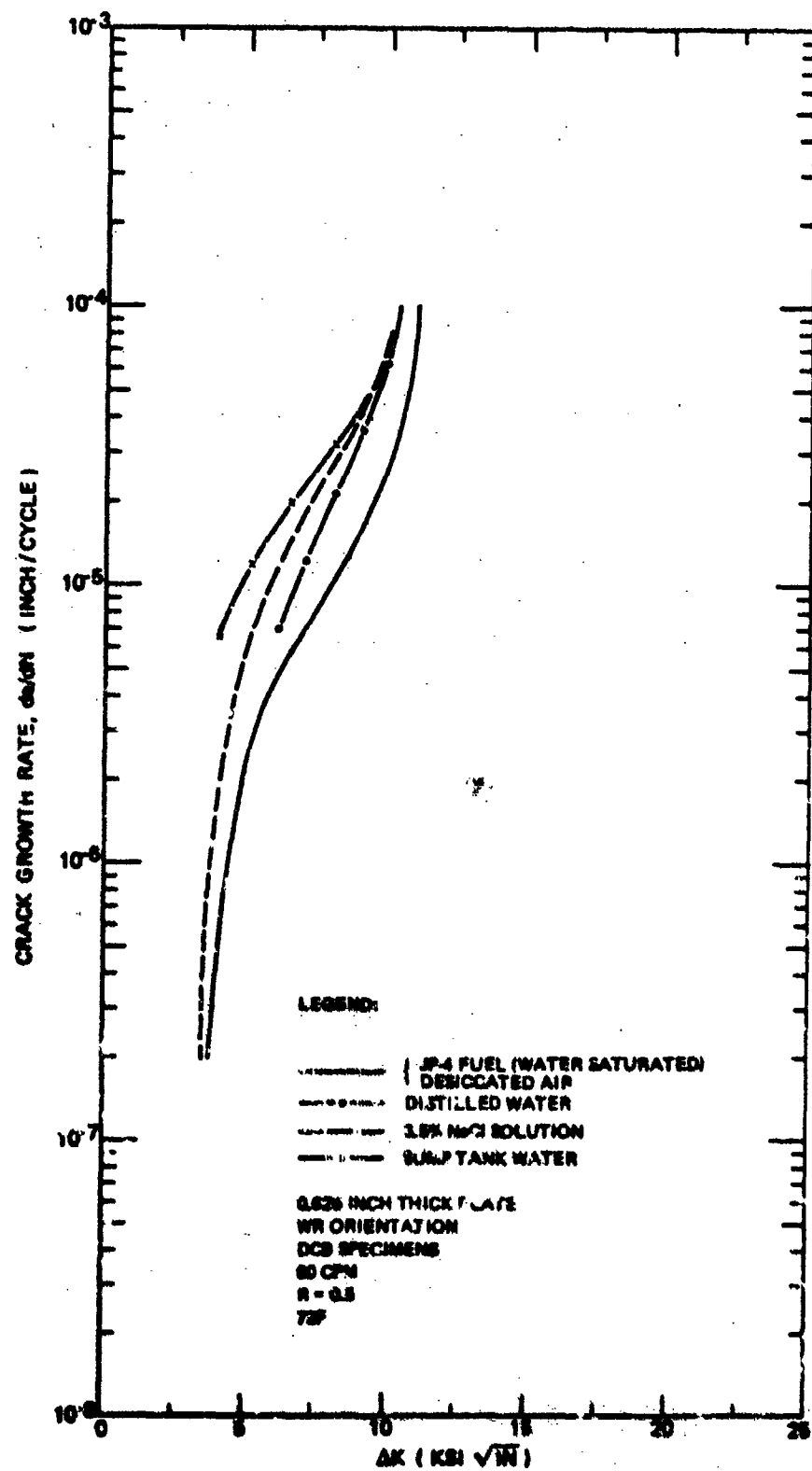


Figure 28: Effect of Environment on Fatigue Crack Growth Rates at $R=0.5$ in 7075-T651 Aluminum Alloy (60 CPM)

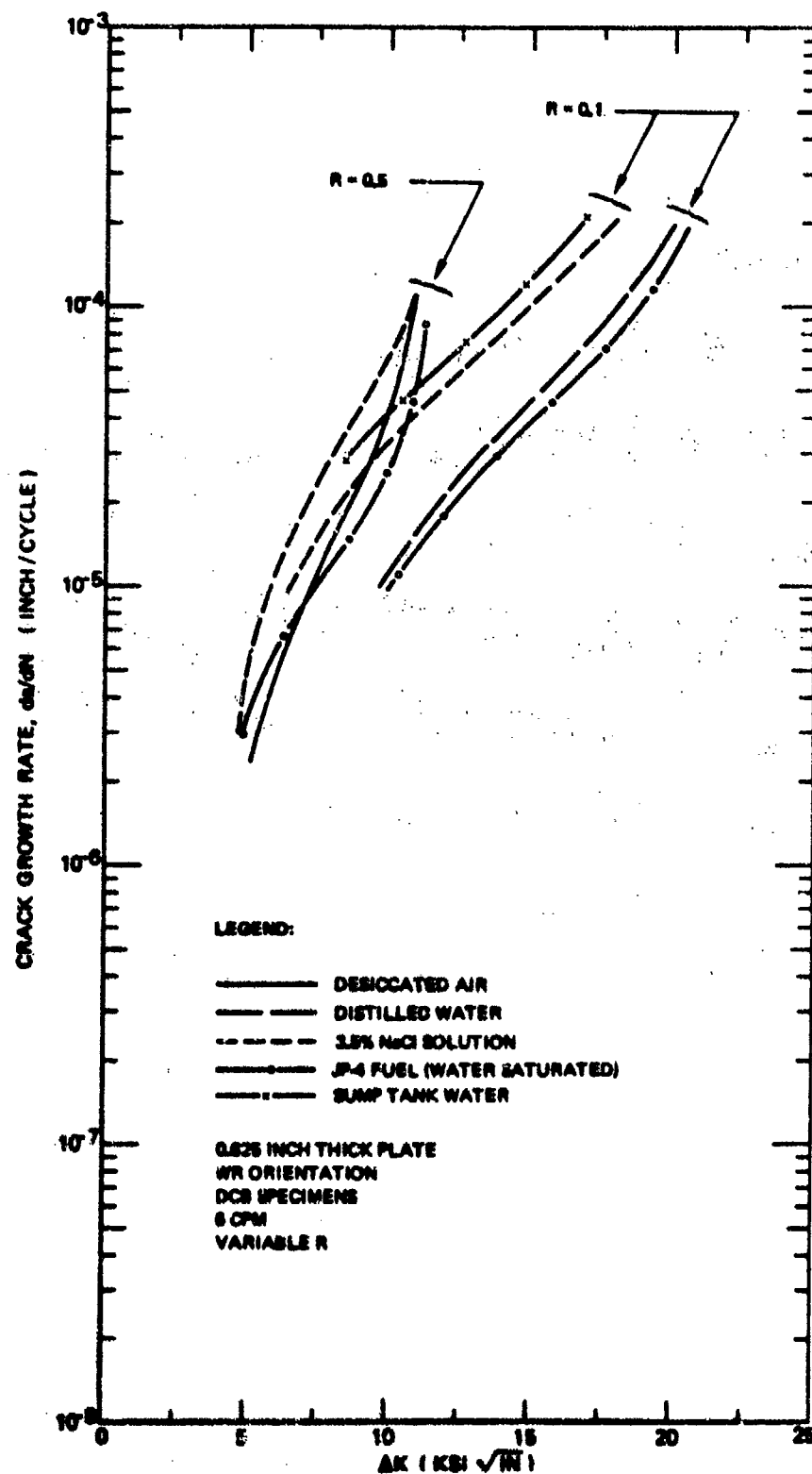


Figure 29: Effect of Environment on Fatigue Crack Growth Rates at 6 CPM in 7075-T651 Aluminum Alloy

Test media affected crack growth rates over the entire range of ΔK values from the threshold to critical values. The effects were most easily noticed at intermediate ΔK was decreased, the slopes of the crack growth rate curves continuously increased and it became more and more difficult to distinguish differences in crack growth rate values. When the slopes became large, very small changes in the location of a data point can create an apparent large change in crack growth rates at a constant ΔK value. Hence, conclusions about low ΔK crack growth rate behaviors must be qualified by stating that such behaviors are difficult to ascertain. Notwithstanding the difficult, Figure 27 shows that the most aggressive test media consistently lowered the apparent threshold stress intensity values and increased crack growth rates at very low ΔK values.

Three tests were conducted in the alternating JP-4 fuel and distilled water environment using a stress ratio of 0.1 and cyclic frequency of 60 cpm; two tests were conducted using a stress ratio of 0.5 and cyclic frequencies of either 6 or 60 cpm. Each test was conducted by growing the crack in increments of 0.15 inch with the specimen alternately submerged in JP-4 fuel and distilled water. The resultant crack growth rate measurements are plotted in Figure 30 and 31. Individual data points for the alternating environment are compared to average crack growth rate curves for both distilled water and JP-4 fuel. The 60 cpm data in Figures 30 and 31 fall either between or close to the average crack growth rate curves for the individual components of the environments. Hence, no unusual effects were generated by alternating the two environments. Some of the 6 cpm data, however, fell considerably above the crack growth rate curves for the components of the alternating environment as shown in Figure 31b. Since other similar tests in this program showed no accelerative effect on crack growth rates due to the alternating of JP-4 fuel and distilled water media, the apparent accelerative effect in Figure 31b is probably due to data scatter.

A single test was conducted on a 7075-T651 aluminum alloy specimen after the crack surfaces had been sprayed with the corrosion inhibitor LSP-3 and allowed to dry for 3 hours. The specimen was tested in distilled water using a stress ratio of 0.5 and cyclic frequency of 60 cpm. The resultant crack growth rate

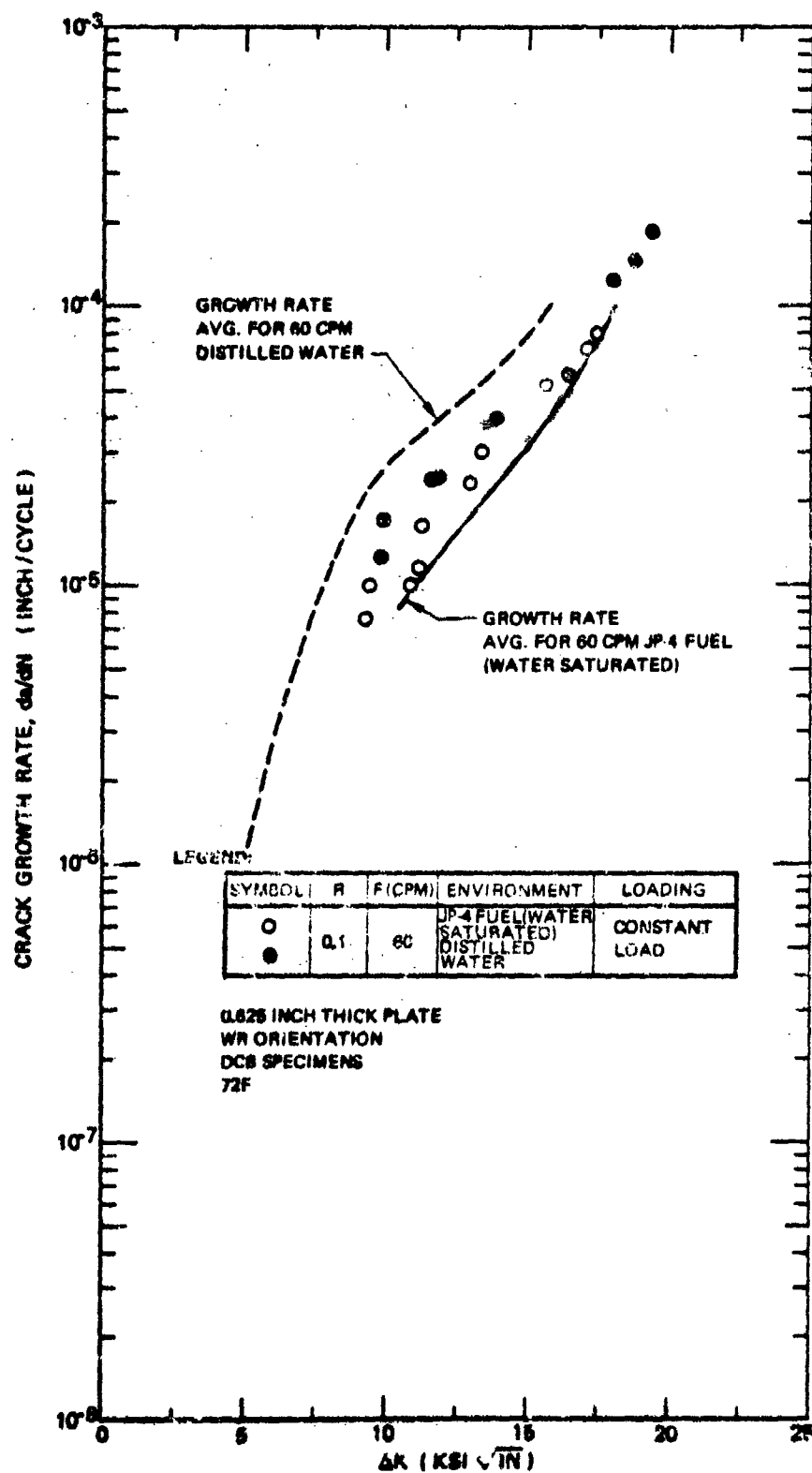
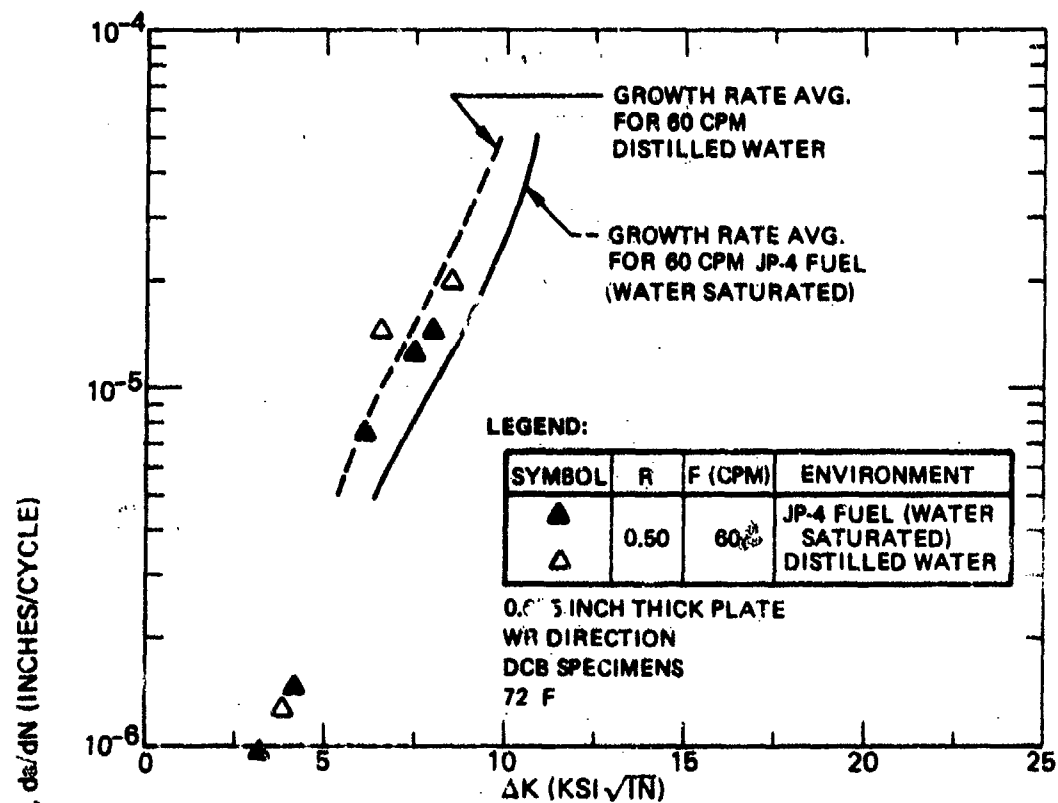
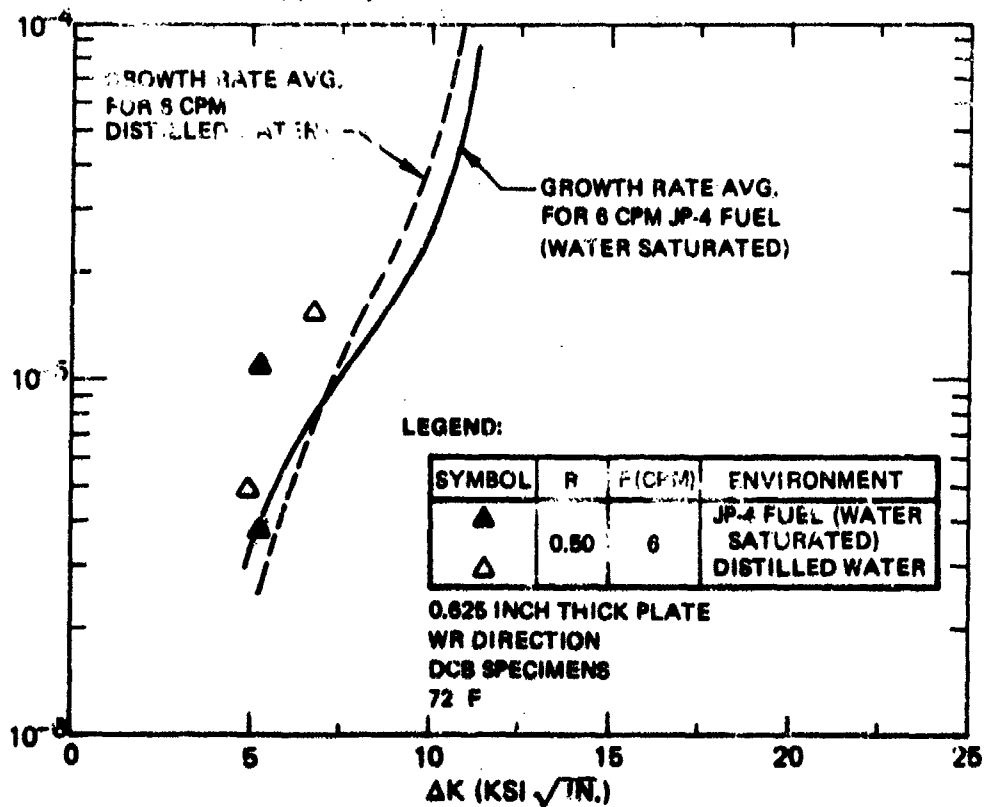


Figure 30: Fatigue Crack Growth Rates for 7075-T651 Aluminum Alloy in Alternating JP-4 Fuel and Distilled Water (60 CPM)



(a) 60 Cpm Results



(b) 6 Cpm Results

Figure 31: Crack Growth Rates for 7075-T651 Aluminum Alloy Plate in Alternating JP-4 Fuel and Distilled Water (60 and 6 CPM)

data are plotted in Figure 32 along with the average crack growth rate curve for distilled water and untreated crack surfaces. The data show that the LPS-3 had little or no effect on fatigue crack growth rate behavior.

Three tests were conducted in dye penetrant (ZL-2A) using cyclic frequencies of both 6 and 60 cpm and stress ratios of both 0.1 and 0.5. The 60 cpm data are plotted in Figure 33 along with average crack growth rate curves for desiccated air. Since desiccated air was one of the least aggressive media used in this program, it is evident that the dye penetrant used in these tests is not detrimental to fatigue crack growth resistance of 7075-T651 aluminum alloy plate. The 6 cpm data are plotted in Figure 34 along with average crack growth rate curves for salt water and desiccated air. The dye penetrant data fall between or below the curves for the 3.5% NaCl solution and desiccated air environments over the range of ΔK values tested.

Temperature

Fatigue crack growth rate tests were conducted on 7075-T651 aluminum alloy specimens at 175F in four media. The resulting crack growth rate data for desiccated air and 3.5% NaCl solution are plotted in Figure 35; data for JP-4 fuel and distilled water are plotted in Figure 36. Average crack growth rate curves obtained at 72F in the same media are also included in Figures 35 and 36. It is evident that an increase in temperature from 72 to 175F had no significant effect on crack growth rate behavior in the four test media.

Tests were also conducted at -65F in air and the resulting crack growth rate data are plotted in Figure 35. It appears that variations in temperature within the range of -65F to +175F have little or no effect on fatigue crack growth rates for the 7075-T651 alloy.

3.1.2.2 Effect of Cyclic Frequency

A reduction in cyclic frequency from 60 to 6 cpm had little or no effect on fatigue crack growth rates of 7075-T651 aluminum alloy plate in any of the environments tested in this program. The result is substantiated by Figures 37 through 41 where 6 cpm crack growth rate data are plotted and compared to corresponding 60 cpm crack growth rate curves for the five principal test

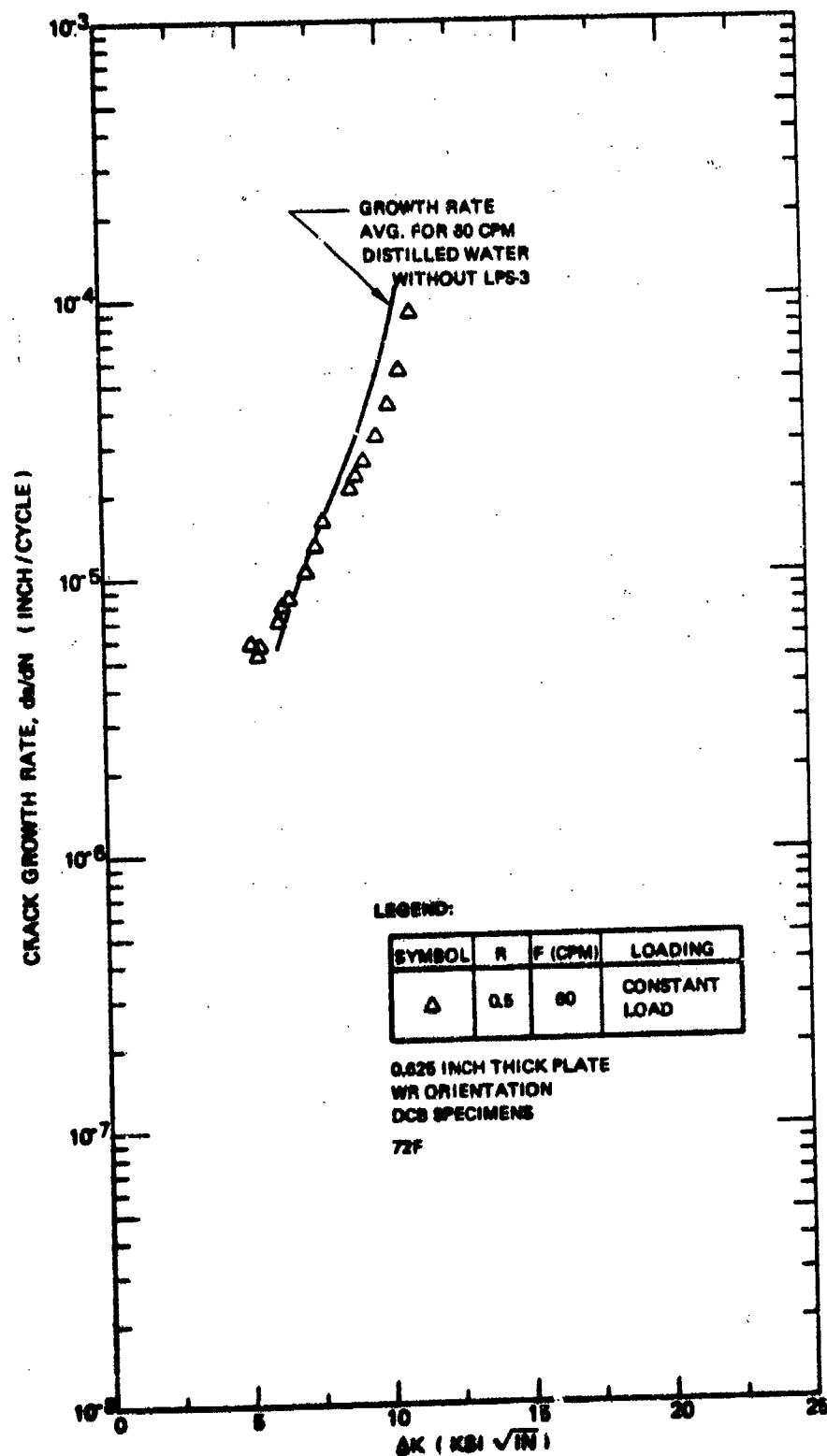


Figure 32: Fatigue Crack Growth Rate for 7075 T651 Aluminum Alloy in Distilled Water, Crack Surface Sprayed With LPS-3 and Dried for 3.0 Hours Prior to Immersion in Test Media (80 CPM)

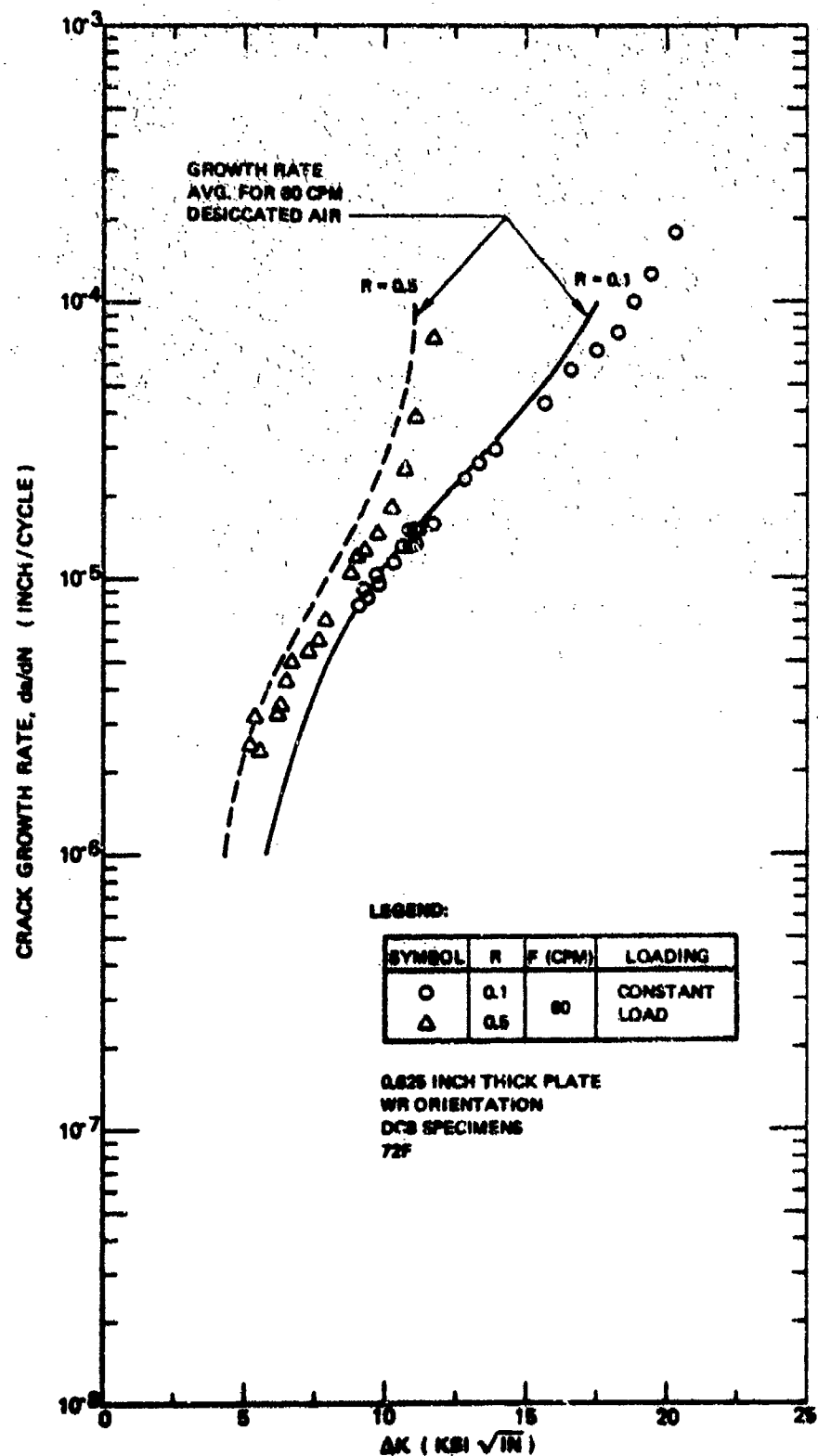


Figure 33: Fatigue Crack Growth Rates for 7075-T651 Aluminum Alloy in Dye Penetrant (Type ZL-2A, 60 CPM)

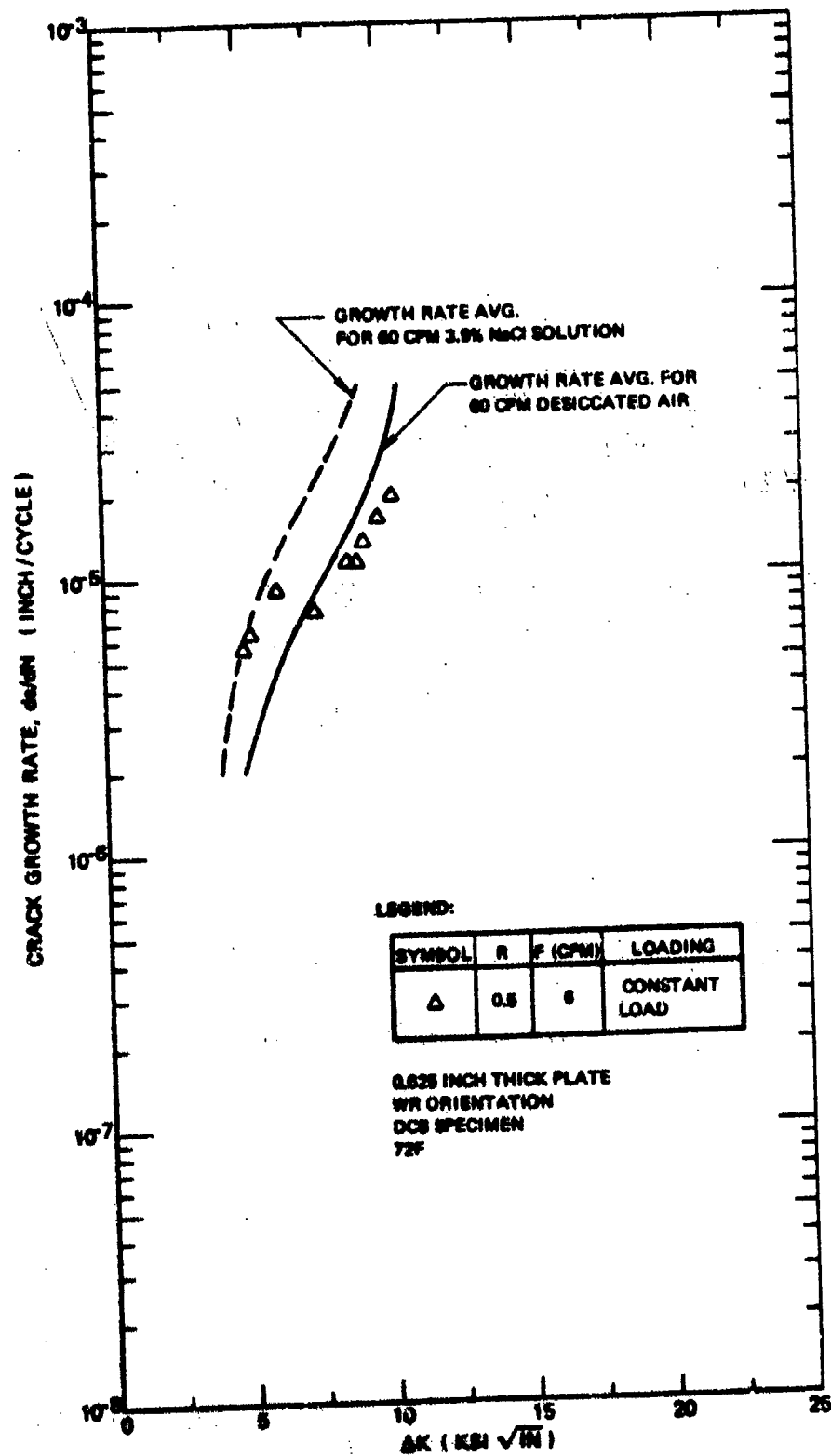


Figure 34: Fatigue Crack Growth Rates for 7075-T651 Aluminum Alloy in Dye Penetrant (Type ZL-2A, 6 CPM)

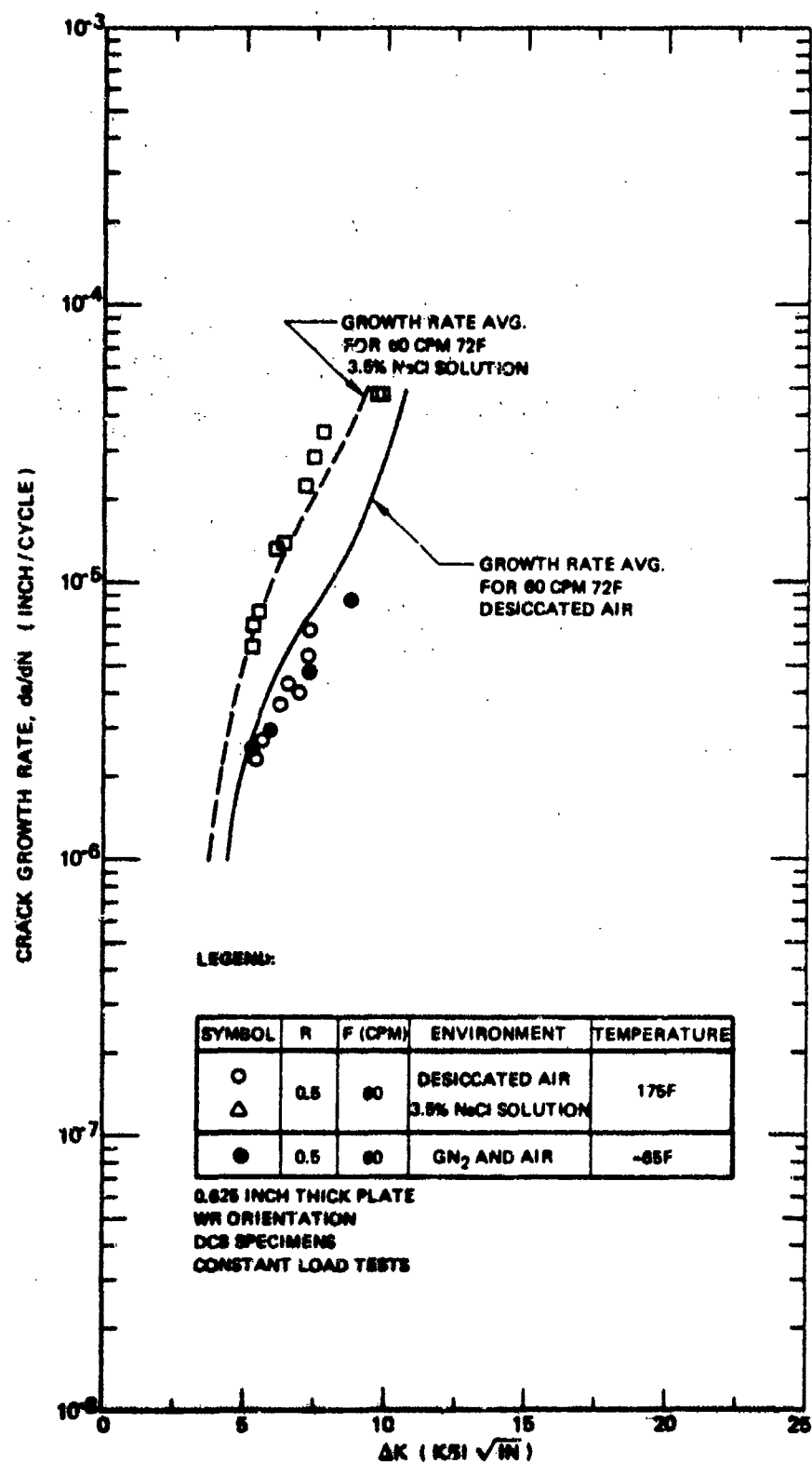


Figure 35: Fatigue Crack Growth Rates for 7075-T651 Aluminum Alloy at -65F and +175F in Desiccated Air and 3.5% NaCl Solution (60 CPM)

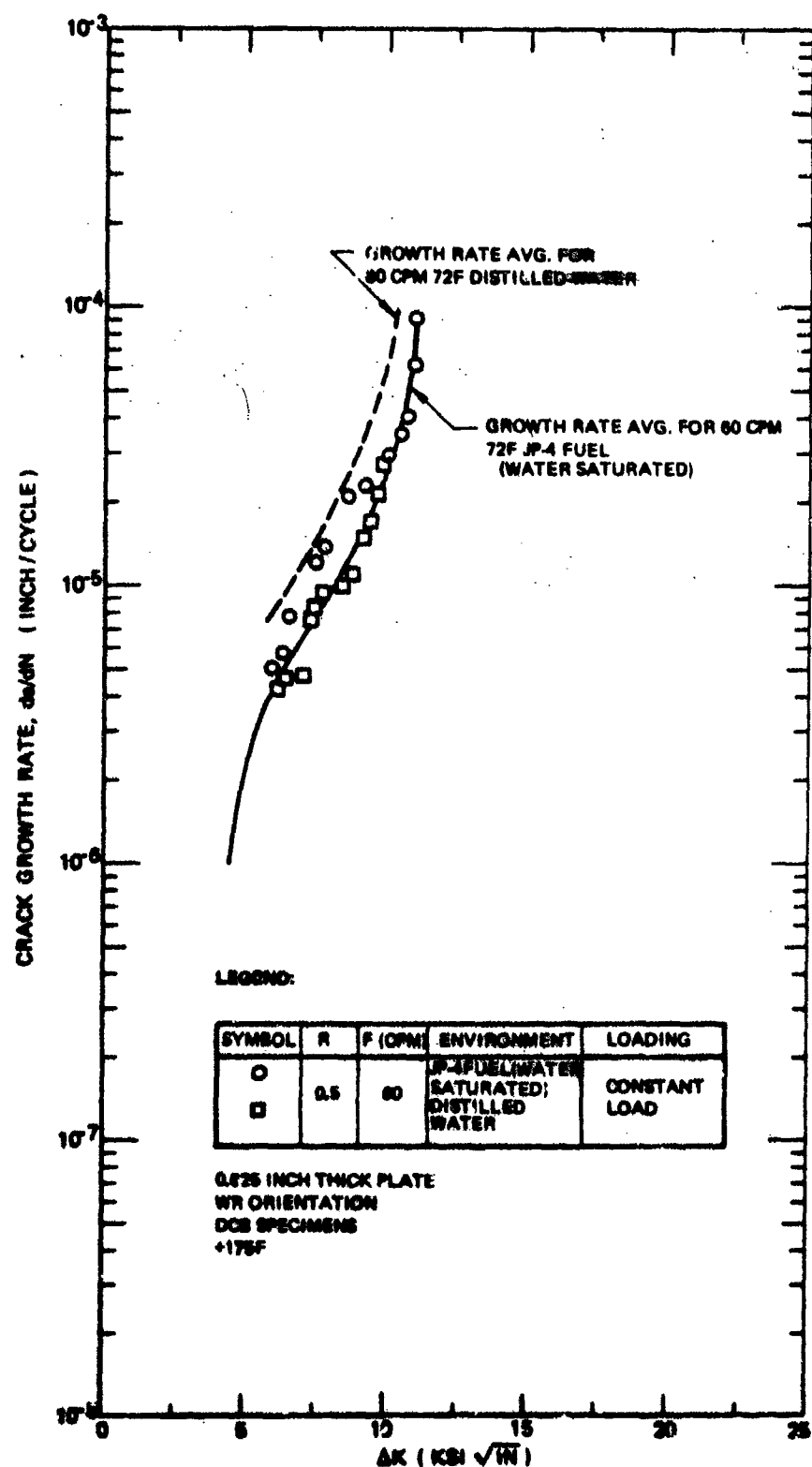


Figure 36: Fatigue Crack Growth Rates for 7075-T651 Aluminum Alloy at +175 in Distilled Water and Water Saturated JP-4 Fuel (60 CPM)

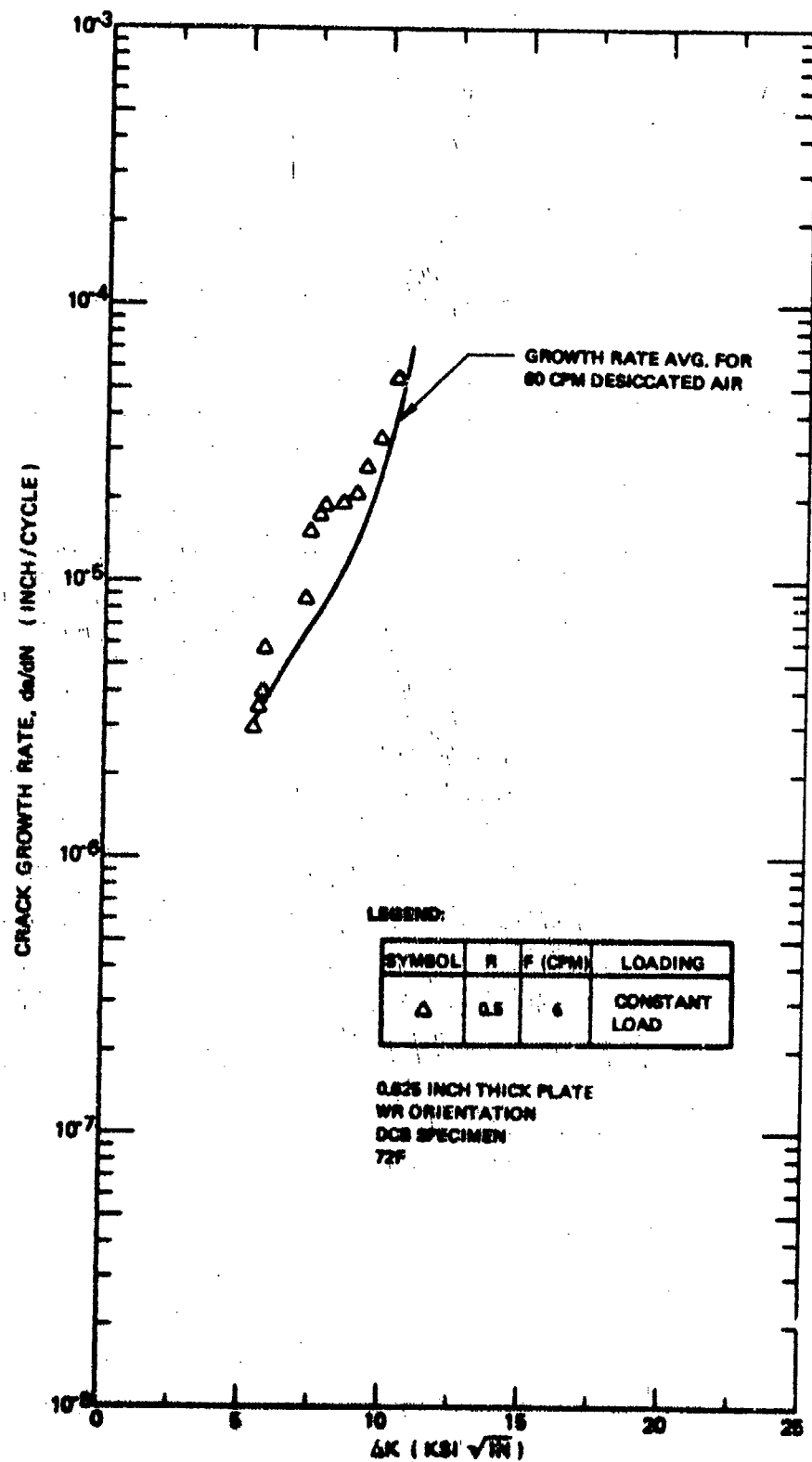


Figure 37: Fatigue Crack Growth Rates for 7075-T651 Aluminum Alloy in Desiccated Air (6 CPM)

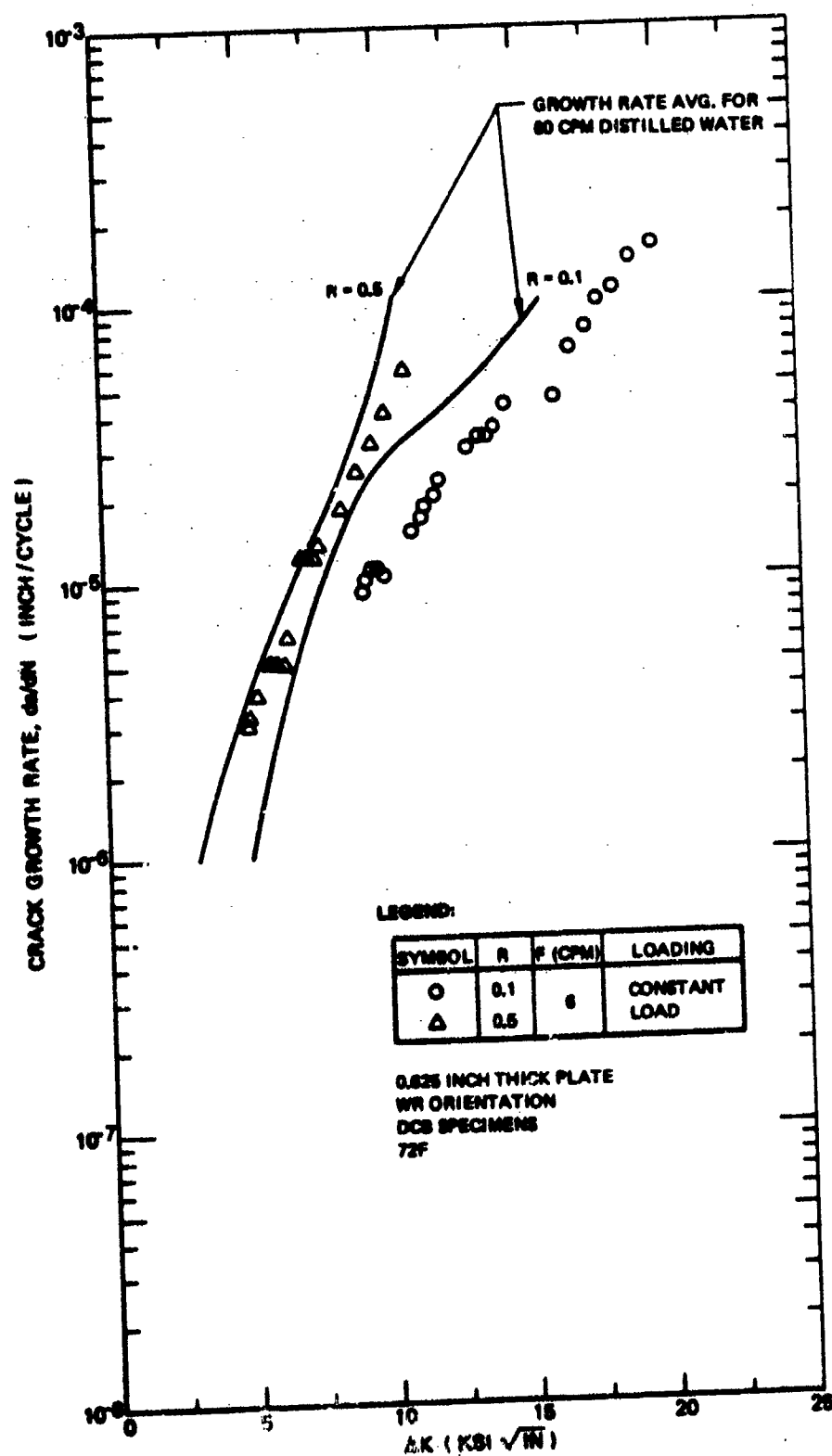


Figure 38: Fatigue Crack Growth Rates for 7075-T651 Aluminum Alloy in Distilled Water (6 CPM)

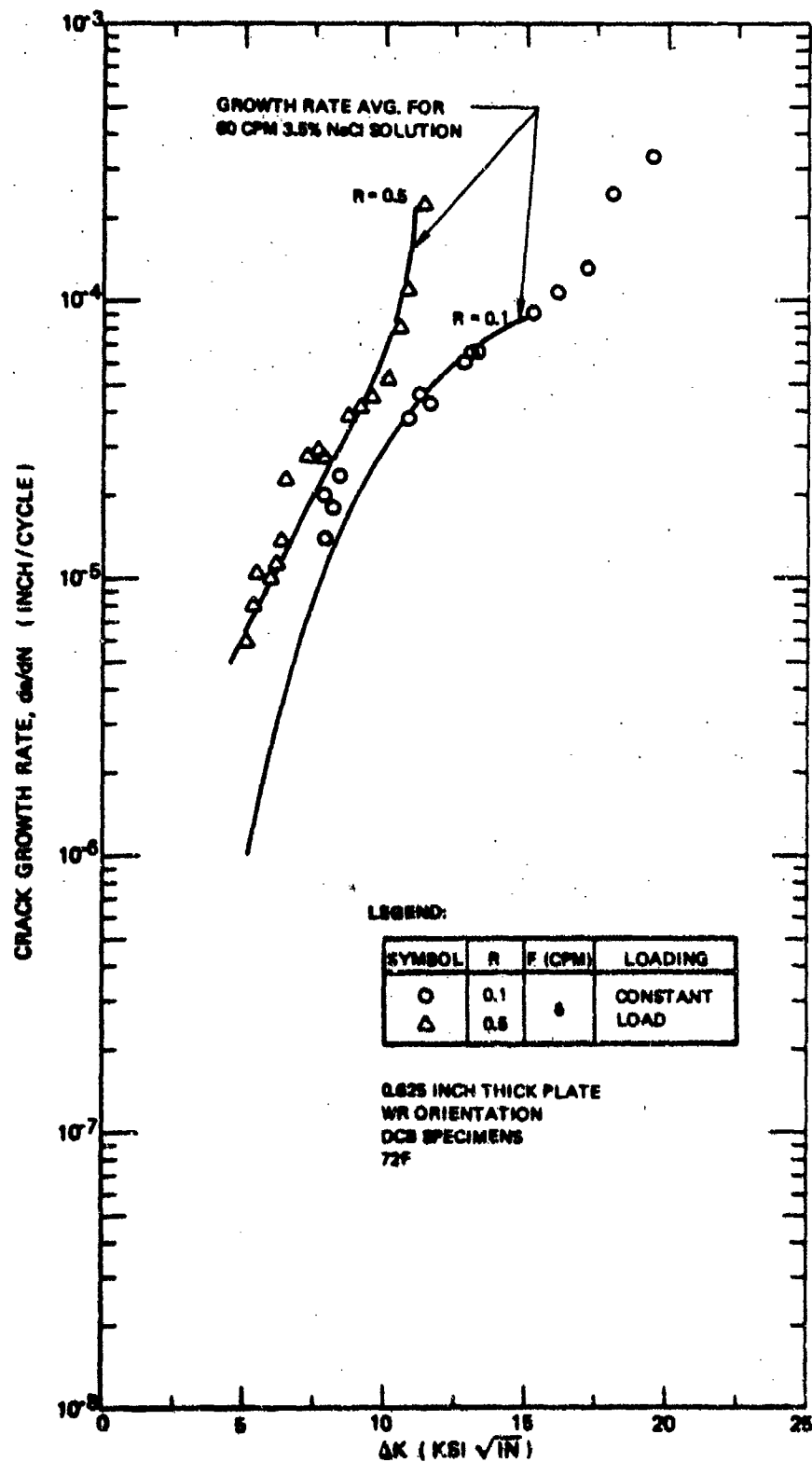


Figure 39: Fatigue Crack Growth Rates for 7075-T651 Aluminum Alloy in 3.5% NaCl Solution (6 CPM)

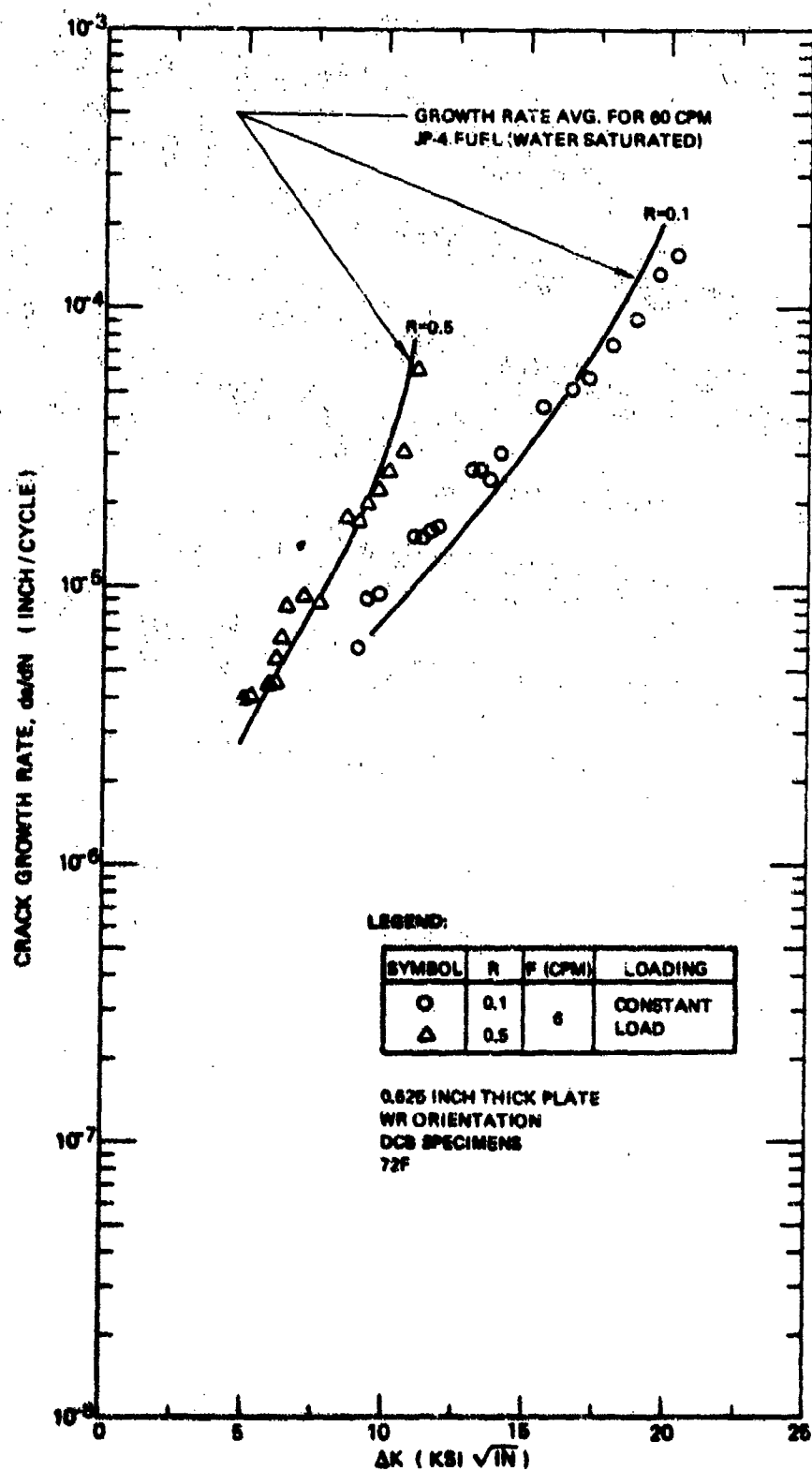


Figure 40: Fatigue Crack Growth Rates for 7075-T651 Aluminum Alloy in Water Saturated JP-4 Fuel (6 CPM)

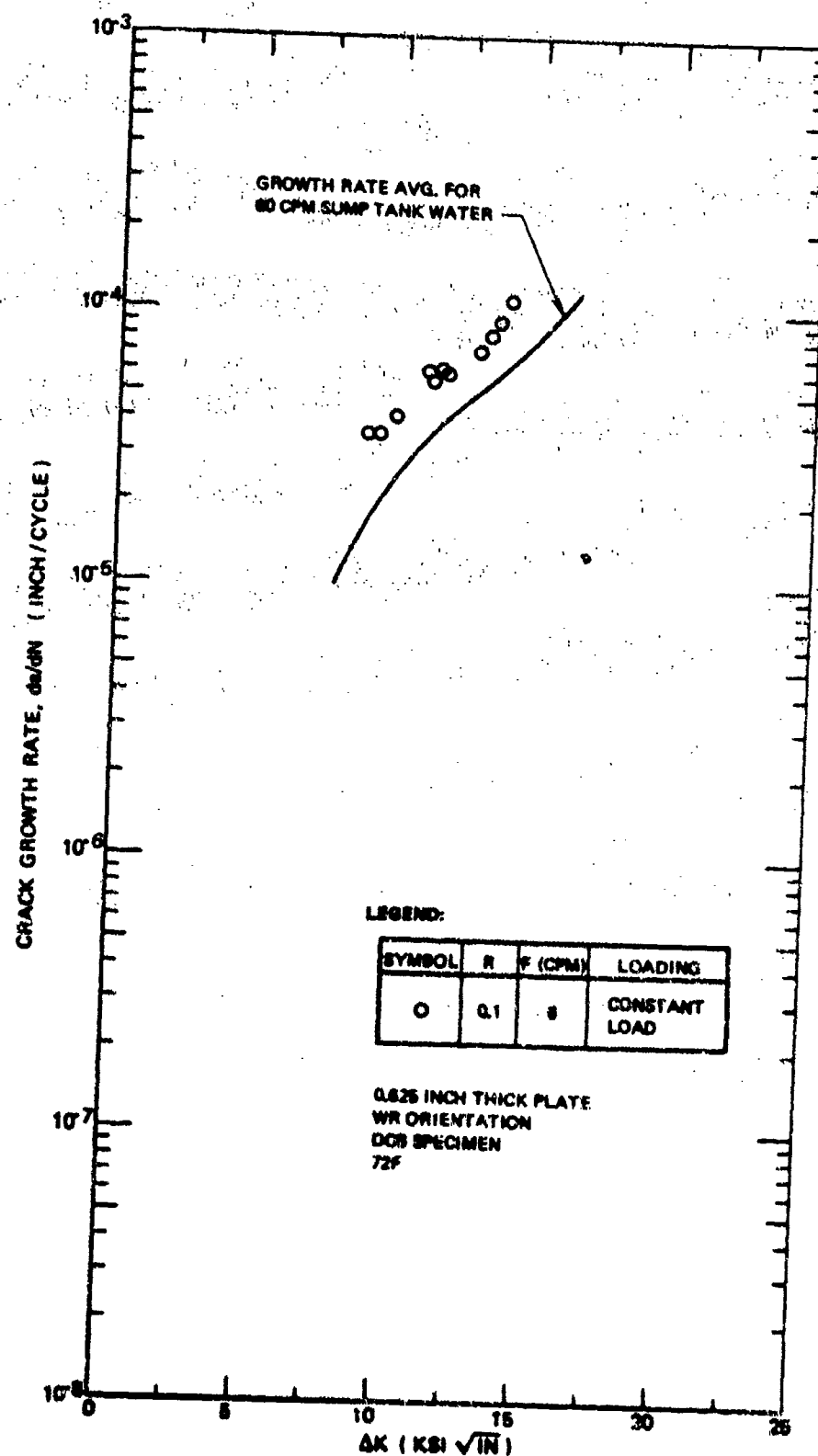


Figure 41: Fatigue Crack Growth Rates for 7075-T651 Aluminum Alloy in Sump Tank Water (6 CPM)

media. The 6 cpm data fell both above and below the 60 cpm curves and only in sump tank water was there any consistent difference between 60 and 6 cpm crack growth rates. In sump tank water, 6 cpm crack growth rates were consistently 1.5 to 2 times the 60 cpm rates. Since this discrepancy is within normal data scatter for crack growth rate tests, it cannot be concluded that it was due solely to a frequency effect.

3.1.2.3 Effect of Specimen Type

Four surface-flawed (SF) specimens were tested so that crack growth rate data obtained from both DCB and SF specimens could be directly compared. Two tests were conducted in each of the 72F test media of desiccated air and 3.5% NaCl solutions. Peak cycle stress levels were varied by a factor of two to determine if stress level had any effect on crack growth rates other than through its contribution to the stress intensity factor. The resulting crack growth rate data are plotted in Figure 42 along with average crack growth rate curves obtained from tests DCB specimens. In air, crack growth rates obtained from SF specimens were slower than corresponding rates obtained from DCB specimens. Although these differences could be due to data scatter, it is believed to be due to the difference in crack propagation directions for the two specimens, namely, WT direction in the SF specimens and WR direction in the DCB specimens. Aluminum alloy hot rolled plate tends to be anisotropic with respect to fatigue crack growth rate resistance with the WT direction having the highest resistance. In contrast, the 3.5% NaCl solution, SF specimen tests yielded higher crack growth rates than did the DCB specimens. Past experience (2) has shown that SF specimens tend to lead to maximum susceptibility to SCC in aggressive environments. In these tests, SF specimens yielded a greater impact of test environment on fatigue crack growth resistance. For example, at a ΔK of $5 \text{ ksi}\sqrt{\text{in}}$, the 3.5% NaCl solution resulted in a twofold increase in crack growth rates in DCB specimens and a tenfold increase in crack growth rates in SF specimens.

Peak cyclic stress level did not appear to have a significant effect on crack growth rates for constant ΔK values. Data for the two peak cyclic stress levels

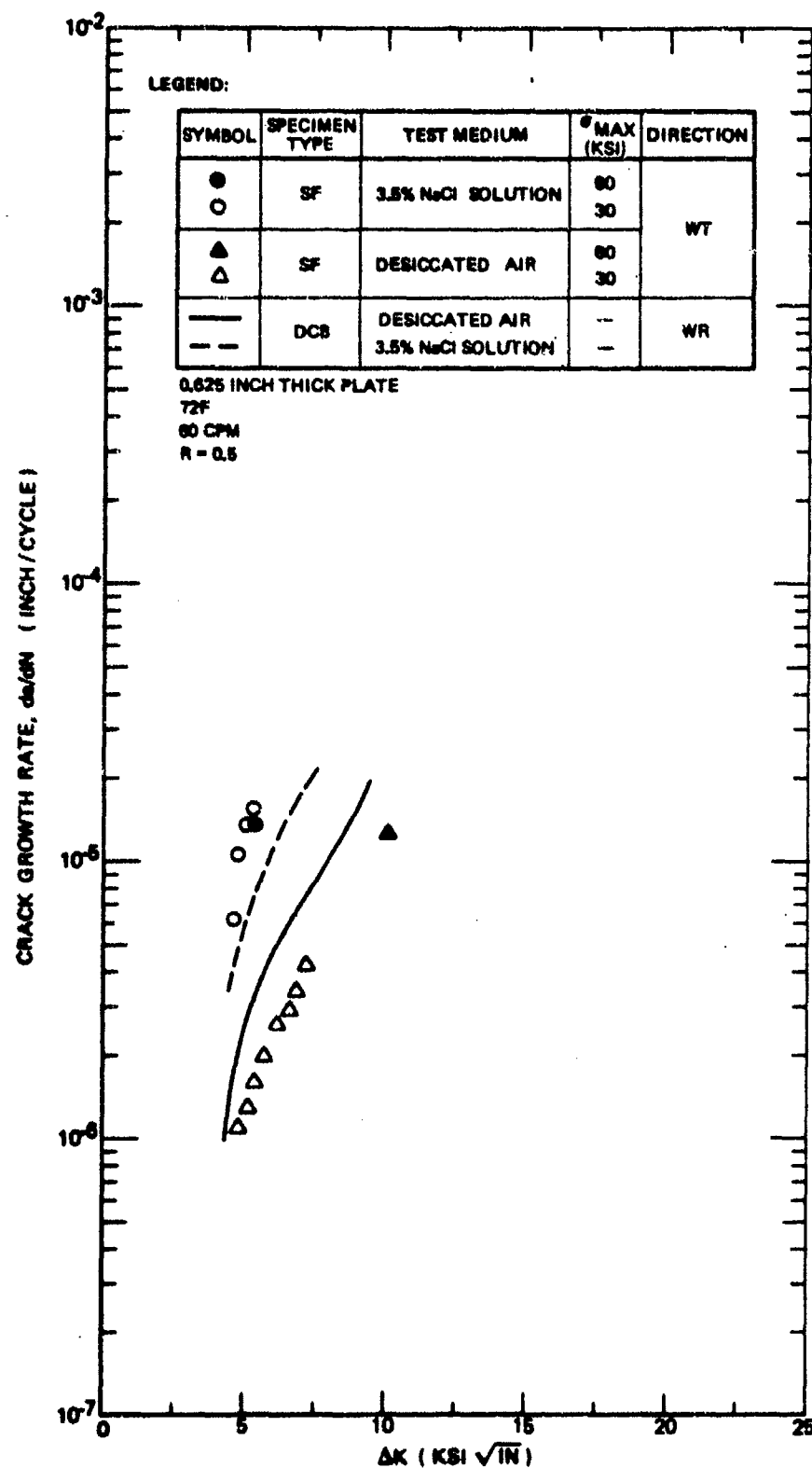


Figure 42: Fatigue Crack Growth Rates Data for 7075-T651 Aluminum Alloy Surface Flawed Specimens (60 CPM)

overlapped only for the 3.5% NaCl solutions and showed no effect of peak cyclic stress level.

3.1.3 Aluminum Alloy 7475-T651 Results

The aluminum alloy 7475 was tested as a high purity form of the 7075 alloy to compare SCC and corrosion fatigue behavior of the two alloys. Six tests were conducted for the 7475 alloy including two corrosion fatigue tests in low humidity air, one stress corrosion cracking test in distilled water, and one stress corrosion cracking and two corrosion fatigue tests in 3.5% NaCl solution.

The chemical content of the 7075 and 7475 alloys was essentially the same except for Fe and Mn contents which were lower in the 7475 alloy than in the 7075 alloy (see Table 2). The 7475 alloy contained significantly less impurities than did the 7075 alloy (see Figures 1 and 4).

3.1.3.1 Stress Corrosion Cracking Tests

One test was conducted in each of 3.5% NaCl solutions and distilled water test media for three months. The resulting crack growth rate data are plotted as a function of stress intensity factor in Figure 43. Average curves drawn through comparable 7075-T651 aluminum alloy SCC data are included in Figure 43 for comparison. For stress intensity factor above $12.5 \text{ ksi}\sqrt{\text{in}}$, SCC rates in the 7475 alloy were faster than in the 7075 alloy. Below $12.5 \text{ ksi}\sqrt{\text{in}}$, there was not much difference in SCC behavior between the two alloys in 3.5% NaCl solution. Hence, the 7475 alloy did not show any improvement over the 7075 alloy in resistance to SCC in the short transverse crack propagation direction.

3.1.3.2 Corrosion Fatigue Tests

Two corrosion fatigue tests were conducted at 60 cpm in each of the 3.5% NaCl solution and low humidity air test media. The resulting crack growth rate data are plotted in Figure 44 along with average crack growth rate curves drawn through comparable 7075-T651 aluminum alloy corrosion fatigue data. For crack growth rates above 5×10^{-7} inches/cycle, the agreement between data for the two alloys is within normal limits of data scatter. However, the trend

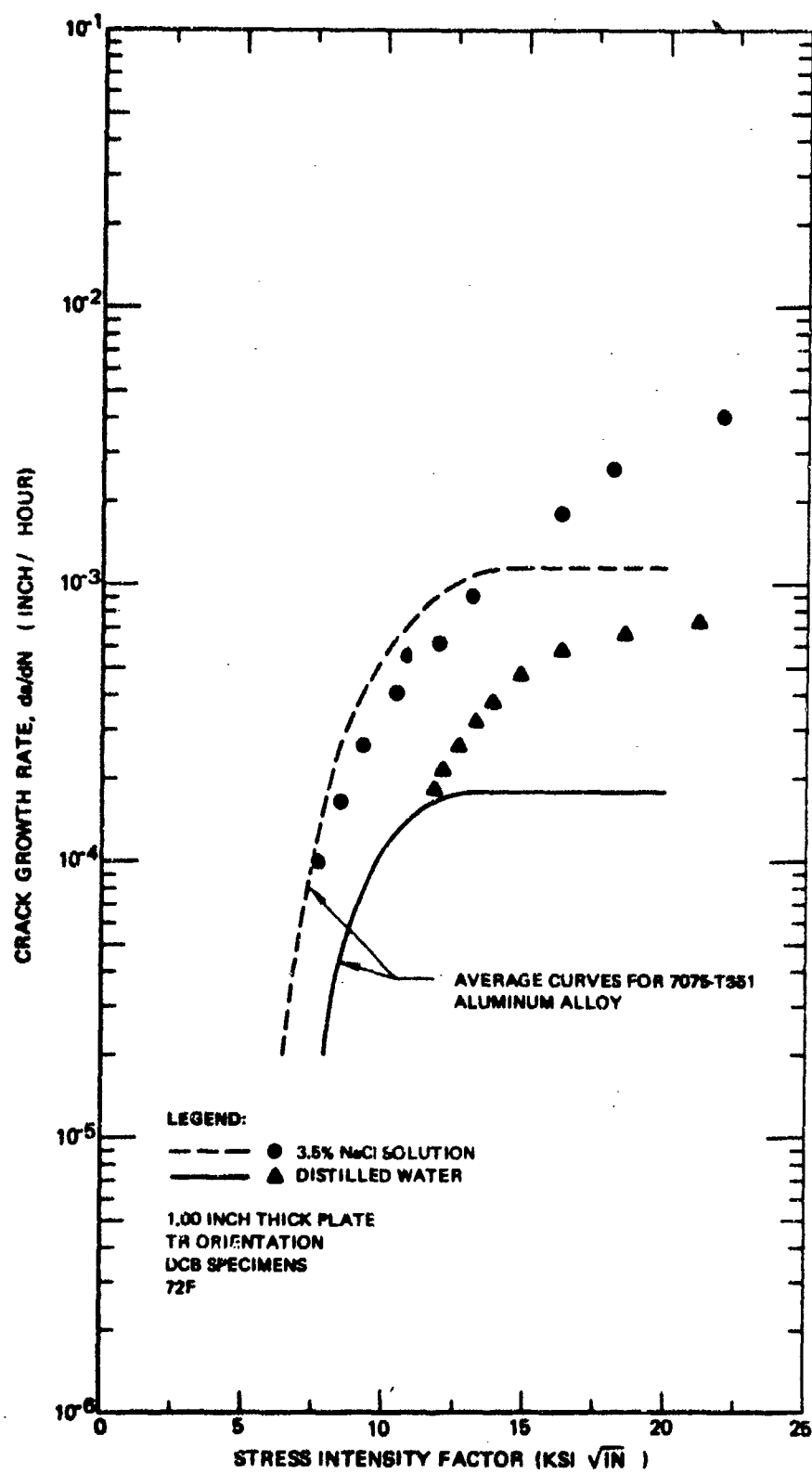


Figure 43: Stress Corrosion Cracking Velocity Data for 7475-T651 Aluminum Alloy

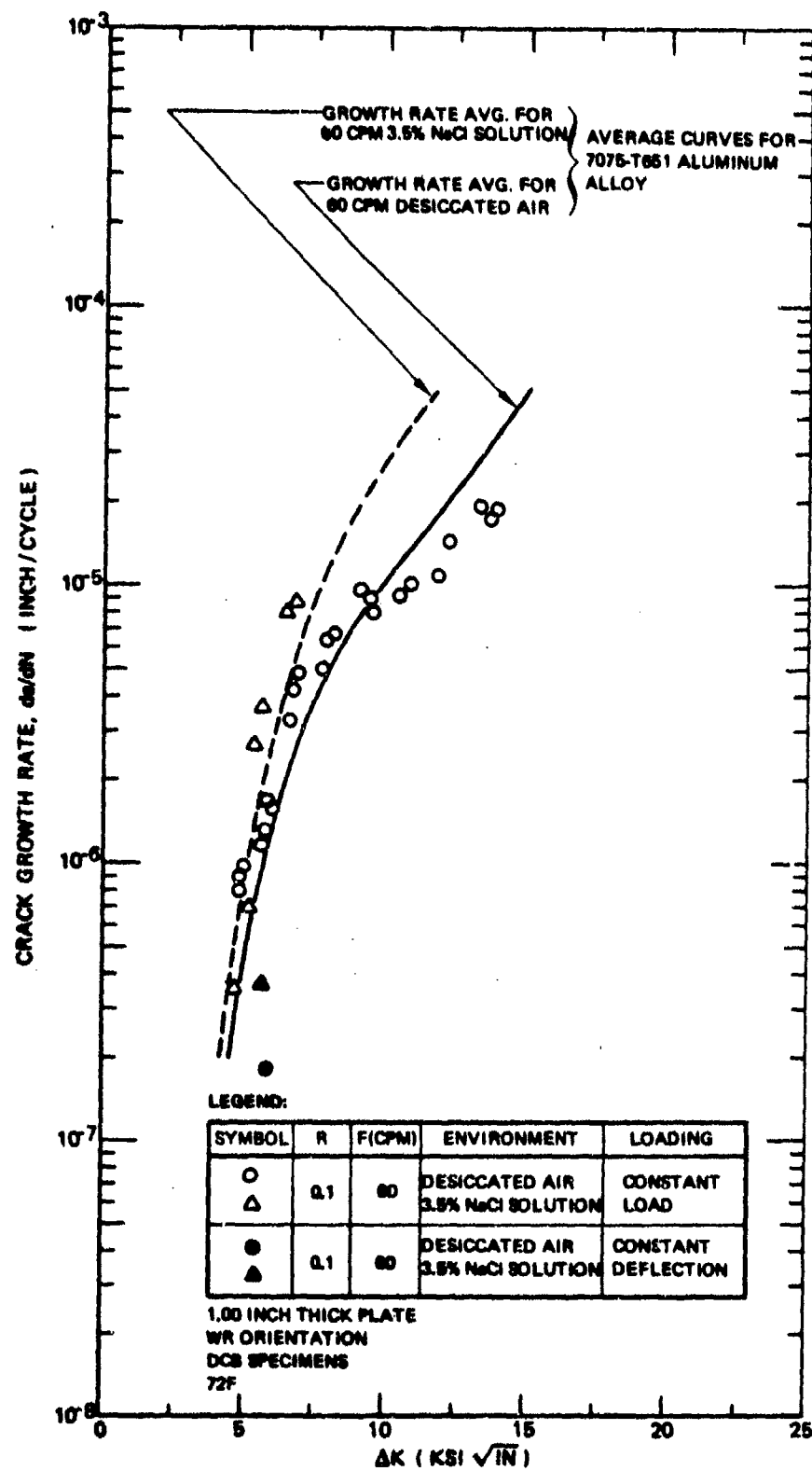


Figure 44: Fatigue Crack Growth Rates for 7475-T651 Aluminum Alloy in Desiccated Air and 3.5% NaCl Solution (60 CPM)

of the data indicates that the 7475 alloy might have a higher threshold stress intensity factor range than does the 7075 alloy. Unfortunately, there were insufficient data to verify this trend.

The work of other investigators has shown that low purity 7000 series aluminum alloys yield crack growth rates at low ΔK values that are equal to or slower than crack growth rates for comparable high purity alloys. Glassman and McEvily⁽⁶⁾ have shown that a reduction in particle content may have detrimental effects on fatigue crack growth resistance; they found that crack growth rates in a 7075-T6 aluminum alloy were slower than in a lower particles content X7275-T6 aluminum alloy. Pelloux⁽⁷⁾ found that reducing particle content in the 7178 aluminum alloy did not retard crack growth. In more recent work, Pelloux and McClintoch have found that particles (dirt) are beneficial and that low purity alloys outperform high purity alloys at low ΔK values. In the present investigation, insufficient crack growth rate data were generated at low ΔK values to provide a good comparison between the higher purity 7475 and lower purity 7075 aluminum alloys.

3.2 Titanium Alloy 6Al-4V Beta Annealed Results

The test program for the Ti-6Al-4V beta annealed alloy is summarized in Table 11. Mechanical property and fracture toughness data are reported in Section 2.1. Results of the stress corrosion cracking and corrosion fatigue tests are described in this section.

3.2.1 Stress Corrosion Cracking Tests

Two preliminary stress corrosion cracking tests were conducted to measure the relative susceptibility to SCC of the RW and WR crack propagation directions in the 6Al-4V beta mill annealed (β A) titanium alloy plate. Two DCB specimens (Figure B7) were wedge loaded and tested in 3.5% NaCl solutions for 120 hours. For the WR direction, the crack grew 0.47 inch while the stress intensity factor decreased from the initial value of 78 ksi $\sqrt{\text{in}}$ to 70 ksi $\sqrt{\text{in}}$; for the

Table 11: Test Program for Ti-6Al-4V Beta Annealed

TEST TYPE	SPECIMEN TYPE	CYCLIC FREQUENCY	STRESS RATIO	ENVIRONMENT																				
				AIR			DISTILLED WATER			3.5% NaCl SOLUTION			JP-4			SUMP TANK			JP-4 + H ₂ O			DYE PEN		
				-65F	72F	175F	-65F	72F	175F	-65F	72F	175F	-65F	72F	175F	-65F	72F	175F	-65F	72F	175F			
MECHANICAL PROPERTY	TENS.			4	4	4																		
FRACTURE TOUGHNESS	CT			2	4	2																		
	SF			2	2	2																		
STRESS CORROSION CRACKING	DCB			2			4			5			4			2								
	SF			1						1												4	1	
CORROSION FATIGUE	DCB	60	0.1	2	2	2	1	2	1	3	2	1	1	2	1	2	2					2		
			0.5	2	2	2	2	2	1	2	2	1	2	2	1	2	2							
			0.8	1							1													
CORROSION FATIGUE	DCB	6	0.1	1			1			1			1											
			0.5	2			2			2			2			2						2		
OVERLOAD	SF	60	0.5	2						2														
OVERLOAD	TDCB	60	0.5	2						2														

RW direction, the crack grew 0.46 inch and the stress intensity factor decreased from 85 ksi $\sqrt{\text{in}}$ to 77 ksi $\sqrt{\text{in}}$. It was concluded that the resistance to SCC of the titanium alloy plate was not very sensitive to test direction and it was decided to test the WR direction in the ensuing tests.

Four subsequent stress corrosion cracking tests were conducted including one test in each of the environments of water saturated JP-4 fuel, distilled water, sump tank water, and 3.5% NaCl solution. Specimen configuration is illustrated in Figure B7. The specimens were pin loaded in a test machine with the crack tip submerged in the test medium and a clip gage was used to monitor maximum crack surface displacement during the loading process. After the desired crack displacement was attained, a pair of circular wedges were inserted in the central hole to wedge open the crack. The specimens were then transferred to test chambers filled with the proper medium and were left there for a period of 506 hours. Periodic observations of crack length showed that no crack growth occurred in any of the test media except 3.5% NaCl solution where a trace of growth was observed. Test results are summarized in Table 12. The result for the 3.5% NaCl solution is in good agreement with the preliminary tests where an apparent K_{ISCC} of 70 ksi $\sqrt{\text{in}}$ was measured for the WR direction of the Ti-6Al-4V beta annealed plate.

3.2.2 Corrosion Fatigue Tests

Test variables included environment, cyclic frequency, specimen type and stress ratio. The effects of environment, frequency, and specimen type on fatigue crack propagation behavior are described in this section. Stress ratio effects are described in Section 4.6.

All data collected from corrosion fatigue tests of the Ti-6Al-4V beta annealed alloy are included in Figure A17 through A32 in Appendix A. In the body of the report, only a limited amount of actual data are shown. For the most part, effects of test variables are illustrated using average curves drawn through the data.

Table 12: SCC Test Results for Ti-6Al-4V Beta Annealed Plate (WR Direction)

SPECIMEN	TEST ENVIRONMENT		INITIAL APPLIED K (KSI $\sqrt{\text{IN.}}$)	INITIAL CRACK LENGTH (IN.)	FINAL CRACK LENGTH (IN.)	COMMENTS
	MEDIUM	TEMP (°F)				
TS-2	JP-4 FUEL	72	79.6	1.96	1.96	NO GROWTH
TS-1	DISTILLED WATER	72	82.5	1.98	1.98	NO GROWTH
TS-3	SUMP TANK WATER	72	81.2	1.97	1.97	NO GROWTH
TS-4	3.5% NaCl SOLUTION	72	69.2	2.02	2.02 ⁺	TRACE OF GROWTH

NOTE: ALL TEST DURATIONS WERE 500 HOURS

3.2.2.1 Effect of Test Environment

Test Media

The effects of the five primary test media on fatigue crack growth rate behavior of the Ti-6Al-4V beta annealed plate are shown in Figures 45 through 49. Average crack growth rate curves in Figure 45 show a consistent effect over the entire range of ΔK values tested. The least aggressive media were desiccated air and water saturated JP-4 fuel and the most aggressive medium was 3.5% NaCl solution. The ratio of maximum to minimum crack growth rates at a given value of ΔK increased from 1.6 to 100 as ΔK decreased from 60 ksi $\sqrt{\text{in}}$ to 14 ksi $\sqrt{\text{in}}$. This ratio is difficult to evaluate at the low ΔK values due to the steepness of the crack growth rate curves. Nevertheless, these data show a large effect of test media on crack growth rates at the low ΔK values. Current calculations indicate that crack growth rates in the range of 10^{-7} to 10^{-5} inch/cycle are of prime interest in calculating crack propagation lives for military aircraft components. Hence, the media with which the components come in contact could have a serious effect on crack growth behavior and some serious thought must be given to potential problems due to environmental exposure.

Since 3.5% NaCl solution is a severe representation of the "worst" corrosive operating environment for airframe components, sump tank water is currently being used in some aircraft development programs as being representative of the "worst" environment. The crack growth rate curves in Figure 45 show that sump tank water is indeed less aggressive than 3.5% NaCl solution, particularly at the low ΔK values. For example, at $\Delta K = 12$ ksi $\sqrt{\text{in}}$, these tests yielded a ratio of crack growth rate in 3.5% NaCl solution to crack growth rate in sump tank water of five. This ratio gradually decreased to 1.4 at $\Delta K = 40$ ksi $\sqrt{\text{in}}$. Previous work (8) has shown that the chloride ion content of the test medium is a key factor in determining the crack growth resistance of titanium alloys. This observation is substantiated by the result that the 3.5% NaCl solution was more aggressive than sump tank water. Hence, some thought should be given as to how concentrated chloride ions can become in potential crack locations.

Two tests were conducted in an alternating distilled water and JP-4 fuel environment at 72F. The resulting data are plotted in Figures 50 and 51 along with comparable average crack growth rate curves for both distilled water and

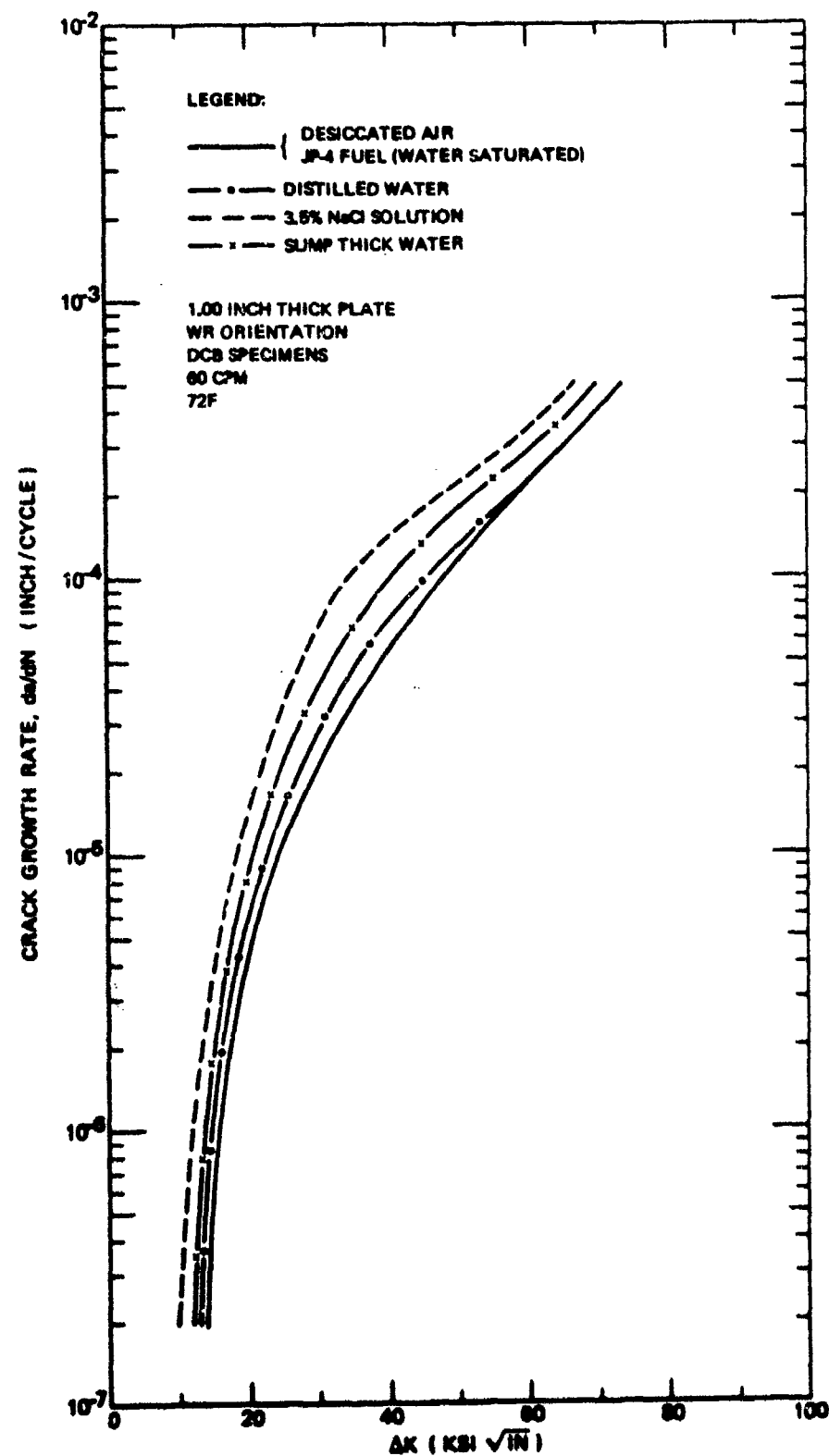


Figure 45: Effect of Environment on Fatigue Crack Growth Rates at $R=0.1$ in 6Al-4V Standard ELI Beta Annealed Titanium Alloy (60 CPM)

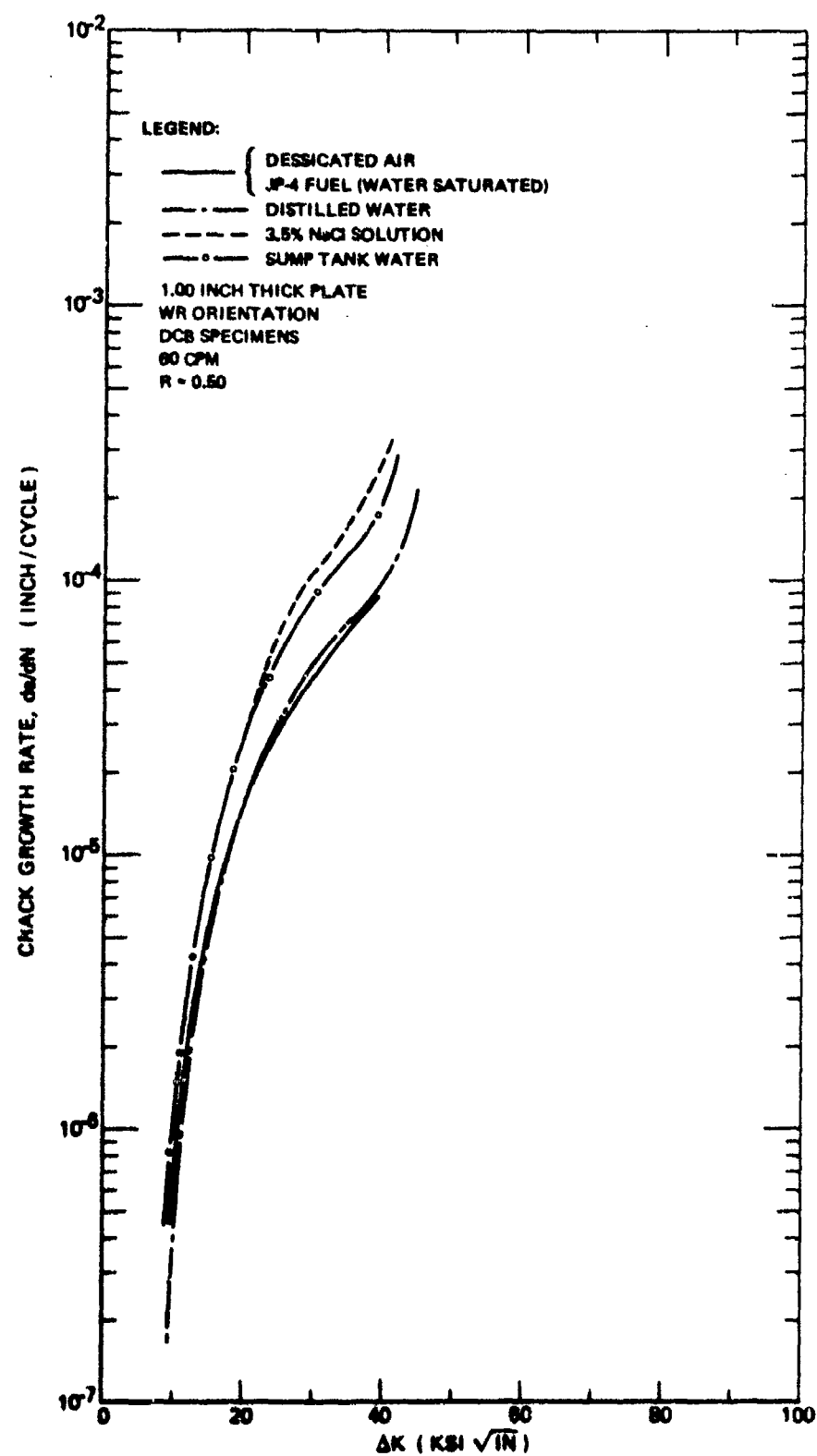


Figure 46: Effect of Environment on Fatigue Crack Growth Rates at $R=0.50$ in 6Al-4V Standard ELI Beta Annealed Titanium Alloy (60 CPM)

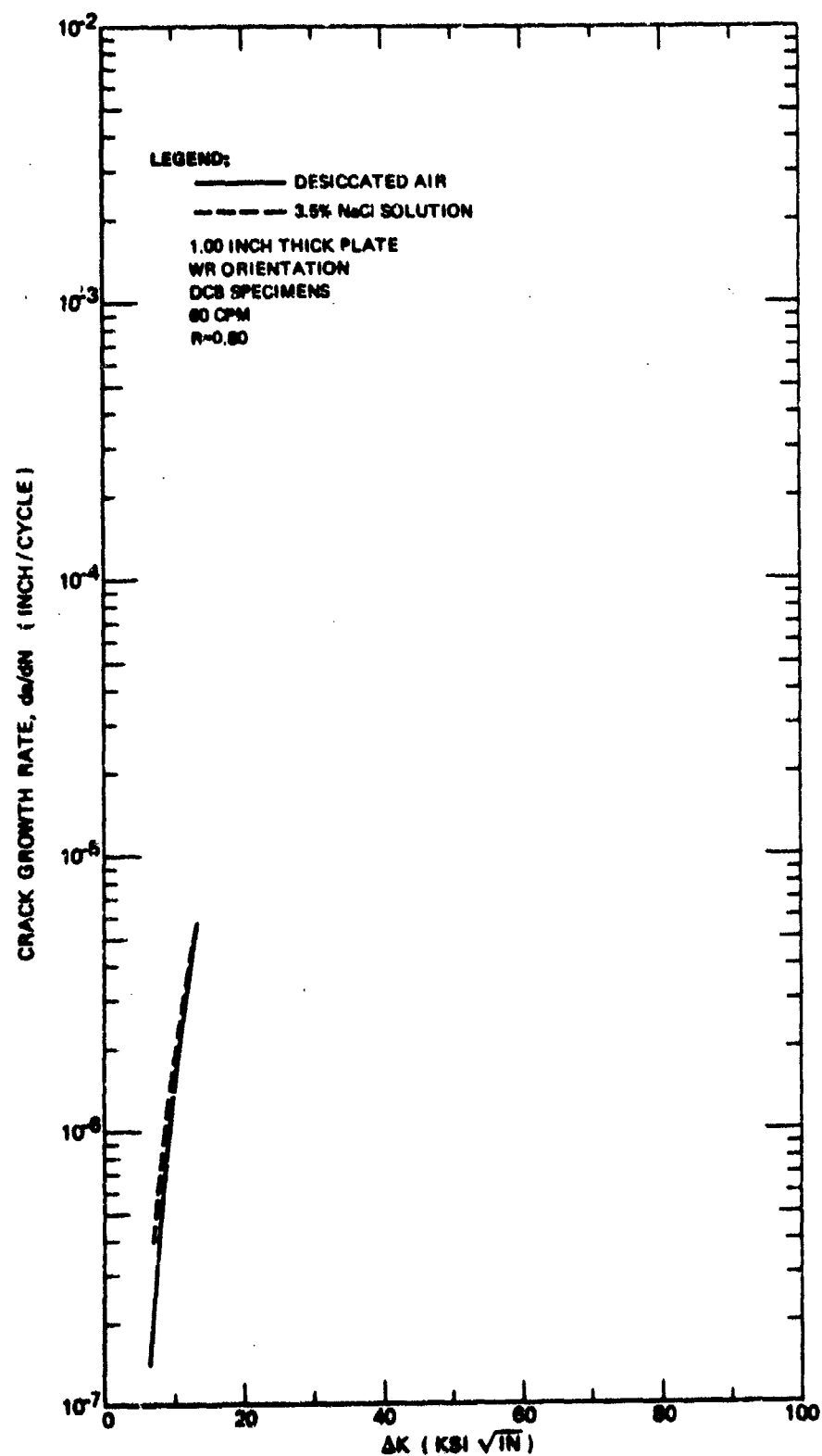


Figure 47: Effect of Environment on Fatigue Crack Growth Rates at R=0.80 in 6Al-4V Standard ELI Beta Annealed Titanium Alloy (60 CPM)

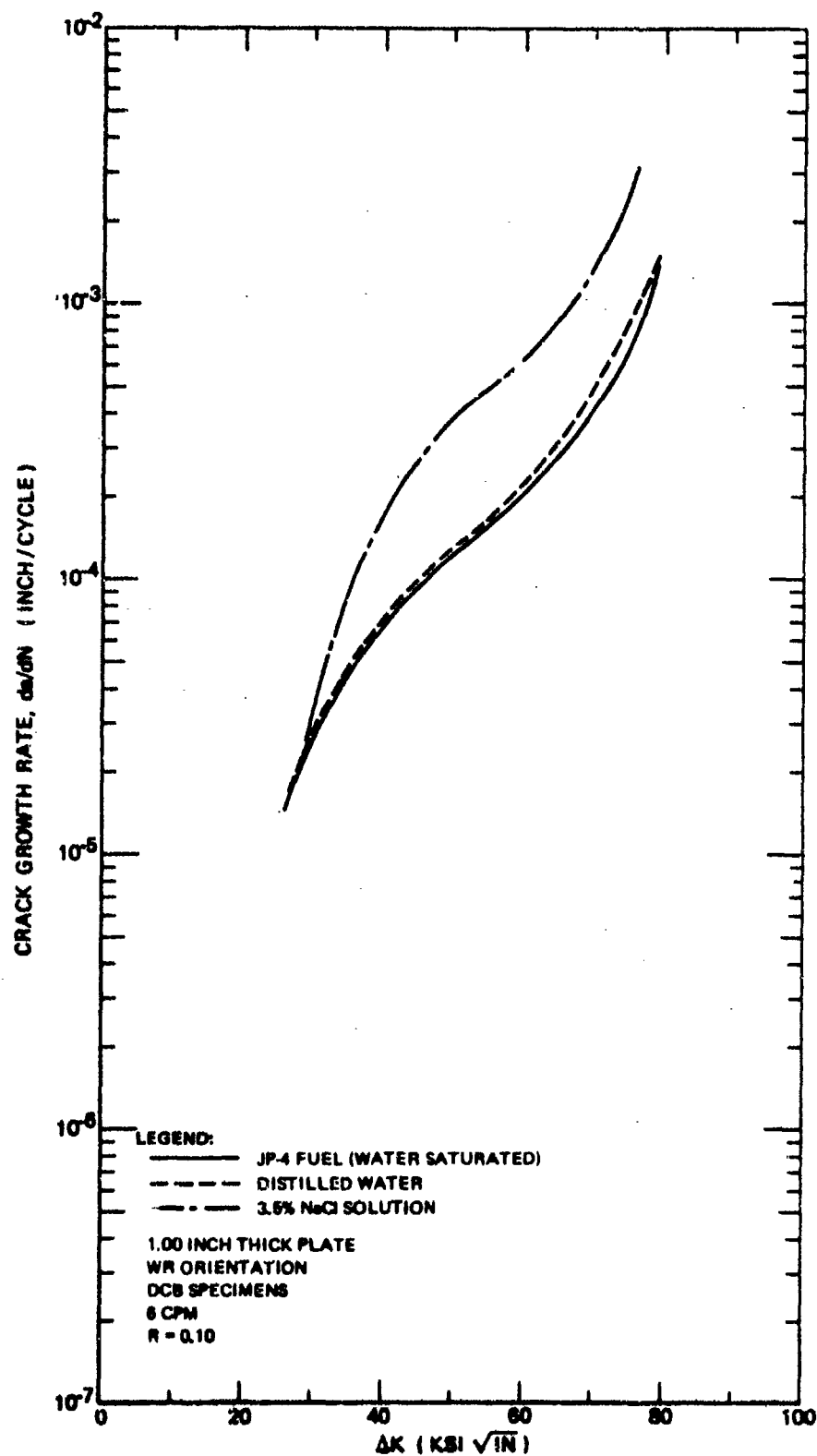


Figure 48: Effect of Environment on Fatigue Crack Growth Rates at $R=0.10$ in 6Al-4V Standard ELI Beta Annealed Titanium Alloy (6 CPM)

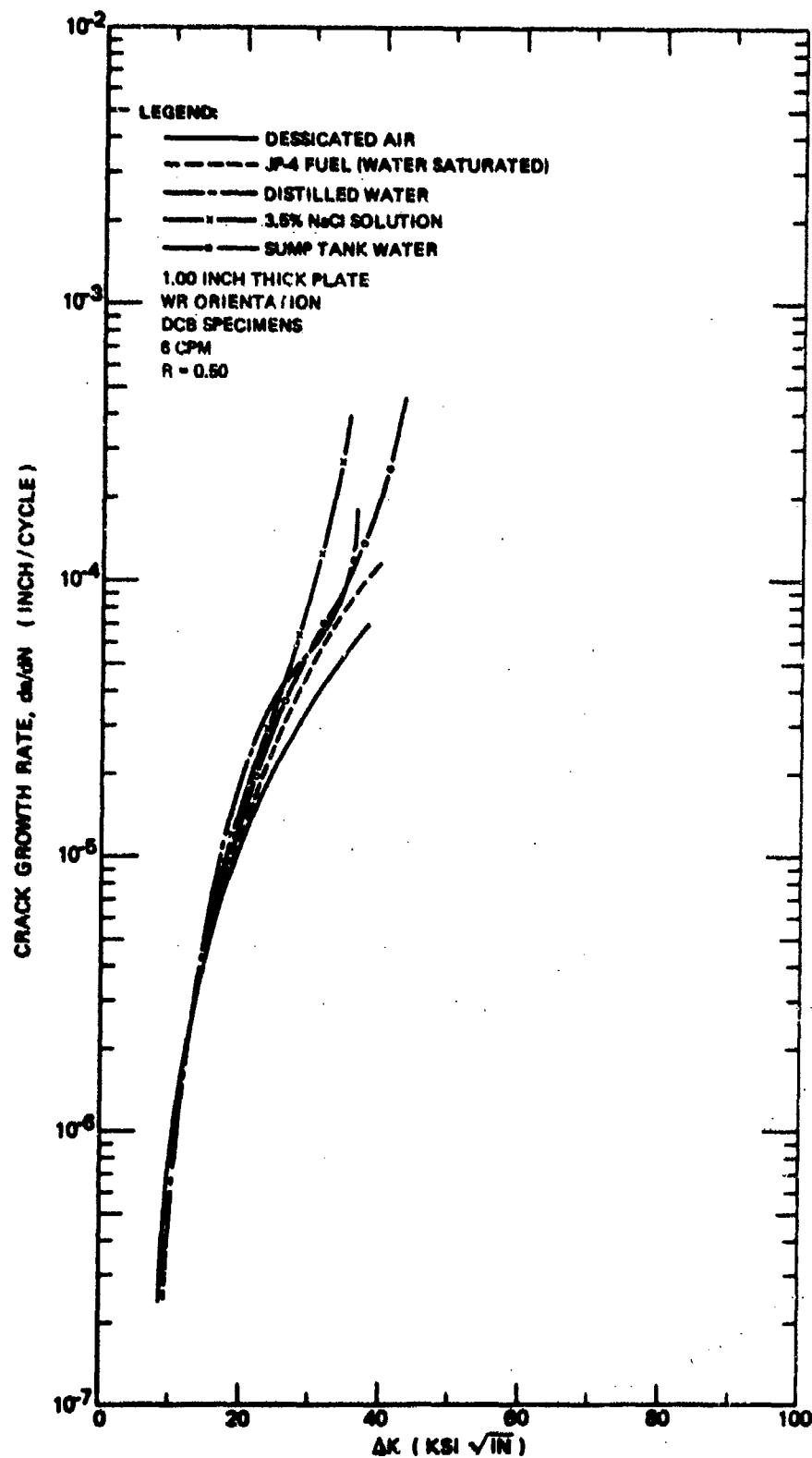


Figure 49: Effect of Environment on Fatigue Crack Growth Rates at $R = 0.50$ in 6Al-4V Standard ELI Beta Annealed Titanium Alloy (6 CPM)

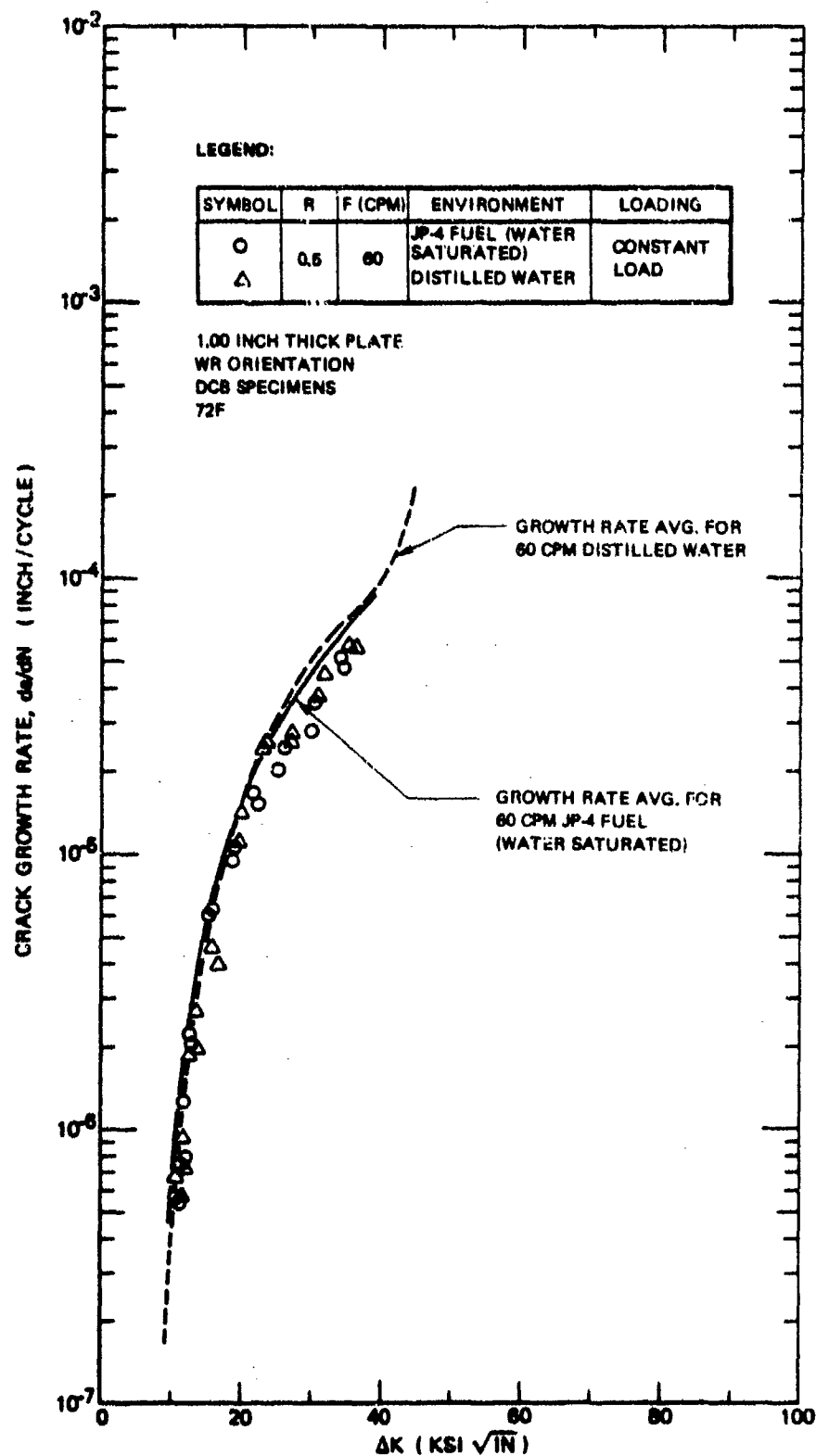


Figure 50: Fatigue Crack Growth Rates for 6Al-4V Standard ELI Beta Annealed Titanium Alloy in Alternating JP-4 Fuel and Distilled Water (60 CPM)

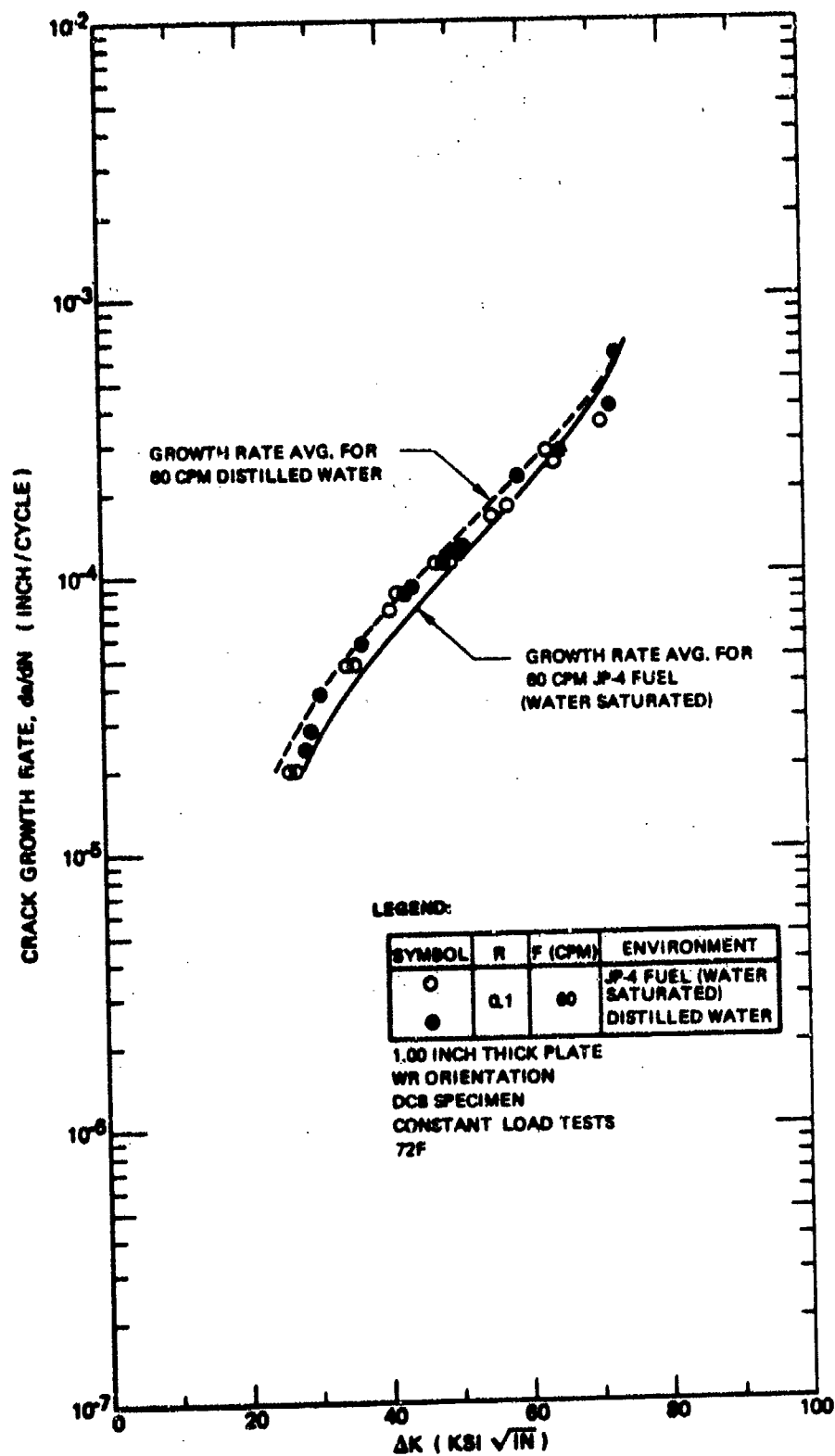


Figure 51: Fatigue Crack Growth Rates for 6Al-4V Standard ELI Beta Annealed Titanium at $R = 0.1$ in Alternating JP-4 Fuel and Distilled Water (60 CPM)

water saturated JP-4 fuel. All of the data for the alternating environment fall between or very close to the average crack growth rate curves for the individual components of the environment. Hence, alternating the test media had no effect on crack growth rate behavior of the Ti-6Al-4V beta annealed alloy.

A single 72F test was conducted in dye penetrant using a stress ratio of 0.5 and cyclic frequency of 6 cpm. The resulting data in Figure 52 show that type ZL-2A dye penetrant is equivalent to desiccated air in its effect on crack growth rate behavior.

A single 72F test was conducted in distilled water after the crack surfaces had been sprayed with the corrosion inhibitive compound LPS-3 and dried for 3 hours. The test involved a stress ratio of 0.5 and cyclic frequency of 60 cpm. The resulting data are plotted in Figure 53 where it is evident that the data fall close to the average crack growth rate curve for distilled water with no corrosion inhibitor. However, distilled water had only a very mild accelerative effect on fatigue crack growth rates relative to desiccated air and so the corrosion inhibitor would not be expected to have a large effect on crack growth rate behavior in distilled water.

Temperature

Corrosion fatigue tests were conducted at 175F in four environments to evaluate the effects of elevated temperatures on fatigue crack growth behavior of the Ti-6Al-4V beta annealed alloy. The crack growth rate data for all four test media are plotted in Figure 54. Average crack growth rate curves for both 3.5% NaCl solution and desiccated air at 72F are included for comparison. The comparison shows that an increase in temperature from 72F to 175F had little or no effect on crack propagation rates over the range of ΔK values tested. Since increase in temperature usually accelerates chemical reactions and decreases yield strength, it was anticipated that if a temperature increase from 72F to 175F had any effect on corrosion fatigue behavior, it would accelerate crack growth rates. However, data for the 3.5% NaCl solution indicates a decelerative effect of the temperature increase on crack growth rates. However, the apparent deceleration is probably due to data scatter since the magnitude of the effect is less than normal data scatter.

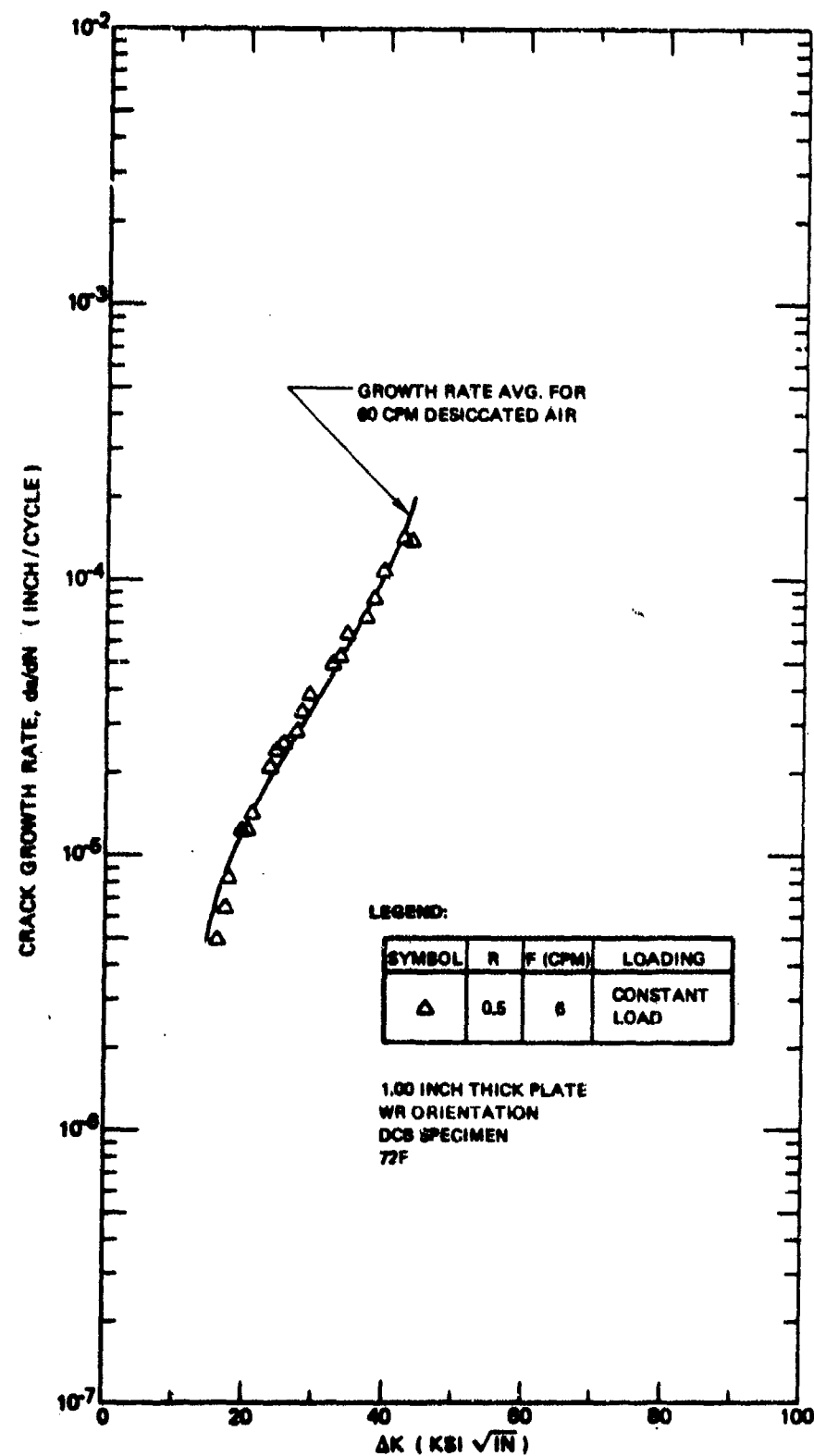


Figure 52: Fatigue Crack Growth Rates for 6Al-4V Standard ELI Beta Annealed Titanium Alloy in Dye Penetrant (Type ZL-2A, 60 CPM)

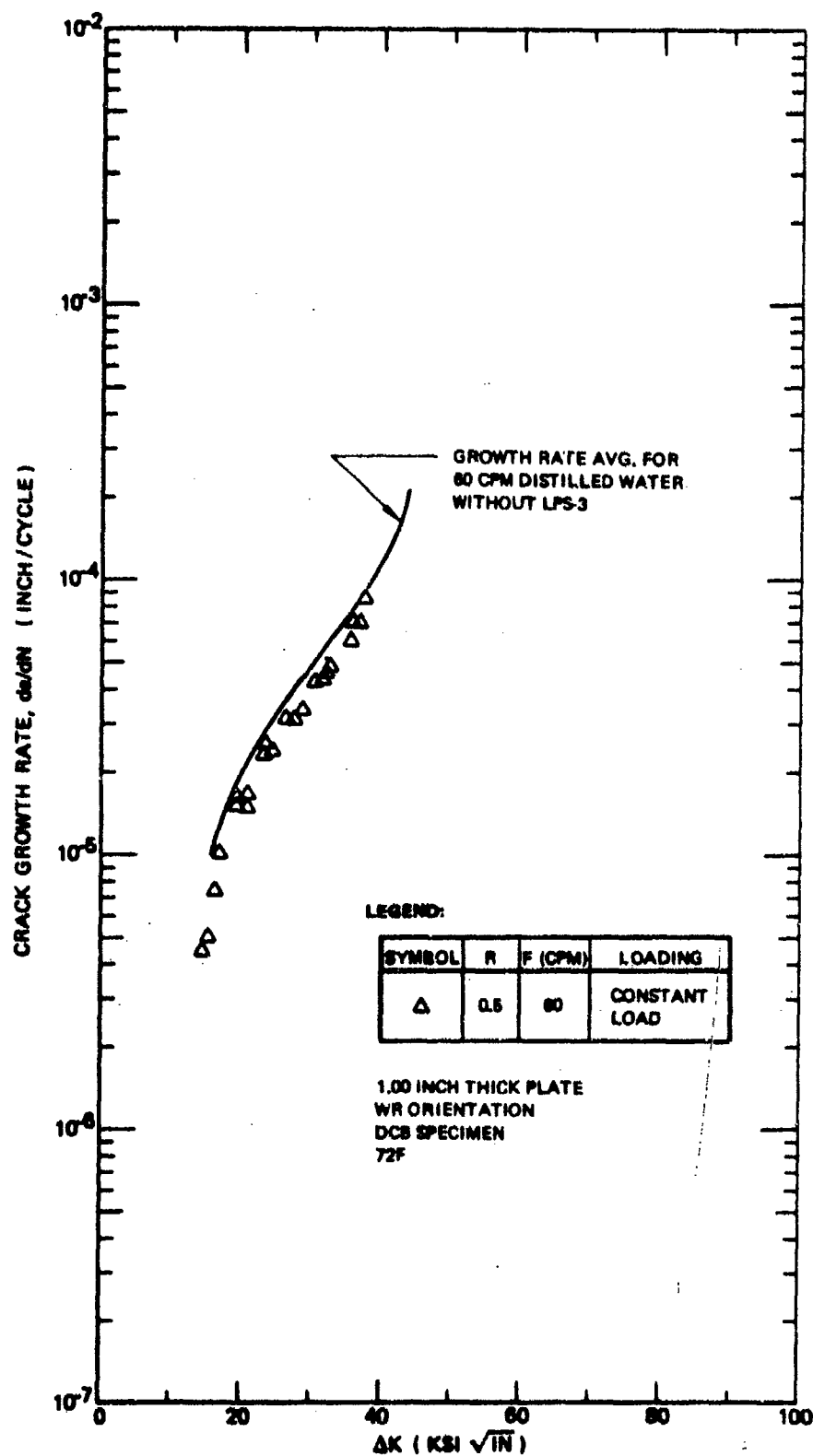


Figure 53: Fatigue Crack Growth Rates for 6Al-4V Standard ELI Beta Annealed Titanium Alloy in Distilled Water, Crack Surface Sprayed With LPS-3 and Dried for 3.0 Hours Prior to Immersion in Test Media (60 CPM)

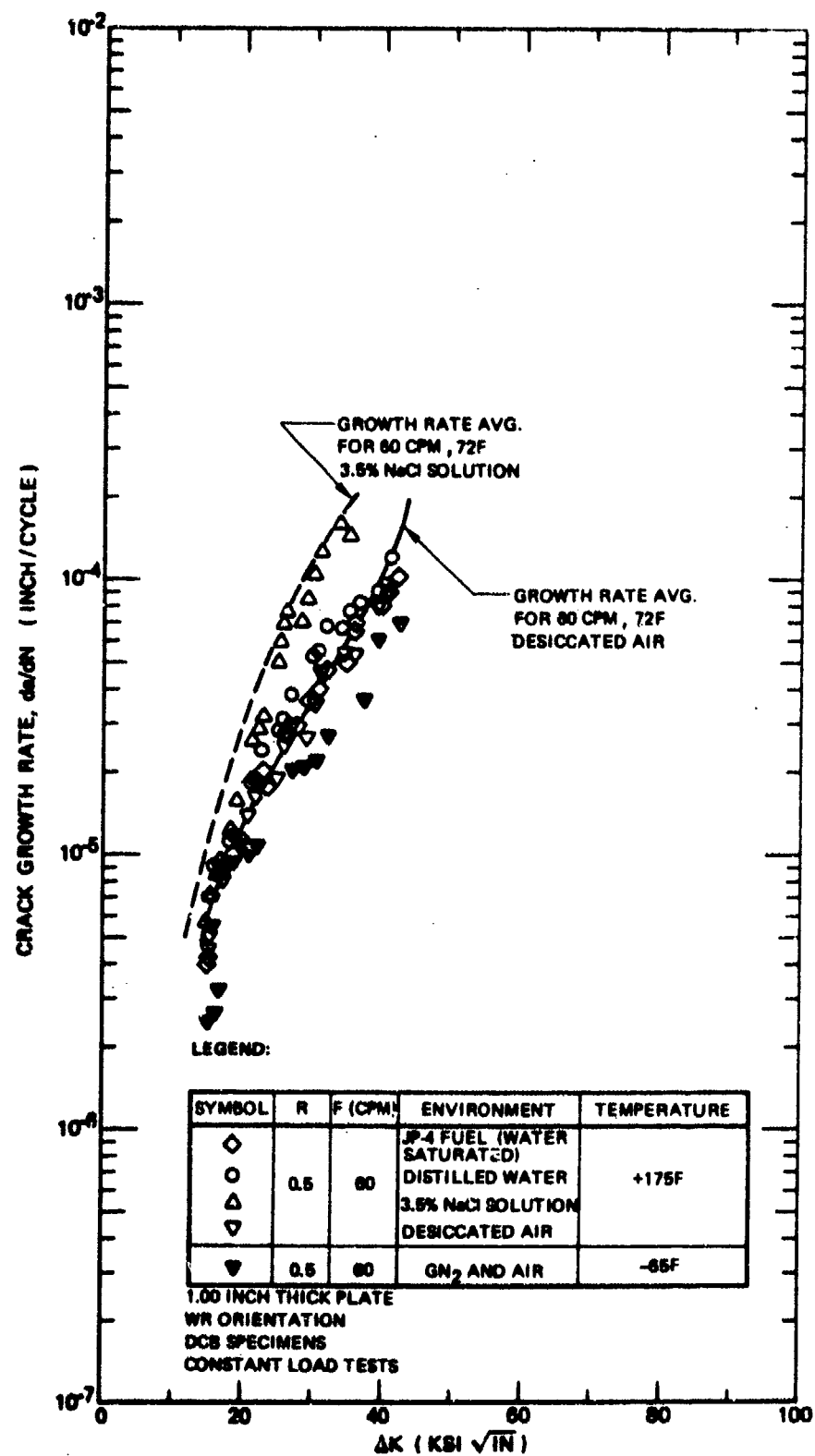


Figure 54: Fatigue Crack Growth Rates for 6Al-4V Standard ELI Beta Annealed Titanium Alloy at -65F and +175F (60 CPM)

Two tests were conducted at -65F in air to explore the effects of colder temperatures on fatigue crack growth rate behavior in the Ti-6Al-4V beta annealed alloy. The resulting crack growth rate data are plotted in Figure 54 along with the +175F data and average 72F crack growth rate curves for desiccated air and 3.5% NaCl solution. The decrease in temperature from +175 to -65F resulted in a modest deceleration in crack growth rates over the entire range of ΔK values tested. However, the differences between the +175 and -65F crack growth rates are less than those arising from normal data scatter.

3.2.2.2 Effect of Cyclic Frequency

A reduction in cyclic frequency from 60 to 6 cpm had little or no effect on fatigue crack growth rate behavior in three of the four media in which tests were conducted. Data for 6 cpm in desiccated air, distilled water, and JP-4 fuel are plotted in Figures 55, 56 and 57, respectively. Average crack growth rate curves drawn through the corresponding 60 cpm data are shown on the same figures for comparison. Close correspondence between the 6 and 60 cpm data was obtained in all three media. In 3.5% NaCl solution, cyclic frequency had a noticeable effect on fatigue crack growth rate behavior. The 6 cpm salt solution data are plotted in Figure 58 along with average crack growth rate curves for the 60 cpm data. There is a crossover between the 6 and 60 cpm crack growth rate curves at a crack growth rate of about 10^{-4} inches/cycle. For crack growth rates in excess of 10^{-4} inches/cycle, tests at 6 cpm yielded faster crack growth rates than did tests at 60 cpm. For lower crack growth rates, the opposite effect occurred. Reasons for the crossover in crack growth rates curves for 6 and 60 cpm are not immediately obvious. The data indicate that for crack growth rates in the range of primary interest, i.e., from 10^{-7} to 10^{-5} inches/cycle, cyclic frequencies within the range of interest for airframe components will not significantly influence corrosion fatigue crack growth behavior in Ti-6Al-4V beta annealed.

3.2.2.3 Effect of Specimen Type

Surface-flawed (SF) specimens were tested in both desiccated air and 3.5% NaCl solution using two different peak cyclic stress levels. The resulting crack growth rate data for the WT direction are plotted in Figure 59 along with

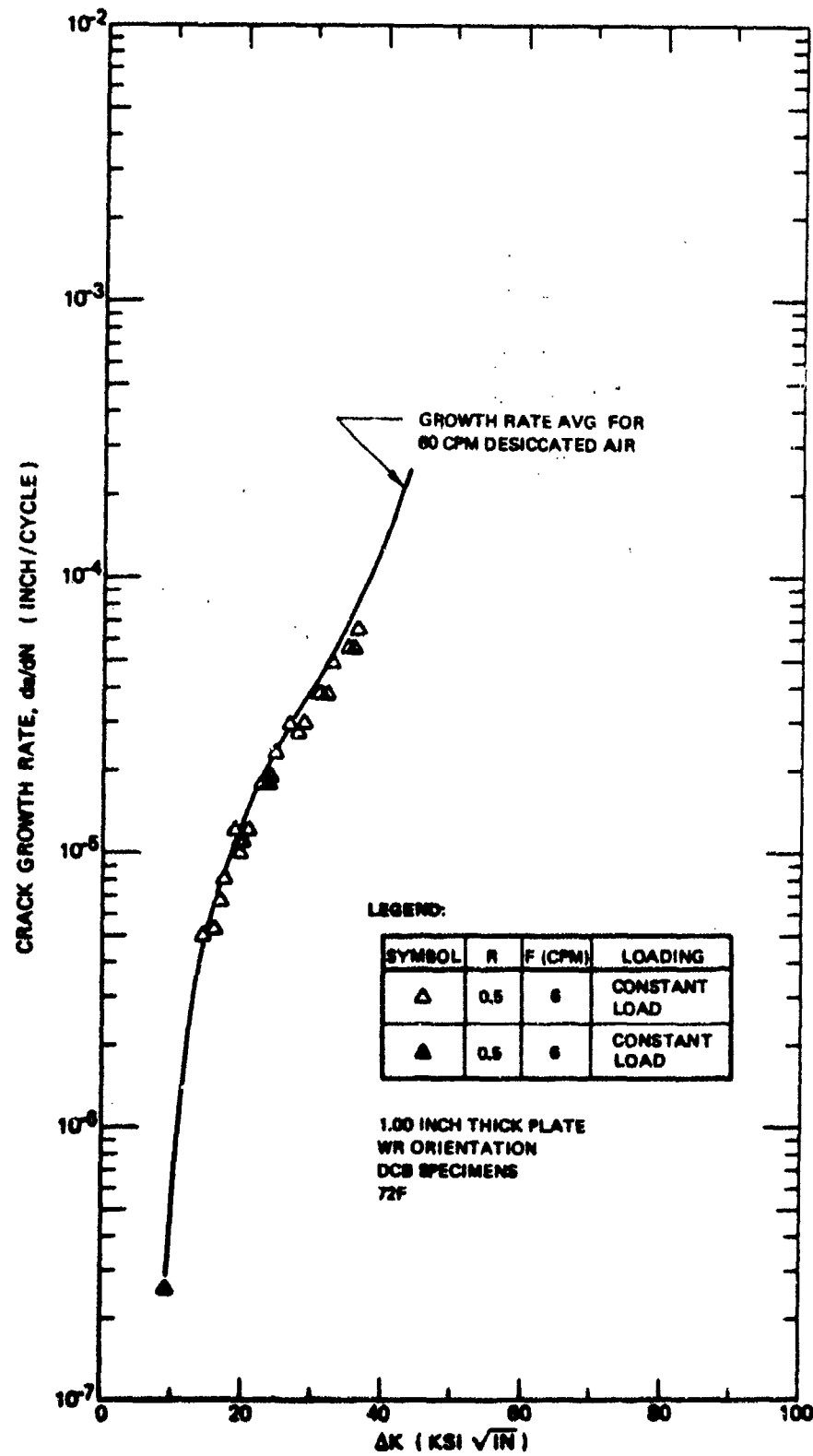


Figure 55: Fatigue Crack Growth Rates for 6Al-4V Standard ELI Beta Annealed Titanium Alloy in Desiccated Air (6 CPM)

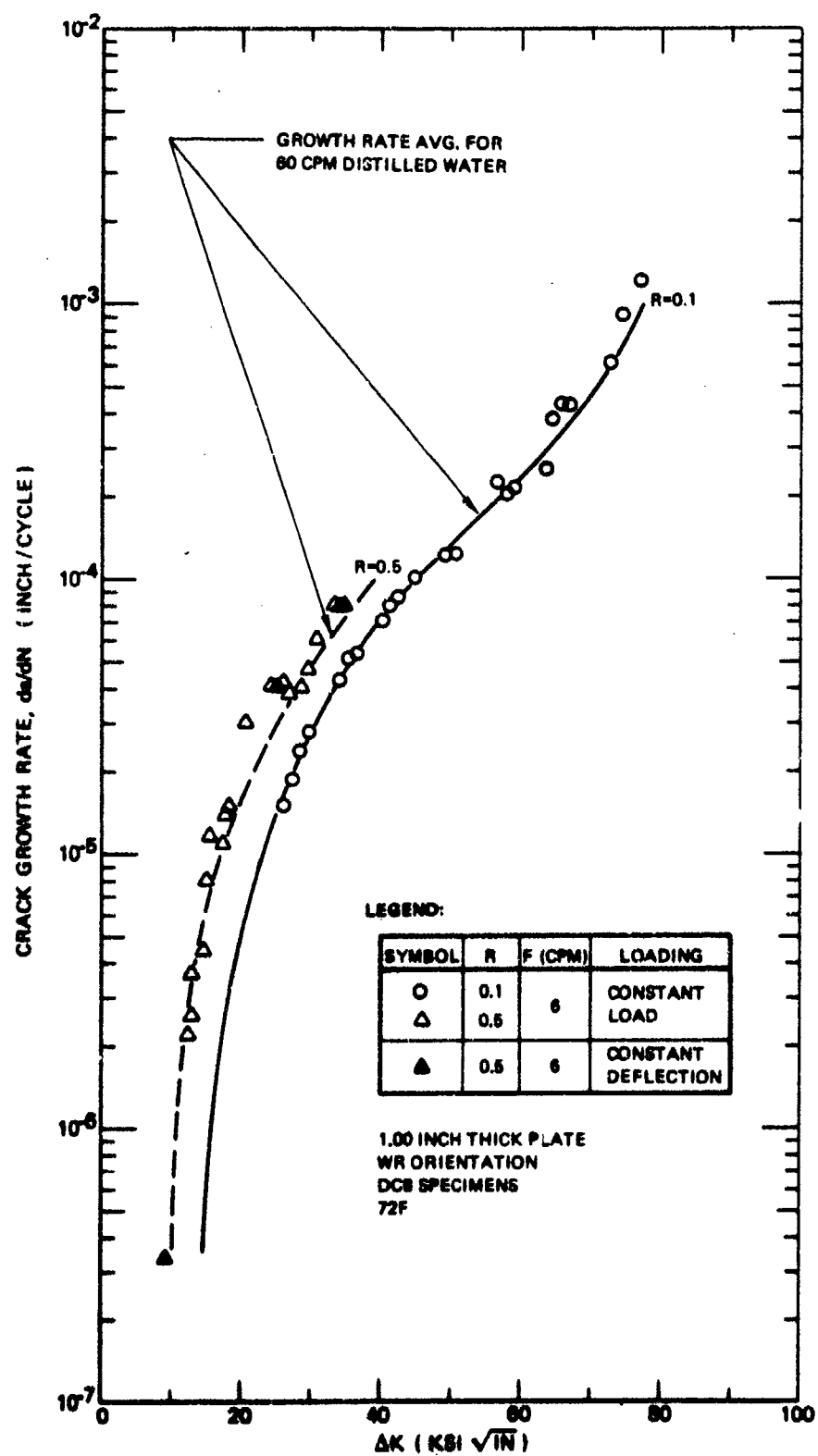


Figure 56: Fatigue Crack Growth Rates for 6Al-4V Standard ELI Beta Annealed Titanium Alloy in Distilled Water (6 CPM)

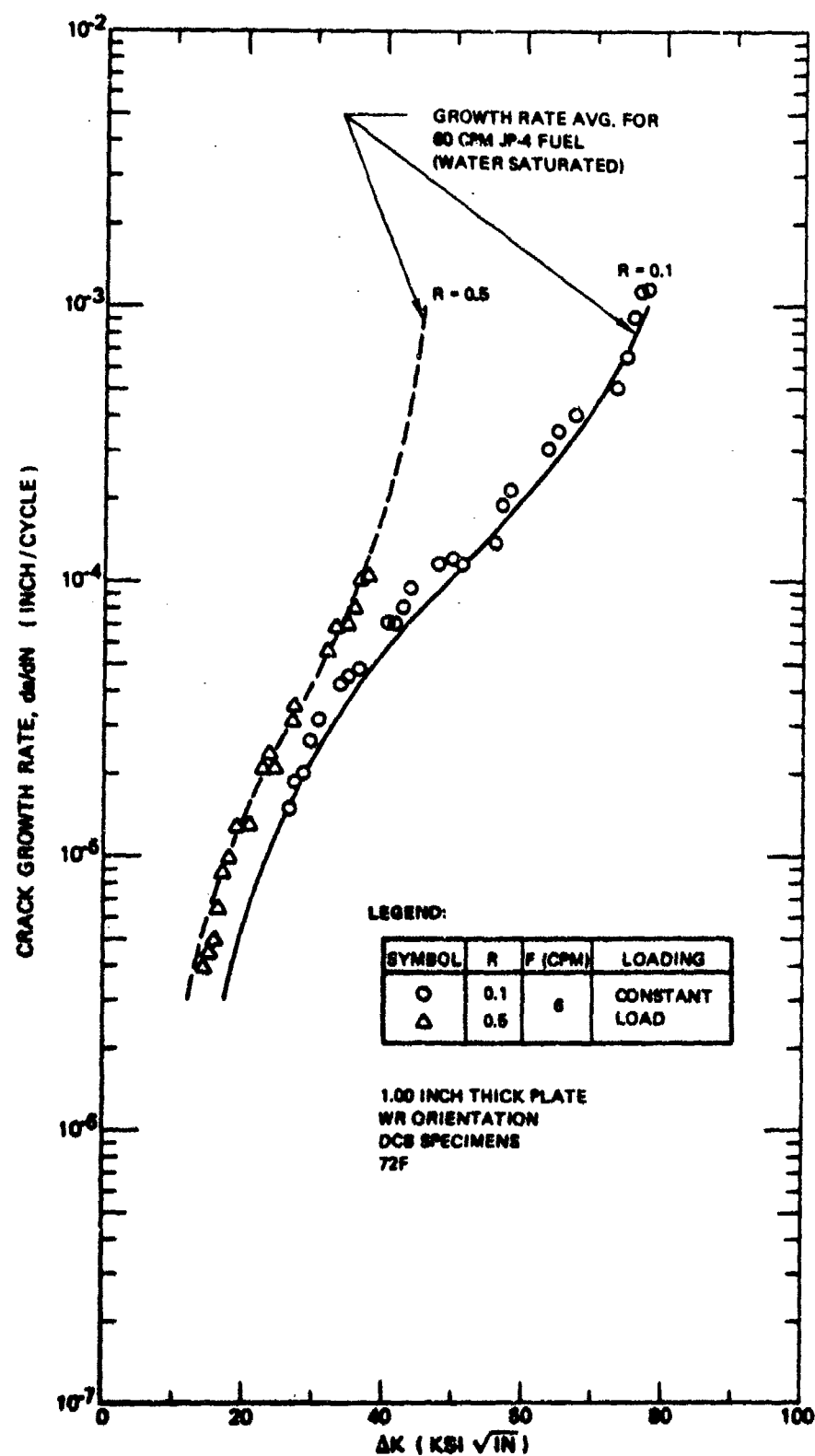


Figure 57: Fatigue Crack Growth Rates for 6Al-4V Standard ELI Beta Annealed Titanium Alloy in Water Saturated JP-4 Fuel (6 CPM)

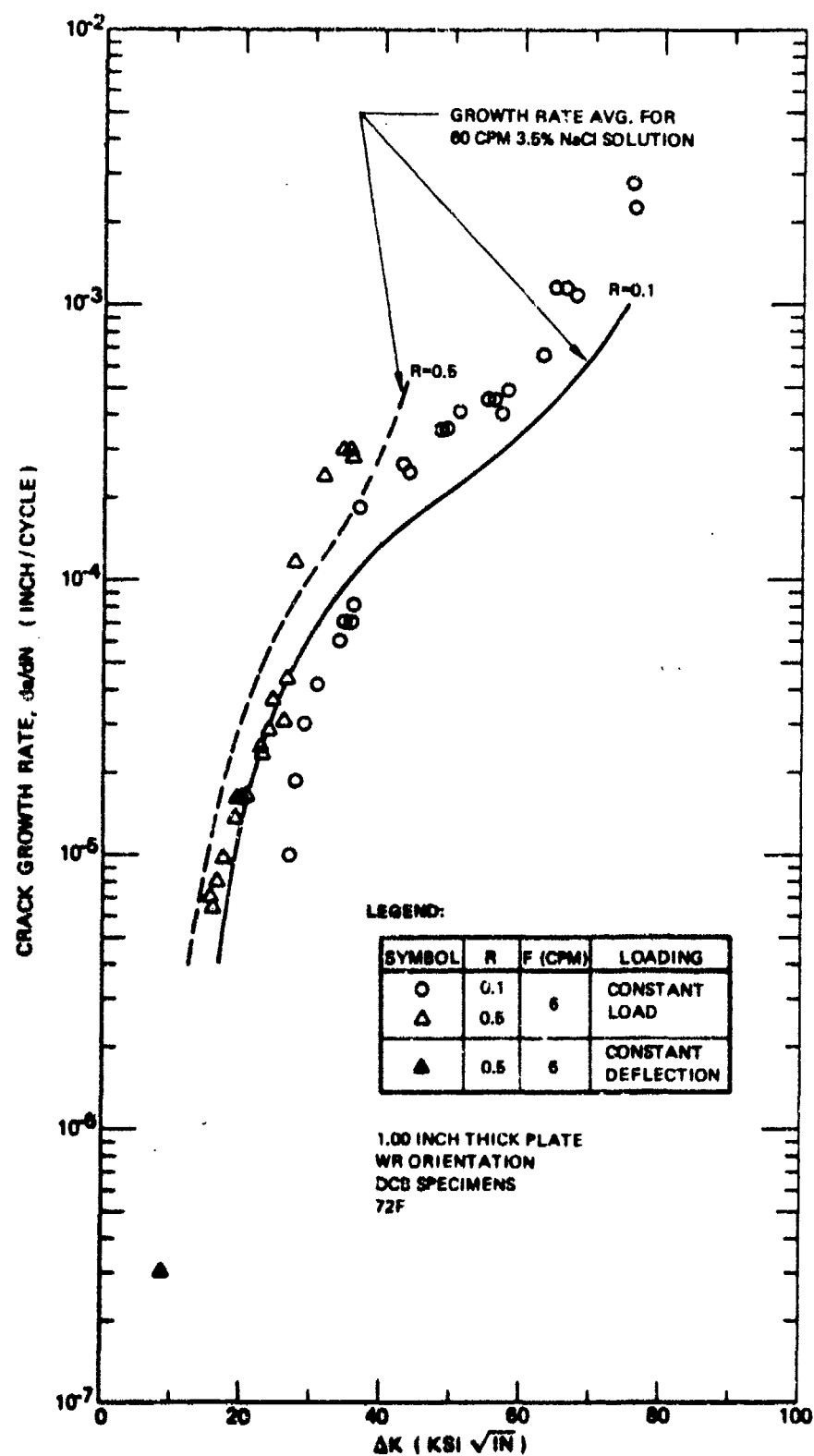


Figure 58: Fatigue Crack Growth Rates for 6Al-4V Standard ELI Data Annealed Titanium Alloy in 3.5% NaCl Solution (6 CPM)

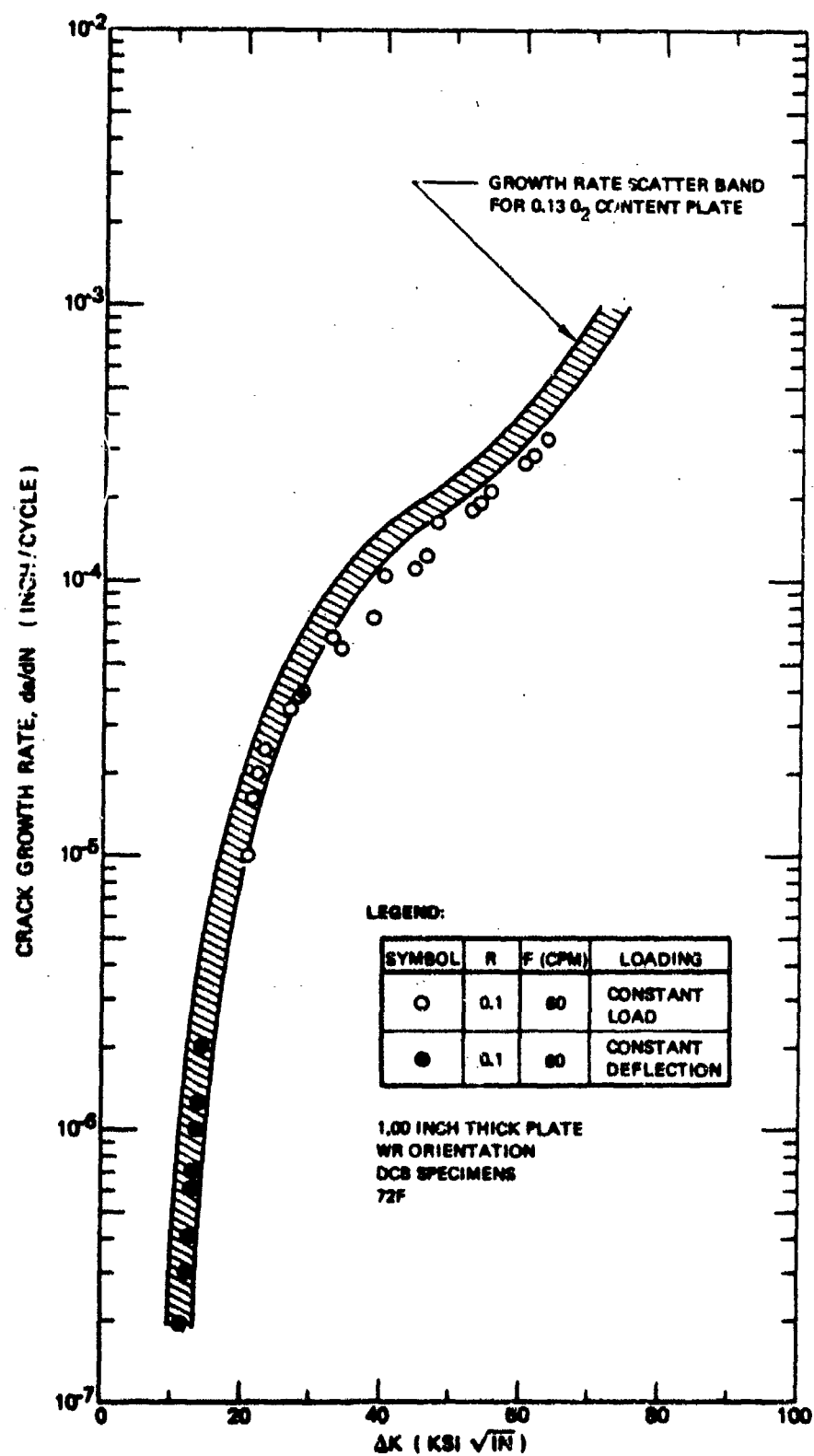


Figure 59: Fatigue Crack Growth Rates for "Super ELI" 6Al-4V Beta Annealed Titanium Alloy in 3.5% NaCl Solution (60 CPM)

average crack growth rate curves for the WR direction obtained from tests of DCB specimens. There is excellent agreement between all data for a given environment regardless of crack propagation directions or peak cyclic stress level.

3.2.2.4 Tests of Low O_2 (Super ELI) Material

Two corrosion fatigue tests were conducted in 3.5% NaCl solution using DCB specimens cut from the "super ELI" Ti-6Al-4V BA plate described in Section 2.1.3. Oxygen content of the "super ELI" plate was 0.06% as compared to 0.13% for the standard ELI Ti-6Al-4V BA plate tested in this program, and K_{ISCC} values for the super and standard ELI plates were 87 and 69 $ksi\sqrt{in}$, respectively. The intent of the tests was to measure the effect of O_2 content on fatigue crack growth rates in an aggressive environment.

Crack growth rate data for the super ELI plate are plotted in Figure 60. The scatterband of comparable data for the standard ELI plate are also shown in the same figure. Any differences between crack growth rate data for the two materials were sufficiently small to be considered insignificant.

It had been hoped that the mechanism lending to increased SCC resistance with decreased oxygen content would also lead to similar increases in corrosion fatigue crack growth resistance. However, even though the apparent K_{ISCC} value was higher for the super ELI plate, the corrosion fatigue resistance for both the super and standard ELI grade plates was essentially identical.

The results described above need to be verified before any conclusions with regard to the effect of oxygen content on corrosion fatigue crack growth resistance can be drawn. Chemistry and K_{ISCC} measurements for the super ELI specimens tested in this program were made at locations in the parent plate different from the area from which the test specimens were cut. Hence, chemistry variations within the parent plate could have led to less favorable chemistry in the test samples than was thought to exist.

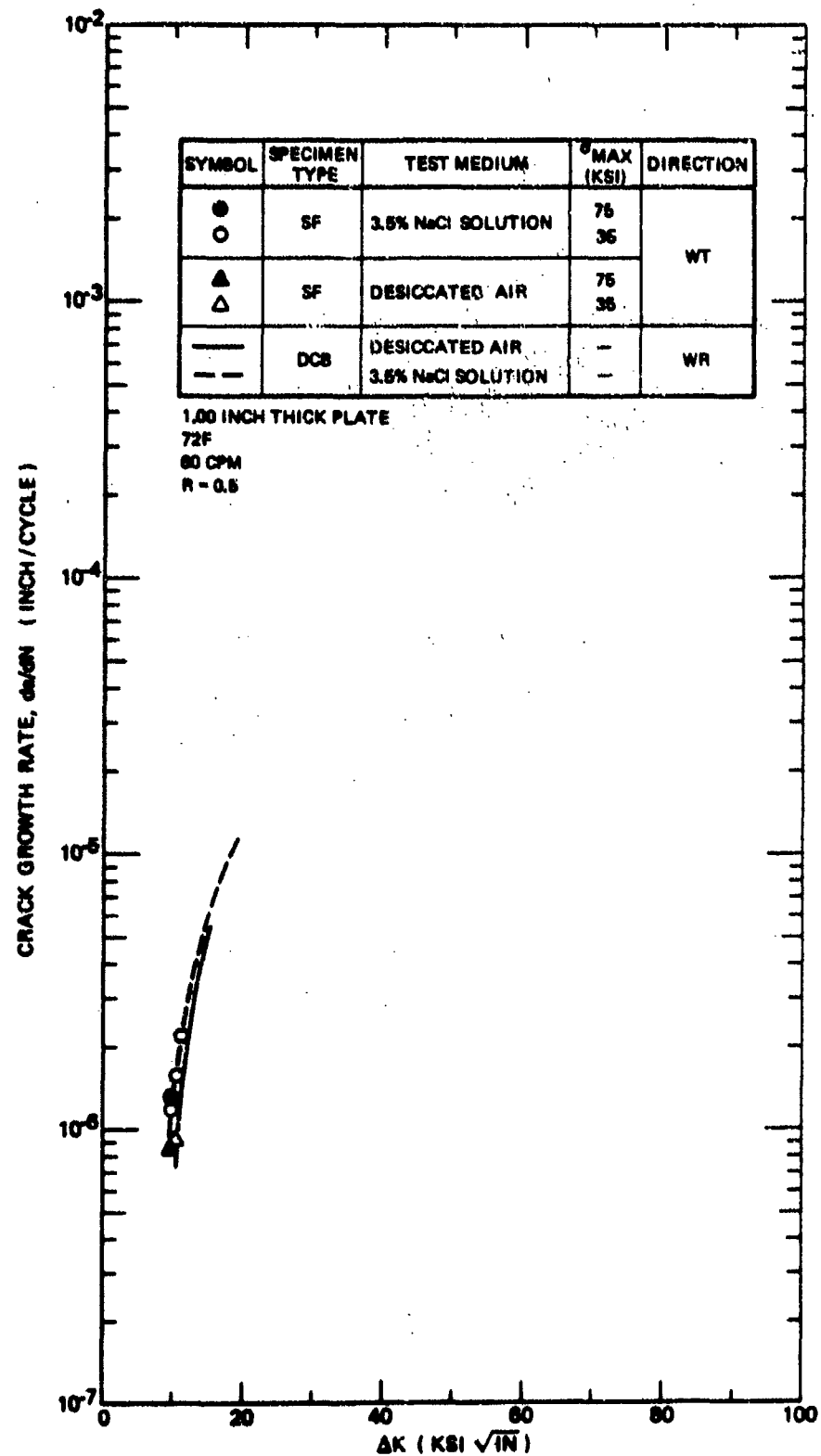


Figure 60: Fatigue Crack Growth Rate Data for 6Al-4V Standard ELI Beta Annealed Titanium Alloy Surface Flawed Specimens (60 CPM)

3.3 Titanium Alloy 6Al-4V Recrystallize Annealed

The test program for the Ti-6Al-4V RA alloy is summarized in Table 13. Mechanical property and fracture toughness data are reported in Section 2.1 Results of the stress corrosion cracking, corrosion fatigue and thermal processing effect tests are described in this section.

3.3.1 Stress Corrosion Cracking Tests

Five stress corrosion cracking tests were conducted including one test in each of the 72F environments of low humidity air, distilled water, water saturated JP-4 fuel, sump tank water, and 3.5% NaCl solution. Double cantilever beam specimens (Figure B7) were used to conduct the tests. Specimens were loaded to a constant deflection with the crack tip submerged in the test media, and were then placed in the required test media within enclosed chambers. Test results are summarized in Table 14. Periodic observations of crack length over a period of 325 hours showed that no SCC occurred in low humidity air, distilled water or water saturated JP-4 fuel. In both the sump tank water and 3.5% NaCl solutions, stress corrosion cracking initiated at the outset of the test and proceeded at a uniform rate of about one inch per hour until crack growth abruptly stopped. The amounts of SCC observed in the sump tank water and 3.5% NaCl solutions were 0.69 and 0.78 inches, respectively. The calculated K_{ISCC} values were 45 and 61 $\text{ksi}\sqrt{\text{in}}$ for the 3.5% NaCl solution and sump tank water media, respectively. The K_{ISCC} values are 48 and 65 percent of the 72F fracture toughness, respectively.

3.3.2 Corrosion Fatigue Tests

Major test variables included environment, cyclic frequency, thermal processing, and stress rates. A limited number of tests were conducted to evaluate the effects of specimen configuration on crack growth rates. The effects of environment, cyclic frequency, thermal processing, and specimen type on corrosion fatigue crack growth rates are described and discussed in this section. Results of a limited number of crack closure measurements are also included in this section. Stress ratio effects are described in Section 4.6.

Table 13: Test Program for Ti-6Al-4V Recrystallize Annealed

TEST TYPE	SPECIMEN TYPE	CYCLIC FREQUENCY	STRESS RATIO	ENVIRONMENT																				
				AIR			DISTILLED WATER			3.5% NaCl SOLUTION			JP-4			SUMP TANK			JP-4 + H ₂ O			DYE PEN		
				-65F	72F	175F	-65F	72F	175F	-65F	72F	175F	-65F	72F	175F	-65F	72F	175F	-65F	72F	175F			
MECHANICAL PROPERTY	TENS.			4	14	4																		
FRACTURE TOUGHNESS	CT			2	14	2																		
	SF			2	2	2																		
STRESS CORROSION CRACKING	DCB			2			4			10	4		2				2			4			4	
	SF			1						1												1		
CORROSION FATIGUE	DCB	60	0.1	4			1			7	1		1			2							2	
			0.5	2	2	2	2	1		2	1		2	1		2			2					
			0.8	1						1														
	DCB	6	0.1	1			1			1			1										2	
OVERLOAD	SF	60	0.5	2						2														
	TDCB	60	0.5	2						2														

Table 14: SCC Test Results for Ti-6Al-4V Recrystallize Annealed Plate (WR Direction)

SPECIMEN	TEST ENVIRONMENT		INITIAL APPLIED K KSI $\sqrt{\text{IN.}}$	INITIAL CRACK LENGTH (IN.)	FINAL CRACK LENGTH (IN.)	FINAL K KSI $\sqrt{\text{IN.}}$
	MEDIUM	TEMP (°F)				
NTSC-4	AIR	72	88.9	2.00	2.00	88.9
NTSC-8	DISTILLED WATER	72	85.9	2.00	2.00	85.9
NTSC-5	JP-4 FUEL	72	84.8	2.00	2.00	84.8
NTSC-6	SUMP TANK WATER	72	85.5	2.00	2.69	60.6
NTSC-7	3.5% NaCl SOLUTION	72	66.0	2.00	2.78	45.0

NOTE: ALL TEST DURATIONS WERE 325 HOURS

All data collected from corrosion fatigue tests of the Ti-6Al-4V RA alloy are included in Figures A33 through A49 in Appendix A. In the body of this report all of the data are not shown. In some cases, average crack growth rate curves are used to represent the data and to illustrate specific effects.

3.3.2.1 Effect of Test Environment

Test Media

The effect of the five primary test media on fatigue crack growth rate behavior is illustrated in Figures 61 through 65. The least aggressive test media were desiccated air and water saturated JP-4 fuel, both of which yielded identical results. The most aggressive media were 3.5% NaCl solution and sump tank water, both of which yielded identical curves up to ΔK values of $24 \text{ ksi}\sqrt{\text{in}}$; at higher ΔK values, the 3.5% NaCl solution resulted in larger crack growth rates than did the sump tank water. Distilled water resulted in a modest acceleration in crack growth rates relative to the air and fuel media. This ratio of maximum to minimum crack growth rates for given ΔK values was relatively constant over the entire range of ΔK values tested and ranged from about 2 at the highest ΔK values to 3 at the lowest ΔK values.

The two potential models of the "worst" environments for airframe components, namely sump tank water and 3.5% NaCl solution, yielded essentially identical crack growth rates over the range of rates believed to be of primary importance to crack propagation life calculations for airframe components, i.e., 10^{-7} to 10^{-5} inches/cycle. The deviation between crack growth rates in the two media occurred when peak stress intensity factors during the loading cycles reached a value of $24 \text{ ksi}\sqrt{\text{in}}$. This value of stress intensity factor is about one-half the K_{ISCC} value measured in 3.5% NaCl solution. The relative behavior of the RA processed alloy in the sump tank and salt water media was different from that for the beta processed alloy in that the latter alloy yielded faster crack growth in 3.5% NaCl solution over the entire range of ΔK values tested. This behavioral difference could not be predicted on the basis of the SCC test results.

Five tests were conducted in an alternating distilled water and JP-4 fuel environment at 72F. The resulting data are plotted in Figure 66 along with comparable average crack growth rate curves for both distilled water and water saturated JP-4

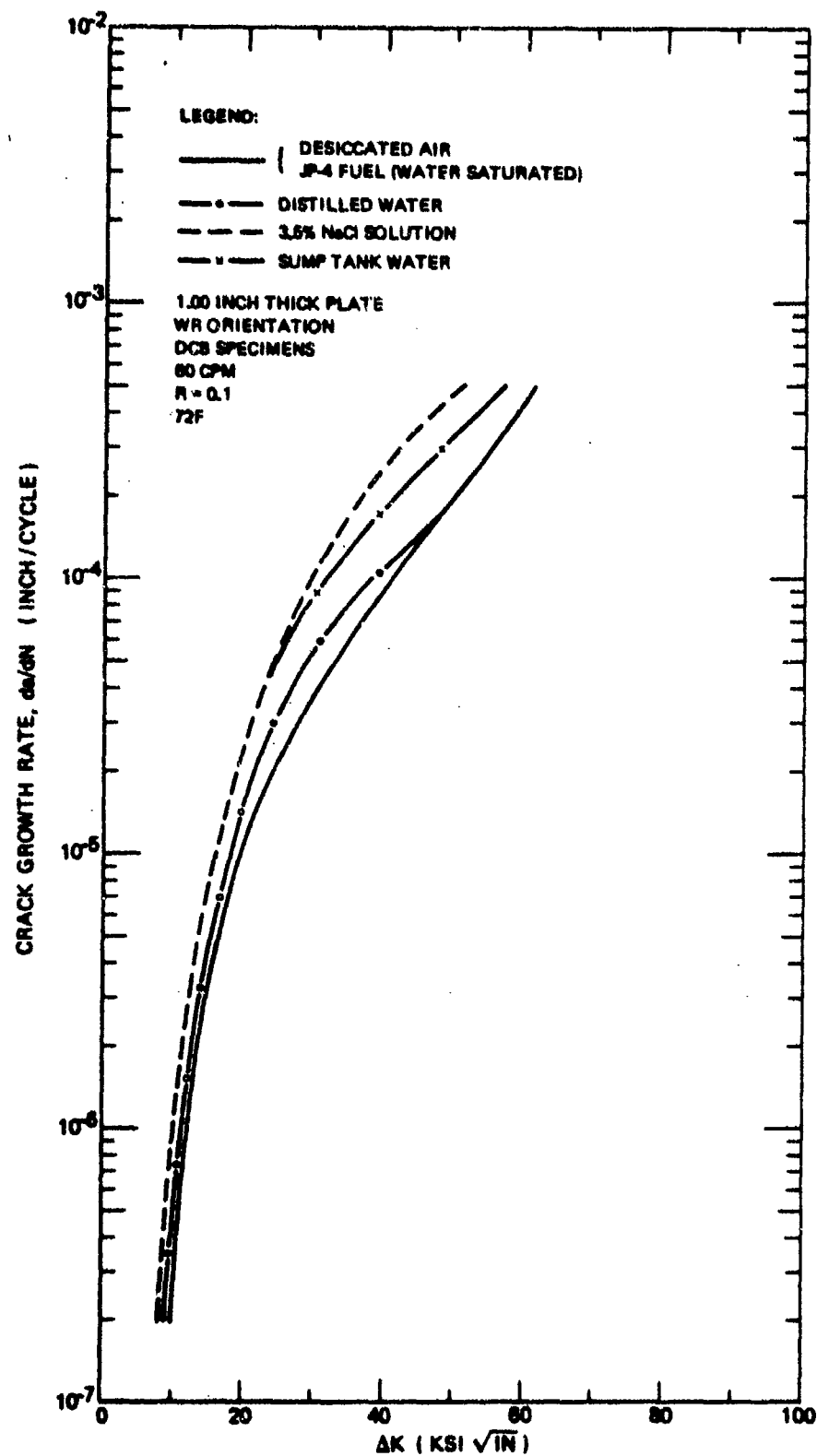


Figure 61: Effect of Environment on Fatigue Crack Growth Rates at $R=0.1$ in 6Al-4V Recrystallize Annealed Titanium Alloy (60 CPM)

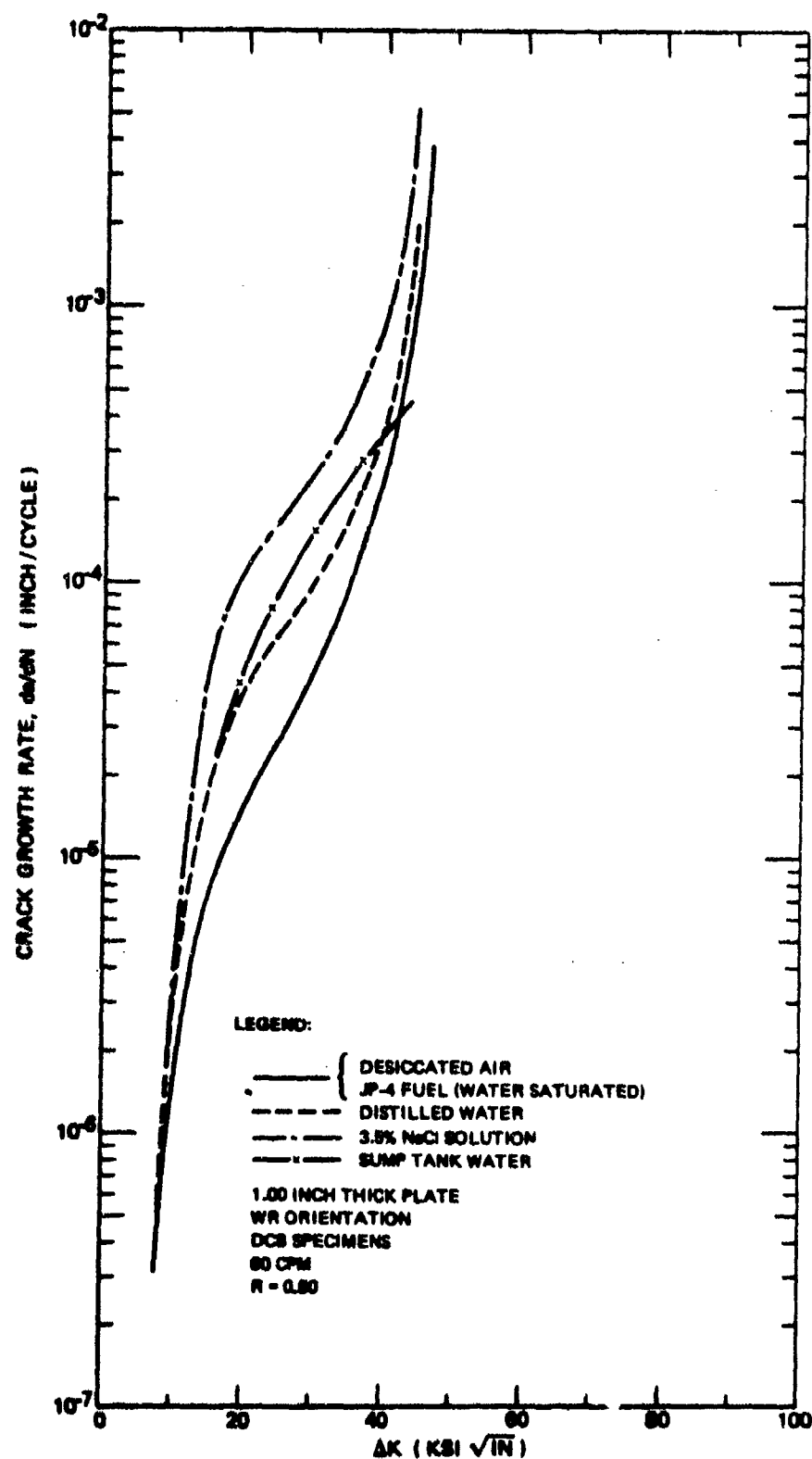


Figure 62: Effect of Environment on Fatigue Crack Growth Rates at $R = 0.50$ in 6Al-4V Recrystallized Annealed Titanium Alloy (60 CPM)

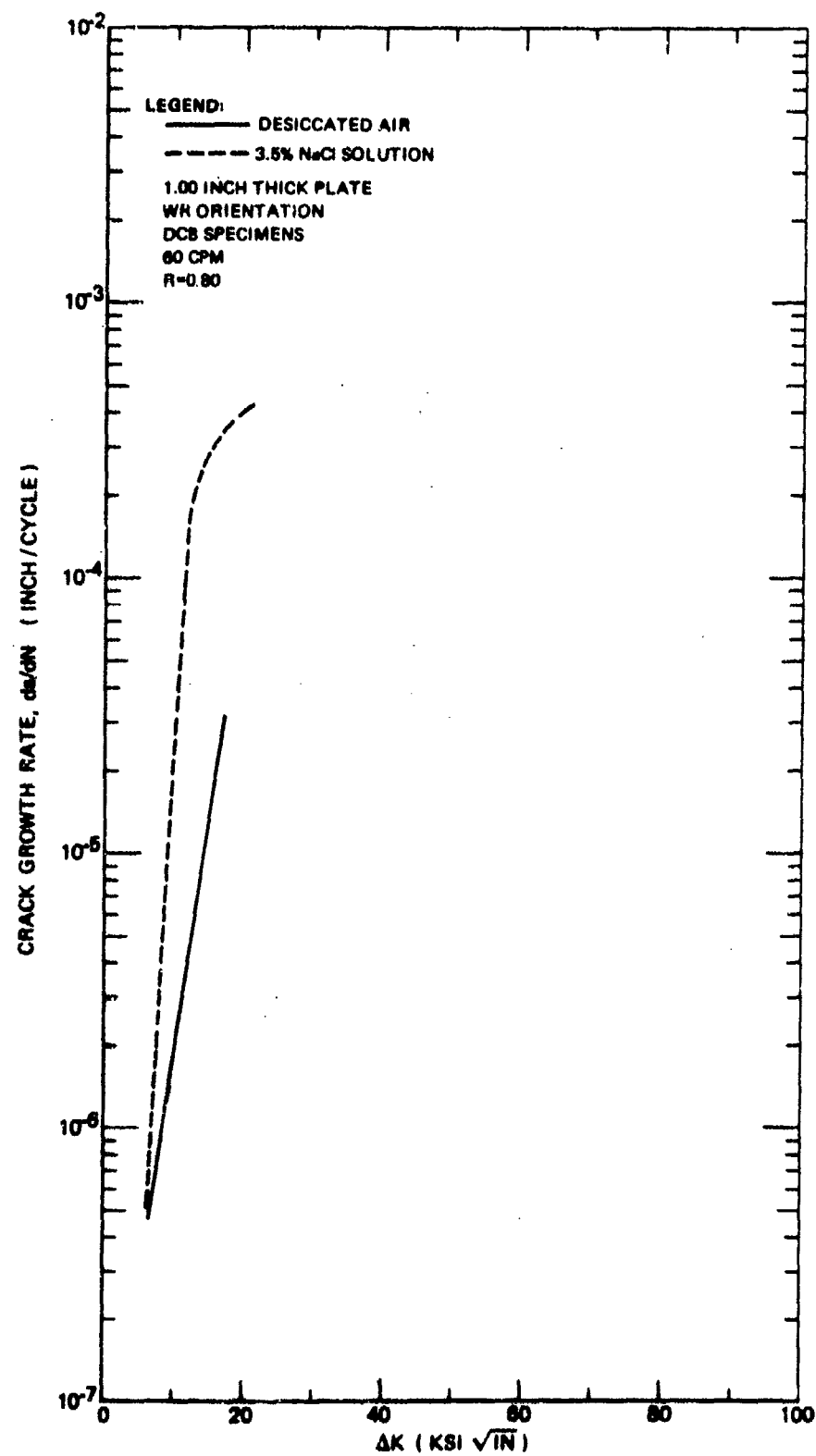


Figure 63: Effect of Environment on Fatigue Crack Growth Rates at $R = 0.50$ for 6Al-4V Recrystallized Annealed Titanium Alloy (60 CPM)

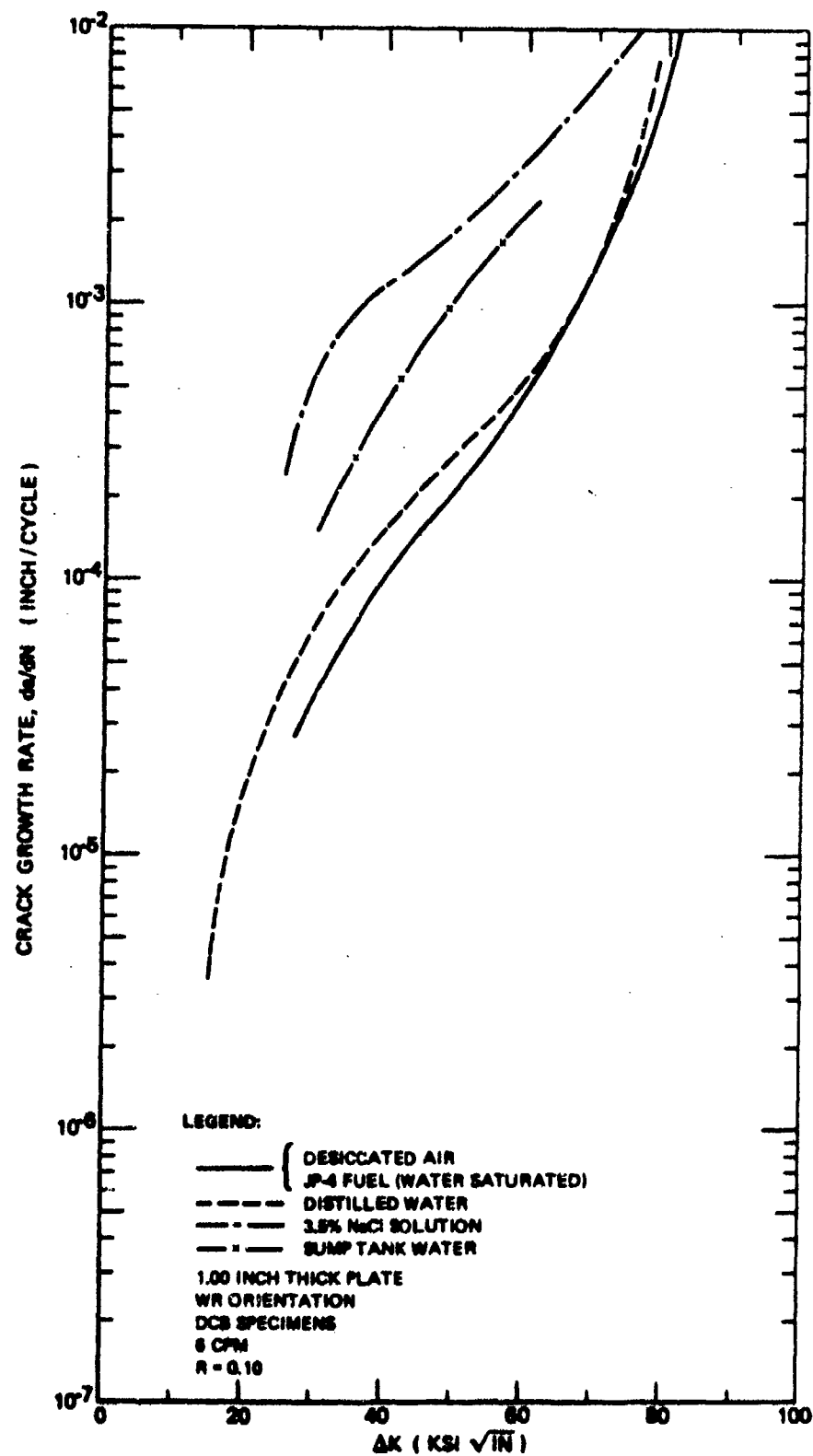


Figure 64: Effect of Environment on Fatigue Crack Growth Rates at $R = 0.10$ in 6Al-4V Recrystallized Annealed Titanium Alloy (6 CPM)

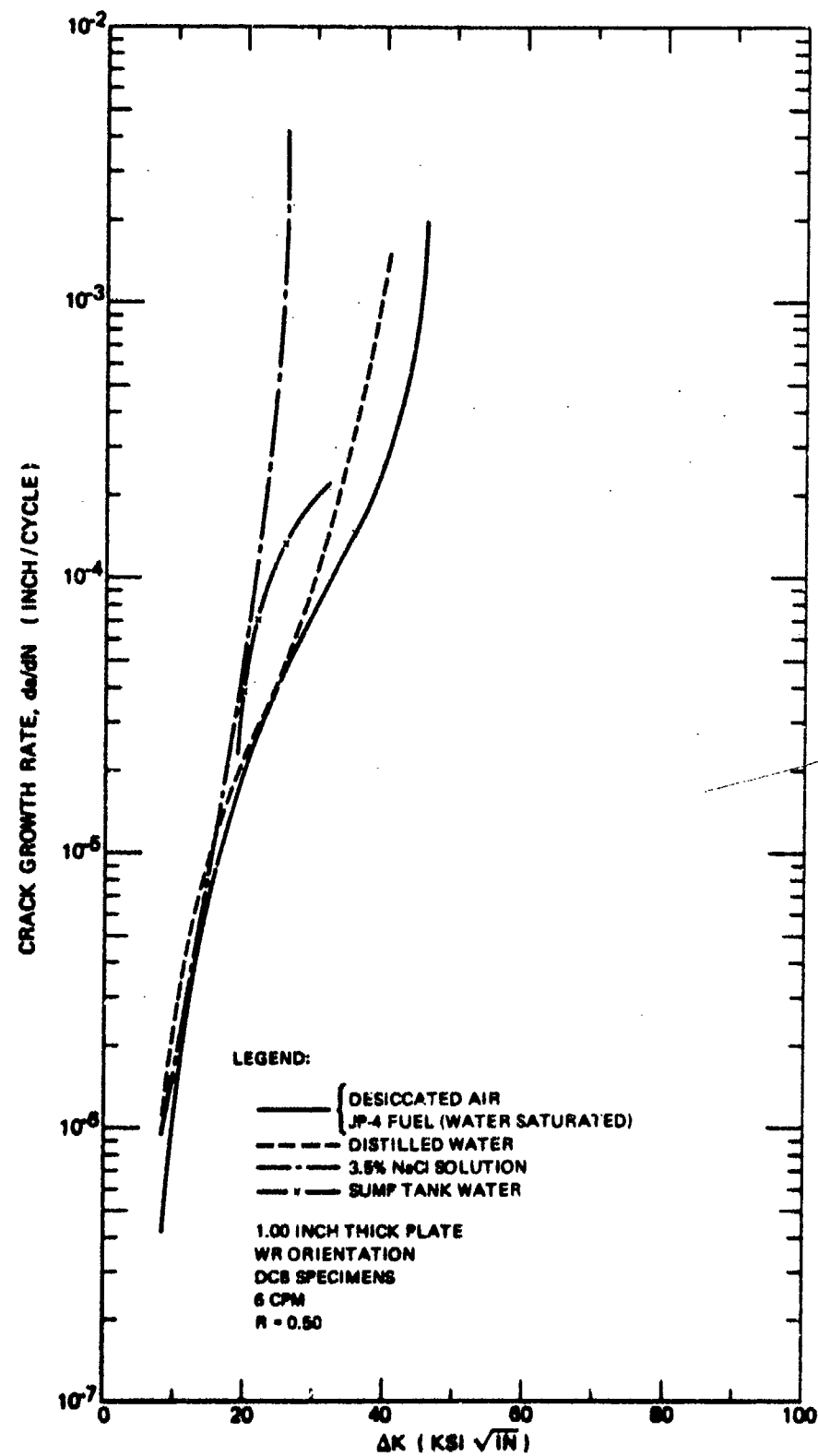


Figure 65: Effect of Environment on Fatigue Crack Growth Rates at $R = 0.50$ in 6Al-4V Recrystallized Annealed Titanium Alloy (6 CPM)

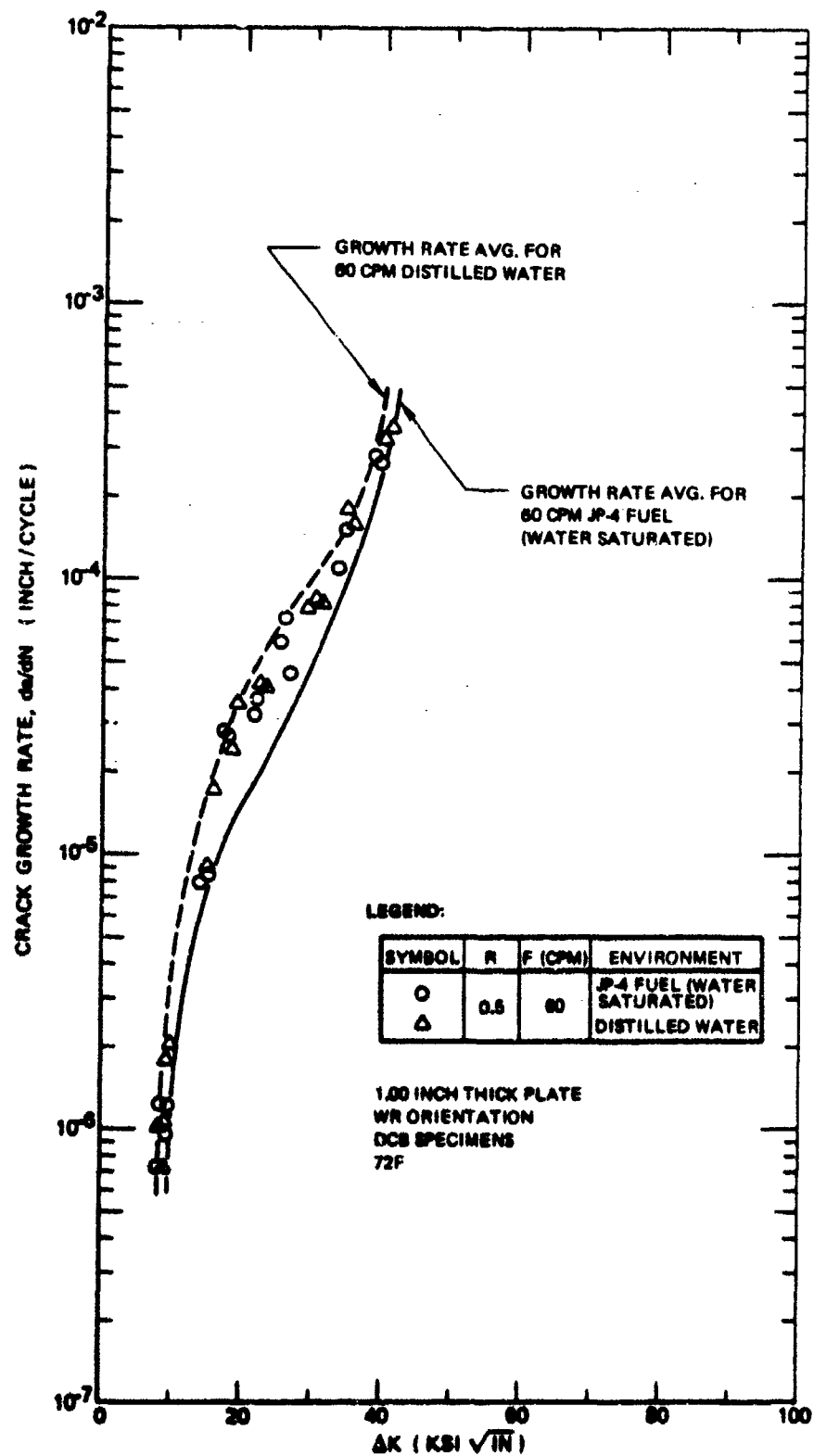


Figure 66: Fatigue Crack Growth Rates for 6Al-4V Recrystallized Annealed Titanium Alloy in Alternating JP-4 Distilled Water (60 CPM)

fuel. All of the data for the alternating environment fall on or between the average crack growth rate curves for the individual components of the alternating environment. This result is identical to that obtained from tests of the other primary alloys in the alternating environment.

Three 72F tests were conducted in type ZL-2A dye penetrant using a stress ratio of 0.5 and cyclic frequencies of both 6 and 60 cpm. The resulting data are plotted in Figure 67 where it can be seen that cyclic frequency had no effect on crack growth rates and that the dye penetrant was equivalent to the least aggressive environments tested in this program (desiccated air and JP-4 fuel) in its effect on fatigue crack growth rates.

Two tests were conducted in distilled water after the crack surfaces had been sprayed with the corrosion inhibitive compound LPS-3 and dried for 3.0 hours. Tests were conducted at 72F using stress ratios of both 0.1 and 0.5. The resulting crack growth rate data are plotted in Figure 68 along with corresponding average crack growth rate curves for distilled water with no corrosion inhibitor. The data for specimens that were treated with the corrosion inhibitor fall below the average curves and are equivalent to the crack growth rate data obtained from tests in desiccated air. This result is indicative of a beneficial effect on crack growth rates of the corrosion inhibitor. However, previously discussed results for the 7075-T651 aluminum and Ti-6Al-4V beta annealed alloys showed no effect of the corrosion inhibitor or crack growth rate behavior in distilled water. This knowledge combined with the fact that the apparent effect of LPS-3 in Figure 68 is small leads to the speculation that the apparent effect may be due to data scatter rather than the LPS-3.

Temperature

Corrosion fatigue tests were conducted at 175F in four media to evaluate the effects of elevated temperatures on fatigue crack growth behavior of the Ti-6Al-4V RA alloy. The resulting crack growth rate data for all four media are plotted in Figure 69 along with average crack growth rate curves resulting from comparable tests at 72F. In all but the 3.5% NaCl solution, the data for 175F tests fall on or below the 72F crack growth rate curves. In the 3.5% NaCl solution, there was considerable scatter in the data, but the majority of data points fell significantly above the 72F crack growth rate curve; the trend of the

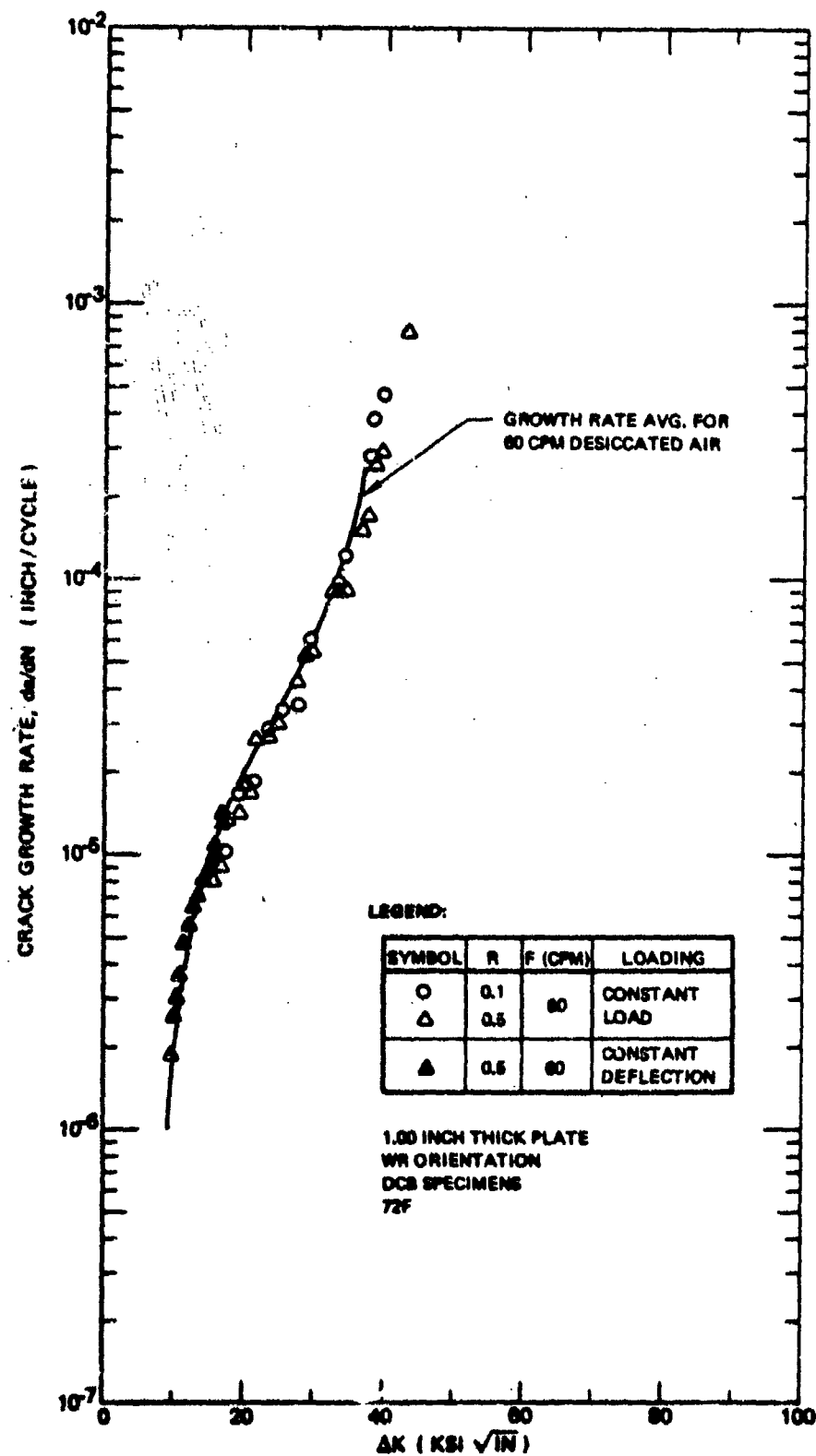


Figure 67: Fatigue Crack Growth Rates for 6Al-4V Recrystallized Annealed Titanium Alloy in Dye Penetrant (Type ZL-2A, 60 CPM)

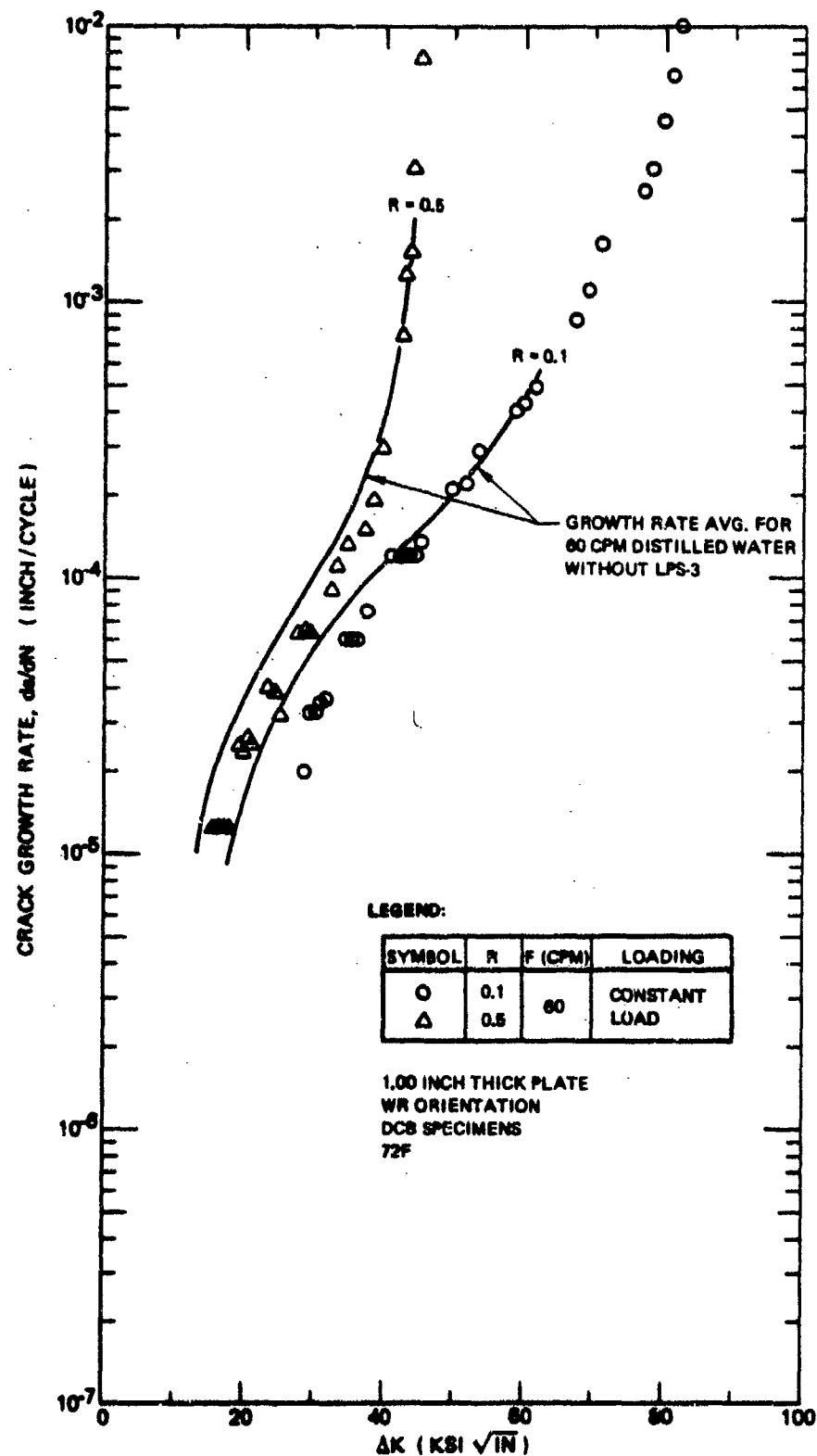


Figure 68: Fatigue Crack Growth Rates for 6Al-4V Recrystallize Annealed Titanium Alloy in Distilled Water, Crack Surfaces Sprayed With LPS-3 and Dried for 3.0 Hours (60 CPM)

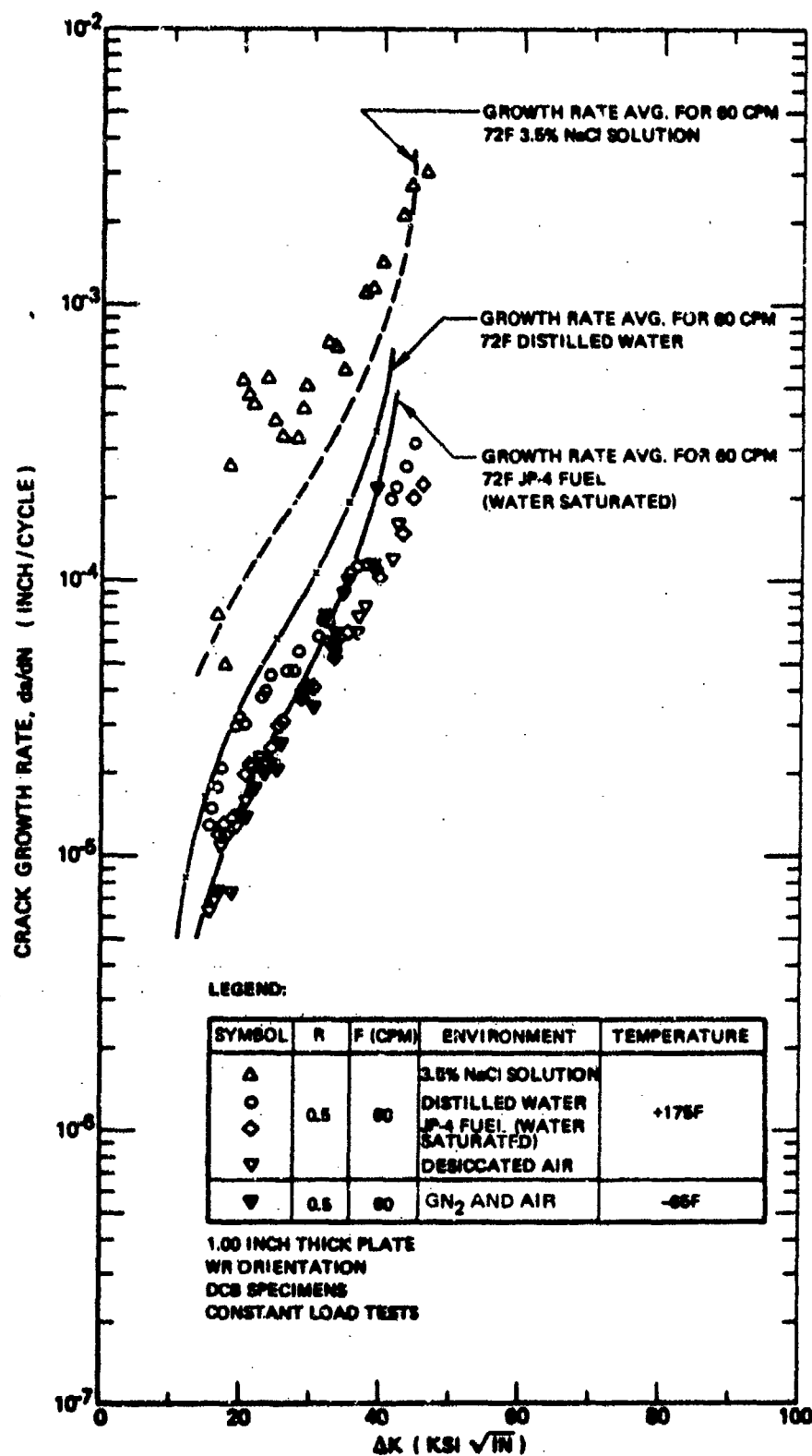


Figure 69: Fatigue Crack Growth Rates for 6Al-4V Recrystallized Annealed Titanium Alloy at -65F and +175F (60 CPM)

data indicates that over the range of crack growth rates of prime importance to airframe life problems, (da/dN less than 10^{-4} inches/cycle) an increase in temperature from 72 to 175F would not have any detrimental effect on crack growth rates.

Two tests were conducted at -65F to evaluate this effect of colder temperatures on crack growth rates in the Ti-6Al-4V RA alloy. The resulting crack growth rate data are plotted in Figure 69 along with the +175F data. The decreases in temperature from +175 to -65F had no significant effect on crack growth rate behavior over the range of ΔK values tested.

3.3.2.2 Effect of Cyclic Frequency

Tests to evaluate the effect of a reduction in cyclic frequency from 60 to 6 cpm were conducted in the five prime test media at 72F. The crack growth rate data resulting from the 6 cpm tests are plotted in Figures 70 through 74 along with average crack growth rate curves drawn through the 60 cpm data. The effect of a reduction in cyclic frequency from 60 to 6 cpm on crack growth rate behavior was dependent on the test media. In the non-aggressive media of desiccated air and JP-4 fuel, the reduction in cyclic frequency had no detectable effect on crack growth rate behavior as shown in Figure 70 and 71. In the mildly aggressive medium of distilled water, cyclic frequency appeared to have a modest effect on crack growth rate behavior. For ΔK values above $30 \text{ ksi}\sqrt{\text{in}}$, the 6 cpm crack growth rates tended to be faster than comparable 60 cpm rates; below $30 \text{ ksi}\sqrt{\text{in}}$, the 6 cpm rates for $R=0.5$ tended to be slower than comparable 60 cpm rates. However, none of the difference were larger than one normally expects from data scatter. In the more aggressive media of 3.5% NaCl solution and sump tank water, the effect of a decrease in cyclic frequency was to accelerate crack growth rates at ΔK values above about $20 \text{ ksi}\sqrt{\text{in}}$ by approximately an order of magnitude, and to decelerate crack growth rates below $20 \text{ ksi}\sqrt{\text{in}}$. This result is an amplification of the trend noted in the distilled water data.

3.3.2.3 Specimen Configuration Effect

Three corrosion fatigue tests were conducted using large "compact" tension specimens having overall dimensions of 1.0 inch thick by 7.2 inch high by

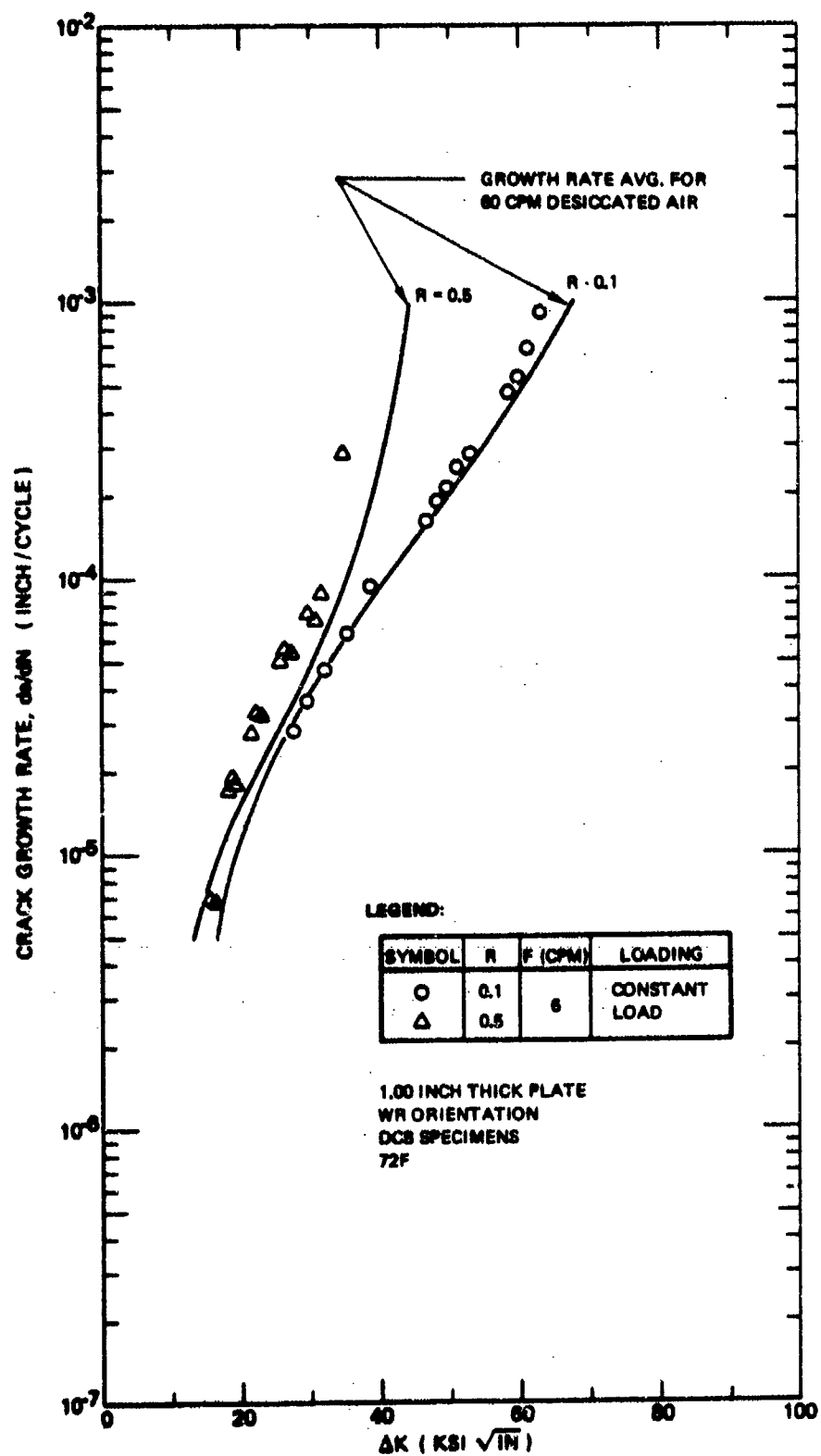


Figure 70: Fatigue Crack Growth Rates for 6Al-4V Recrystallize Annealed Titanium Alloy in Desiccated Air (6 CPM)

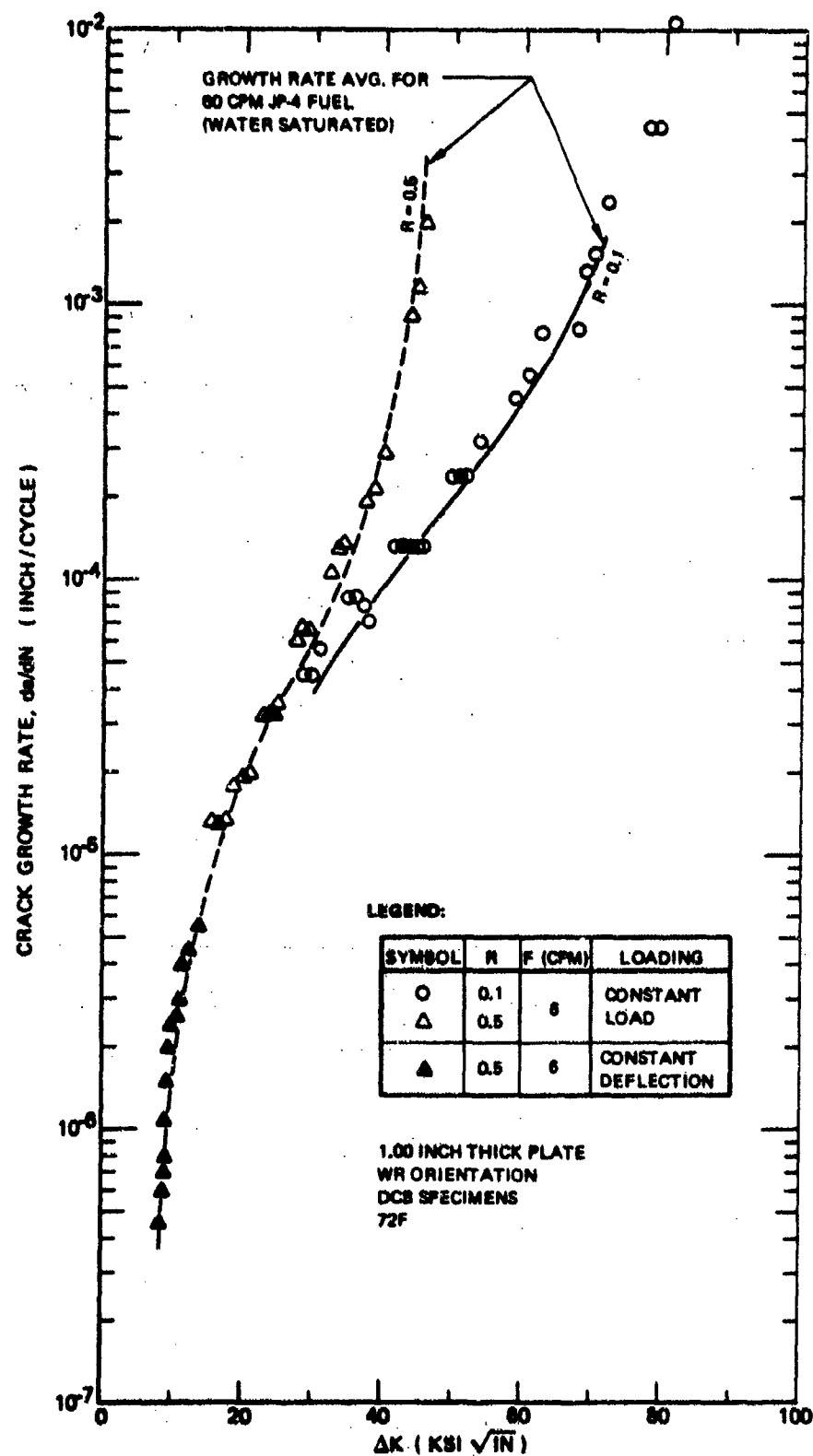


Figure 71: Fatigue Crack Growth Rates for 6Al-4V Recrystallized Annealed Titanium Alloy in Water Saturated JP-4 Fuel (6 CPM)

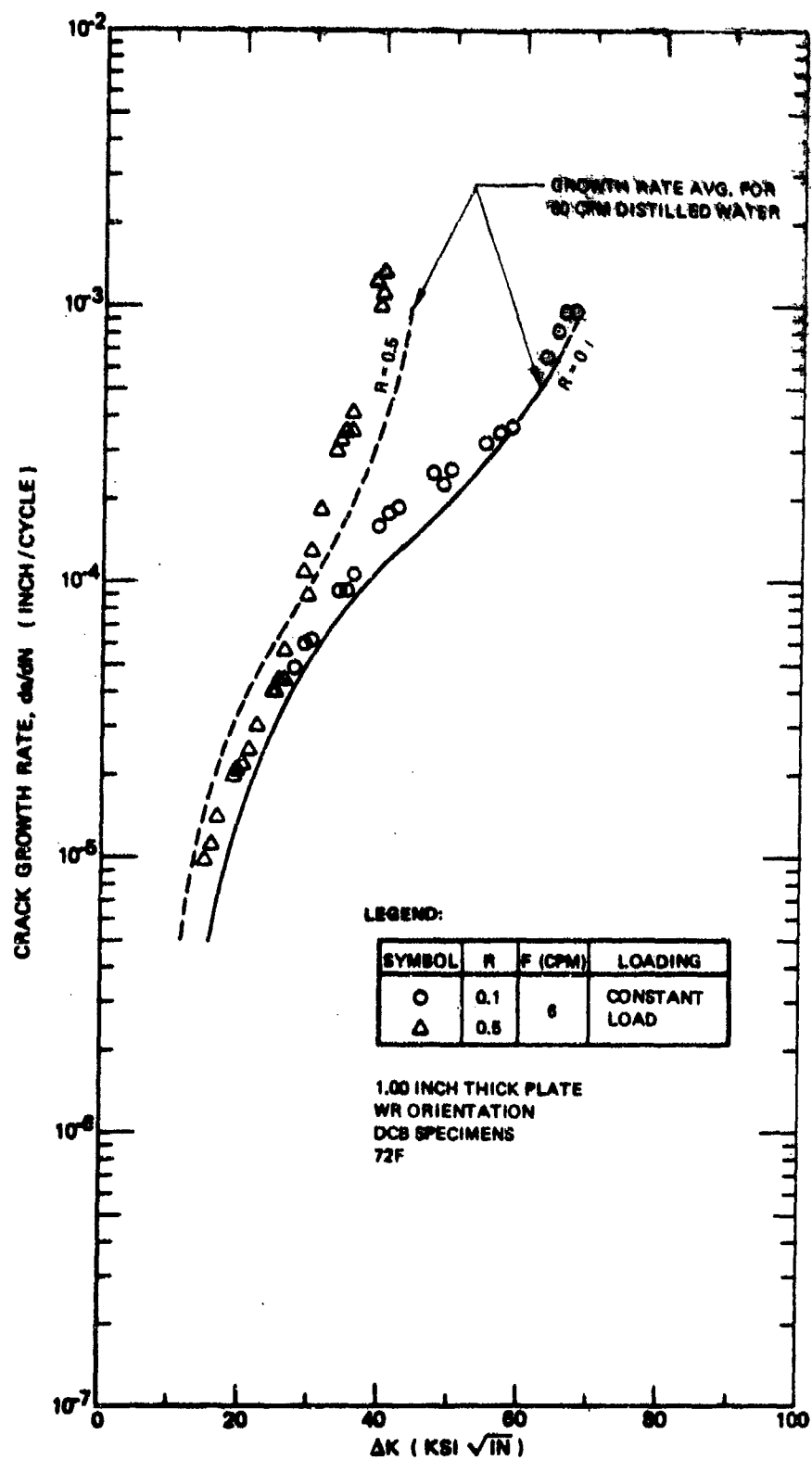


Figure 72: Fatigue Crack Growth Rates for 6Al-4V Recrystallized Annealed Titanium Alloy in Distilled Water (6 CPM)

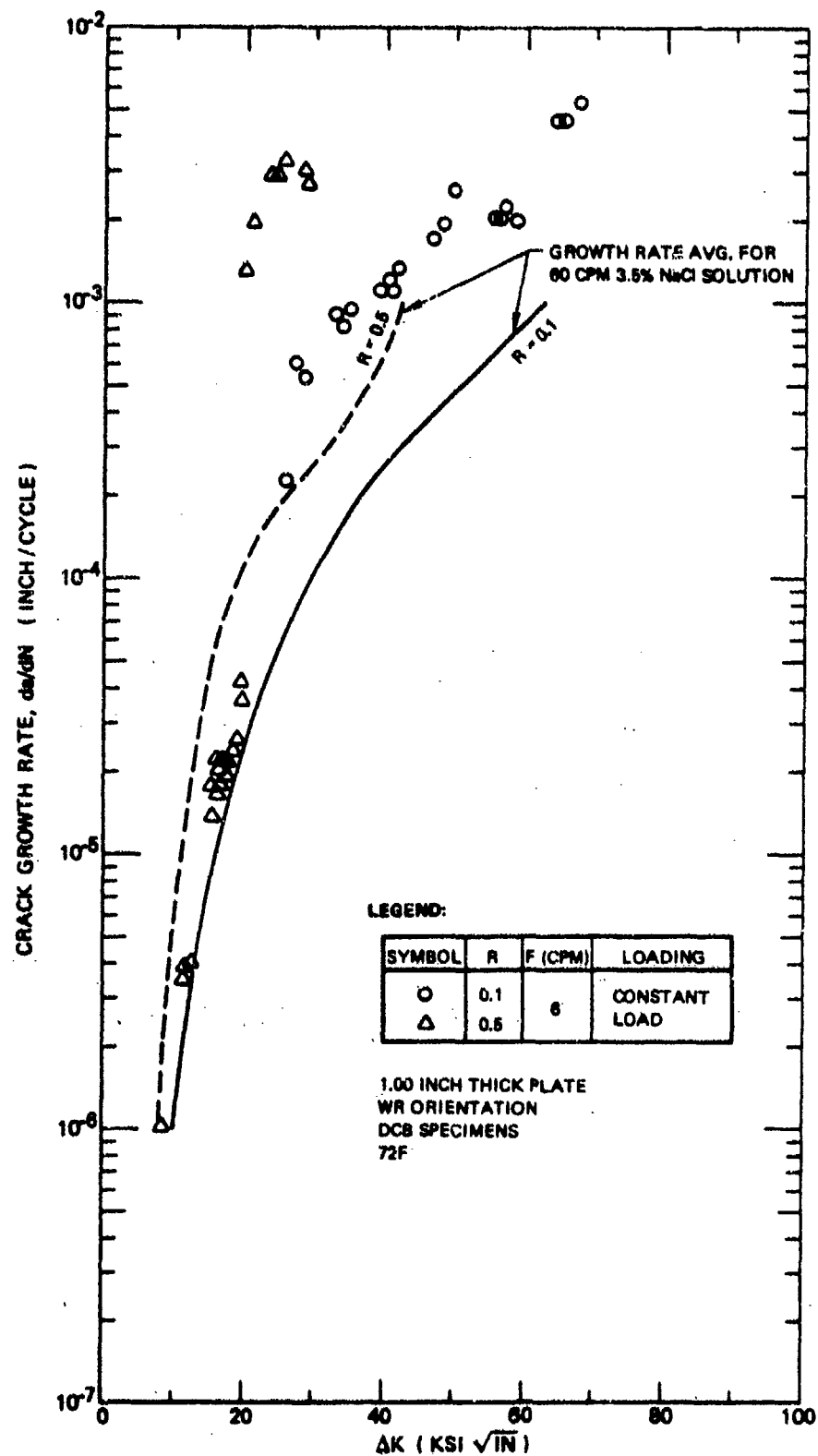


Figure 73: Fatigue Crack Growth Rates for 6Al-4V Recrystallized Annealed Titanium Alloy in 3.5% NaCl Solution (6 CPM)

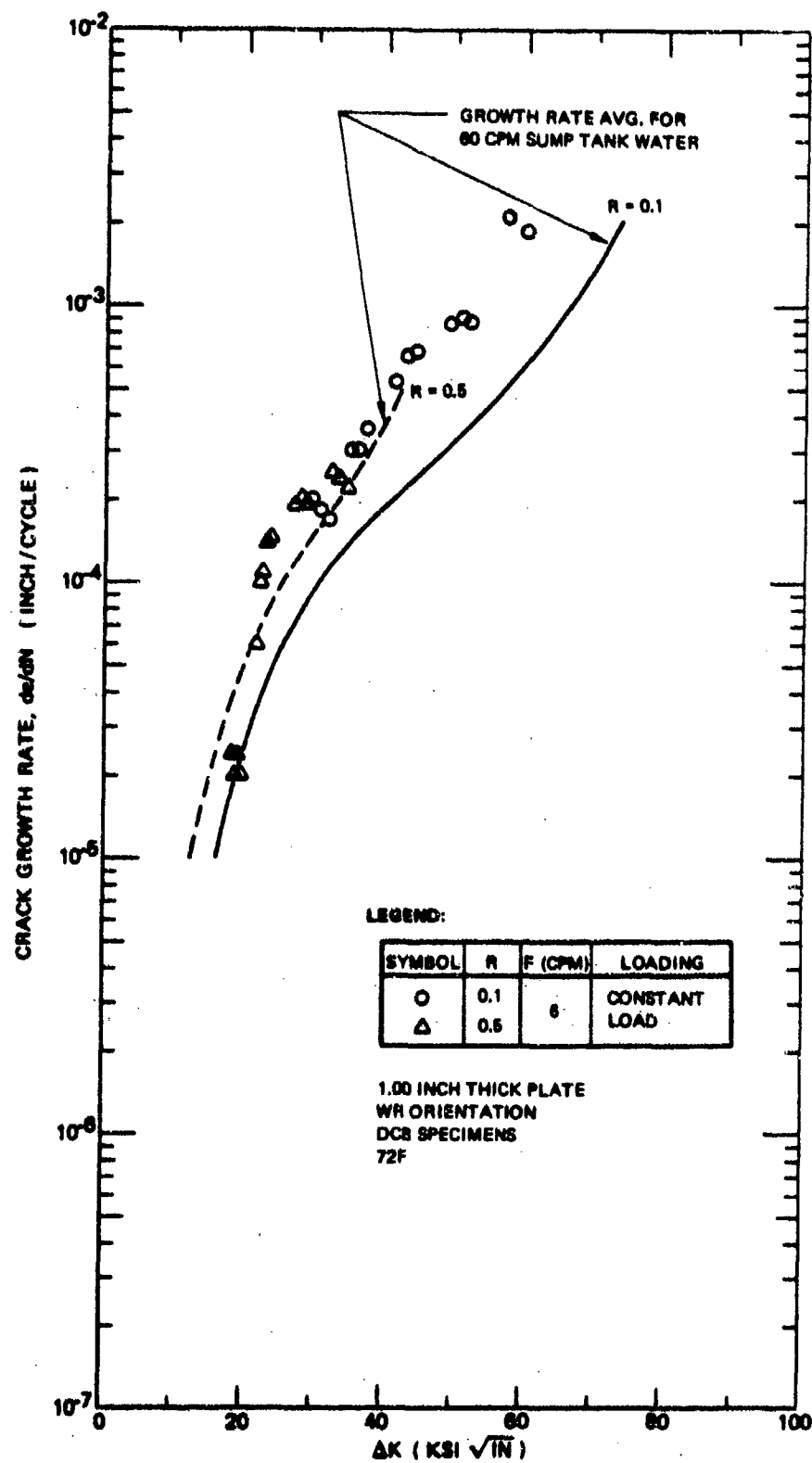


Figure 74: Fatigue Crack Growth Rates for 6Al-4V Recrystallized Annealed Titanium Alloy in Sump Tank Water (6 CPM)

8.9 inch long (Figure B12). The specimen arms were sufficiently high that side grooves were not required to restrict the growing crack to its original plane. The resulting crack growth data obtained in low humidity air and 3.5% NaCl solution are plotted in Figure 75 along with average crack growth rate curves obtained in the present investigation. The agreement between the data obtained using large compact tension specimens and the average crack growth rate curves resulting from tests in this program is good.

Two surface-flawed specimens were tested in both desiccated air and 3.5% NaCl solution using two different peak cyclic stress levels. The resulting WT direction crack growth rate data are plotted in Figure 76 along with average crack growth rate curves for the WR direction obtained from tests of DCB specimens. All data for a given environment agree regardless of specimen type and peak cyclic stress level.

3.3.2.4 Crack Closure Measurements

A series of crack closure measurements were made on titanium alloy CT specimens to investigate the crack closure behavior of the CT specimen configuration. These measurements were undertaken as an aid to future investigations concerned with developing fatigue crack growth models, and with the application of laboratory crack growth rate data to the prediction of minimum crack propagation life for full scale components.

Procedures

The crack closure behavior of Ti-6Al-4V RA compact tension specimens was investigated by periodically measuring crack opening displacements near the crack tip in specimens subjected to programmed loads. Specimen configuration is illustrated in Figure B12 in Appendix B.

Specimens were instrumented with clip gages spring loaded against knife edges spot welded to the specimen surface immediately above and below the crack as illustrated in Figure 77. The spot welds were located 0.05, 0.10 and 0.25 inches away from the tip of the crack, and 0.02 inches above the plane of the crack. Gages that were 0.05 and 0.25 inch from the crack tip were located on one side of the specimen with the middle gage on the other side of the specimen. Crack

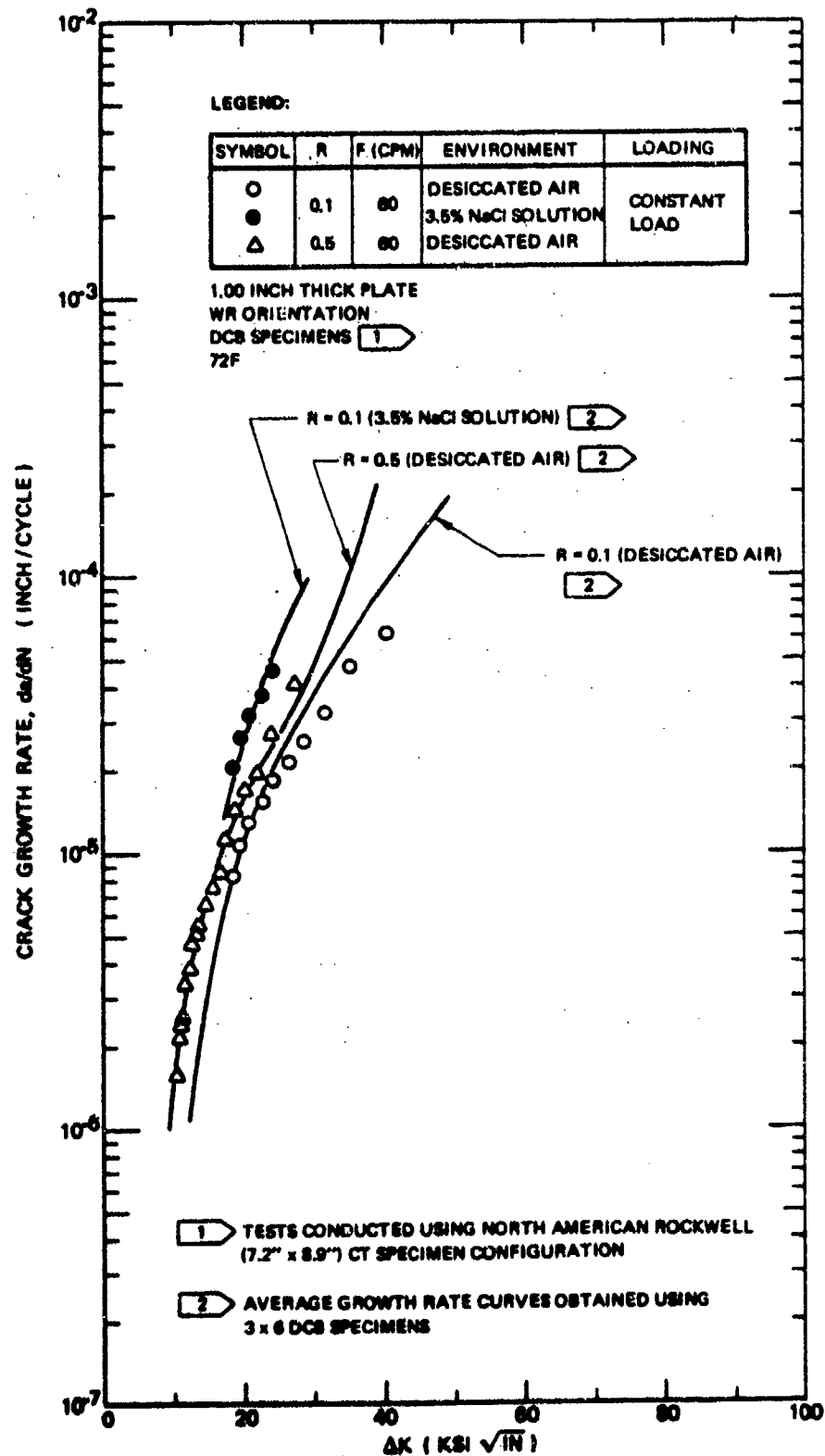


Figure 75: Fatigue Crack Growth Rates for 6Al-4V Recrystallized Annealed Titanium Alloy (Obtained Using North American Rockwell Specimen Configuration)

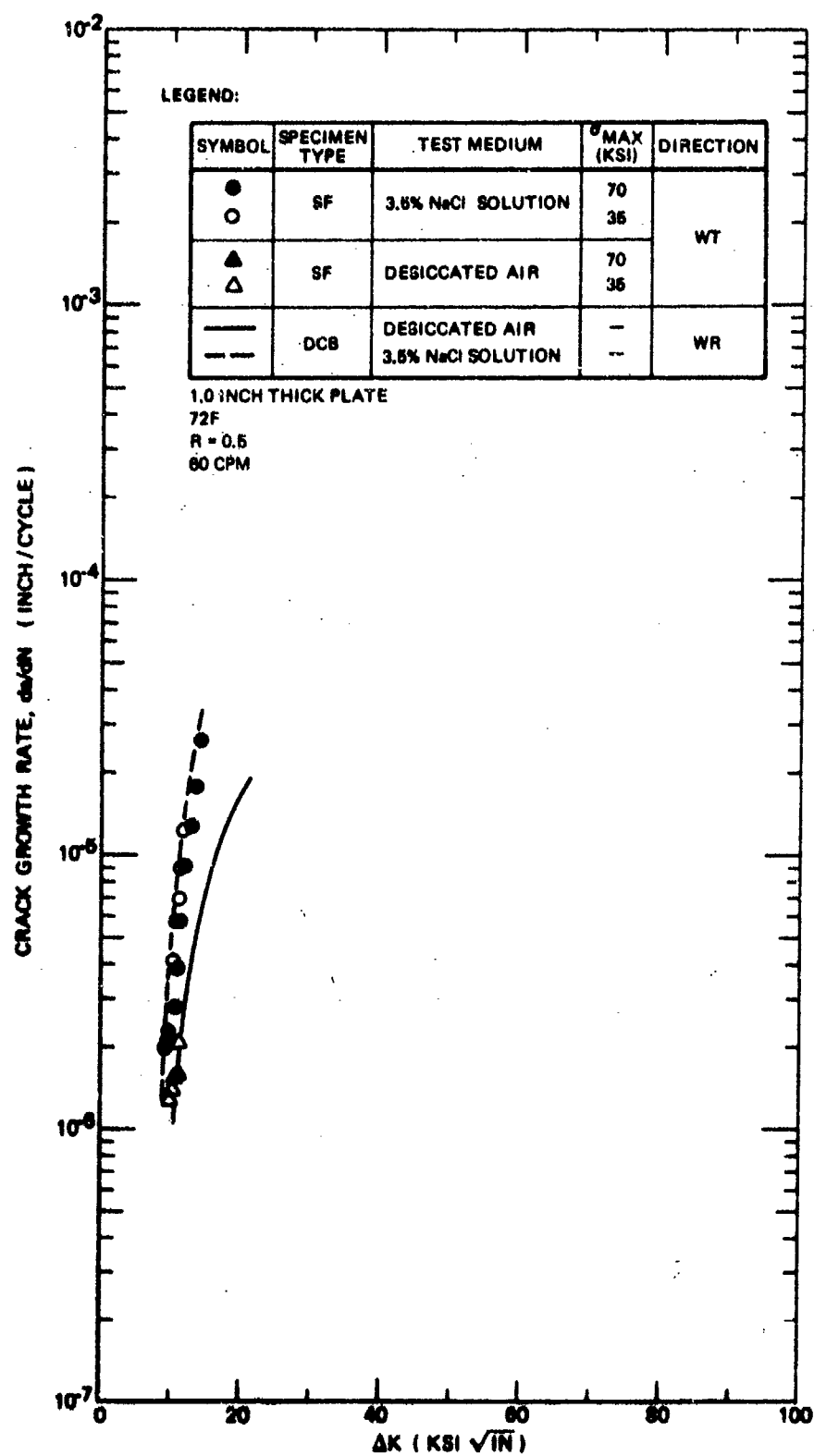


Figure 76: Fatigue Crack Growth Rate Data for 6Al-4V Recrystallized Annealed Titanium Alloy Surface Flawed Specimens

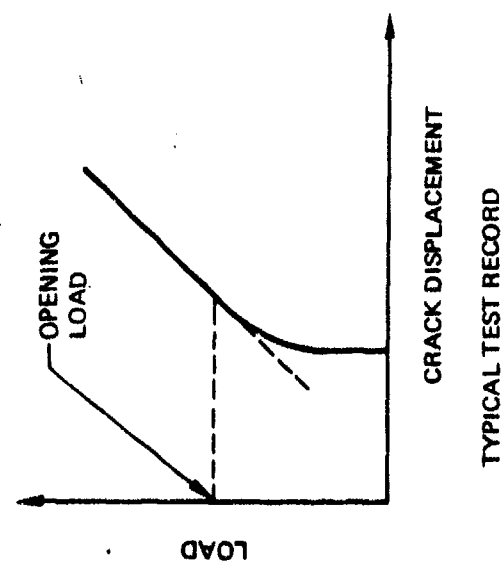
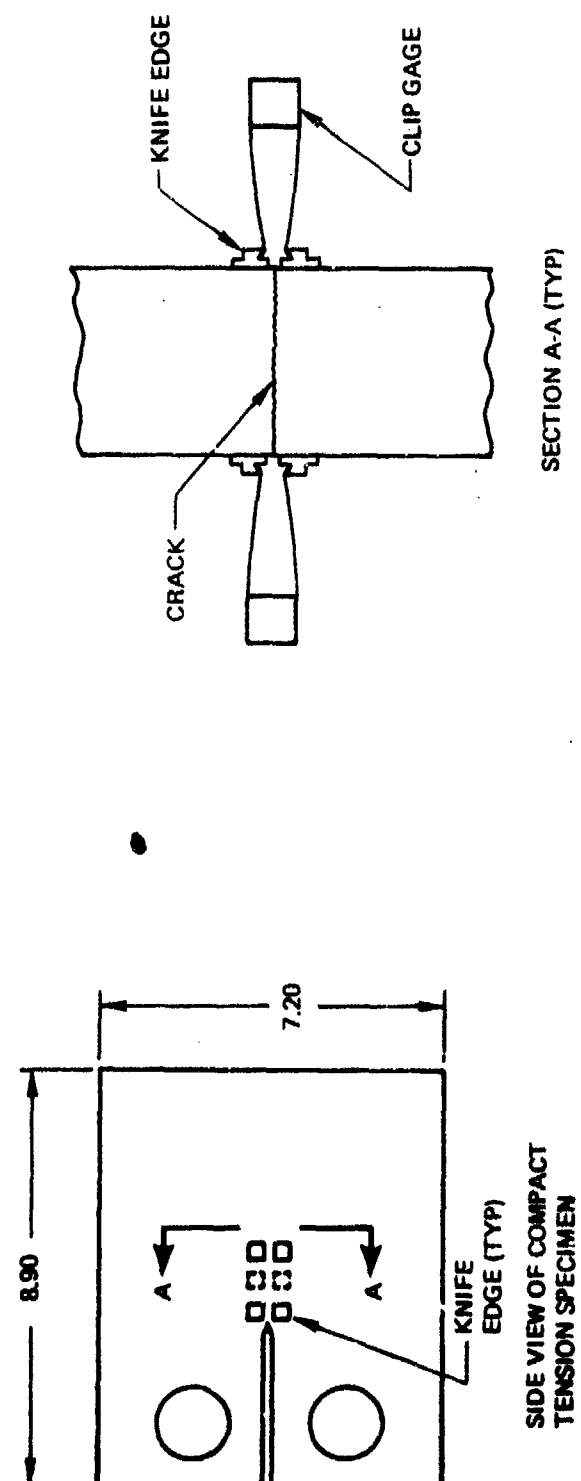


Figure 77: Clip Gage Locations For Crack Closure Measurements

opening was recorded as a function of applied load using an X-Y plotter with crack displacement recorded on the abscissa and load recorded on the ordinate.

Specimens were cycled at 72F in air using the loading program illustrated in Figure 78. The loading program involved cycling at three different peak cyclic load levels in a low-high-low-high sequence using a stress ratio of 0.1. During each loading block, the crack was grown over an increment of about 0.2 to 0.3 inches as shown on the abscissa in Figure 78. At the locations in the loading program designated by the letter A, crack closure measurements were repeated three times during the last three cycles of the loading block. At locations designated by the letter B, crack closure measurements were made on the first and second, fifth and sixth, and ninth and tenth cycle of the loading block.

Results

Examples of the crack displacement versus load recordings obtained in these tests are shown in Figure 80. The three recordings were simultaneously obtained during a single loading of the test specimen. The sensitivity of the crack displacement scale was decreased as the gages became further away from the crack tip. This was done so that each recording filled the 11 x 17 inch graph paper. This change in recording sensitivity may have had some influence on the measured values of minimum loads at which the crack was entirely open. This will be discussed in the following evaluation of results.

The minimum value of load at which the crack was entirely open (P_o) was taken as the load corresponding to the point of tangency between the sloping straight line and curved portions of the test record, as shown in Figure 77. The value of P_o was used to calculate the minimum stress intensity factors at which the crack was entirely open, K_{op} . In Figure 79, K_{op} is plotted as a function of distance from the crack tip at which the measurement was made (l_o) for each of the three load levels in the loading program. As the load level was increased, there was an increasing tendency for K_{op} to decrease with increase in l_o . It is believed that this result was due, at least in part, to the intentional decrease in instrumentation sensitivity with increase in l_o . The decrease in sensitivity led to lower and lower apparent tangency points between the sloping straight line and curved portions of the diagram and, hence, to lower values of K_{op} . Accordingly, the value of P_o obtained from the clip gages located 0.05 inch away from the crack tip was used to calculate values of K_{op} .

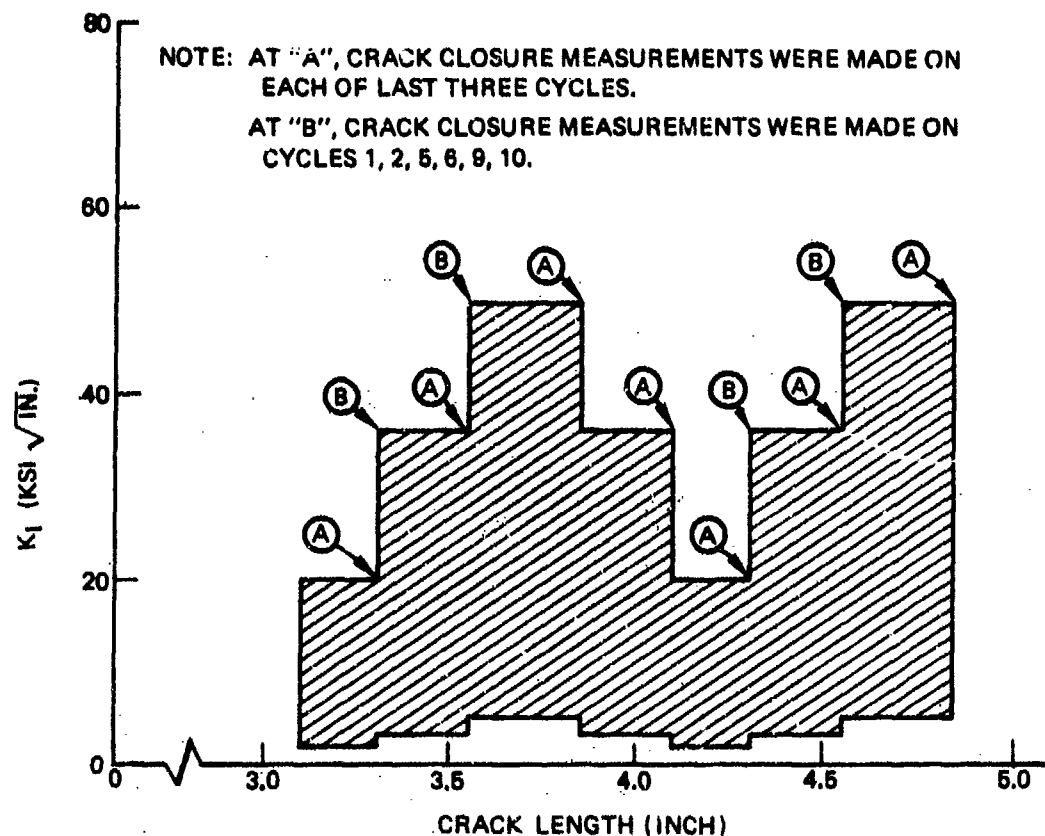


Figure 78: Loading Program Used For Crack Closure Measurements

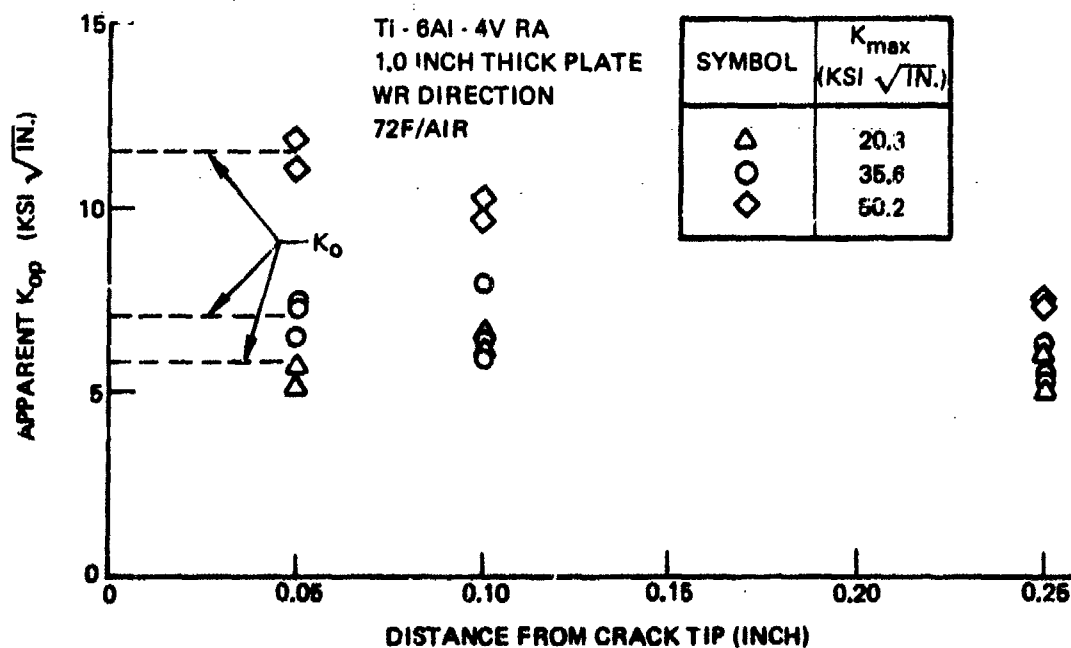


Figure 79: Effect of Measurement Location on Apparent Stress Intensity Factor at Onset of Crack Closure

Ti-6Al-4V RA
 1.00 INCH THICK PLATE
 WR ORIENTATION
 72 F AIR
 CRACK LENGTH = 3.85 IN.

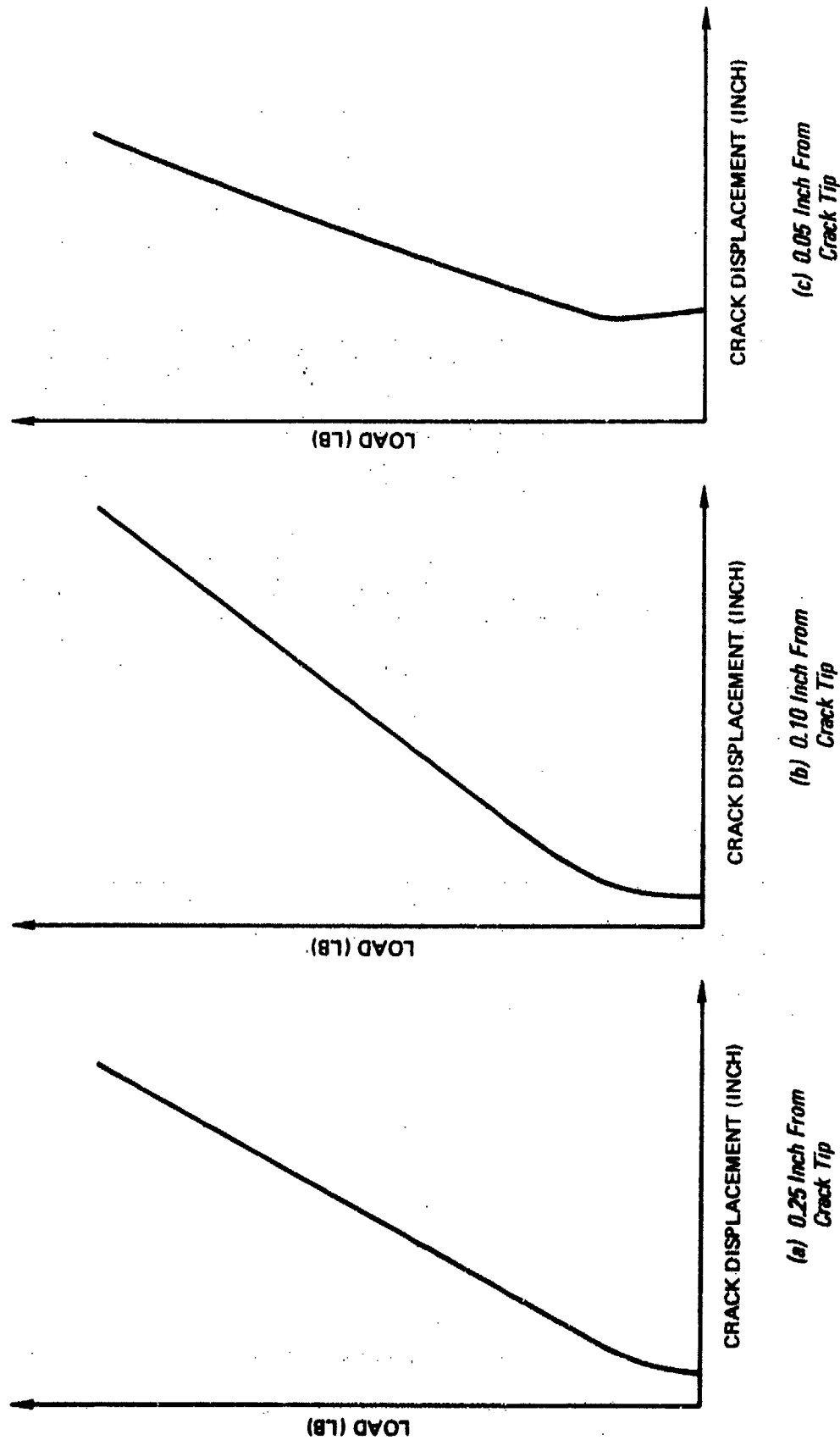


Figure 80: Examples of Crack Displacement Vs. Load Recordings Obtained During Crack Closure Measurements

The values of K_{op} appeared to be a constant percentage of the peak stress intensity factor used to generate the crack growth. This is illustrated in Figure 81 where the three data points obtained in this investigation are included in a scatter band having the bounds $K_{op} = 0.20 K_{max}$ and $K_{op} = 0.30 K_{max}$. Included in the same figure are comparable results reported by Elber (9), Shih and Wei (10), and Katcher and Kaplan (11). Both the Elber and Shih and Wei results differ considerably from those reported herein. Elber's data were obtained from thin aluminum specimens tested under conditions of net section yielding. Hence, the applicability of Elber's data is questionable. Shih and Wei's results were obtained from tests of 0.2 inch thick Ti-6Al-4V center-cracked panels, whereas the results herein were obtained from 1.0-inch-thick-specimens. The results that Katcher and Kaplan obtained from tests of 1.0-inch thick Ti-6Al-4V RA DCB specimens are in good agreement with the results obtained in this program. The effects of specimen thickness on crack closure behavior have yet to be investigated and it is not known whether or not difference in thickness contributed to the disagreements between Shih and Wei's results and those obtained in this program and in (10).

Stress intensity factors at the onset of crack tip closure (K_{op}) showed no tendency to vary with crack length, or during the first ten cycles of high load cycling following lower load cycling. This result is illustrated in Figure 82 where K_{op} is plotted as a function of crack length for the last cycle of the low stress cycling (point A) and the tenth cycle of the subsequent high stress cycling (point B). It is evident that crack length did not affect the value of K_{op} for a given (K_m), and that K_{op} did not change significantly during the first ten cycles of the high stress cycling. This result is consistent with the transient acceleration in crack growth rates that is often observed immediately after an increase in peak cyclic load.

Discussion

All of the crack closure measurements of which the authors are aware have been made at the surface of test specimens. At the present time, the relationship between surface measurements and conditions at the interior of the specimen are unclear. This uncertainty needs to be resolved before the effects of crack closure on crack growth rate can be determined.

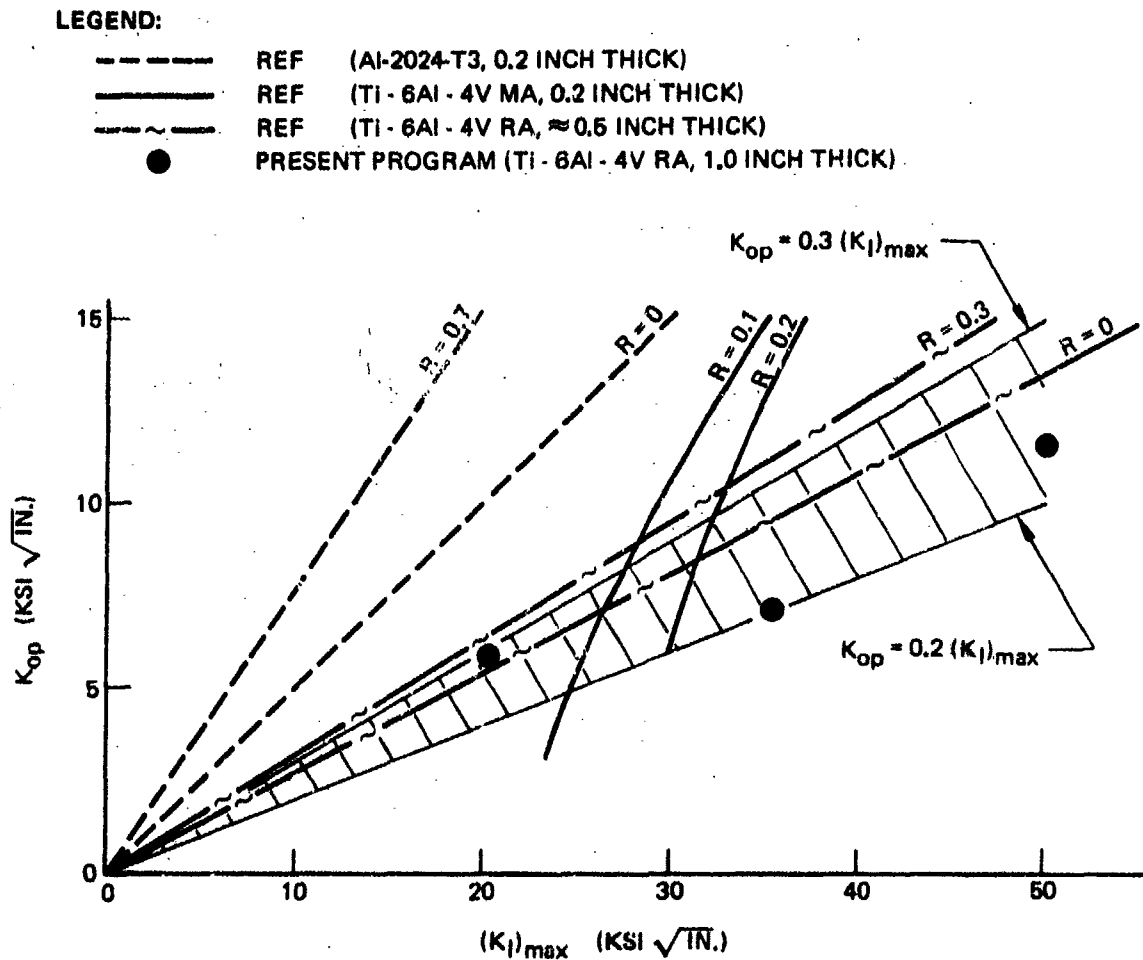


Figure 81: Effect of Peak Cyclic Stress Intensity Factor on Stress Intensity Factor at the Onset of Crack Closure

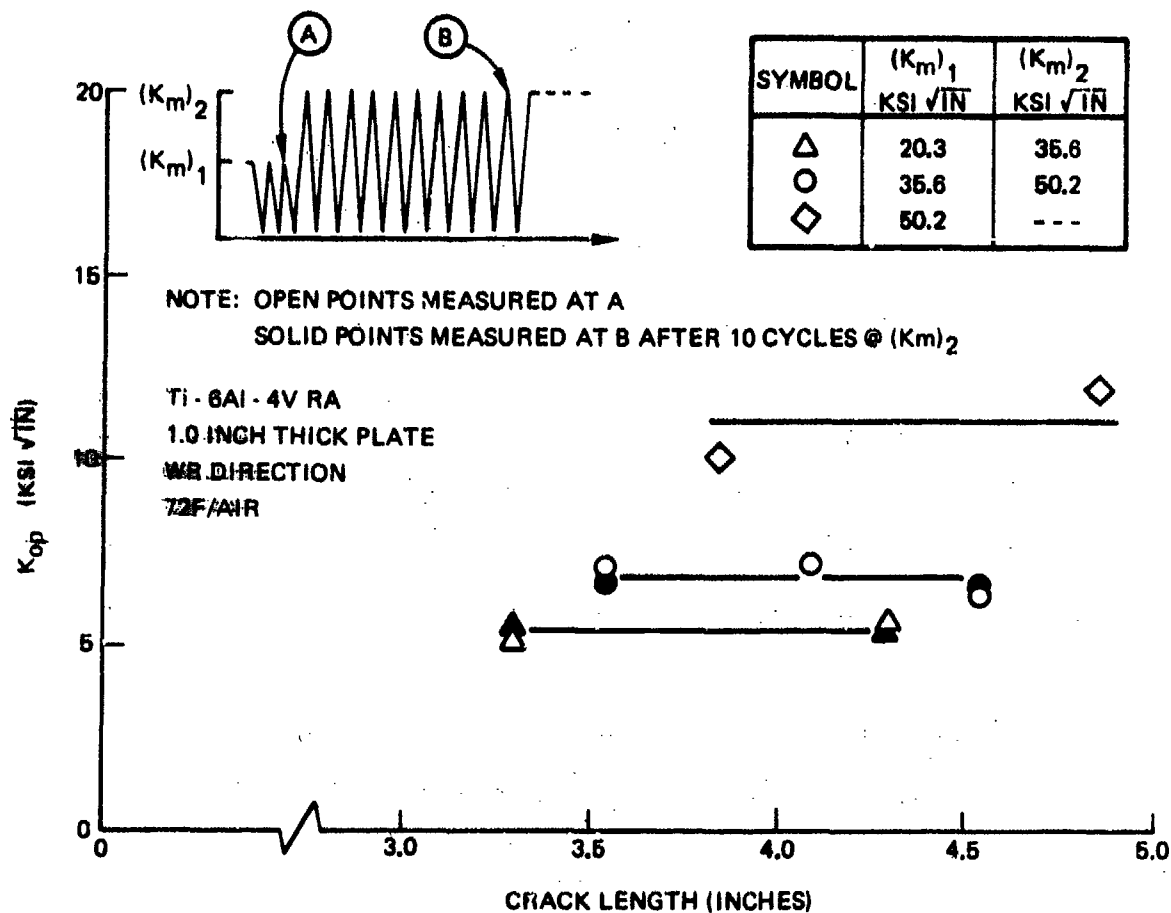


Figure 82: Effect on Crack Length and Load Increase on Stress Intensity Factor at Which Crack Closure Occurs

It appears that stress ratio effects on fatigue crack growth rate behavior do not result solely from crack closure effects. If surface measurements are accepted as being representative of average conditions throughout the thickness of the specimen, the crack would be expected to remain open at all times for stress ratios in excess of about 0.2 to 0.3, and stress ratio effects would not be observed for stress ratios above this range. However, the data in this report and in the literature demonstrate that stress ratios above 0.3 have a significant effect on fatigue crack growth rate behavior.

Summary

The crack closure measurements made in this program showed that:

- Crack closure at the specimen surface occurs during fatigue crack growth testing for R ratios below about 0.25 in Ti-6Al-4V RA compact tension specimens.
- After sufficient uniform stress cycling to stabilize conditions, the onset of crack closure occurs at a stress intensity factor value that is a reasonably constant percentage (about 25%) of the peak cyclic stress intensity factor.
- Crack closure behavior is independent of crack length for long cracks.
- After an increase in peak cyclic load, it takes more than ten uniform load cycles before the closure load starts to increase to the new value associated with the higher peak cyclic stress level.

3.3.2.5 Thermal Processing Effects

Tests were conducted to evaluate the effects of variations in metallurgical characteristics imparted to the Ti-6Al-4V RA alloy by various thermal cycles. The original intent was to evaluate the effects of grain size and cooling rate on the fracture and crack growth resistance properties of this alloy. Small

plates were heated to temperatures near the beta transus and were slow cooled to grow the primary alpha grains. The plates were then reheated to 1400F and either air cooled or slow cooled at 50 F/hour to study effects of possible ordering of the alpha phase of the material. However, the thermal cycles used to cause grain growth also resulted in large variations in microstructure throughout each of the plates from which the test specimens were cut. The microstructural variations had a large influence on fracture and crack growth resistance as described in the following paragraphs.

Metallurgical Effects

Various thermal cycles were employed on 1 x 10 x 14 inch plates of Ti-6Al-4V RA plate material to achieve alpha phase grain growth. Initial trials involved heating the material near the predicted beta transus and slow cooling the the alpha-beta temperature range. The beta transus of the material was predicted to be 1790F utilizing ingot composition and an empirical relationship. The following thermal cycle was employed:

1775F 1 hr Furnace Cool at 50F/Hr to 1400F. Air Cool from 1400F to Room Temperature.

Microstructural examination after heat treatment revealed that all samples had been heated above the beta transus. This was evidenced by a large grained basketweave structure, devoid of equiaxed primary alpha phase.

Next, the beta transus was determined experimentally by microstructural evaluation of samples heated to various temperatures and was found to be $1793 \pm 10F$.

A second set of plates were heat treated using the same thermal cycle except that a thermocouple was placed between the plates during heat treatment. Microstructural examination of samples cut from the corners of the plates after heat treatment indicated that two of the plates had been heated above the beta transus and the third plate had not. Grain size measurements indicated that the equiaxed alpha grain size had increased 50% in the third plate. Two of the

plates, designated 33 (alpha-beta) and 44 (basketweave) were then exposed to the following additional thermal cycle:

1400F 1 Hr Furnace Cool at 50F/Hr to 900F

This cycle was expected to result in higher stress corrosion susceptibility than observed in the as-received plate and to allow a comparison of results for both the basketweave morphology and the alpha-beta morphology.

A cyclic thermal treatment was employed on additional material in an attempt to grow the primary alpha grains by more than 50%. Metallurgical samples were exposed to the following cyclic thermal treatment:

1770F 45 minutes then cycled between 1600F and 1770F for 6 hours. 1700F for 16 hours (overnight) and heated to 1770F for 10 minutes and furnace cooled at 25F/hr to 1650F, then 100F/Hr to 1400F, then air cooled from 1400F to room temperature.

Grain size measurements on the metallurgical samples indicated an increase in alpha grain size of nearly 100%. Based on these results, two additional 1 x 10 x 14 inch plate samples were given the above cyclic thermal treatment to achieve large alpha grains. The plate samples, designated 55 and 66, were heat treated in a similar manner except that the increased sample size and larger furnace required slower heat-up and cool-down rates. To assure adequate temperature control, three thermocouples were used to monitor temperatures. The test plates were stacked in the furnace with an additional 1-inch thick plate on top to minimize furnace temperature variations. Subsequently, sample 55 was heated to 1400F-one hour and air cooled, and sample 66 was furnace cooled from 1400F at 50F/hr to 900F and then air cooled.

Subsequent metallurgical examination of samples cut from corners of the plates and examination of the fracture faces of various test specimens revealed that the microstructure varied throughout each plate as shown in Figure 83. Some regions in each plate had large transformed beta grains (basketweave morphology)

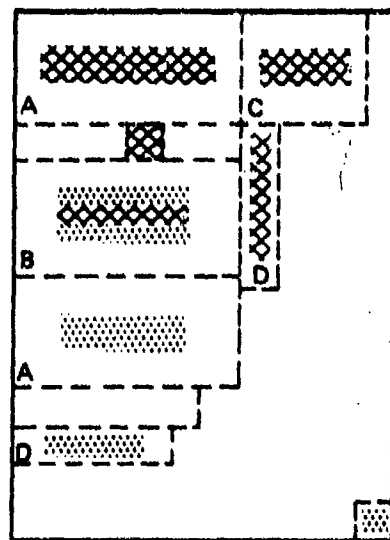


PLATE 33

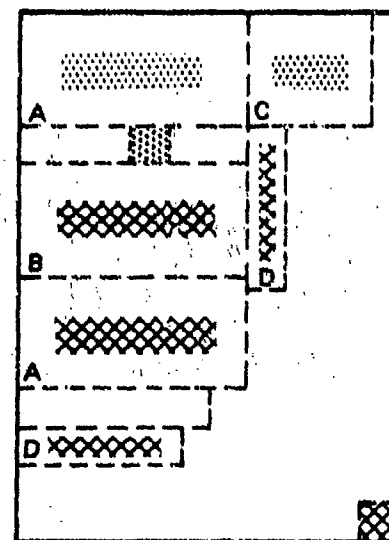


PLATE 44

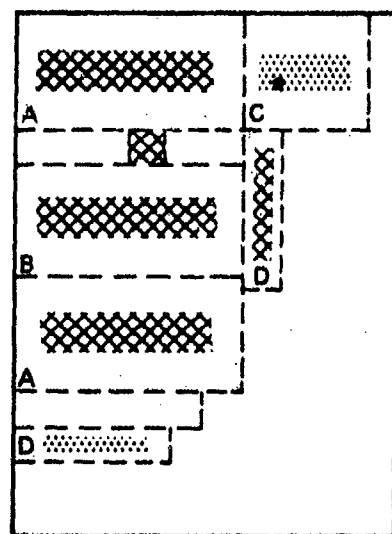


PLATE 55

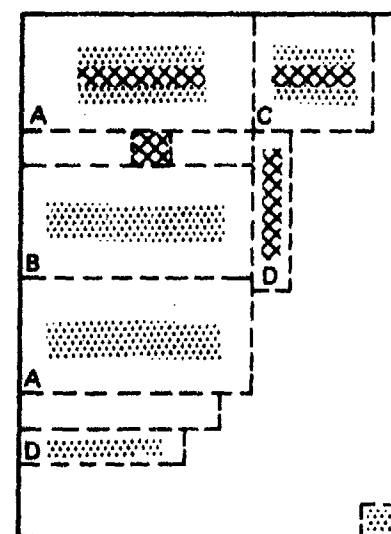


PLATE 66

LEGEND:

MORPHOLOGY	SYMBOL
BASKETWEAVE	
ALPHA-BETA	
BASKETWEAVE CENTER ALPHA-BETA EDGES	

SPECIMEN TYPE	IDENTIFICATION
DCB (CORROSION FATIGUE)	A
DCB (STRESS CORROSION)	B
CT (FRACTURE TOUGHNESS)	C
TENSILE	D

Figure 83: Cutting Diagrams and Microstructural Variations for Thermally Cycled Ti-6Al-4V RA Plates

with the remaining regions composed of equiaxed alpha-beta morphology. Examples of alpha-beta microstructure and basketweave microstructure showing large primary alpha grains are shown in Figure 84 and 85, respectively. An example of variation in microstructure within a given plate is demonstrated in Figure 86 where both basketweave and equiaxed alpha-beta morphology in plate 66 are shown. Since the equiaxed alpha microstructure occurred in regions near the original plate surfaces, the difference in microstructure is most likely a result of compositional differences. Lower oxygen and aluminum content in the center of the plate would lower the beta transus temperature in that area. If microstructural variations had been caused by temperature variations within the plate during heat treatment, the surface microstructure would then have been the basketweave morphology. The microstructural variations within each plate sample necessitated an examination of the fracture face of each test specimen so that it could be categorized with respect to microstructure.

A dramatic change in crystallographic texture was observed with the change in microstructure. Basal plane pole figures were determined for specimens 44CF-1 (from plate 44). The texture for the equiaxed alpha microstructure of specimen 44CF-1 (Figure 87 and Table 15) compares favorably with that of the as-received material. The majority of basal planes were oriented normal to the transverse direction. The texture for the basketweave microstructure of specimen 44CF-2 (Figure 88 and Table 15) was extremely different with about 60% of the basal planes oriented normal to the longitudinal direction. This was the most severe texture encountered to date at Boeing for a thermally produced basketweave microstructure.

Effects on Mechanical Properties

Mechanical properties for the four plates used to fabricate test specimens are listed in Table 16. The specimens used to measure longitudinal and transverse grain properties were cut from different locations within each plate and in three of the four plates, the specimen from a single plate exhibited markedly different microstructures. All transverse specimens had a basketweave microstructure with the majority of the basal planes oriented normal to the longitudinal direction. Hence, ultimate and yield strengths for the transverse

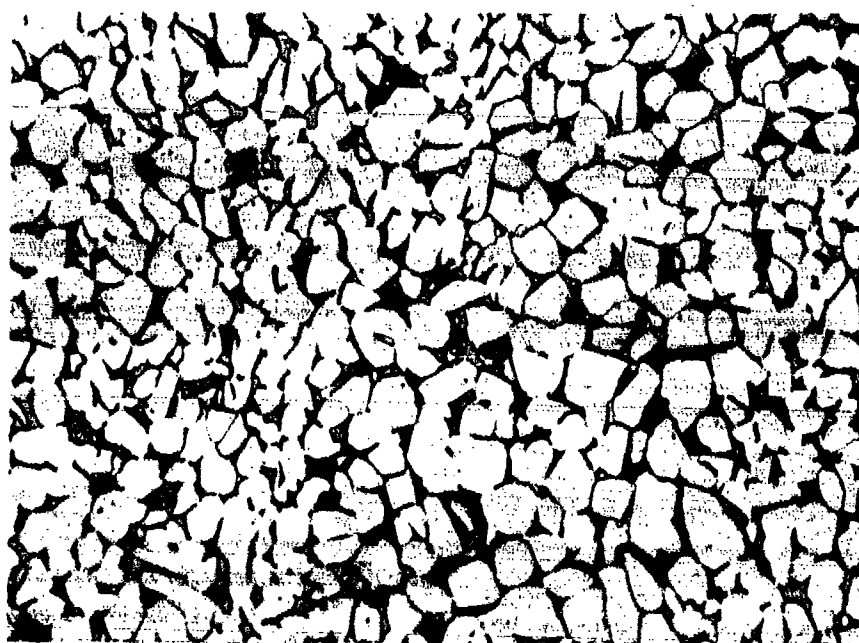


Figure 84: Equiaxed Alpha-Beta Microstructure of Ti-6Al-4V,
Specimen 55K-1 (200X)

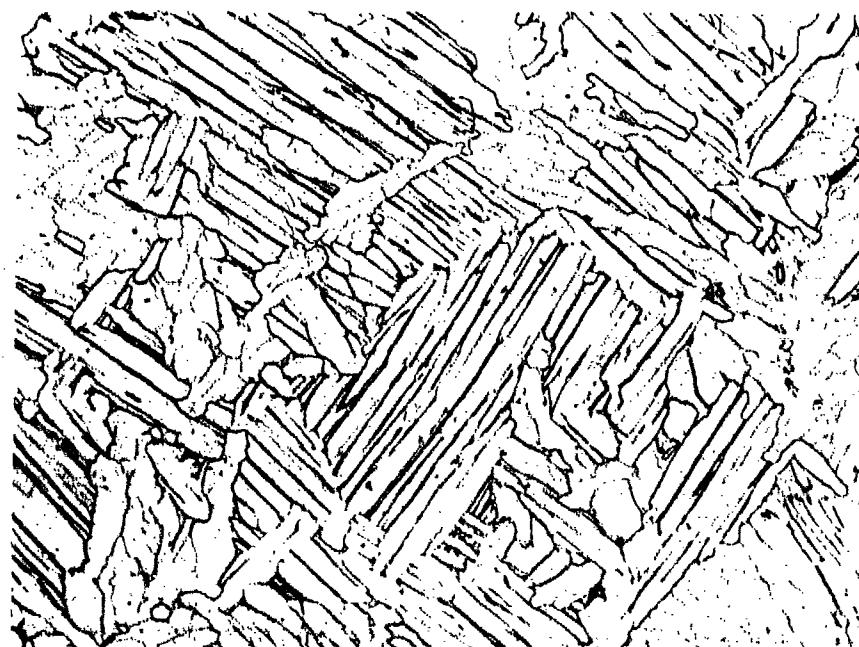
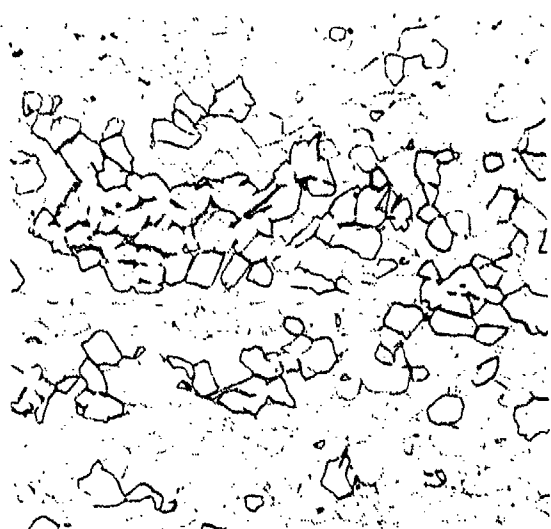


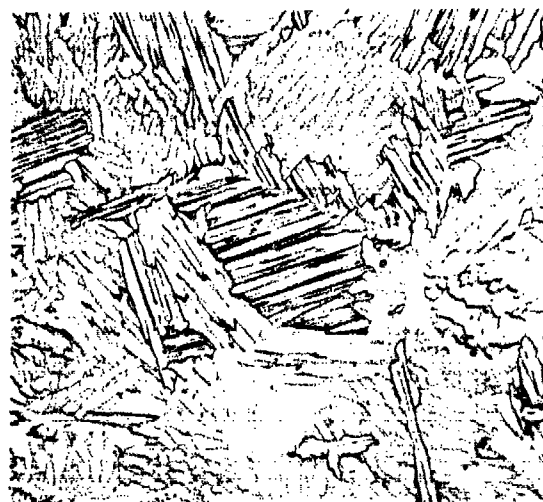
Figure 85: Basketweave Microstructure of Ti-6Al-4V
Specimen 44K-1 (200X)



200 X

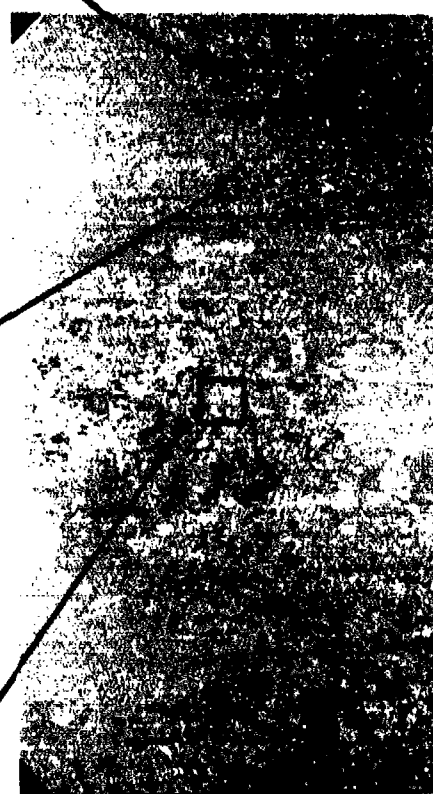


200 X



100 X

TOP SURFACE



BOTTOM SURFACE

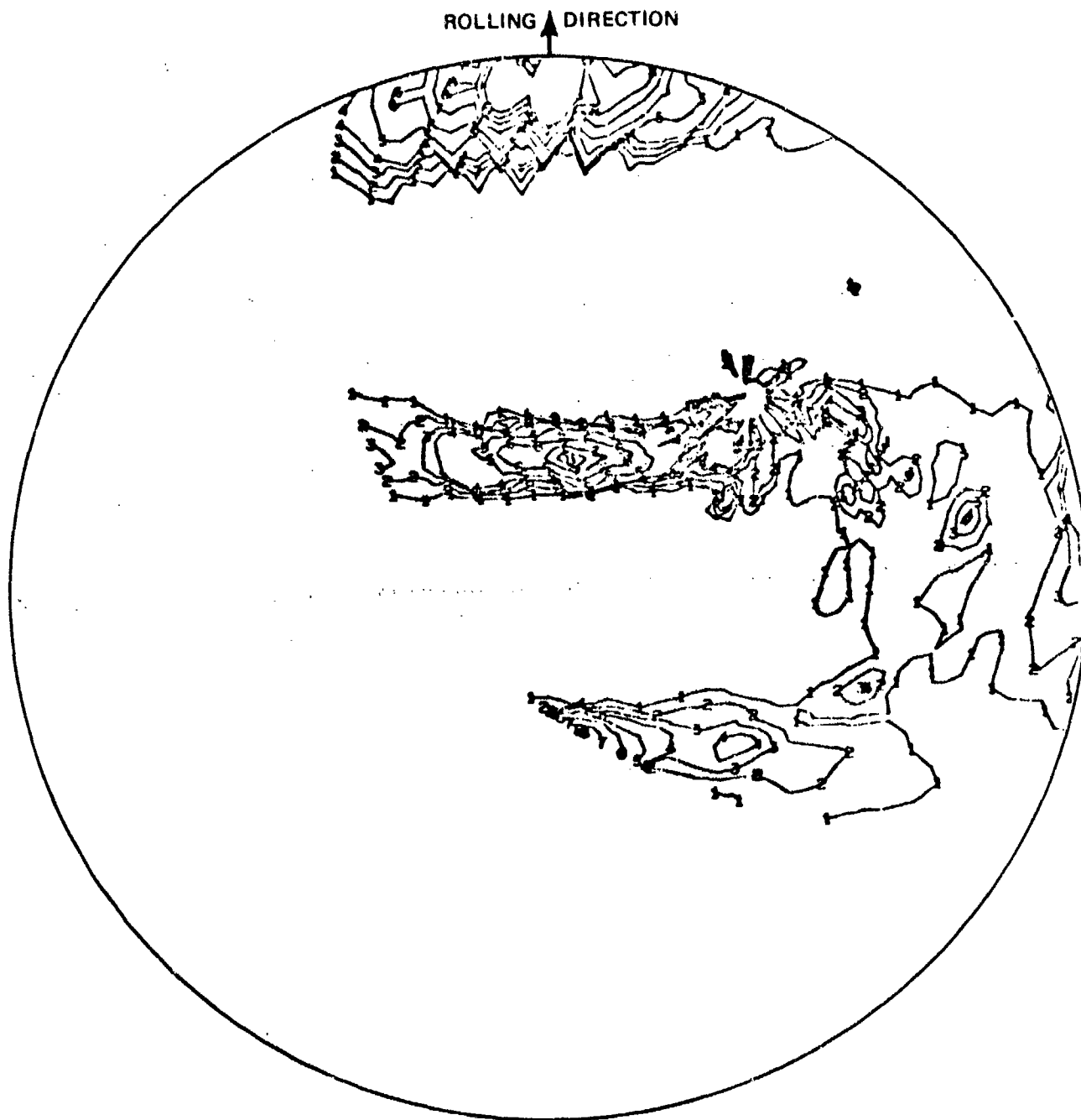
4 X

Figure 86: Macrostructure of Fracture Toughness Specimen 66K-1 Showing Both the Equiaxed Alpha and Basketweave Grain Morphologies



CONTOUR LINES	1	2	3	4	5	6	7	8	9	0
TIMES RANDOM INTENSITY	0.5	1.0	1.5	2.0	4.0	8.0	14.0	20.0	25.0	30.0

Figure 87: Basal Plane Pole Figure for Equiaxed Alpha-Beta Microstructure Resulting from Cyclic Heat Treatment of Plate 44



CONTOUR LINES	1	2	3	4	5	6	7	8	9	0
TIMES RANDOM INTENSITY	0.5	1.0	1.5	2.0	4.0	8.0	14.0	20.0	25.0	30.0

Figure 88: Basal Plane Pole Figure for Basketweave Microstructure Resulting from Cyclic Heat Treatment of Plate 44

Table 15: Quantitative Texture Factors and Moduli for Ti-6Al-4V Alloy Subjected to Various Thermal Cycles

MATERIAL	HEAT TREATMENT	TEXTURE FACTORS*			MODULI (KSI X 10 ⁻³)**		
		%I _L	%I _T	%I _{ST}	E _L	E _T	E _{ST}
Ti-6Al-4V (PLATE 44) EQUIAXED ALPHA MICROSTRUCTURE	CYCLED FROM 1600F + 1700F FOR ~ 12 HRS AND FURNACE COOLED	29.6	44.1	26.3	15.8	17.0	15.6
Ti-6Al-4V (PLATE 44) BASKETWEAVE MICROSTRUCTURE	SAME AS ABOVE	50.5	16.7	23.8	18.2	15.1	15.5
Ti-6Al-4V RA EQUIAXED ALPHA-BETA MICROSTRUCTURE	AS RECEIVED	34.0	41.2	24.8	16.2	16.7	15.5

*SEE TABLE 6

**CALCULATED FROM X-RAY POLE FIGURE INTENSITIES

Table 16: Mechanical Property Test Results at 72F for Ti-6Al-4V Plate Subjected to Various Thermal Cycles

PLATE NO.*	MICROSTRUCTURE	GRAIN DIRECTION	ULTIMATE TENSILE STRENGTH (KSI)	YIELD STRENGTH 0.2% OFFSET (KSI)	ELONGATION IN 2.0 IN (%)	REDUCTION IN AREA (%)
33	ALPHA-BETA BASKETWEAVE	LONGITUDINAL	129.6	120.9	8	33
		TRANSVERSE	120.1	108.5	8	25
44	BASKETWEAVE BASKETWEAVE	LONGITUDINAL	133.3	125.2	8	25
		TRANSVERSE	121.8	110.4	8	17
55	ALPHA-BETA BASKETWEAVE	LONGITUDINAL	138.1	127.6	7	24
		TRANSVERSE	133.3	117.8	4	12
66	ALPHA-BETA BASKETWEAVE	LONGITUDINAL	136.3	125.0	8	25
		TRANSVERSE	126.2	115.0	7	22

*SEE SECTION 3.3.2.4 FOR DETAILS OF THERMAL PROCESSING

direction tended to be lower than for the longitudinal direction. The anisotropy in strength is best illustrated by the results for plate 44 that were obtained from specimens having similar microstructures. In plates 33, 55, and 66, the longitudinal specimens had an alpha-beta microstructure with little texturing.

The additional thermal processing of the as-received Ti-6Al-4V RA plate had no effect on the tensile strength values as long as the alpha-beta microstructure was retained. However, both elongation and reduction in area were reduced by the additional thermal processing regardless of microstructure. This reduction was greatest for the transverse direction of the transformed basketweave microstructure.

Results of static fracture toughness tests for the WR direction of the four test plates are included in Table 17. Again, the microstructure of test specimens varied. For specimens having an alpha-beta microstructure, fracture toughness values tended to be slightly higher than the values of 90.4 and 94.6 ksi $\sqrt{\text{in}}$ measured for the as-received plate. For specimens having a basketweave microstructure, fracture toughness was noticeably greater than for the alpha-beta specimens. These results are typical since beta processed titanium alloys normally tend to have higher fracture toughness than comparable alpha-beta processed alloys, although the as-received materials for this program had comparable fracture toughness values.

Effects on Susceptibility to Stress Corrosions Cracking

Results of stress corrosion cracking tests of specimens taken from each of the four thermally cycled plates are listed in Table 18. Microstructural characteristics of the various specimens had a significant influence on test results. The specimen cut from plate 33 had the microstructure pictured in Figure 86; the central 0.5 inch thick band of the plate had a basketweave microstructure and the outer 0.15 each thick bands had an alpha-beta microstructure. The fracture surface of the test specimen is shown in Figure 89. In the WR direction, more SCC, occurred in the outer alpha-beta regions of the plate than in the basketweave central zone. In the basketweave region, there was a tendency for

Table 17: Fracture Toughness Test Results for Ti-6Al-4V Subjected to Various Thermal Cycles (WR Direction and CT Specimens)

PLATE * NO.	MICROSTRUCTURE	AVERAGE CRACK LENGTH (IN)	PEAK LOAD (K)	P _Q @ 5% OFFSET (K)	K _Q ^(a) (KSI√IN)
33	BASKETWEAVE	1.277	18.60	16.68	109.9
44	ALPHA-BETA	1.430	13.40	12.69	99.5
55	ALPHA-BETA	1.410	11.82	12.25	95.6
66	BASKETWEAVE + ALPHA-BETA	1.317	16.85	15.44	111.3

*SEE SECTION 3.3.2.4 FOR DETAILS OF THERMAL PROCESSING

(a) SPECIMENS DID NOT MEET ASTM E399-70T THICKNESS REQ'MENTS.

Table 18: SCC Test Results in 72F/3.5% NaCl Solution for Ti-6Al-4V Subjected to Various Thermal Cycles

PLATE * NO.	MICROSTRUCTURE	TEST DIRECTION	INITIAL CRACK LENGTH (IN)	FINAL CRACK LENGTH (IN)	FINAL STRESS INTENSITY FACTOR (KSI√IN)
33	BASKETWEAVE PLUS ALPHA-BETA (FIGURE 88)	WR	1.375	1.470	68.3
44	BASKETWEAVE	WR	1.400	(a)	—
55	BASKETWEAVE	WR	1.410	(a)	—
66	ALPHA-BETA	WR	1.375	1.550	42.9
55	BASKETWEAVE	RW	0.980	1.12	46.3

*SEE SECTION 3.3.2.4 FOR DETAILS OF THERMAL PROCESSING

(a) CRACK GREW PERPENDICULAR TO ORIGINAL PLANE (I.E., IN RW DIRECTION)

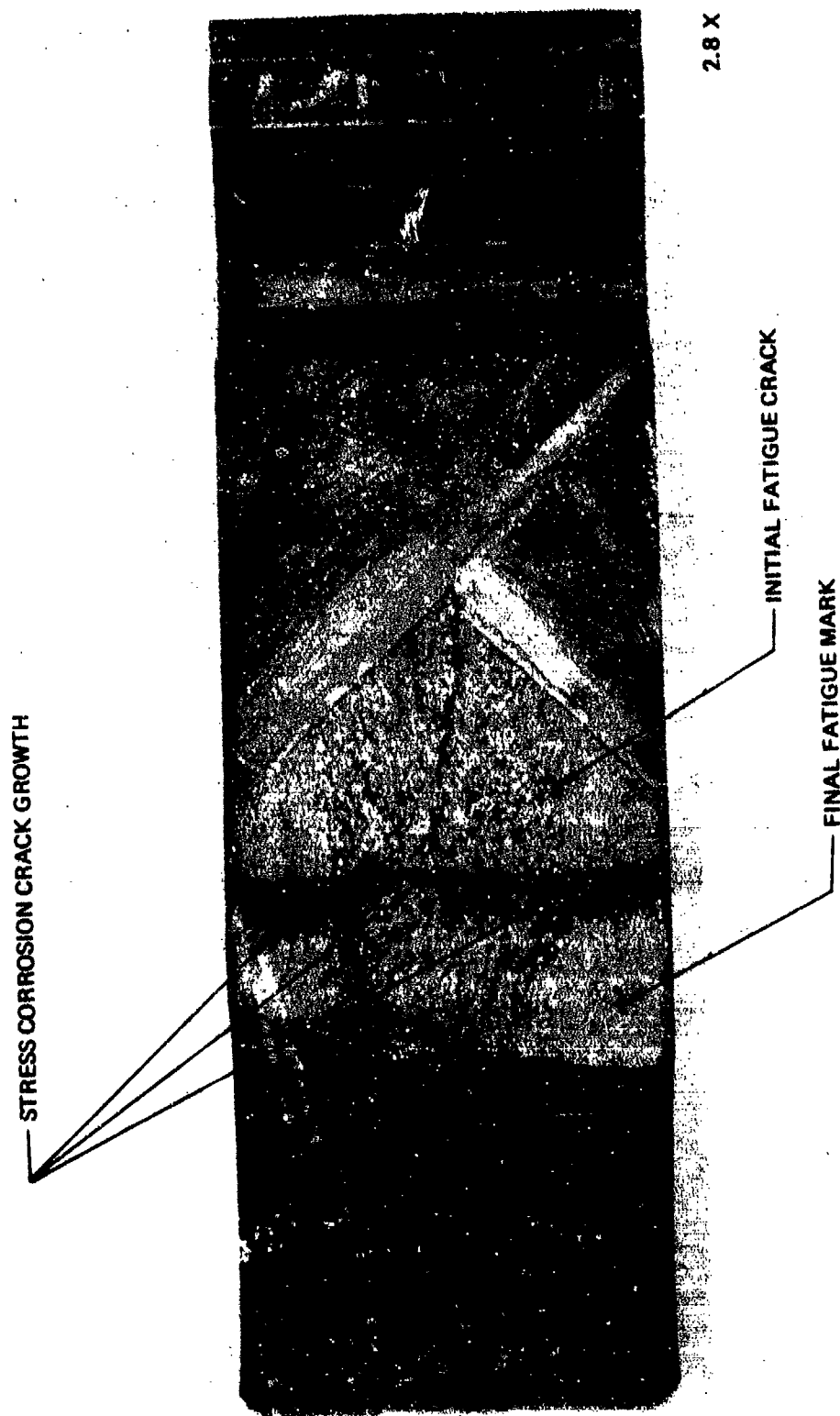


Figure 89: Fracture Surface of Stress Corrosion Specimen 33L I-1 (Plate 33)

SCC to occur in the RW directions, i.e., perpendicular to the original crack plane. This result was probably due to the severe texturing of the basketweave material as illustrated in Figure 88. Test specimens cut from plates 44 and 55 both had a basketweave microstructure. There was only a small amount of SCC in each specimen and the SCC that did occur propagated primarily perpendicular to the original crack plane i.e. in the RW direction. Since the majority of the basal planes were normal to the longitudinal direction in the basketweave material, it should be more susceptible to SCC in the RW than in the WR crack propagation direction. Finally the specimen taken from plate 66 had an alpha-beta microstructure with alpha grain size about double that of the as-received plate. This specimen underwent the most SCC of any of the four specimens tested and the apparent K_{ISCC} was $42.9 \text{ ksi}\sqrt{\text{in}}$ as compared to the K_{ISCC} for the as-received material of $45 \text{ ksi}\sqrt{\text{in}}$.

In summary only one of the four specimens tested had an alpha-beta microstructure similar to the as-received plate. The grain size in the specimen was about double that of the as-received plate and the specimen had been slow cooled at 50F/hour through the critical temperature range from 1400F to 900F. Neither this moderate increase in grain size or slow cooling had any significant effect on SCC susceptibility of the material. The other three specimens had either a basketweave or mixed basketweave/alpha-beta microstructure and were not directly comparable to the as-received plate. The basketweave microstructure was severely textured with the majority of the basal planes oriented normal to the longitudinal direction and was most susceptible to SCC in the RW crack propagation direction.

Effects on Corrosion Fatigue Crack Growth Rates

Corrosion fatigue tests were conducted in 3.5% NaCl solution at 72F on two specimens from each of the four test plates. One of the two specimens was tested under constant peak cyclic load and the other under constant peak cyclic deflection conditions. Results are plotted on graphs of crack growth rate versus ΔK in Figure 90. Again, results were affected by differences in microstructure from specimen to specimen.

The most striking result of the corrosion fatigue test was the wide variation in crack growth rates. At ΔK of $20 \text{ ksi}\sqrt{\text{in}}$ for instance, crack growth rates

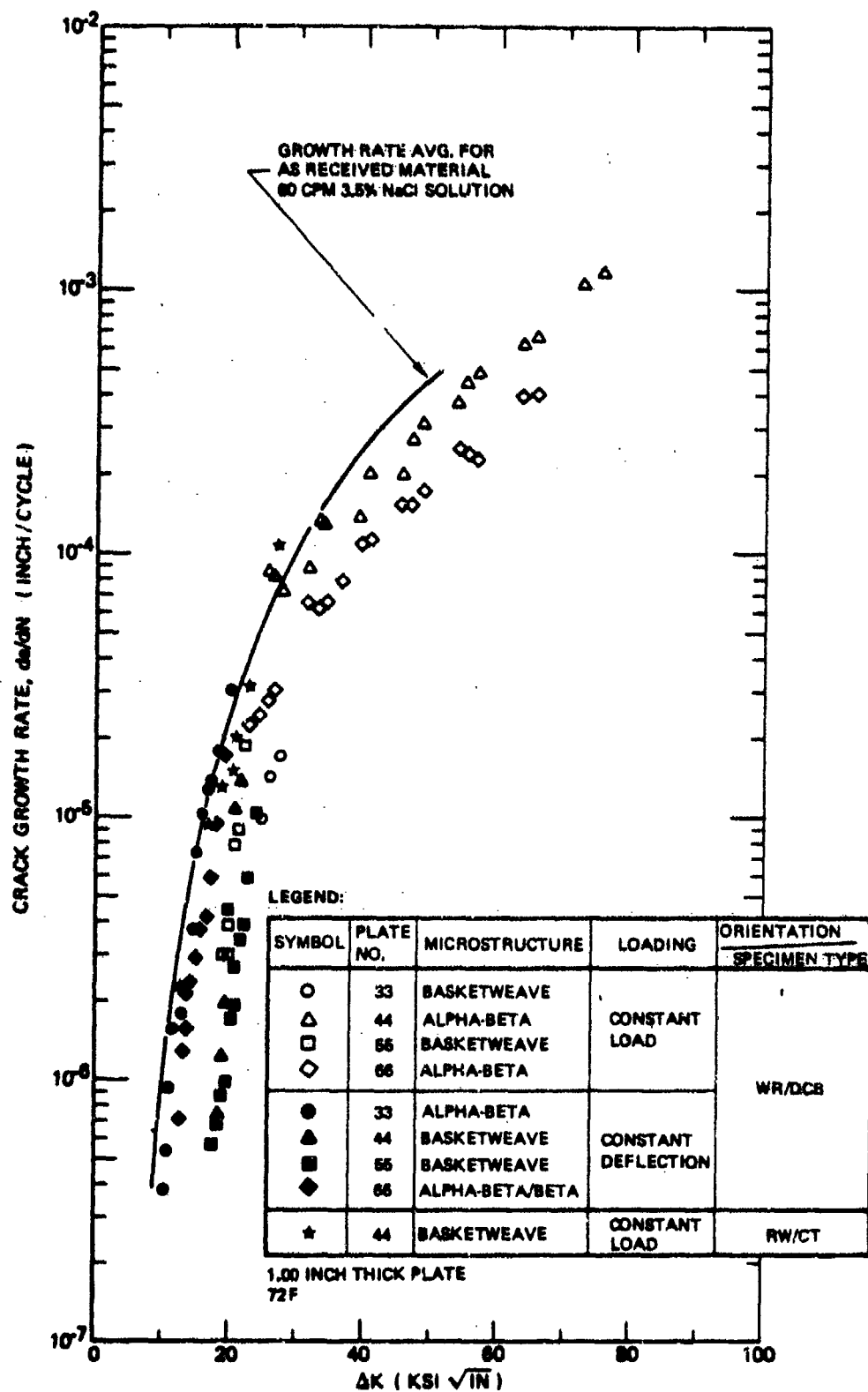


Figure 90: Corrosion Fatigue Crack Growth Rates for Thermal Processing Effect Tests (6Al-4V Annealed Titanium Alloy in 3.5% NaCl Solution)

varied over one and one-half orders of magnitude. The fastest crack growth rate occurred in specimens having an alpha-beta microstructure and the slowest rates for the WR crack propagation direction in specimens having a basketweave microstructure. However, the basketweave material was highly textured and crack propagation rates for the RW direction were about the same as the fastest rates measured for the WR direction of the specimens having an alpha-beta microstructure.

All additional thermal treatments applied to the as-received material had either no effect or a decelerative effect on corrosion fatigue crack growth rate. The crack growth rate curve for the as-received material is included in Figure 90 for comparison and lies on or above all but three data points. Data points indicated by solid circles, open triangles, and open diamonds in Figure 90 were obtained from specimens having an alpha-beta microstructure with grain size about double that of the as-received material, and were slow cooled at 50F/hour through the critical temperature range. Neither the increased grain size nor slow cooling had a detrimental effect on crack growth rate under the conditions existent in these tests. There is always the possibility that if cyclic speed had been slower, or if composition of the material had been different within specification limits, that an acceleration in crack growth rates due to increased grain size or slow cooling would have been observed. However, these tests indicate that for conditions representative of gust loadings in aircraft structure, the effects of overheating or slow cooling of Ti-6Al-4VRA material will not be detrimental to crack propagation life of the components.

Summary

Specimens of Ti-6Al-4V RA material were heated near the beta transus and were slow cooled to: (1) grow the primary alpha grains and (2), result in ordering of the alpha phase. Mechanical property, fracture toughness, stress corrosion cracking, and corrosion fatigue tests were conducted to determine the effects of grain size and ordering on fracture and crack growth resistance. After testing was underway, it was discovered that the thermal processing had resulted in wide variations in microstructure within each test plate. Both Alpha-beta and basketweave microstructures were observed throughout each test plate.

Both alpha-beta and basketweave microstructures were observed throughout each test plate. Alpha grain size varied from 1.5 to 2 times that of the as-received material but no ordering was detected by thin foil electron diffraction microscopy. The basketweave material was extremely textured with about 60% of the basal planes oriented perpendicular to the longitudinal direction.

Differences in microstructure had the largest effect on fracture and crack growth resistance. In the WR crack propagation direction, the textured basketweave material had superior fracture toughness, SCC resistance, and corrosion fatigue resistance. For the RW direction, the SCC and corrosion fatigue resistance of the basketweave material was nearly the same as for the as-received Ti-6Al-4V RA plate. A significant result was that none of the potentially detrimental thermal processing applied to the Ti-6Al-4V RA material degraded the fracture and crack growth resistance properties of the as-received material which is believed to be representative of high quality Ti-6Al-4V RA alloy plate.

3.4 Steel Alloy Test Results

The test program for 9Ni-4Co-0.3C (240 ksi) steel alloy plate is summarized in Table 19. Mechanical property and fracture toughness tests were conducted for both the longitudinal (RW) and long transverse (WR) directions. Stress corrosion cracking tests were conducted for the short transverse (TR) and WR crack propagation directions. Corrosion fatigue tests were conducted for only the WR direction. Results of mechanical property and fracture toughness tests are reported in Section 2.1. Results of the stress corrosion cracking and corrosion fatigue tests are described in the following sections 3.4.1 and 3.4.2.

3.4.1 Stress Corrosion Cracking Tests

Six stress corrosion cracking (SCC) tests were conducted including five in distilled water and one in water saturated JP-4 fuel. The distilled water tests included four tests for the WR crack propagation direction and one test for the TR crack propagation direction.

Results of tests conducted in distilled water are plotted in Figure 91. The specimen was wedge loaded to generate a stress intensity factor of $80 \text{ ksi}\sqrt{\text{in.}}$

Table 19: Test Program for 9Ni-4Co-0.3C (240 KSI) Steel Alloy Plate

TEST TYPE	SPECIMEN TYPE	CYCLIC FREQUENCY	STRESS RATIO	ENVIRONMENT																							
				AIR			DISTILLED WATER			3.5% NaCl SOLUTION			JP-4			SUMP TANK			JP-4 + H ₂ O			DYE PEN					
				-65F	72F	175F	-65F	72F	175F	-65F	72F	175F	-65F	72F	175F	-65F	72F	175F	-65F	72F	175F	-65F	72F	175F			
MECHANICAL PROPERTY	TENS.			8	8	8																					
FRACTURE TOUGHNESS	CT			2	2	2																					
	SF			2	2	2																					
STRESS CORROSION CRACKING	DCB						5						1														
	SF																										
CORROSION FATIGUE	DCB	60	0.1	2	1	1	3	1		2	1		2	1	1					1	1			1			
			0.5	1						1			1														
			0.8	1																							
CORROSION FATIGUE	DCB	6	0.1				1	1		1	1		1	1						1							
			0.5	1			1	1		1	1		1	1													
OVERLOAD	SF	60	0.5																								
	TDCB	60	0.5																								

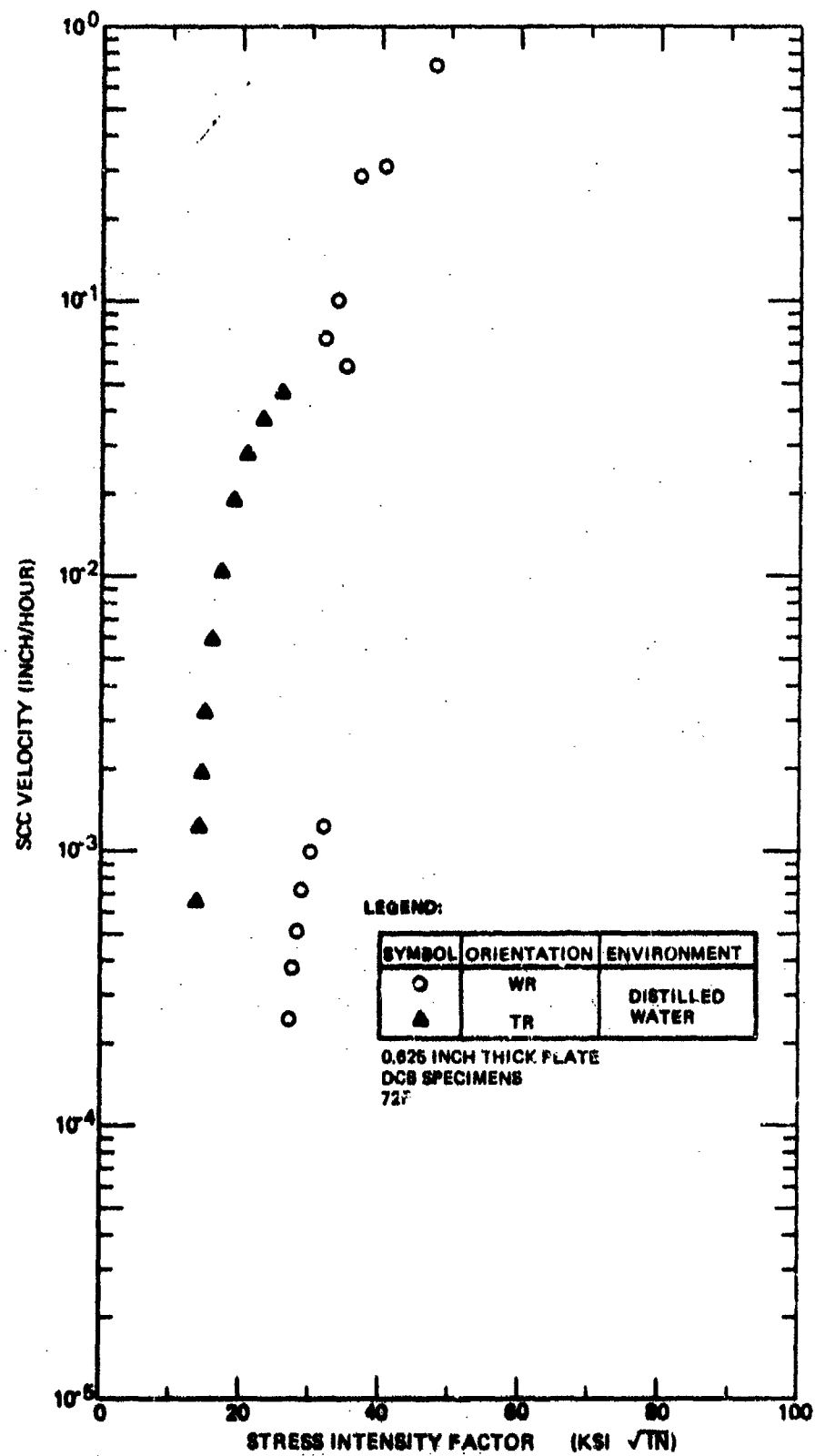


Figure 91: Stress Corrosion Cracking Velocity Data for 9Ni-4Co-0.3C Steel Alloy in Distilled Water

Crack growth initiated immediately but the crack deviated from its original plane and grew into the specimen arms. It was estimated that the initial crack velocity was about 2×10^{-4} inches/second as shown by the bar in the upper right of Figure 91. After the initial test, all other specimens were tested without side grooves. A second specimen was wedge loaded in distilled water to generate a stress intensity factor of $32 \text{ ksi}\sqrt{\text{in}}$ at the crack tip. After an incubation period of about 24 hours, the crack began to grow and the velocity data indicated by the open circles in the lower part of Figure 91 were taken. The stress intensity factor was then increased to $47 \text{ ksi}\sqrt{\text{in}}$ after which the rate of crack propagation increased dramatically; the crack propagated in its original plane for only a short distance at a rate of about 2×10^{-4} inches/second, then rotated into the specimen arm. A third specimen was wedge loaded to generate a stress intensity factor of $40 \text{ ksi}\sqrt{\text{in}}$ and the crack growth rate data indicated by the open circles in the upper part of Figure 91 were taken.

A single SCC test was conducted for the TR crack propagation direction after considerable short transverse splitting was observed on the fracture faces of corrosion fatigue specimens tested in distilled water. The specimen (Figure B5) was wedge-loaded in distilled water to generate a stress intensity factor of $25 \text{ ksi}\sqrt{\text{in}}$. Crack propagation initiated immediately and continued in the original crack plane for a distance of 1.8 inches before the test was discontinued. Periodic measurements of crack length were used to calculate the SCC velocities plotted as solid triangles in Figure 91. It is evident that the TR direction was extremely prone to SCC in distilled water with the apparent K_{ISCC} value being less than $14 \text{ ksi}\sqrt{\text{in}}$ or about 13 percent of the fracture toughness for the WR crack propagation direction.

A single SCC test was conducted in JP-4 fuel. The specimen was initially wedge loaded to generate a stress intensity factor of $47.5 \text{ ksi}\sqrt{\text{in}}$ and tested for five days without any indication of SCC; the stress intensity factor was subsequently increased to 60, 73.2 and $83 \text{ ksi}\sqrt{\text{in}}$ for seven, three and 345 days, respectively, without undergoing SCC. It is evident that the JP-4 fuel is a very mild environment for the 9Ni-4Co-0.3C steel alloy.

It had been hoped at the outset of this program that the 9Ni-4Co alloy would yield higher K_{IC} and K_{ISCC} values than comparable strength 4330 alloys. The resulting fracture toughness values were better than those normally obtained from the 4330 alloy at the 220-240 strength level, i.e., $100 + ksi\sqrt{in}$ versus $70-80 ksi\sqrt{in}$. However, the aqueous environment K_{ISCC} for the WR direction showed no improvement over typical values for 4330 steel. In addition, a particularly severe susceptibility to SCC in the TR direction was observed. However, the latter result was probably influenced by the banding in the particular batch of 9Ni-4Co-0.3C steel alloy plate tested in the program.

3.4.2 Corrosion Fatigue Tests

The program of corrosion fatigue tests for the 9Ni-4Co-0.3C steel alloy plate is summarized in Table 19. Tests were conducted in seven different test media at 72F using three different stress ratios (0.1, 0.5 and 0.8) and two cyclic frequencies (6 and 60 cpm). The effects of these variables on fatigue crack propagation are described in this section.

All crack growth rate data collected for the 9Ni-4Co-0.3C steel alloy is included in Figures A50 through A62 in Appendix A. All data are not shown in the body of the report. Rather, average crack growth rate curves drawn through the data are used to illustrate specific effects.

3.4.2.1 Effect of Test Media and Cyclic Frequency

The effect of test media on fatigue crack growth rates was highly dependent on cyclic frequency. At 60 cpm, tests in seven different media yielded very little variation in crack growth rates as illustrated in Figure 92. The scatter bands in Figure 92 encompass all the crack growth rate data obtained in the seven test media for stress ratios of 0.1 and 0.5. For given ΔK , the largest ratio of maximum to minimum crack growth ratio was 3 for a stress ratio of 0.5 and crack growth rates near 10^{-5} inches/cycle. At 6 cpm, there was a marked effect of cyclic frequency on crack growth rate behavior as shown in Figures 93 and 94. Testing was discontinued before crack growth rates at low ΔK values were evaluated and the effects of the decrease in test frequency

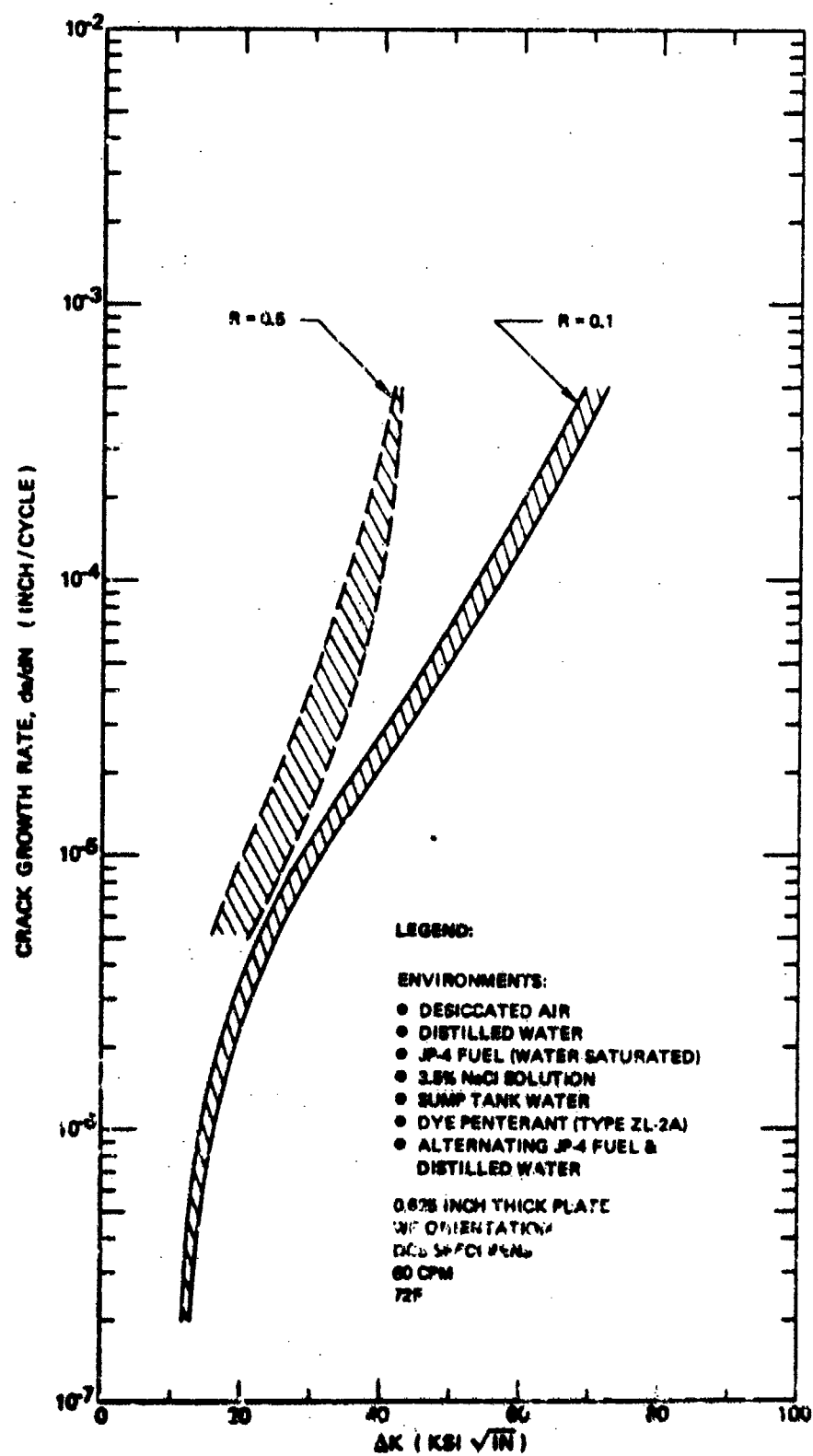


Figure 92: Envelopes of Average Fatigue Crack Growth Rates for 9Ni-4Co-0.3C Steel Alloy in Seven (7) Environments (60 CPM)

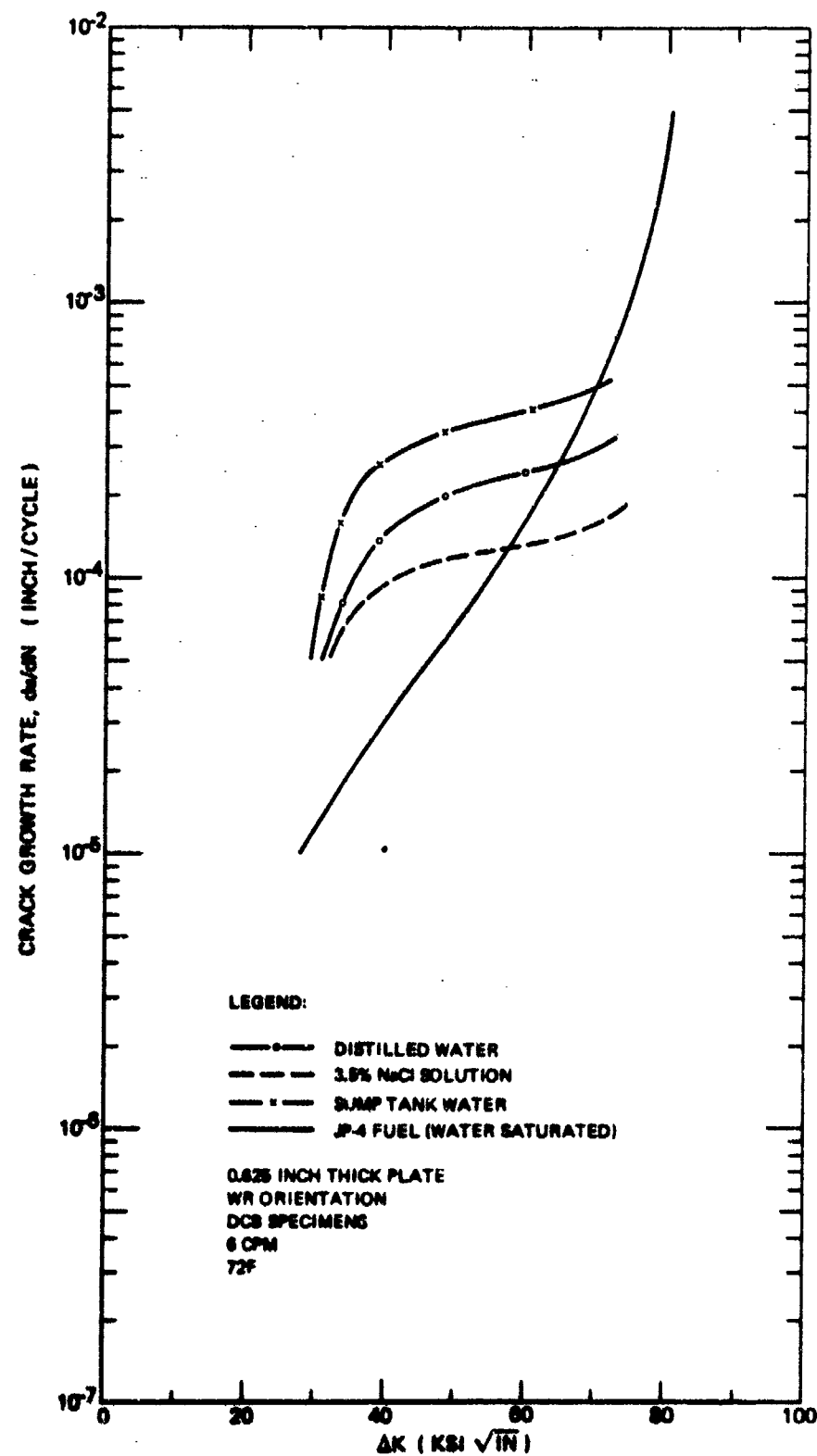


Figure 93: Effect of Environment on Fatigue Crack Growth Rates at $R=0.1$ in 9Ni-4Co-0.3C Steel Alloy (6 CPM)

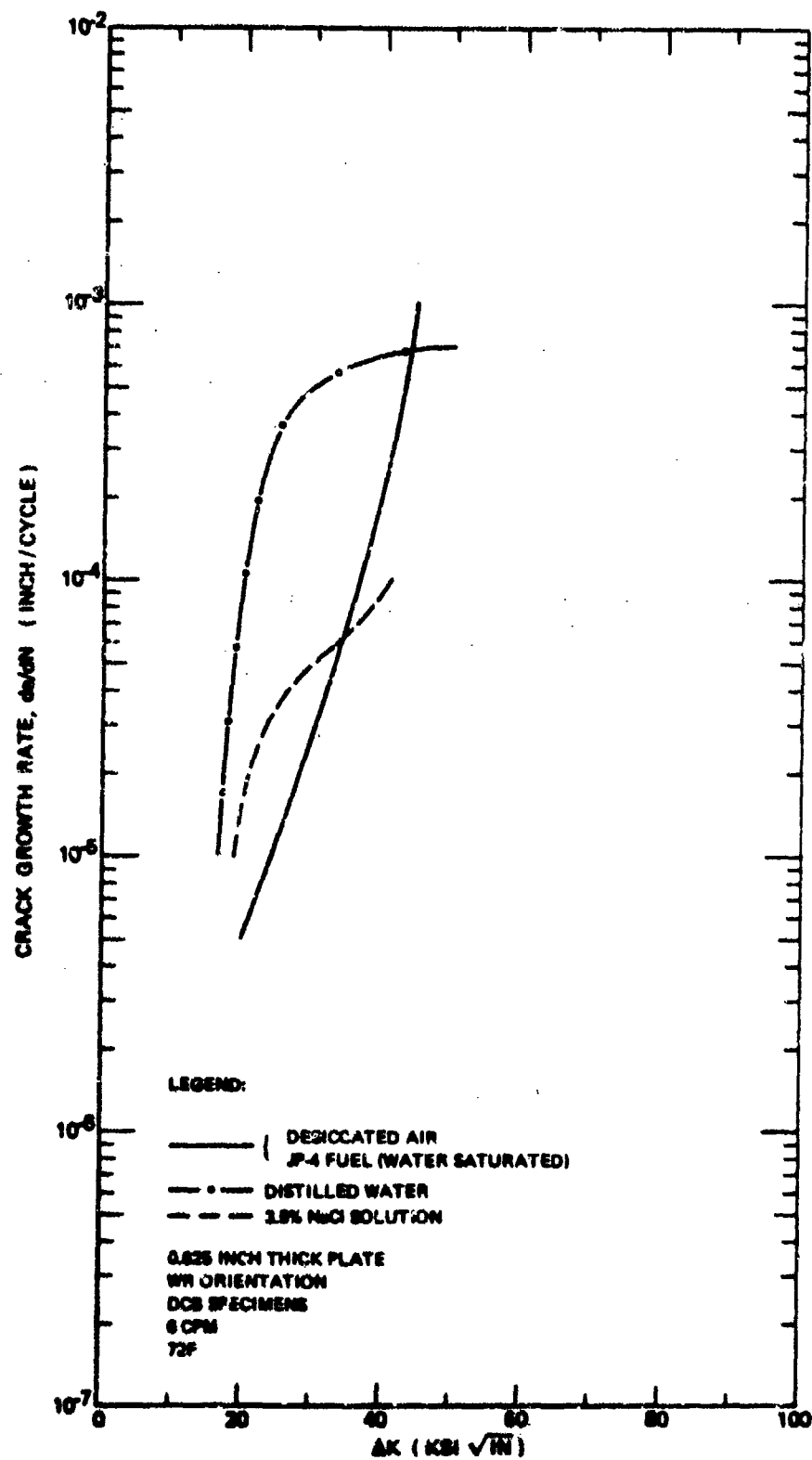


Figure 94: Effect of Environment on Fatigue Crack Rates at $R=0.5$ in 9Ni-4Co-0.3C Steel Alloy (6 CPM)

were not fully characterized. However, it does appear the the marked acceleration in crack growth rates due to the decrease in cyclic frequency began at K_{\max} levels near the apparent K_{ISCC} value of about $26 \text{ ksi}\sqrt{\text{in}}$. Below $K_{\max} = 26 \text{ ksi}\sqrt{\text{in}}$, the effect of cyclic frequency on crack growth rates is probably less drastic than the effects shown in Figures 93 and 94.

3.5 • Overload Effect Tests

Thirty overload effect tests were conducted to evaluate the effect of single overloads on subsequent fatigue crack growth rate behavior. Ten tests were conducted for each of three alloys including 7075-T651 aluminum, Ti-6Al-4V beta annealed, and Ti-6Al-4V recrystallize annealed, as summarized in Table 20. Three different peak overload stress intensity factors (K_o) were tested to represent overloads early ($K_o = 62.5\% K_{cr}$), midway ($K_o = 75\% K_{cr}$), and late ($K_o = 90\% K_{cr}$) in the life of an airframe component. The subsequent peak cyclic stress intensity factors (K_{\max}) were chosen to yield overload ratios (K_o/K_{\max}) of 1.5 and 1.8. Parallel test programs were conducted in desiccated air and 3.5% NaCl solution to evaluate overload effects in both mild and aggressive media.

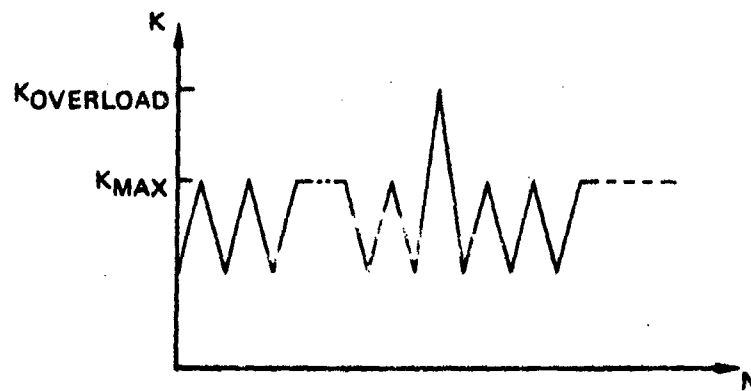
3.5.1 Test Procedures

Overload effect tests were conducted by subjecting tapered double cantilever beam specimens (Figure B13) to loading profiles consisting of two block of uniform load cycles separated by a single overload. All tests were conducted using a cyclic frequency of 60 cpm and stress ratio of 0.5. Specimens were instrumented with clip gages spring loaded against knife edges integrally machined at the mouth of the crack as shown in Figure B11. The clip gages were used to continuously record crack displacement as a function of loading cycles.

Tests were conducted in both desiccated air and 3.5% NaCl solution. Tests in desiccated air were performed with the specimen surrounded by a sealed plastic bag containing sufficient desiccant to reduce the relative humidity to about 10%. Tests in 3.5 solution were conducted with the crack tip continuously submerged in the solution.

Table 20: Overload Effects Test Program

ALLOYS	TEST MEDIA	K _{OVERLOAD} (% K _Q)	K _{MAX} (% K _{cr})	R	NUMBER OF TESTS
Al - 7075-T651 Ti - 6Al-4V βA Ti - 6Al-4V RA	DESICCATED AIR 3.5% NaCl SOLUTION	90	$\left\{ \begin{matrix} 60 \\ 50 \end{matrix} \right\}$	0.5	12
		75	$\left\{ \begin{matrix} 50 \\ 41.7 \end{matrix} \right\}$	0.5	12
		62.5	41.7	0.5	6



Multiple tests were conducted on each specimen. Five tests were conducted on each aluminum alloy specimen and either two or three tests were conducted on each titanium alloy specimen. Individual tests included the application of two blocks of uniform load cycles separated by an overload. During the application of each block of uniform load cycles, the crack was grown a distance approximately equal to the value of $(K_o/\sigma_{ys})^2$ where K_o is the value of peak stress intensity factor during the overload cycle, and σ_{ys} is the yield strength of the material. Different stress levels were used for each successive test and the crack growth that occurred during each block of cycles was identifiable on the fracture surfaces of the test specimens.

3.5.2 Methods for Evaluating Results

Results for overload effect tests were determined both by evaluation of test records of crack displacement versus cycles, and observation of the fracture faces of test specimens. An example of a crack displacement versus cycles record is shown in Figure 95. The initial straight line portion of the record (AB) was obtained during uniform stress cycling prior to application of the overload. An overload was applied at point B and the crack displacement increased to point C during the overload. Uniform stress cycling was then resumed and the curved portion (CD) of the record was obtained. At point D, the test record returned to the straight line DE which was parallel to the initial straight line portion AB. Test records were used to determine:

(1) the number of delay cycles caused by the application of the overload, ΔN_d , and (2) the crack length over which the effects of the overloads were observed, Δa_d . The value of Δa_d was proportional to $\Delta \delta_d$ which was measured from the test record as shown in Figure 95. The relationship between crack growth that occurred during the overload (Δa_o) was measured directly from the fracture face of the test specimen. The number of baseline loading cycles that would have been required to growth the crack the same distance that it grew during the overload (ΔN_o) was calculated by dividing Δa_o by the average rate at which the crack was growing prior to application of the overload. The relationship of both Δa_o and ΔN_o to the test record is shown in Figure 95.

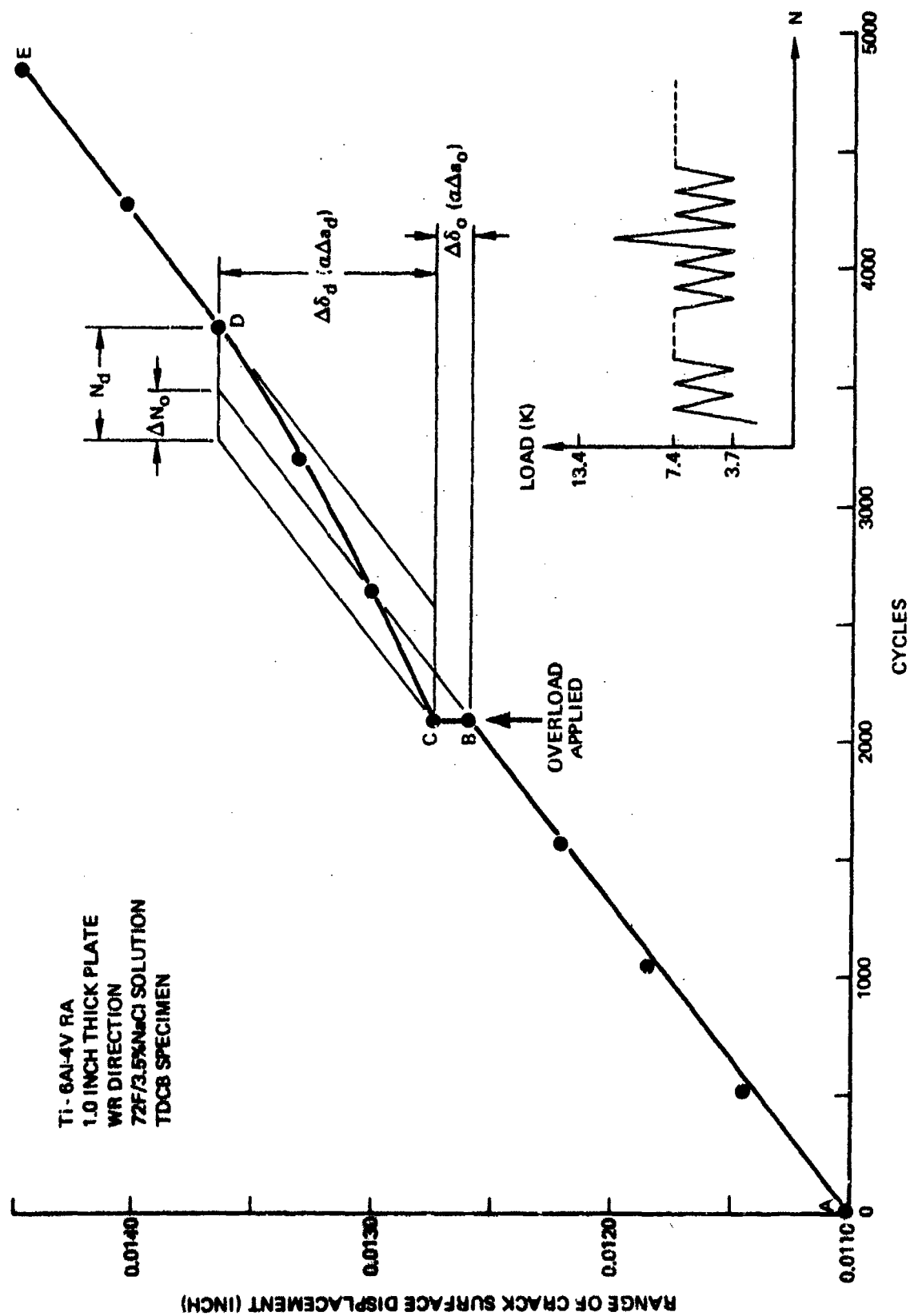


Figure 95: Example of Test Records Obtained From Overload Tests

3.5.3 Results and Discussion

Test parameters and results for each of the Ti-6Al-4V beta annealed, Ti-6Al-4V recrystallized annealed, and 7075-T651 aluminum alloy tests are listed in Tables 21, 22 and 23, respectively. Results obtained from tests in desiccated air are listed in the upper parts of the tables; comparable results from tests in 3.5% NaCl solution are listed in the lower parts of the tables. Individual values of delay cycles (ΔN_d), crack growth caused by the overload (Δa_o), number of baseline cycles that would have been required to grow the crack a distance equal to Δa_o (ΔN_o), and length of crack over which the overload effect was observed (Δa_d) are listed in the tables.

All tests did not yield results of equal consistency and so the consistency of each set of data have been indicated in the tables of results. Where the consistency was very good, the data were very easy to evaluate and no subjective interpretations were required. When the consistency of the data was poor, subjective interpretations of the data were required and the accuracy with which the values of ΔN_d and Δa_d could be evaluated deteriorated. The majority of the data obtained from titanium alloy tests exhibited good consistency. On the other hand, the aluminum alloy tests yielded fairly inconsistent data. The reason for the inconsistent aluminum alloy data was that only very small changes in crack deflection occurred between the application of the overload and the time at which the crack grew out of the influence of the overload. The plastic zone size for the 7075-T651 alloy was on the order of 0.01 inch as compared to total crack lengths in excess of 2.5 inches. Hence, the change in crack length and crack deflection over which the overload effects occurred were too small to be reliably detected by the instrumentation used in those tests. The plastic zone size for the titanium alloys was on the order of 0.1 inch and the instrumentation was sufficiently sensitive to detect changes in crack growth behavior as the crack traversed the plastic zone formed by the overload. Consequently, most of the following discussion will be directed to titanium alloy data.

In the titanium alloys, environment had a strong effect on the number of delay cycles resulting from the application of an overload. This is illustrated in Figure 96 where delay cycles (ΔN_d) are plotted as a function of overload ratio (K_o/K_{max}) for both titanium alloys. For the Ti-6Al-4V RA alloy, a substantial

Table 21: Results of Overload Effect Tests on 6Al-4V Standard ELI Beta Annealed Titanium Alloy Plate (TDCB Specimens—WR Orientation)

ENVIRONMENT	ΔK (KSI $\sqrt{\text{IN}}$)	K_{MAX} (KSI $\sqrt{\text{IN}}$)	K_{OVERLOAD} (KSI $\sqrt{\text{IN}}$)	$\frac{K_o}{K_{\text{MAX}}}$	ΔN_D (~)	ΔN_o (~)	Δa_D (IN)	Δa_o (IN)	$\frac{\Delta a_D}{0.2 (K_o/a_{ys})^2}$	CONSISTENCY OF DATA
DESSICATED AIR @ 72F	19.5	38.9	58.3	1.50	2,600	150	0.067	0.002	1.6	VERY GOOD
	19.5	38.9	69.9	1.80	10,000	770	0.084	0.010	1.4	VERY GOOD
	19.5	38.9	69.9	1.80	11,400	1,900	0.078	0.025	1.3	VERY GOOD
	23.3	46.6	69.9	1.50	2,930	2,380	0.058	0.005	1.0	VERY GOOD
	23.3	46.6	83.9	1.80	5,050	4,760	0.066	0.010	0.7	VERY GOOD
	28.0	55.9	83.9	1.50	400	290	0.020	0.010	0.2	GOOD
3.5% NaCl SOLUTION @ 72F	19.5	38.9	58.3	1.50	0	110	0	0.003	0	FAIR
	19.5	38.9	69.9	1.80	6,400	110	0.039	0.003	0.7	GOOD
	23.3	46.6	69.9	1.50	1,400	90	0.139	0.005	2.3	VERY GOOD
	23.3	46.6	83.9	1.11	2,840	370	0.056	0.020	0.6	VERY GOOD
	28.0	55.9	83.9	1.50	1,200	230	0.174	0.020	1.9	VERY GOOD

SEE FIGURE 95 FOR DEFINITION OF SYMBOLS

Table 22: Results of Overload Effect Tests on 6Al-4V Recrystallize Annealed Titanium Alloy Plate (TDCB Specimens—WR Orientation)

ENVIRONMENT	ΔK (KSI $\sqrt{\text{IN}}$)	K_{MAX} (KSI $\sqrt{\text{IN}}$)	K_{OVERLOAD} (KSI $\sqrt{\text{IN}}$)	$\frac{K_0}{K_{\text{MAX}}}$	ΔN_d^* (~)	ΔN_0^* (~)	Δa_d^* (IN)	Δa_0^* (IN)	$\frac{\Delta a_d}{0.2 (K_0/\sigma_{ys}^2)}$	CONSISTENCY OF DATA
DESICCATED AIR @ 72F	19.3	38.6	57.9	1.50	3500	100	0.096	0.002	2.3	GOOD
	19.3	38.6	69.6	1.80	7300	400	0.094	0.008	1.5	FAIR
	23.2	46.4	69.6	1.50	~1500	360	(a)	0.010	(a)	GOOD
	23.2	46.4	83.4	1.80	6700	1260	0.078	0.035	0.9	GOOD
	27.8	55.6	83.4	1.50	(a)	1100	(a)	0.055	(a)	POOR
3.5% NaCl SOLUTION @ 72F	19.3	38.6	57.9	1.50	450	20	0.124	0.002 ^(b)	3.0	VERY GOOD
	19.3	38.6	69.6	1.80	565	100	0.042	0.010	0.7	VERY GOOD
	23.2	46.4	69.6	1.50	~0	30	~0	0.005	~0	GOOD
	23.2	46.4	83.4	1.80	660	190	0.183	0.030	2.1	VERY GOOD
	27.8	55.6	83.4	1.50	~0	450	~0	0.100	~0	FAIR

(a) NOT DETERMINED

(b) ESTIMATED

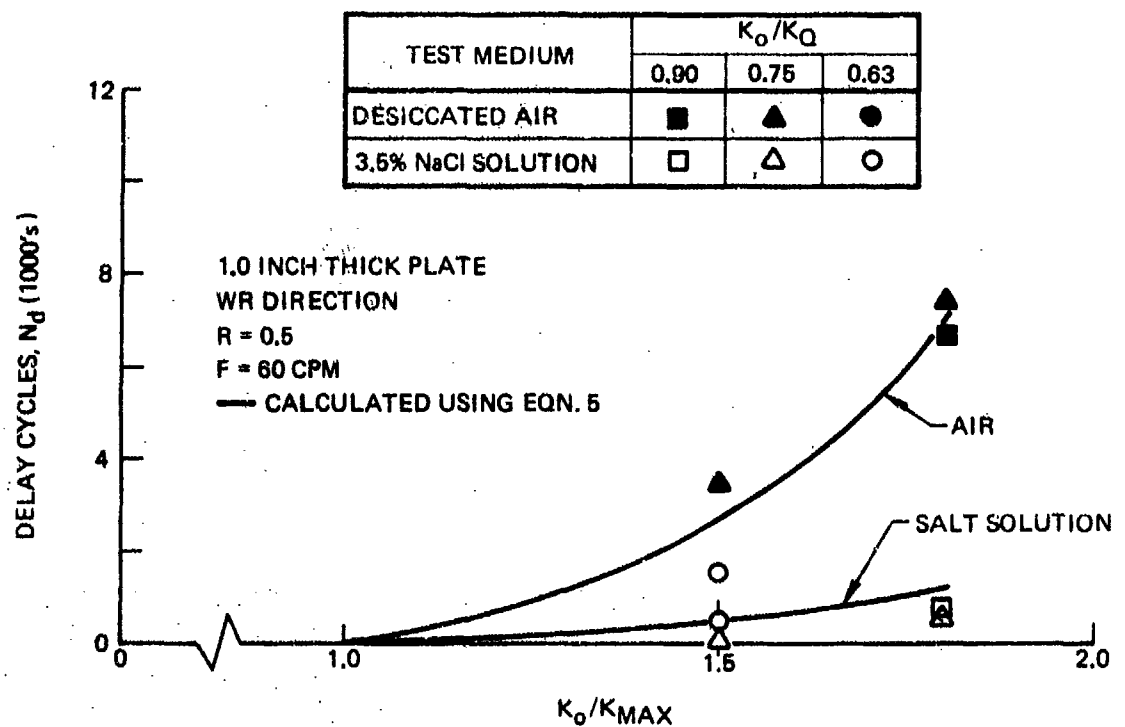
* SEE FIGURE 95 FOR DEFINITION OF SYMBOLS

Table 23: Results of Overload Effect Tests on 7075-T651 Aluminum Alloy Plate
TDCB Specimen—WR Orientation

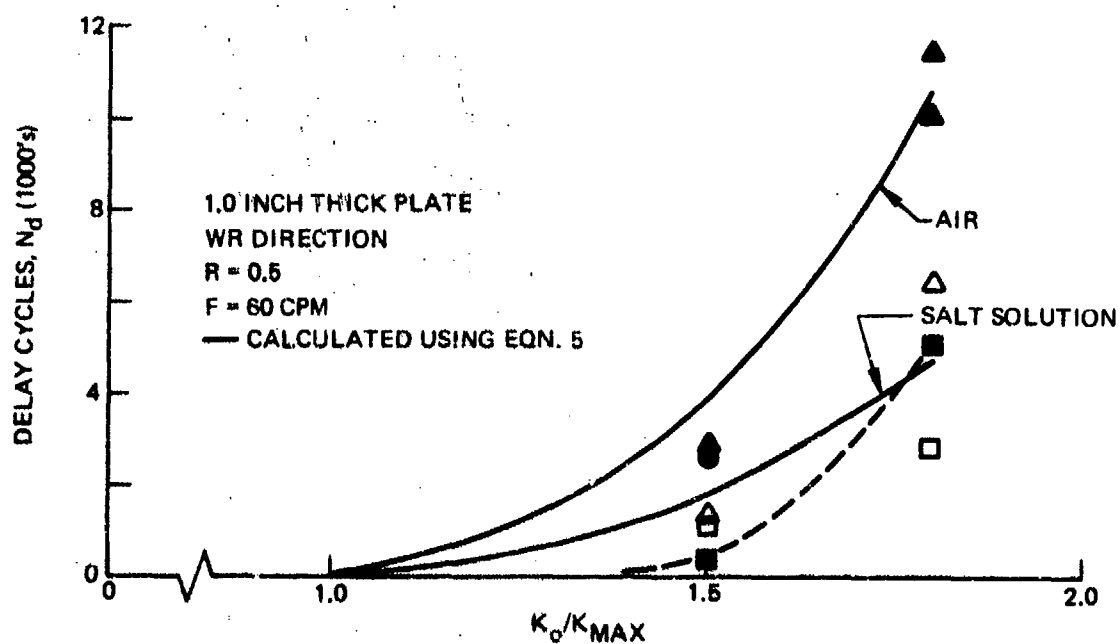
ENVIRONMENT	ΔK (KSI $\sqrt{\text{IN}}$)	K_{MAX} (KSI $\sqrt{\text{IN}}$)	K_{OVERLOAD} (KSI $\sqrt{\text{IN}}$)	$\frac{K_o}{K_{\text{MAX}}}$	ΔN_d (~)	ΔN_o (~)	Δa_d (IN)	Δa_o (IN)	$\frac{\Delta a_d}{0.2 (K_o/\sigma_{ys})^2}$	CONSISTENCY OF DATA
DESSICATED AIR @ 72F	4.60	9.20	13.80	1.50	40,000	833	0.035	0.002	5.8	FAIR
	4.60	9.20	16.50	1.80	ND	833	ND	0.002	ND	POOR
	5.50	11.00	16.50	1.50	25,000	300	0.030	0.001	3.5	POOR
	5.50	11.00	19.80	1.80	4,000	600	0.039	0.002	3.2	POOR
	6.60	13.20	19.80	1.50	4,000	170	0.016	0.001	1.3	POOR
	6.90	13.80	16.60	1.20	3,600	150	0.042	0.001 ^(a)	4.9	GOOD
3.5% NaCl SOLUTION @ 72F	4.60	9.20	13.80	1.50	8,850	370	0.006	0.002	1.0	POOR
	4.60	9.20	16.50	1.80	8,000	370	0.024	0.002	3.0	FAIR
	5.50	11.00	16.50	1.50	3,890	260	0.030	0.002	3.8	FAIR
	5.50	11.00	19.80	1.80	4,800	260	0.040	0.002	3.3	GOOD
	6.60	13.20	19.80	1.50	4,300	140	0.022	0.002	1.8	POOR

(a) ESTIMATE

SEE FIGURE 95 FOR DEFINITION OF SYMBOLS



(a) Ti-6Al-4V RA Results



(b): Ti-6Al-4V BA Results

Figure 96: Effect of Overload Ratio on Delay Cycles for Titanium Alloy Overload Tests

number of delay cycles were obtained from the tests in desiccated air. However, the presence of the 3.5% NaCl solution reduced the number of delay cycles to near zero. For the Ti-6Al-4V beta annealed alloy, the reduction in numbers of delay cycles due to the 3.5% NaCl solution was less marked than in the Ti-6Al-4V RA plate.

When the peak stress intensity factors during the overloads reached 90% of the corresponding critical stress intensity factor, the number of delay cycles for Ti-6Al-4V β A tests was reduced from values of delay cycles obtained from tests having lower peak stress intensity factors. In contrast, the Ti-6Al-4V RA tests did not yield such a trend. These trends are illustrated in Figure 96 where data for three different values of K_o/K_{cr} ratios of 0.90 agree with data obtained from tests using K_o/K_{cr} ratios of 0.75 and 0.63. For the Ti-6Al-4V β A alloy, the data for overload ratios of 0.9 fall considerably below the data for lesser overload ratios. This result was probably influenced by the ductile tear that occurs during overloads to high percentages of the ultimate load.

Overloads resulted in detrimental as well as beneficial effects. During the application of the overloads, the crack extended considerably more than would have been predicted using uniform stress crack growth rate data. For example, the overload cycle for the test listed on the top line of Table 21 resulted in 0.002 inches of crack growth. The overload cycle had a ΔK of $38.8 \text{ ksi}\sqrt{\text{in}}$ and stress ratio of 0.33. The uniform load crack growth rate data in Figure A17 yields a crack growth rate of about 10^{-4} inch for the overload cycle, i.e., an order of magnitude less than the actual growth. This result is typical of all overloads applied on these tests. An acceleration in crack growth rate during high stress cycles following low stress cycles has been previously observed by several investigators (12, 13).

The change in crack length required to eliminate the effects of the prior overloads (Δa_d) was compared to the size of the plastic zone formed by the overload to see if a consistent relationship between the two quantities existed. Plastic zone sizes were estimated to be $0.2 (K_o/\sigma_{ys})^2$ (14). Ratios of $\Delta a_d/0.2 (K_o/\sigma_{ys})^2$ are listed in the next to last column in the tables. For titanium alloy tests in which a K_o/K_{max} ratio of 1.8 was used, the values of $\Delta a_d/0.2 (K_o/\sigma_{ys})^2$ varied

from 0.6 to 2.1 and average 1.1. When a K_o/K_{max} ratio of 1.5 was used, the values varied from 0 to 3 with an average of 1.2. Hence, it appears that on the average, the effects of overloads on subsequent crack propagation ratios are dissipated after the crack has grown approximately one plastic zone size or $0.2 (K_o/\sigma_{ys})^2$ for plane strain conditions.

The total effect of the overloads on the number of cycles required to grow the crack a given distance is indicated by the quantity $(\Delta N_d - \Delta N_o)$, i.e., delay cycles less the equivalent cyclic damage caused by the overload; this quantity is plotted as a function of the ratio of K_{max}/K_o in Figure 97. It is evident that as K_o approaches K_{cr} , the beneficial effect of overloads decreases rapidly. There is insufficient data to allow easy quantification of the results, but it does appear that overloads do not have a detrimental effect on crack propagation life until the peak overload stress intensity factor (K_o) reaches 90% of the critical stress intensity factor. However, beneficial effects of overloads start to diminish when K_o exceeds about 60-70% of the critical stress intensity factor. More tests are required to firmly establish the aforementioned trends.

Results for the 7075-T651 aluminum alloy in Table 23 seem to show trends similar to those observed in the titanium alloy results. The effect of overloads on crack growth rate appeared to be less pronounced in 3.5% NaCl solution than in desiccated air. Also, the beneficial effect of overloads diminished as the peak overload stress intensity factor approached the corresponding critical value.

Several methods of calculating the effect of overloads on subsequent crack growth rate have been proposed (15, 16, 17). The methods due to Wheeler (15) and Willenborg (16) have received the most attention. Unfortunately, a considerable amount of effort would be required to evaluate the results in terms of these methods. A more simple but unpublished procedure for calculating delay cycles due to overloads has been in use at Boeing for some time. The Boeing method was based on data published by Porter (17) and calculates crack growth rate after the application of an overload using the equation

$$\frac{da}{dN} \text{ after overload} = \frac{da}{dN} \text{ uniform load} \times \left(\frac{K_{max}}{K_o} \right)^2 \text{ for } 0 < \Delta a < 0.2 \left(\frac{K_o}{\sigma_{ys}} \right)^2 \quad (5)$$

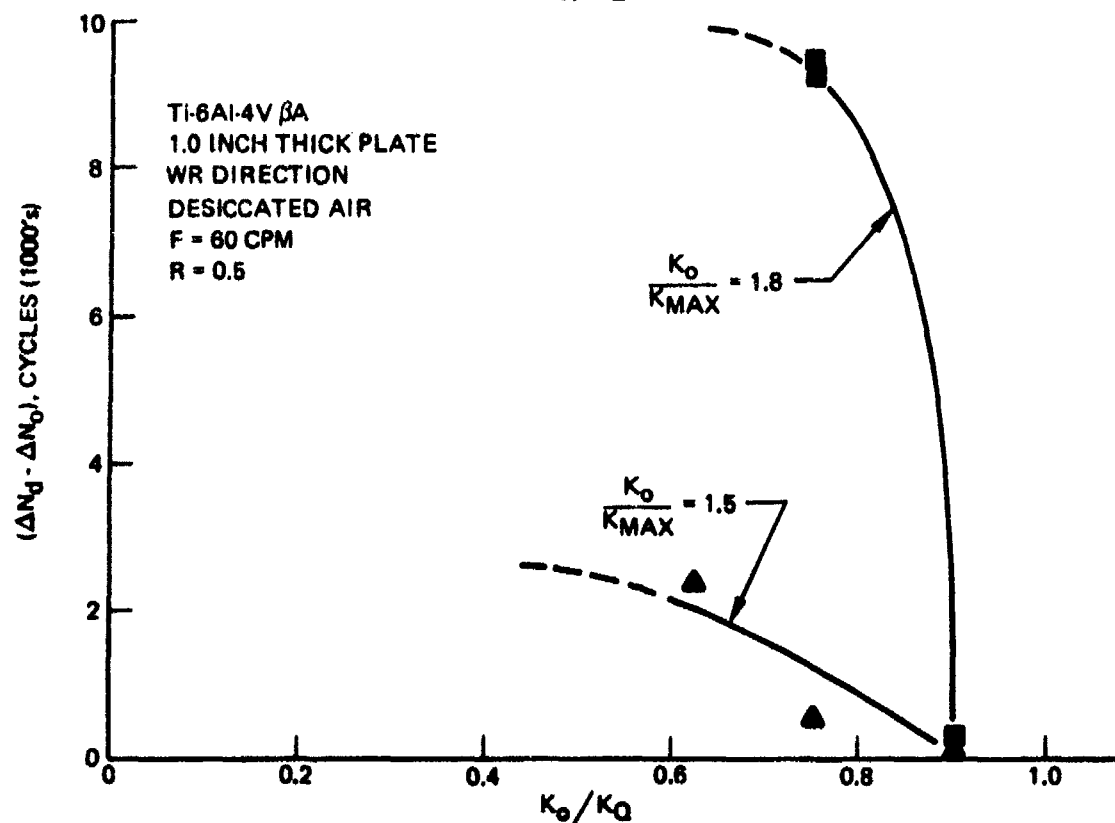
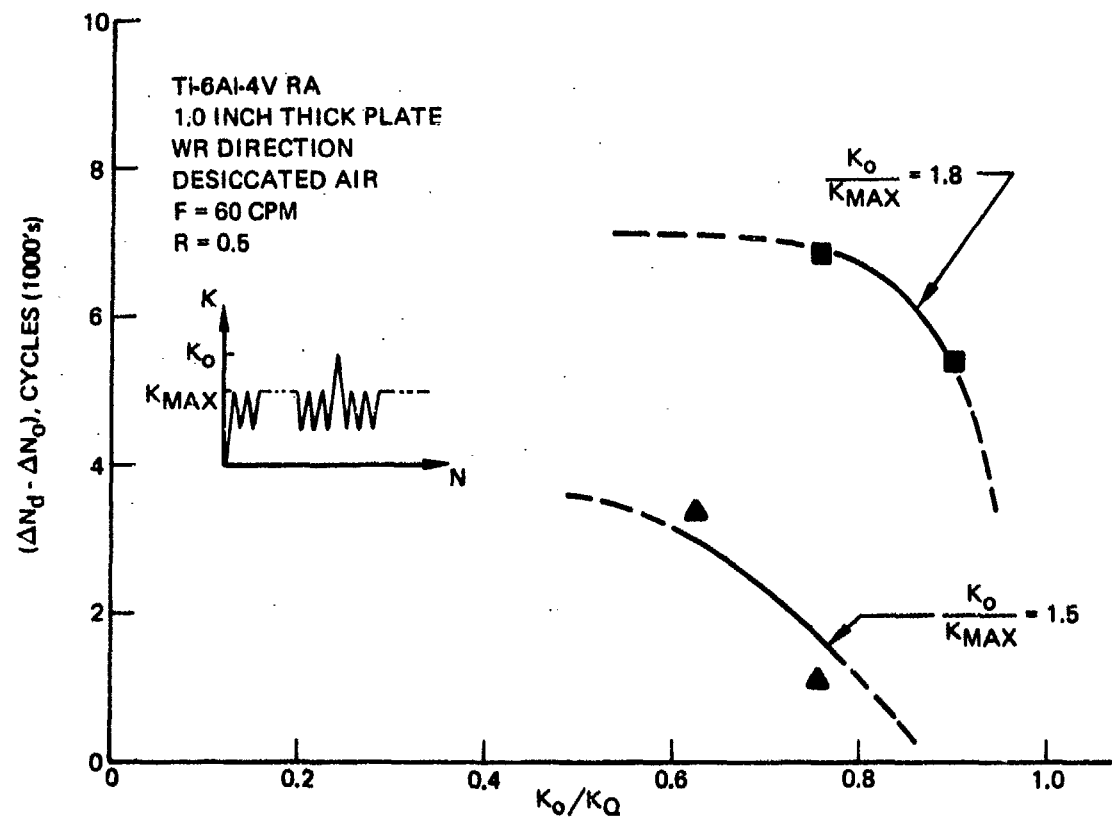


Figure 97: Effect of Peak Overload Stress Intensity Factor on Change in Cyclic Life

Equation 5 was used to calculate delay cycles for the titanium tests and results of the calculation are shown by the solid curves in Figure 96. The agreement between calculations and test data is quite good except for the Ti-6Al-4V β A alloy tests in which $K_o = 0.9 K_{cr}$.

Other investigators have reported that during the transient crack growth rate deceleration that occurs after overloads, the maximum deceleration does not occur immediately after the application of the overload; rather, crack growth rates decelerate to minimum values, then gradually accelerate back to the values that would have occurred in the absence of the overload. In the present tests it did appear that maximum crack growth rate deceleration occurred during the first low stress cycle after the overload. However, the instrumentation used was not sufficiently sensitive to accurately detect crack growth rate behavior during the initial cycles after the overload.

3.5.4 Summary

The following observations were made during evaluation of the overload test data:

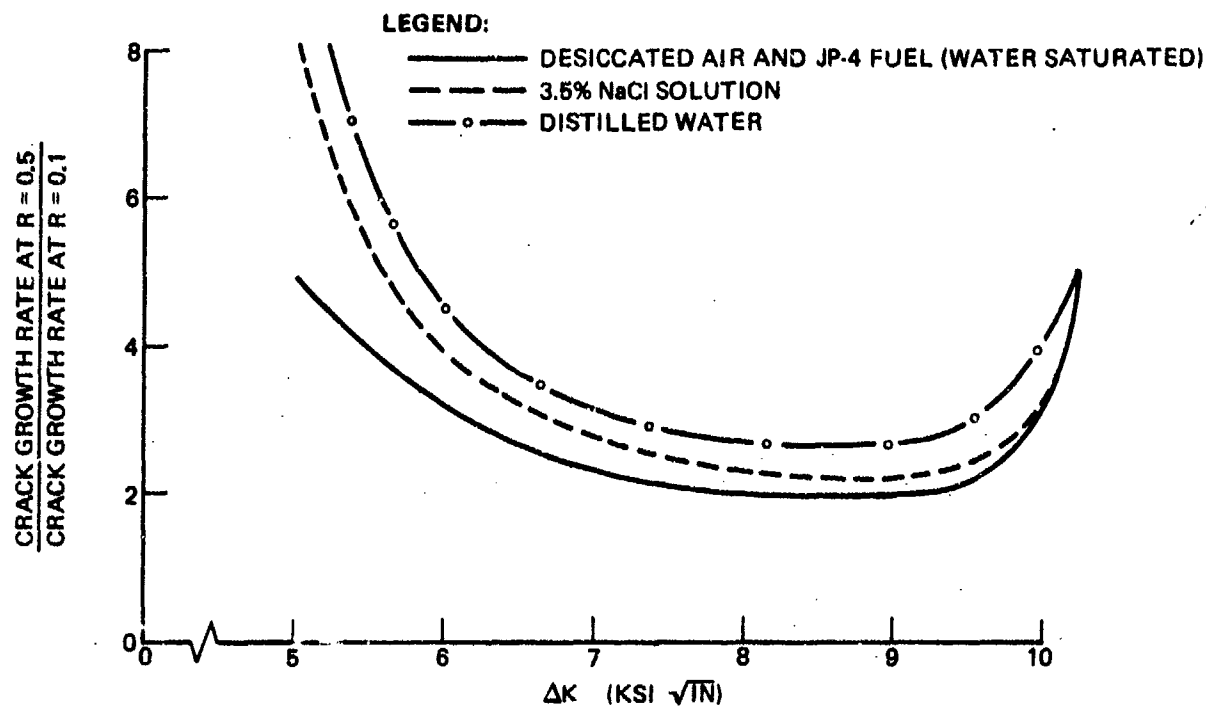
- The application of overloads resulted in a transient retardation in crack growth rates following the overload. The increase in cyclic life caused by an overload varied with ratio of overload stress to cyclic stress, ratio of overload stress to fracture stress, and test medium.
- The amount of crack growth that occurred during the overloads was significantly greater than the corresponding uniform load crack growth rate for the overload cycle.
- Overloads increased cyclic life up to peak overload to fracture stress (σ_o/σ_{cr}) ratio of 0.9. Extrapolation of the data to higher values of overload ratio led to predicted detrimental effects of overloads. For $\sigma_o/\sigma_{cr} > 0.9$, the beneficial effect of crack growth rate retardation is more than offset by the detrimental effect of crack growth occurring during the overload. Maximum beneficial effects were not realized until (σ_o/σ_{cr}) was decreased to less than about 0.6.

- The beneficial effects of overloads were much greater in desiccated air than in 3.5% NaCl solution. The differences between results for the two media was due to differences in uniform stress crack growth rates for the two media.
- The delay cycles caused by the overloads were predicted with acceptable accuracy by Equation 5.
- The presently available methods of calculating the effect of overloads on crack propagation life maybe unconservative, at least to the extent that accelerated crack growth that occurs during overload is not accounted for. For peak overload to critical stress ratios less than about 0.6, the errors resulting from the accelerated growth during the overload should be negligible.

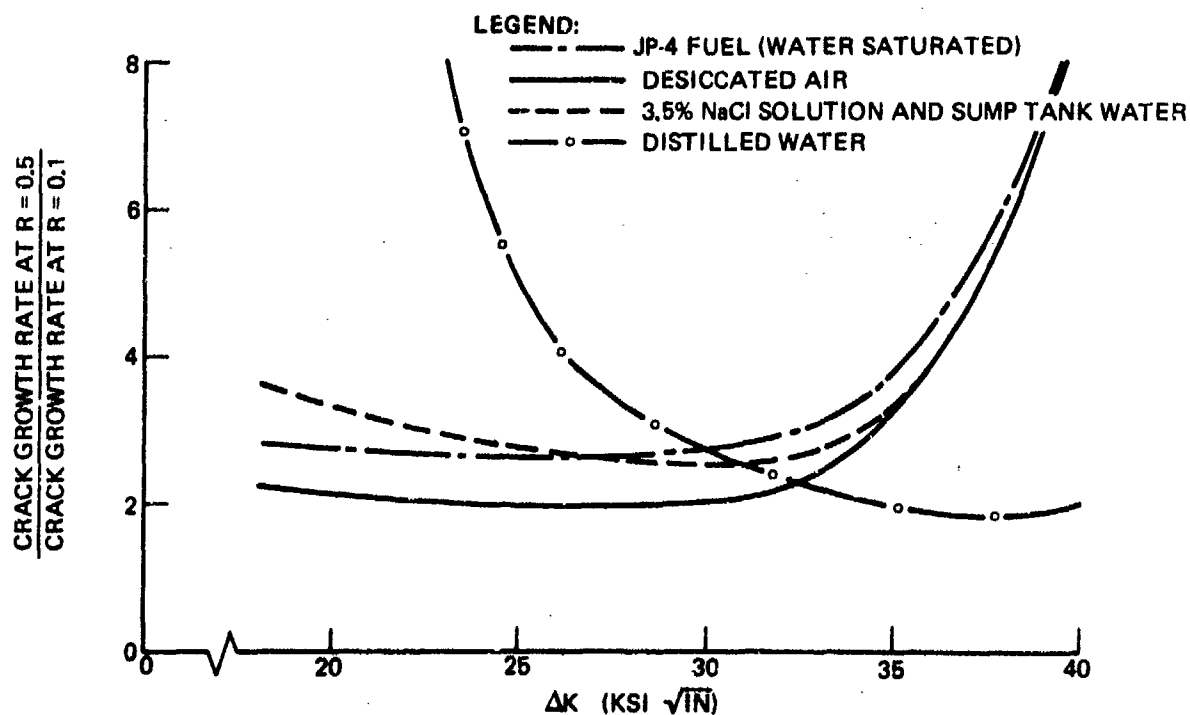
3.6 Stress Ratio Effects

The effects of stress ratio on crack growth rates were evaluated by plotting ratios of crack growth rate at $R=0.5$ and 0.8 to crack growth rate at $R=0.1$ as a function of ΔK . The procedure was followed for each of the four prime alloys and five test media, namely, 7075-T651 aluminum, 9Ni-4Co-0.3C steel, 6Al-4V β A titanium and 6Al-4V RA titanium in desiccated air, water saturated JP-4 fuel, distilled water, 3.5% NaCl solution, and sump tank water. The majority of applicable data were generated at 60 cpm using stress ratios of $R=0.1$ and 0.5 . The resulting stress ratio effects are shown in Figures 98 and 99. There was only a limited amount of data which could be used to evaluate stress ratio effects for $R=0.8$ and the results are shown in Figure 100. A summary of stress ratio effects for data generated using a cyclic frequency of 6 cpm is included in Table 24, and results are plotted in Figure 101.

The effect of stress ratio on crack growth rates was dependent on the value of ΔK at which crack growth was taking place. For low ΔK values, the rates of increase in crack growth rates with increase in stress ratio tended to large values. This trend was due to the existence of apparent threshold stress



(a) 7075-T651 Aluminum Alloy



(b) 9Ni-4Co-0.3C Steel Alloy

Figure 98: Effect of Stress Ratio on Corrosion Fatigue Crack Growth Rate Behavior of Aluminum and Steel Alloys at 60 CPM

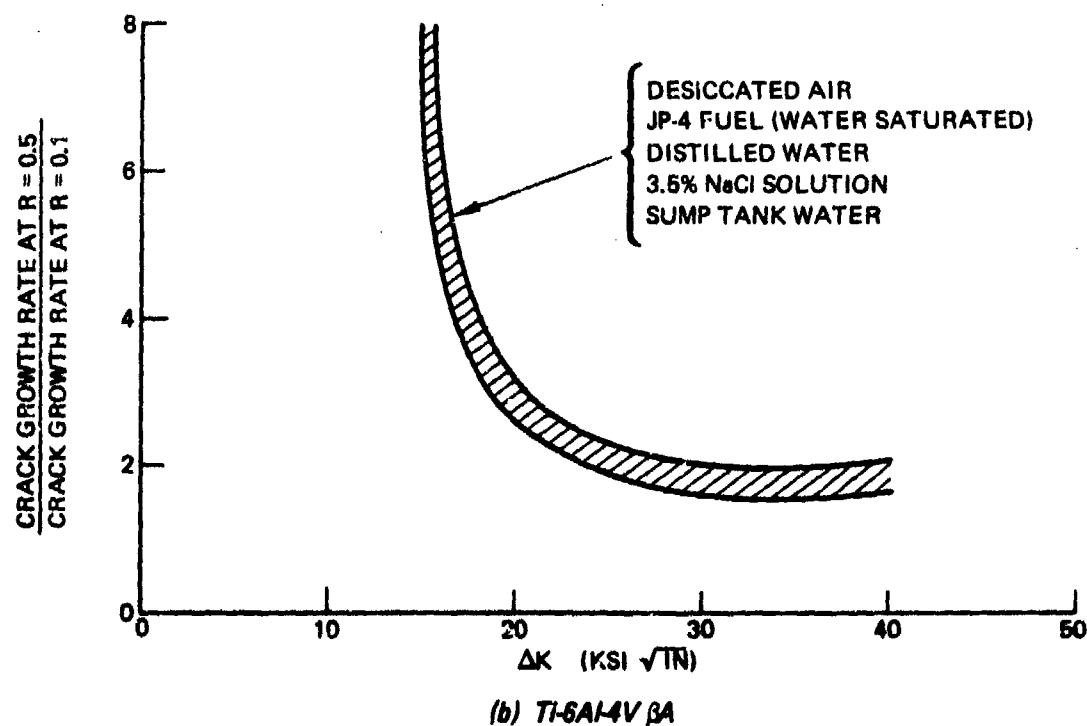
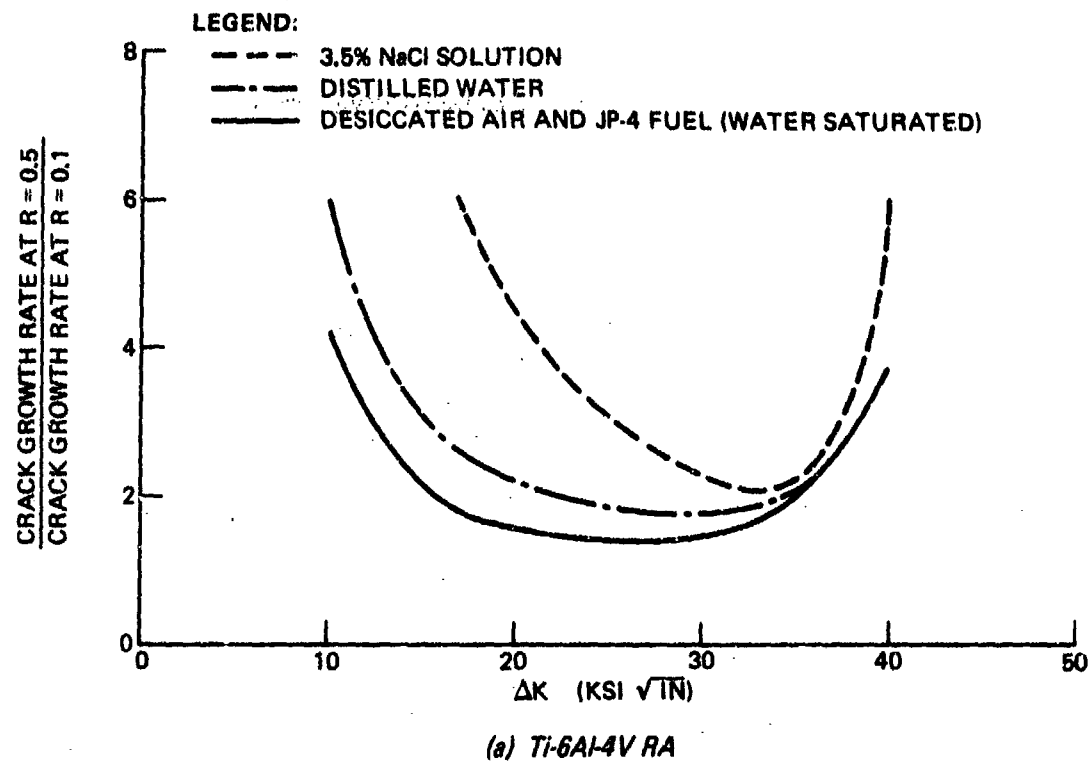
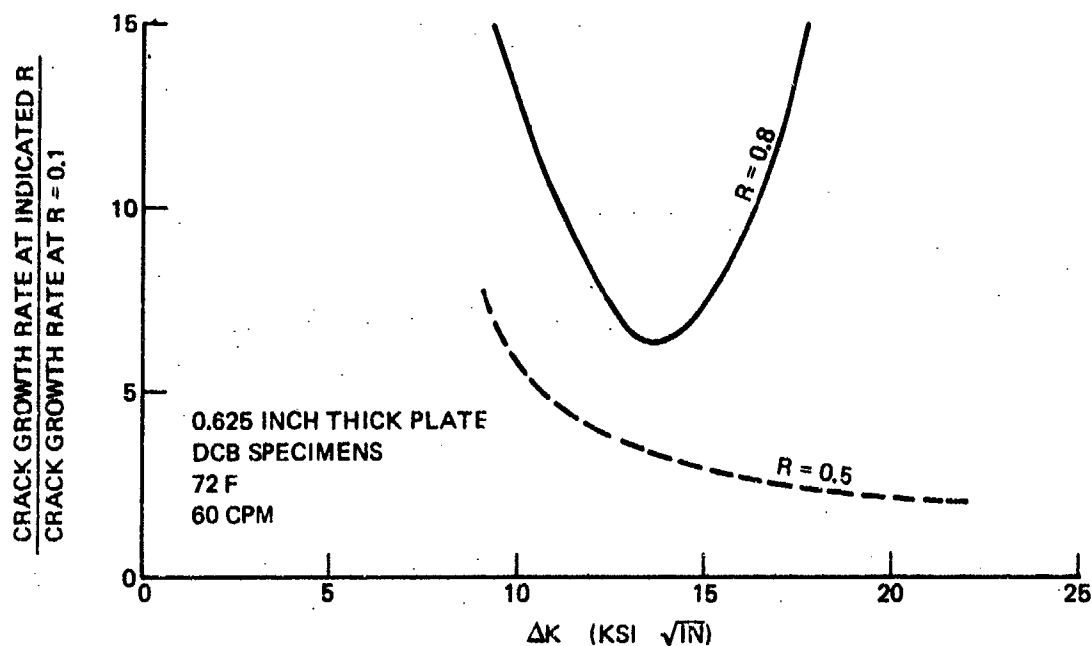
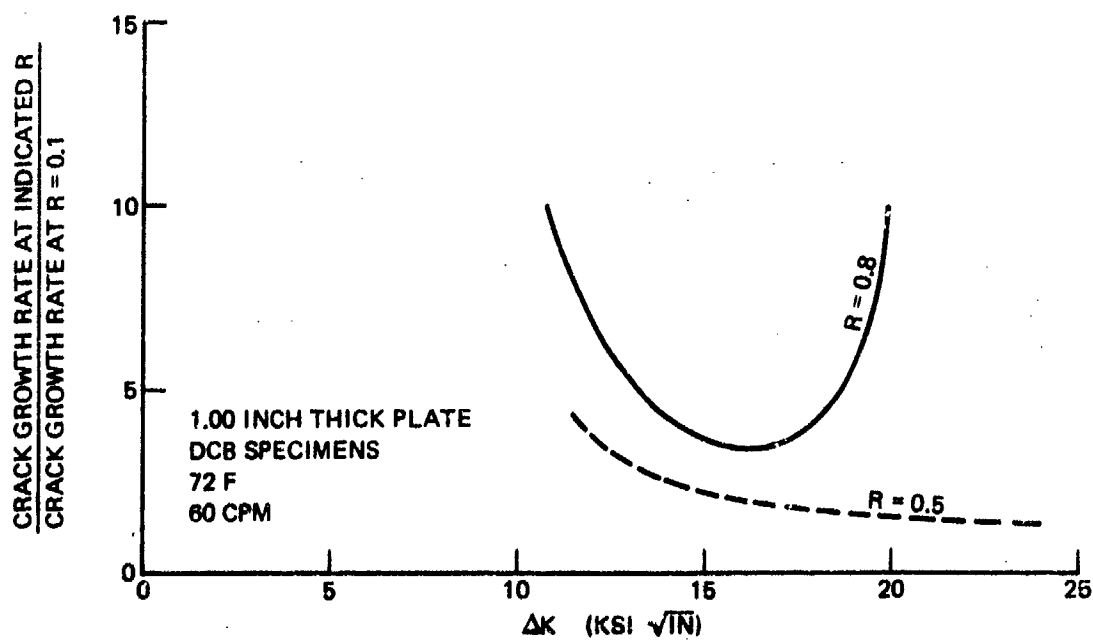


Figure 99: Effect of Stress Ratio on Corrosion Fatigue Crack Growth Rate Behaviors of Titanium Alloys at 60 CPM



(a) 9Ni-4Co-0.3C Steel Alloy



(b) Ti-6Al-4V RA

Figure 100: Effect of Stress Ratio on Fatigue Crack Growth Rates for Steel and Titanium Alloys in Desiccated Air

Table 24: Summary of Stress Ratio Effects Resulting from 6 CPM Tests

ALLOY	TEST MEDIUM	COMMENTS
7075-T651 ALUMINUM	AIR JP-4 FUEL (WATER SATURATED) DISTILLED WATER	NOT ENOUGH DATA OVERLAP BETWEEN $R = 0.1$ AND $R = 0.5$ TO EVALUATE R EFFECTS
	3.5% NaCl SOLUTION	SAME AS 60 CPM EFFECTS FOR $\Delta K > 7 \text{ KSI } \sqrt{\text{IN}}$. NO DATA OVERLAP BELOW $\Delta = 7 \text{ KSI } \sqrt{\text{IN}}$.
9Ni-4Co-0.3C STEEL	AIR JP-4 FUEL (WATER SATURATED)	NOT ENOUGH DATA OVERLAP TO EVALUATE R EFFECTS. TRENDS INDICATE EFFECT SHOULD BE SAME AS 60 CPM EFFECTS.
	3.5% NaCl SOLUTION	DATA FOR BOTH $R = 0.1$ AND $R = 0.5$ FALL IN ONE SCATTER BAND BETWEEN $\Delta K = 30$ AND $45 \text{ KSI } \sqrt{\text{IN}}$
	DISTILLED WATER	SEE FIGURE 101
6Al-4V β A TITANIUM	AIR	NO DATA FOR $R = 0.1$
	JP-4 FUEL (WATER SATURATED) DISTILLED WATER	SAME AS 60 CPM EFFECTS (FIGURE 99) FOR $\Delta K > 25 \text{ KSI } \sqrt{\text{IN}}$
	3.5% NaCl SOLUTION	SEE FIGURE 101
6Al-4V α A TITANIUM	AIR JP-4 FUEL (WATER SATURATED)	SAME AS 60 CPM EFFECTS FOR $\Delta K > 25 \text{ KSI } \sqrt{\text{IN}}$
	DISTILLED WATER	SEE FIGURE 101
	3.5% NaCl SOLUTION	INSUFFICIENT DATA

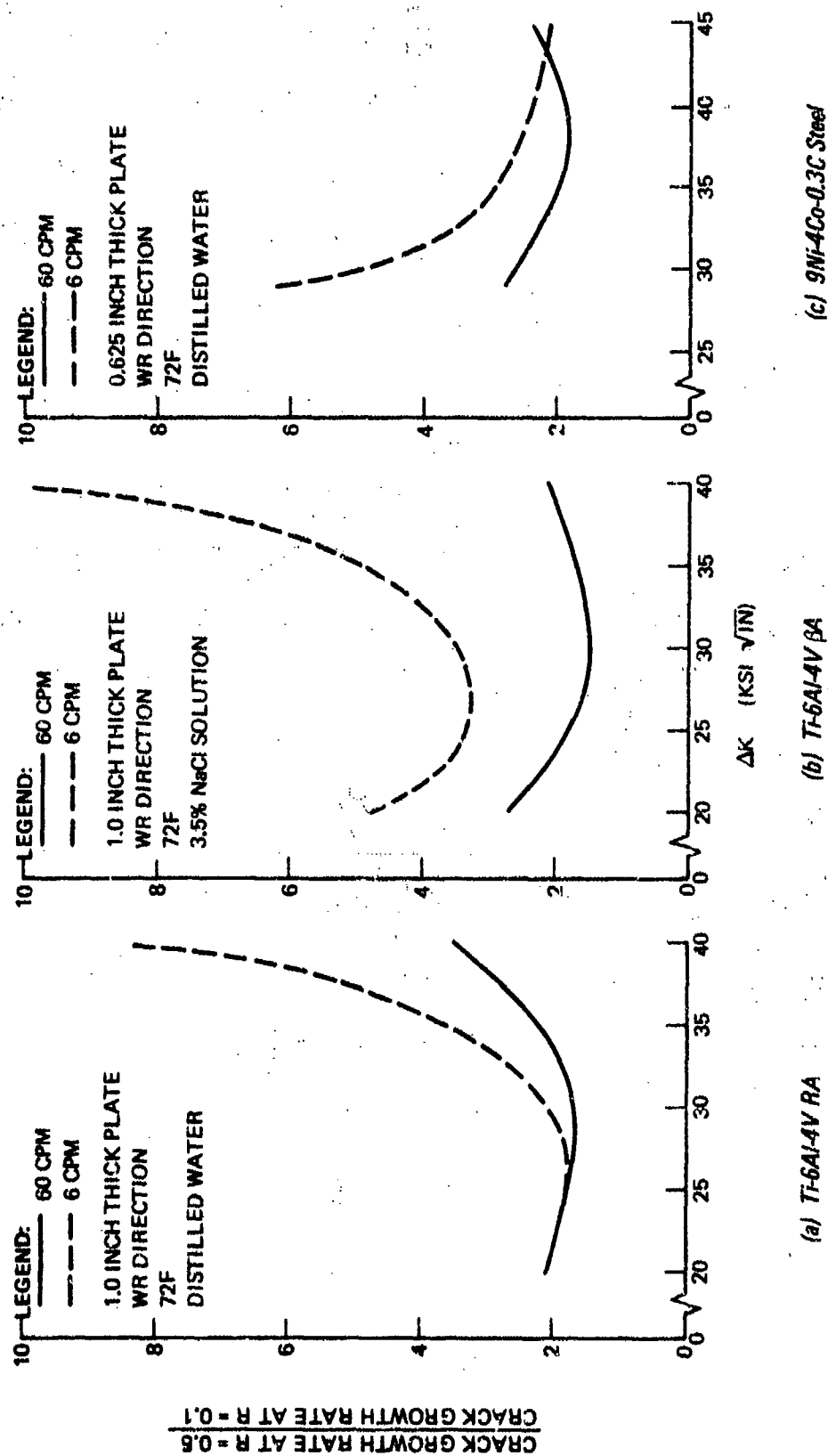


Figure 101: Effect of Cyclic Frequency on Stress Ratio Effects in Titanium and Steel Alloys

intensity ranges (ΔK_{th}) near which crack growth rates asymptotically approached very small values. Since ΔK_{th} for $R=0.1$ was greater than ΔK_{th} for $R=0.5$, the ratio of crack growth rates at $R=0.5$ to those at $R=0.1$ tended to large values when ΔK approached the ΔK_{th} for $R=0.1$. As ΔK values increased, the effect of stress ratio on crack growth rate decreased to a minimum and then once again tended to large values as ΔK approached $K_{cr}(1-R)$ where: K_{cr} is the appropriate critical stress intensity factor and R is the higher of the two stress ratios for which data is being compared. As ΔK approaches $K_{cr}(1-R)$, crack growth rate are accelerated rapidly due to the onset of ductile tear and, hence, the ratio of crack growth rates at the two different R value increases rapidly.

Test media influenced the effects of stress ratio on crack growth rates in three of the four alloys tested. For the 6Al-4V RA titanium alloy, the effects of stress ratio increased with increasing susceptibility to SCC in the test medium. For the 7075-T651 aluminum alloy, distilled water tests yielded higher stress ratio effects than did the 3.5% NaCl solutions even though the apparent K_I values and stress ratio effects between the two media was not large. In the 9Ni-4Co-0.3C steel alloy, stress ratio effects at a cyclic frequency of 60 cpm in air, JP-4 fuel, 3.5% NaCl solution, and sump tank water were different from these in the other media. For the 6Al-4V β A titanium alloy, test medium had only a small effect on stress ratio effects. In general, the results indicate that stress ratio effects are more severe in aggressive environments than in benign environments. This result is probably due in part to the detrimental effects of aggressive media on both ΔK_{th} and on corrosion fatigue crack growth rates.

Cyclic frequency influenced stress ratio effects for some material/environment combinations as summarized in Table 24 and Figure 102. As stated in the table, there was insufficient data overlap to evaluate R effect, at 6 cpm for several material/environment couples. For other couples, stress ratio effects for both 6 and 60 cpm were identical over the range of ΔK values tested. For Ti-6Al-4V RA in distilled water, Ti-6Al-4V β A in 3.5% NaCl solutions, and 9Ni-4Co-0.3C steel in distilled water, stress ratio effects were larger at 6 cpm than 60 cpm as illustrated in Figure 101. For the titanium alloys, the effect of cyclic frequency on stress ratio effect increased with increasing ΔK . This result is consistent with SCC behavior where environmental effects

increase with increasing stress intensity factors. On the other hand, the effect of cyclic frequency on stress ratio effects for the steel alloy decreased with increasing stress intensity factor over the range of ΔK values tested.

In summary, stress ratio effects on corrosion fatigue crack growth rates varied considerably from one material/environment couple to another. In general, stress ratio effects were largest for material/environment combinations that were susceptible to SCC. The higher the susceptibility of the alloy to SCC in the test medium, the greater the stress ratio effects. Environment influenced stress ratio effects by changing values of both apparent ΔK_{th} and crack growth rates. The material/environment couple which exhibited unique behavior was the steel alloy in distilled water. The presence of distilled water resulted in a marked increase in the effect of stress ratio on crack growth rates at low ΔK values and a decrease in stress ratio effect on crack growth rates for moderate ΔK values.

4.0 OBSERVATIONS AND CONCLUSIONS

The following observations and conclusions are based on the results of this program.

4.1 Observations

Alloy

1. For the Ti-6Al-4V alloy, beta annealing led to superior stress corrosion cracking and corrosion fatigue crack growth resistance than did recrystallize annealing. The beta annealed alloy yielded slower crack growth rates for the WR direction under all test conditions. Both annealing treatments led to similar fracture toughness values for each of the WR and WT directions.
2. The 7475-T651 alloy plate had fracture toughness superior to the 7075-T651 alloy plate for the WR crack propagation direction (other directions were not tested). Fatigue crack growth rates for the two alloys in 3.5% NaCl solution did not differ greatly. There was an indication that the 7475 alloy might have had a higher threshold stress intensity factor in fatigue than the 7075 alloy. However, there were insufficient data to substantiate this indication.
3. The 9Ni-4Co-0.3C plate material tested in this program was banded because of suspected improper hot rolling practice and was not considered to be typical of the 9Ni alloy by the producer (Republic Steel). The effect of the banding on test results is unknown. When heat treated to the 240 ksi strength level, the alloy was found to be very susceptible to stress corrosion cracking in aqueous environments. The apparent K_{ISCC} values for the WR and TR crack propagation direction were about 27 and 13 $\text{ksi}\sqrt{\text{in}}$, respectively. Aqueous environments also markedly accelerated corrosion fatigue crack growth rates for fatigue cycles having peak stress intensity factors above about 26 $\text{ksi}\sqrt{\text{in}}$ and cyclic frequencies less than 60 cpm.

Environment

4. Of the seven test media (desiccated air, water saturated JP-4 fuel, distilled water, 3.5% NaCl solution, sump tank water, alternating JP-4 fuel/distilled water, and dye penetrant type ZL-2A), desiccated air and JP-4 fuel were the least detrimental to SCC and corrosion fatigue crack growth resistance; 3.5% NaCl solution and sump tank water were the most detrimental. Fatigue crack growth rates for the alternating JP-4 fuel/distilled water media fell between rates for the individual components of the alternating media. Finally, the effect of dye penetrant on corrosion fatigue cracking was equivalent to that of desiccated air.
5. The relative effects of potential models of the "worst" normal operating environment for airframe components, namely, 3.5% NaCl solution and sump tank water, was dependent on alloy. For the 7075-T651 aluminum and Ti-6Al-4V RA alloys, the effects of the two media were equally detrimental. For Ti-6Al-4V beta annealed, the 3.5% NaCl solution was more detrimental than the sump tank water. For 9Ni-4Co-0.3C steel, the sump tank water was more detrimental than the 3.5% NaCl solution.
6. Spraying the crack surfaces of test specimens with the corrosion inhibitive compound LPS-3 prior to test had no significant effect on SCC and corrosion fatigue crack growth resistance.
7. Changes in test temperature from -65F to +175F had little or no effect on corrosion fatigue crack growth rates.

Cyclic Frequency

8. The effect of change in cyclic frequency from 60 to 6 cpm was dependent on alloy/environment couple. Both accelerations and decelerations in crack growth rate at given ΔK values occurred with decrease in cyclic frequency. It is not possible to generalize the frequency effects noted in this program.

Stress Ratio

9. The magnitude of stress ratio effects on corrosion fatigue crack growth rates varied considerably from one material/environment couple to another. In general, increases in crack growth rate with increase in stress ratio were largest for material/environment combinations that were susceptible to SCC. The higher the susceptibility of the alloy to SCC in the test medium, the greater the stress ratio effects. Environment influenced stress ratio effects by changing values of both apparent ΔK_{th} and crack growth rates. The material/environment couple that exhibited unique behavior was the steel alloy in distilled water. The presence of distilled water resulted in a marked increase in the effect of stress ratio on crack growth rates at low ΔK values, and a decrease in stress ratio effect on crack growth rates for moderate ΔK values.

Crack Propagation Direction

10. Crack growth rates for the WT direction (obtained from tests of surface flawed specimens) and for the WR direction (obtained from tests of double cantilever beam specimens) were in excellent agreement for the two titanium alloys in both desiccated air and 3.5% NaCl solution. In the 7075-T651 aluminum alloy, crack growth rates were slower in air and faster in 3.5% NaCl solution than corresponding rates for the WR direction.

Overload Effects

11. The application of overloads resulted in transient retardation in crack growth rates following the overload. The increase in cyclic life caused by an overload varied with ratio of overload stress to cyclic stress, ratio of overload stress to fracture stress, and test medium.
12. The amount of crack growth that occurred during the overloads was significantly greater than the corresponding uniform load crack growth rate for the overload cycle.
13. Overloads increased cyclic life up to peak overload to fracture stress (σ_o/σ_{cr}) ratios of 0.9. Extrapolation of the data to higher values of overload ratio led to predicted detrimental effects of overloads. For

$\sigma_o/\sigma_{cr} > 0.9$, the beneficial effect of crack growth rate retardation is more than offset by the detrimental effect of crack growth occurring during the overload. Maximum beneficial effects were not realized until (σ_o/σ_{cr}) was decreased to about 0.6 or less.

14. The beneficial effects of overloads were much greater in desiccated air than in 3.5% NaCl solution. The differences between results for the two media were due to differences in uniform load crack growth rates for the two media.
15. The delay cycles caused by the overloads were predicted with acceptable accuracy by Equation 5.

Thermal Processing Effects

16. Thermal cycles used to induce grain growth and ordering in the Ti-6Al-4V RA alloy did not degrade either the SCC or corrosion fatigue crack growth resistance of the plate. Some of the thermal cycles resulted in a highly textured basket-weave structure that was most susceptible to SCC in the RW direction. The K_{ISCC} and crack growth rate values for the RW direction were the same as for the as-received material.

4.2 Conclusions

1. Testing of double cantilever beam specimens is a very good method of generating fatigue crack growth rate data. However, the resulting data are not always applicable to many practical cracking situations in airframe components. This is particularly true for plate materials that exhibit anisotropy in SCC and corrosion fatigue resistance. In such cases, surface flawed specimen tests must be conducted to evaluate crack growth resistance for the thickness direction.
2. Due to the steepness of the crack growth rate versus ΔK correlations at low ΔK values, calculations of crack propagation life for airframe components in which most of the life is consumed by cycling at low ΔK values will be very sensitive to applied stress level.

3. For the Ti-6Al-4V alloy, beta processing is superior to alpha-beta processing from the standpoint of fracture and crack growth resistance.
4. The use of corrosion inhibitive compounds such as LPS-3 will not necessarily decrease crack propagation rates of cracked airframe components.
5. Type ZL-2A dye penetrant is compatible with all alloys tested in this program.
6. Service temperatures within the range of +175F to -65F will not have any significant effect on the crack propagation rates in airframe components fabricated from the aluminum and titanium alloys tested on this program. Service temperatures could have some influence on crack propagation life by changing fracture toughness of the component materials.

REFERENCES

1. C. F. Tiffany, "Fracture Control of Metallic Pressure Vessels", NASA Space Vehicle Design Criteria (Structures) NASA SP-8040, May 1970.
2. L. R. Hall and R. W. Finger, "Stress Corrosion Cracking and Fatigue Crack Growth Studies Pertinent to Spacecraft and Booster Pressure Vessels", NASA CR-120823, National Aeronautics and Space Administration, December 1972.
3. S. Mostovoy, P. B. Crosley and E. J. Ripling, "Use of Crack-Line-Loaded Specimens for Measuring Plane Strain Fracture Toughness", Journal of Materials, Vol. 2, No. 3, September 1967.
4. R. C. Shah and A. S. Kobayashi, "On the Surface Flaw Problem", The Surface Crack: Physical Problems and Computational Solutions, edited by J. L. Swedlow, ASME, November 1972.
5. M. V. Hyatt and M. O. Speidel, "Stress Corrosion Cracking of High Strength Aluminum Alloys", Advances in Corrosion Science and Technology, Vol. 2, edited by M. G. Fontana and R. W. Staehle, Plenum Press 1972.
6. L. H. Glassman and A. J. McEvily, Jr., "Effects of Constituent Particles on the Notch Sensitivity and Fatigue Crack Propagation Characteristics of Aluminum-Zinc-Magnesium Alloys", NASA TN D928, National Aeronautics and Space Administration, April 1962.
7. R. M. N. Pelloux, "Fractographic Analysis of the Influence of Constituent Particles on Fatigue Crack Propagation in Aluminum Alloys", Transactions ASM, Vol. 57, 1964.
8. M. J. Blackburn, J. A. Feeney, and T. R. Beck, "Stress Corrosion Cracking of Titanium Alloy", Advances in Corrosion Science and Technology, Vol. 2, edited by M. G. Fontana and R. W. Staehle, Plenum Press, 1972.

9. W. Elber, "The Significance of Fatigue Crack Closure", ASTM Special Technical Publication 486, 1971.
10. T. T. Shih and R. P. Wei, "A Study of Crack Closure in Fatigue", Lehigh University Report No.
11. M. Katcher and M. Kaplan, "Effect of R Factor and Crack Closure on Aluminum and Titanium Alloys", presented at Sixth Annual Fracture Mechanics Symposium, Philadelphia, August 1972.
12. O. Jonds and R. P. Wei, "An Exploratory Study of Delay in Fatigue Crack Growth", International Journal of Fracture Mechanics, Vol. 7, 1971.
13. J. C. McMillan and R. N. M. Pelloux, "Fatigue Crack Propagation Under Program and Random Loads", ASTM Special Technical Publication 415, 1966.
14. J. R. Rice, "Mechanics of Crack Tip Deformation and Extension by Fatigue", ASTM Special Technical Publication 415, 1966.
15. O. E. Wheeler, "Crack Growth Under Spectrum Loading", Report No. FZM-5602, General Dynamics Corp., Fort Worth Division, June 1970.
16. J. Willenborg, R. M. Engle and H. A. Wood, "A crack Growth Retardation Model Using an Effective Stress Concept", Technical Memorandum 71-1FBR, Air Force Flight Dynamics Library, WPAFB, January 1971.
17. T. R. Porter, "Method of Analysis and Prediction for Variable Amplitude Fatigue Crack Growth", Eng. Fracture Mech., Vol. 4, No. 4, December 1972.

APPENDIX A

TEST DATA

This appendix contains all the detailed test data generated during this program. Included are mechanical property, static fracture toughness and corrosion fatigue data for aluminum alloy 7075-T651 and 7475-T651, titanium alloys 6Al-4V beta annealed and 6Al-4V recrystallized annealed, and steel alloy 9Ni-4Co-0.3C. The location of the various types of data within this appendix is identified in Table A1.

Table A1: Index of Test Data

ALLOY	TYPE OF DATA	LOCATION
ALUMINUM 7075-T651	Mechanical Property Fracture Toughness Corrosion Fatigue	Table A2 Tables A3, A4 Figures A1 Through A15
ALUMINUM 7475-T651	Corrosion Fatigue	Figure A16
TITANIUM 6Al-4V BETA ANNEALED	Mechanical Property Fracture Toughness Corrosion Fatigue	Table A5 Tables A6, A7 Figures A17 Through A32
TITANIUM 6Al-4V RA	Mechanical Property Fracture Toughness Corrosion Fatigue	Table A8 Tables A9, A10 Figures A33 Through A49
STEEL 9Ni-4Co-0.3C	Mechanical Property Fracture Toughness Corrosion Fatigue	Table A11 Tables A12, A13 Figures A50 Through A62

Table A2: Mechanical Property Data for 7075-T651 Aluminum Alloy Plate

GRAIN DIRECTION	TEMPERATURE (°F)	SPECIMEN NUMBER	ULTIMATE TENSILE STRENGTH (KSI)	0.2% OFFSET YIELD STRENGTH (KSI)	ELONGATION IN 2.0 INCH GAGE LENGTH (%)
LONG.	72	AL-1	86.7	79.0	9.9
		AL-2	88.1	81.2	13.7
	-65	AL-3	93.9	86.2	11.6
		AL-4	94.2	86.4	10.9
	+175	AL-5	81.5	74.2	14.5
		AL-6	81.7	75.4	10.6
TRANS.	72	AT-5	89.9	82.4	10.6
		AT-6	86.8	78.9	10.5
	-65	AT-3	90.2	80.8	10.3
		AT-4	89.9	80.9	10.6
	+175	AT-1	80.5	73.8	9.2
		AT-2	83.0	75.8	9.0

Table A3: Fracture Toughness (K_{Ic}) Data for 7075-T651 Aluminum Alloy Plate

SPECIMEN TYPE	ORIENTATION	TEMP (°F)	K_{Ic} (KSI $\sqrt{IN.}$)
COMPACT TENSION	WR	-65	21.0
			21.8
COMPACT TENSION	WR	+72	23.1
			22.4
COMPACT TENSION	WR	+175	24.0
			24.4
DCB (FIG. 1)	WR	+72	22.8
			22.4
			21.9
			21.8
			22.2
DCB (FIG. 1)	RW	+72	31.5
			32.0

Table A4: Static Fracture Data for 7075-T651 Aluminum Alloy SF Specimens

SPECIMEN GAGE		FLAW		TEST TEMP (°F)	LOAD AT		APPROX WT FRACTURE TOUGHNESS* (KSI $\sqrt{\text{IN.}}$)
WIDTH (IN.)	THICKNESS (IN.)	DEPTH, a (IN.)	WIDTH, 2c (IN.)		POPIN (K)	FAILURE (K)	
3.00	0.404	0.170	0.708	+72	53.7	56.0	31.7
3.00	0.402	0.172	0.717	+72	56.3	58.6	33.6
3.00	0.405	0.172	0.720	-65	50.1	52.8	29.9
3.00	0.401	0.174	0.718	-65	49.6	55.0	31.6
3.00	0.404	0.177	0.715	+175	58.3	60.2	34.8
3.00	0.403	0.176	0.715	+175	58.2	59.8	34.7

*FRACTURE TOUGHNESS = $1.1 \sigma \sqrt{\pi a/Q}$

Table A5: Tensile Properties of 6Al-4V Beta Annealed Titanium Alloy Plate

SPECIMEN NUMBER	DIA (IN.)	AREA (IN. ²)	TEST ENVIRONMENT	TEST TEMPERATURE (°F)	ULTIMATE STRENGTH (KSI)	0.2% OFFSET YIELD STRENGTH (KSI)	ELONGATION (% PER 2.0 INCHES)	REDUCTION IN AREA (%)
TBL-1	0.2479	0.0483	AIR	72	133.6	124.2	10	20
TBL-2	0.2496	0.0489		72	133.6	123.3	10	22
TBL-3	0.2501	0.0491		-65	152.4	145.8	7	18
TBL-4	0.2506	0.0493		-65	152.4	143.9	8	19
TBL-5	0.2499	0.0490		175	121.7	108.5	10	27
TBL-6	0.2501	0.0491		175	121.4	108.3	10	26
TBT-1	0.2498	0.0490	AIR	72	133.8	123.8	10	24
TBT-2	0.2494	0.0489		72	133.8	121.6	10	24
TBT-3	0.2499	0.0490		-65	152.3	144.6	8	22
TBT-4	0.2497	0.0490		-65	152.3	143.2	8	20
TBT-5	0.2489	0.0487		175	121.6	107.5	12	27
TBT-6	0.2498	0.0490		175	122.1	109.1	12	27

Table A6: Static Fracture Toughness Data for 6Al-4V Beta Annealed Titanium (CT Specimens)

SPECIMEN NO.	TEST TEMP (°F)	AVERAGE CRACK LENGTH (IN.)	PEAK LOAD (K)	P _Q 5% OFFSET (K)	K _Q KSI $\sqrt{\text{IN.}}$
T5	-65	1.290	15.12	14.62	93.0
T6	-65	1.327	14.12	13.68	92.0
T1	72	1.385	13.07	12.55	91.0
T2	72	1.272	16.02	15.34	95.5
T3	+175	1.288	17.36	15.95	101.4
T4	+175	1.267	17.15	15.53	95.8

Table A7: Static Fracture Data for 6Al-4V Beta Annealed Titanium Surface-Flawed Specimens

SPECIMEN NUMBER	SPECIMEN GAGE		FLAW		TEST TEMP (°F)	FAILURE LOAD (KIPS)	APPROXIMATE WT FRACTURE TOUGHNESS (KSI $\sqrt{\text{IN.}}$)
	WIDTH (INCH)	THICKNESS (INCH)	DEPTH, ^a (INCH)	WIDTH, 2 ^c (INCH)			
TBS-5	3.4995	0.3238	0.210	0.885	-65	140.4	103.6
TBS-4	3.5008	0.3196	0.210	0.885	-65	140.4	106.0
TBS-1	3.4975	0.3332	0.213	0.905	+72	121.8*	>87.5
TBS-2	3.4994	0.3272	0.206	0.885	+72	129.6	95.2
TBS-3	3.4992	0.3253	0.208	0.890	+175	119.7	89.3
TBS-6	3.4980	0.3304	0.216	0.890	+175	117.3	86.5

*SPECIMEN FAILED AT GRIP


Table A8: Mechanical Property Measurements for 6Al-4V Recrystallize Annealed Titanium 1.0-Inch Thick Plate

GRAIN DIRECTION	TEMP (°F)	ULTIMATE STRENGTH (KSI)	YIELD STRENGTH (KSI)	ELONGATION IN 2.0 IN. (%)	REDUCTION IN AREA (%)
TRANS.	175	128.1 128.1	112.5 113.0	12 13	33 37
	72	137.0 137.2	125.1 125.8	12 12	39 37
	-65	154.6 154.0	145.1 143.8	10 10	28 29
LONG.	175	128.0		12	28
	72	138.4 137.5	126.2 124.5	13 12	39 37
	-65	153.7 150.7	143.2 141.0	10 10	30 27

Table A9: Static Fracture Toughness Data for 6Al-4V Recrystallize Annealed Titanium Alloy 1.0-Inch Thick Plate (CT Specimens—WR Direction)

SPECIMEN NUMBER	TEST TEMP (°F)	AVERAGE CRACK LENGTH (INCH)	PEAK LOAD (KIPS)	P _Q 5% OFFSET (KIPS)	K _Q (KSI $\sqrt{\text{IN.}}$)
NTS-1	72	1.333	13.42	12.91	94.6
NTS-2	72	1.333	13.12	12.32	90.4
NTS-3	-65	1.355	11.60	11.20	84.8
NTS-4	-65	1.317	12.00	11.53	83.0
NTS-5	+175	1.327	15.20	13.56	103.7
NTS-6	+175	1.345	14.70	13.88	101.3

Table A10: Static Fracture Data for 6Al-4V Recrystallize Annealed Titanium Alloy Surface-Flawed Specimens

SPECIMEN NUMBER	SPECIMEN GAGE		FLAW		TEST TEMP (°F)	FAILURE LOAD (KIPS)	APPROXIMATE WT FRACTURE TOUGHNESS (KSI $\sqrt{\text{IN.}}$)
	WIDTH (INCH)	THICKNESS (INCH)	DEPTH, a (INCH)	WIDTH, $2c$ (INCH)			
NTSS-1	3.5023	0.3268	0.217	0.897	-65	138.4	103 
NTSS-2	3.5021	0.3223	0.215	0.890	-65	138.0	103
NTSS-3	3.5022	0.3252	0.215	0.890	+72	126.5	94
NTSS-4	3.5022	0.3262	0.212	0.895	+72	123.8	92
NTSS-5	3.5020	0.3252	0.212	0.890	+175	121.0	91
NTSS-6	3.5017	0.3279	0.210	0.890	+175	120.0	88


 SPECIMEN WAS INITIALLY LOADED TO $K_{IE} = 106.7 \text{ KSI } \sqrt{\text{IN.}}$ (LOAD = 127.0 KIPS) WITH $a = 0.210 \text{ INCH}$, $2c = 0.897 \text{ INCH}$, LOAD DROPPED TO ZERO DUE TO TEST MACHINE FAILURE; SPECIMEN WAS THEN RELOADED.

Table A11: Tensile Properties of Heat Treated 9Ni-4Co-0.3C Steel Alloy

GRAIN DIRECTION	TEMP (°F)	ULTIMATE STRENGTH (KSI)	YIELD STRENGTH (KSI)	ELONGATION IN 2.0 IN. (%)	REDUCTION IN AREA (%)
LONG.	175	235.6 235.1	201.2 203.5	8 8	57 57
	72	244.7 243.2	207.1 209.1	— —	— —
	-65	255.6 256.0	222.5 221.8	7 7	51 46
TRANS	175	235.0 235.1	203.2 202.7	8 7	56 51
	72	239.8 240.1	204.0 203.7	— —	— —
	-65	254.4 254.7	211.4 215.7	7 7	46 47

Table A12: Fracture Toughness Data for 9Ni-4Co-0.3C Steel Alloy

SPECIMEN TYPE	CRACK PROPAGATION DIRECTION	TEST TEMPERATURE (°F)	PLANE STRAIN FRACTURE TOUGHNESS (K_{Ic}) (KSI $\sqrt{IN.}$)	FRACTURE TOUGHNESS (KSI $\sqrt{IN.}$)
COMPACT TENSION	WR	-65	88.1 86.1	— —
DOUBLE CANTILEVER BEAM	WR	72	— —	107.5 104.5
COMPACT TENSION	WR	175	104.6 105.5	— —

Table A13: Static Fracture Data for 9Ni-4Co-0.3C Steel Alloy Surface-Flawed Specimens

SPECIMEN NUMBER	SPECIMEN GAGE		FLAW		TEST TEMP (°F)	FAILURE LOAD (KIPS)	APPROXIMATE WT FRACTURE TOUGHNESS (KSI $\sqrt{IN.}$)
	WIDTH (INCH)	THICKNESS (INCH)	DEPTH, a (INCH)	WIDTH, $2c$ (INCH)			
SS-3	2.2532	0.3968	0.140	0.565	-65	132.9	91.9
SS-4	2.2618	0.3962	0.138	0.555	-65	140.4	96.0
SS-1	2.2578	0.4000	0.138	0.560	+72	156.9	106.7
SS-2	2.2553	0.4065	0.137	0.560	+72	159.0	106.4
SS-5	2.2564	0.4032	0.138	0.550	+175	160.8	108.7
SS-6	2.2542	0.3967	0.137	0.550	+175	156.9	107.8

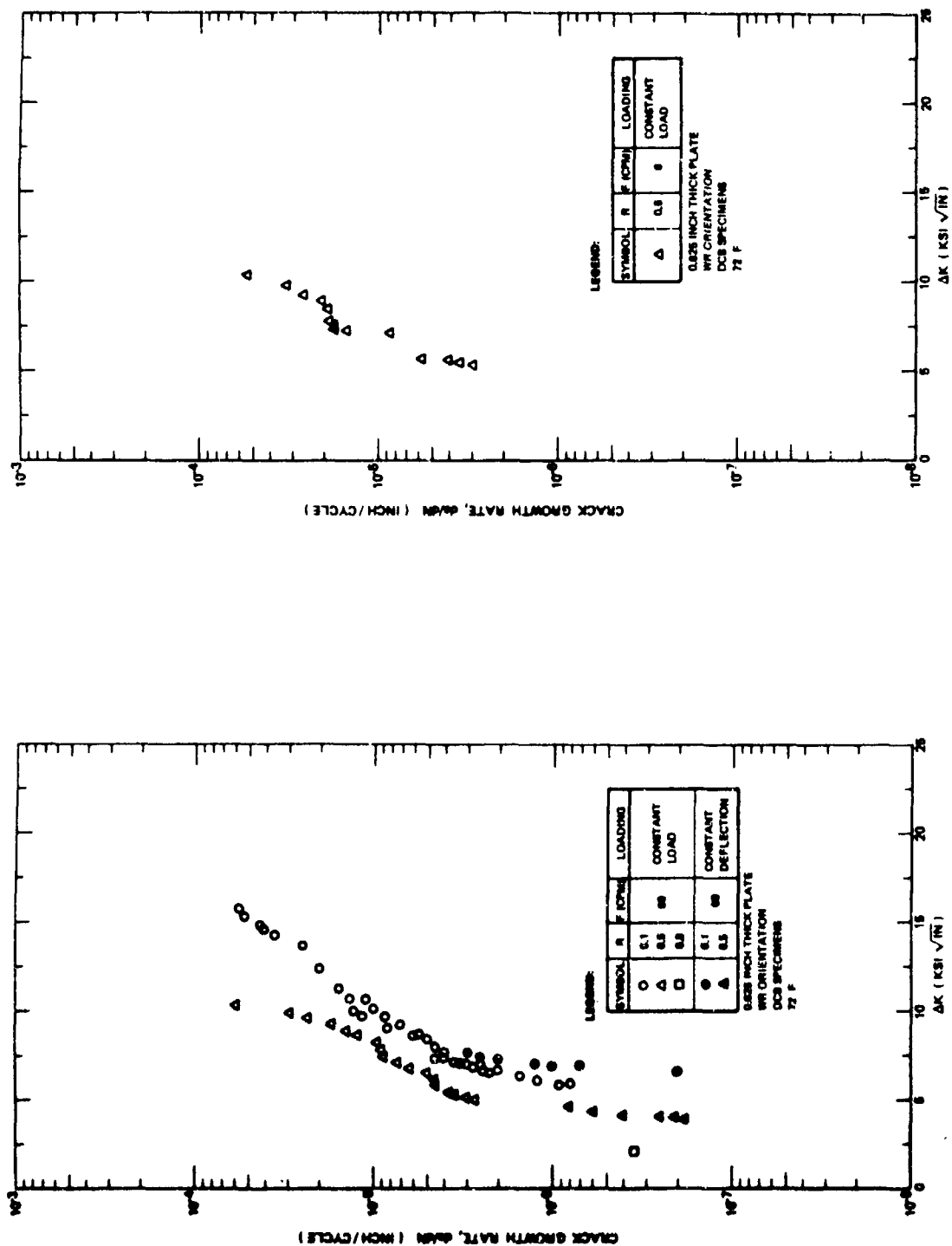


Figure A1: Fatigue Crack Growth Rates For 7075-T651 Aluminum Alloy in Desiccated Air

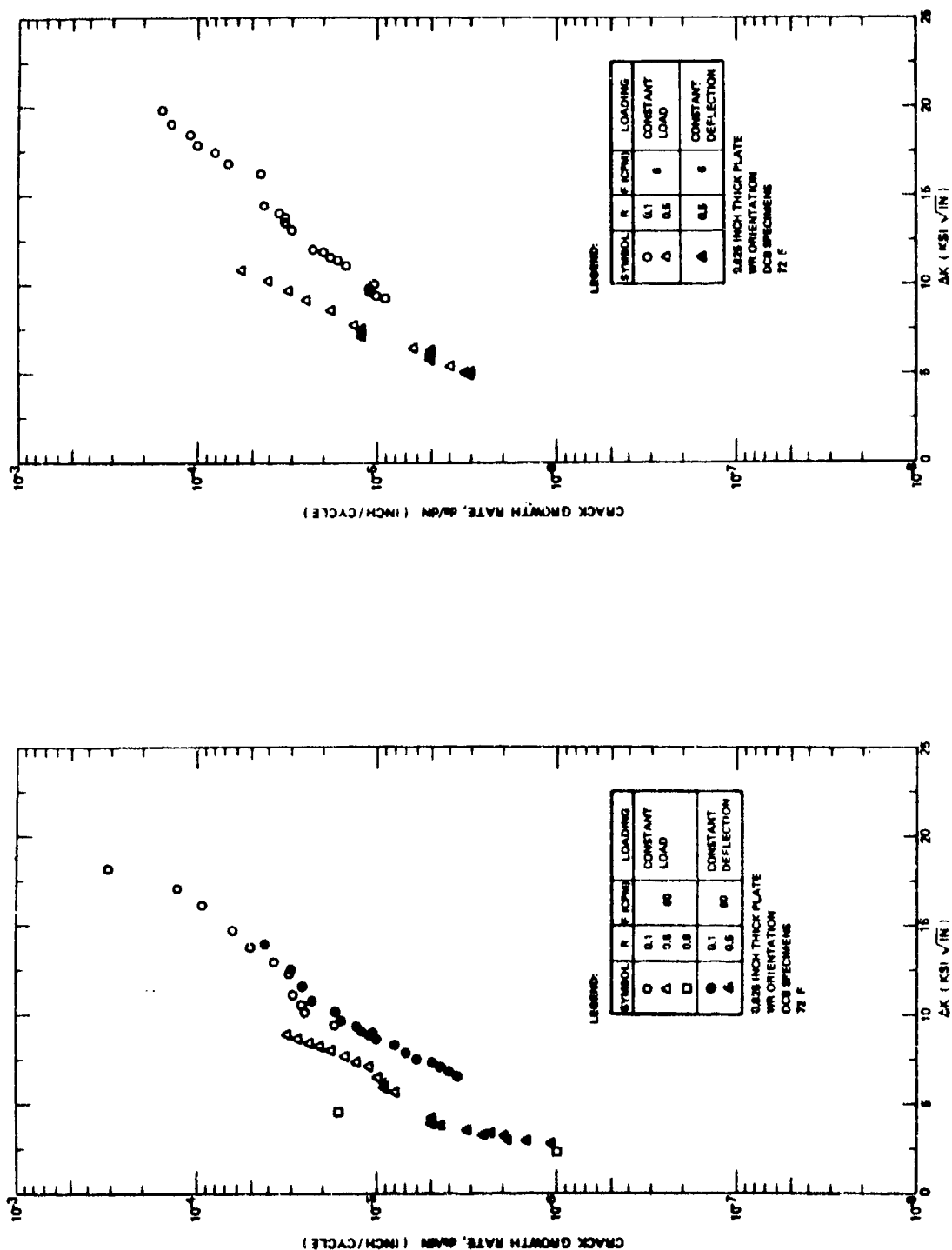


Figure A2: Fatigue Crack Growth Rates For 7075-T651 Aluminum Alloy in Distilled Water

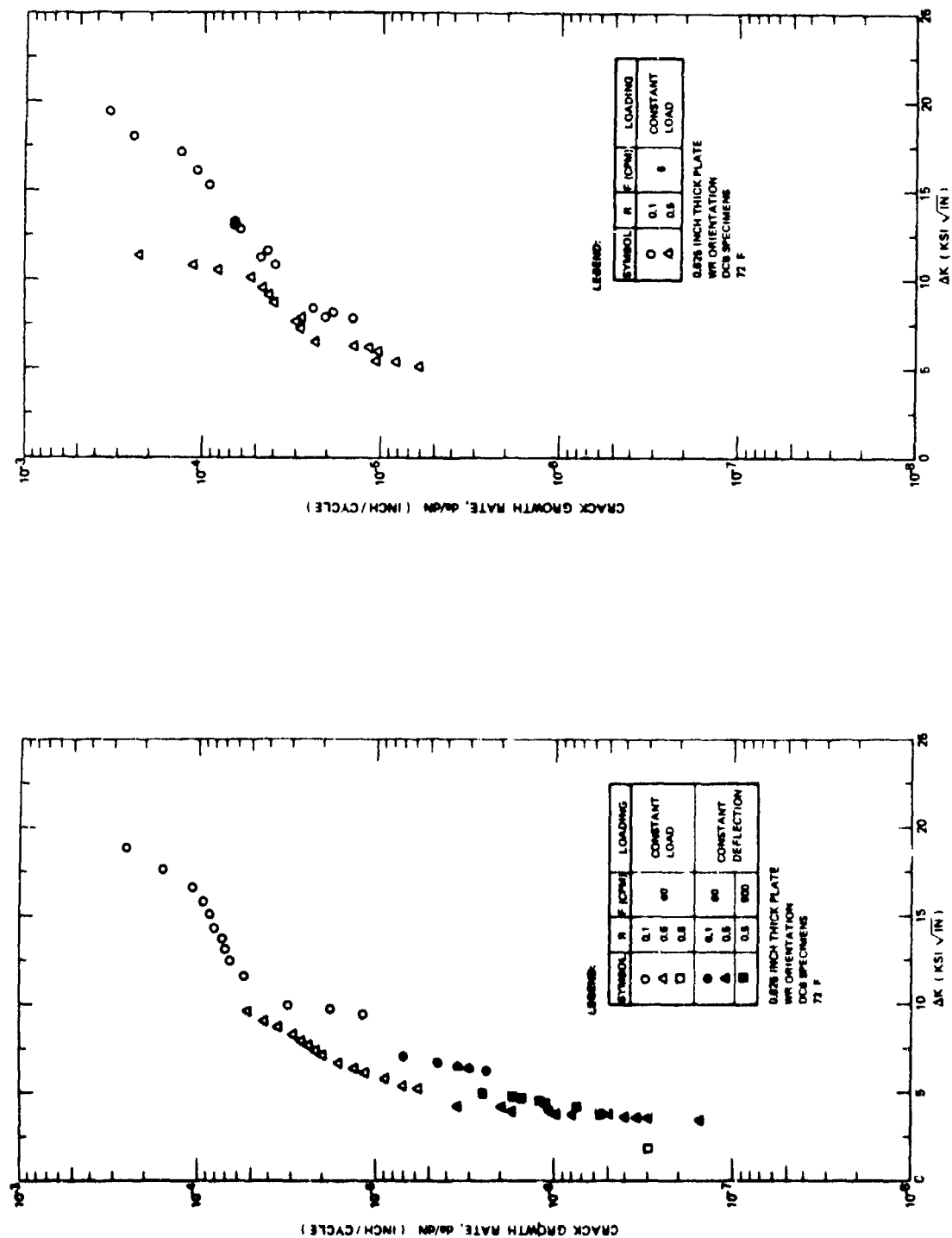


Figure A3: Fatigue Crack Growth Rates For 7075-T651 Aluminum Alloy in 3.5% NaCl Solution

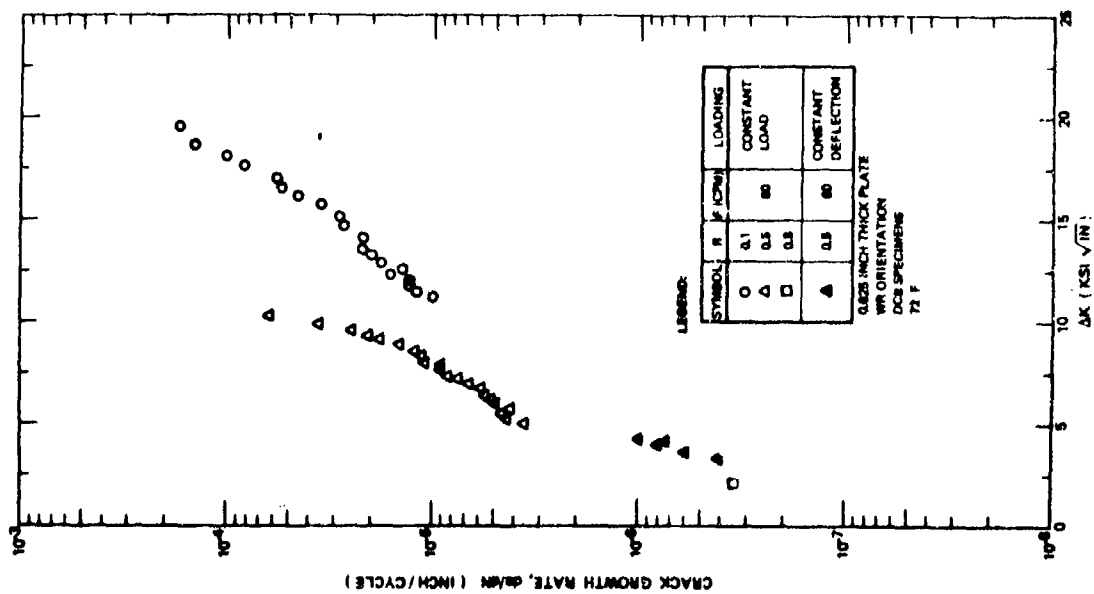
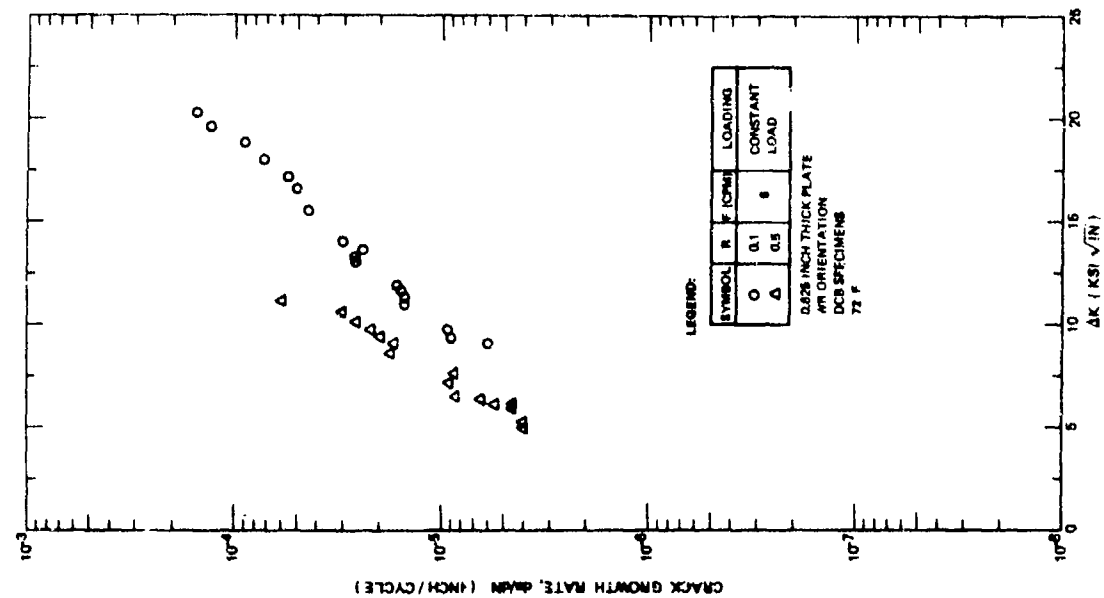


Figure A4: Fatigue Crack Growth Rates For 7075-T651 Aluminum Alloy in Water Saturated JP-4 Fuel

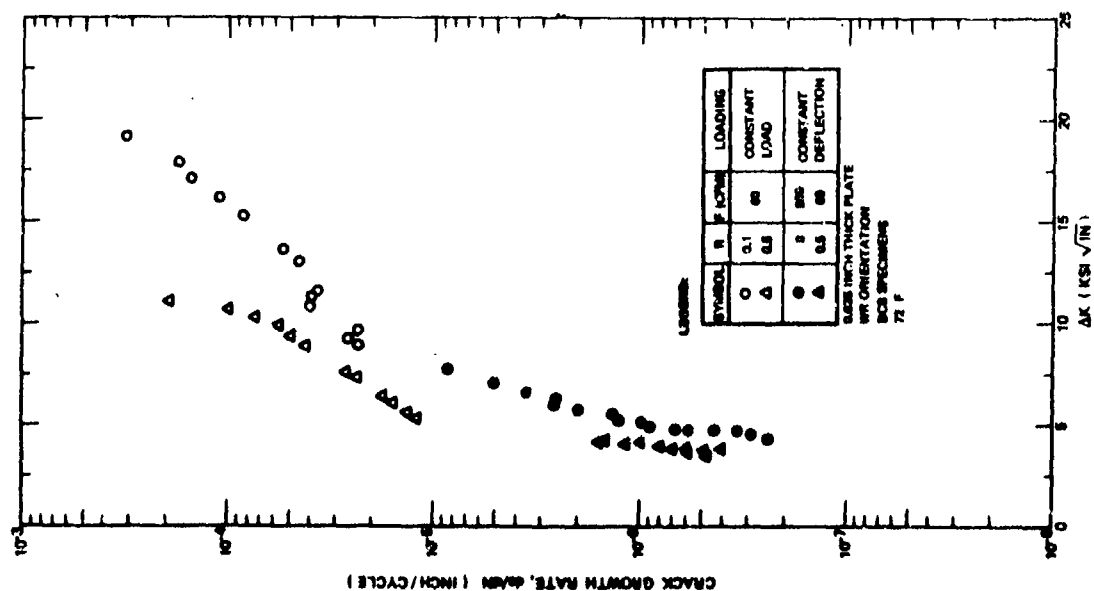
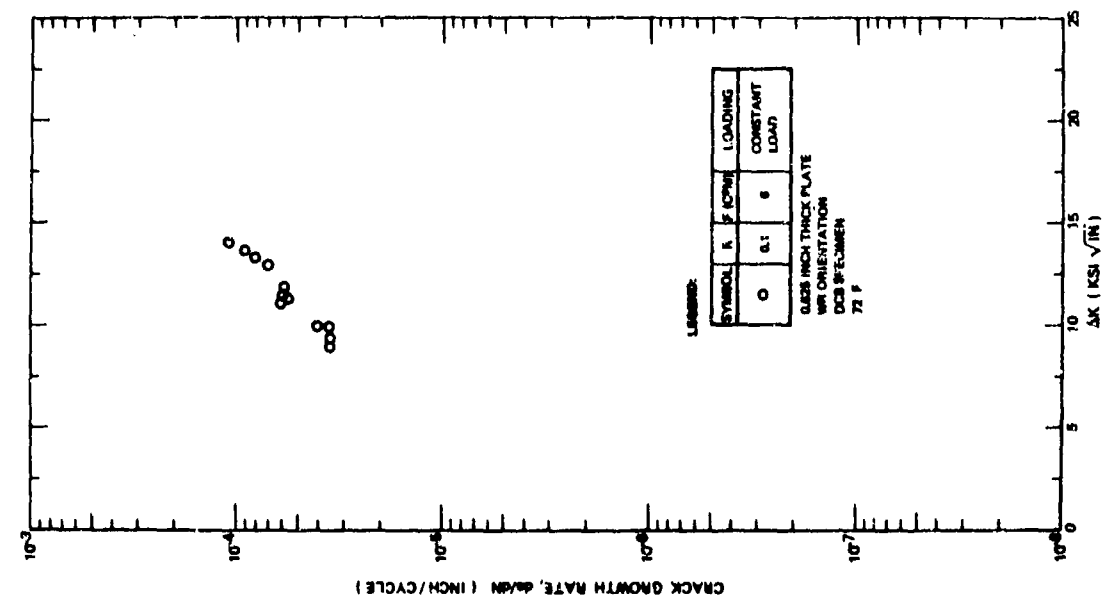


Figure A5: Fatigue Crack Growth Rates For 7075-T651 Aluminum Alloy in Sump Tank Water

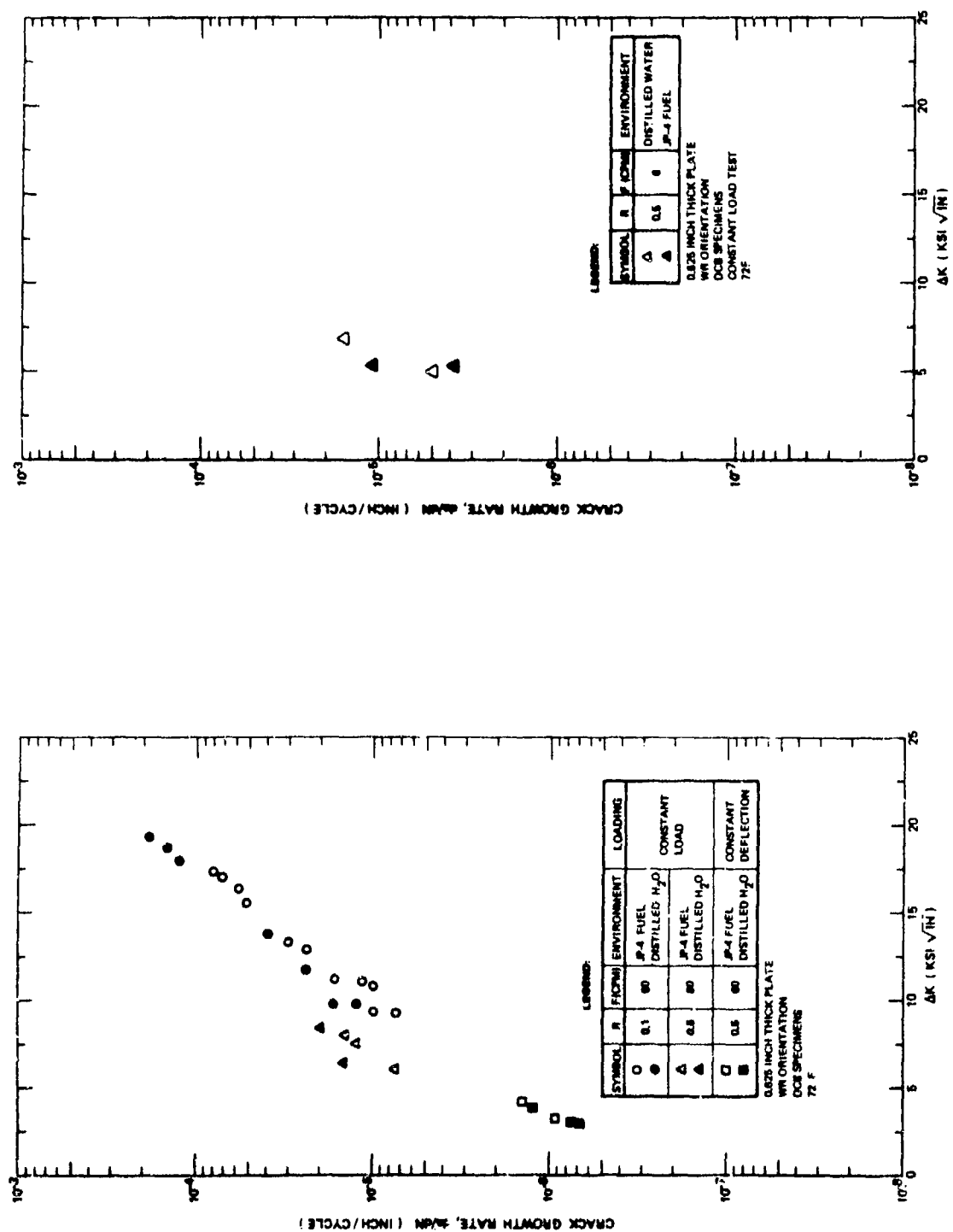


Figure A6: Fatigue Crack Growth Rates For 7075-T651 Aluminum Alloy in Alternating JP-4 Fuel and Distilled Water

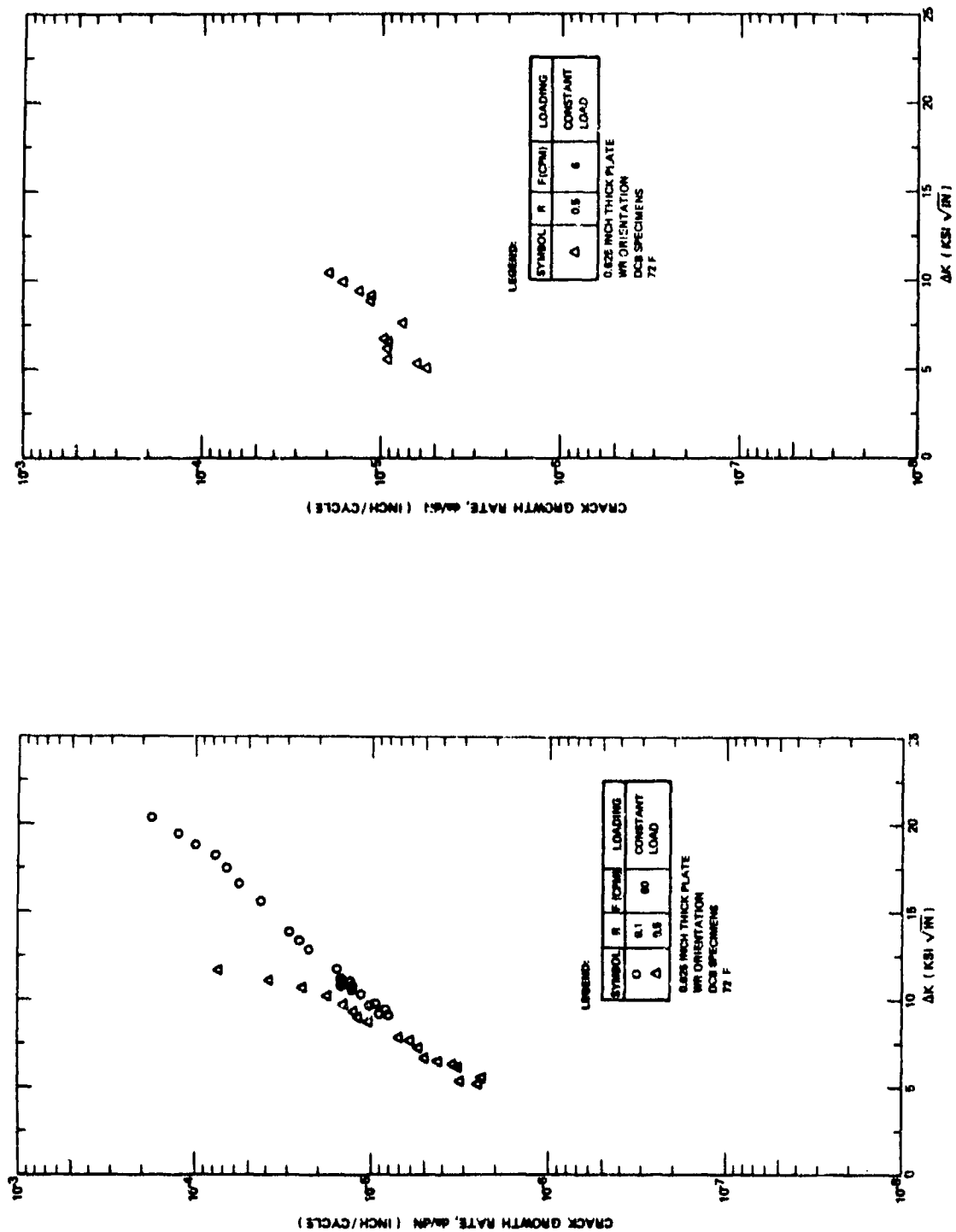


Figure A7: Fatigue Crack Growth Rates For 7075-T651 Aluminum Alloy in Dye Penetrant (Type ZL-2A)

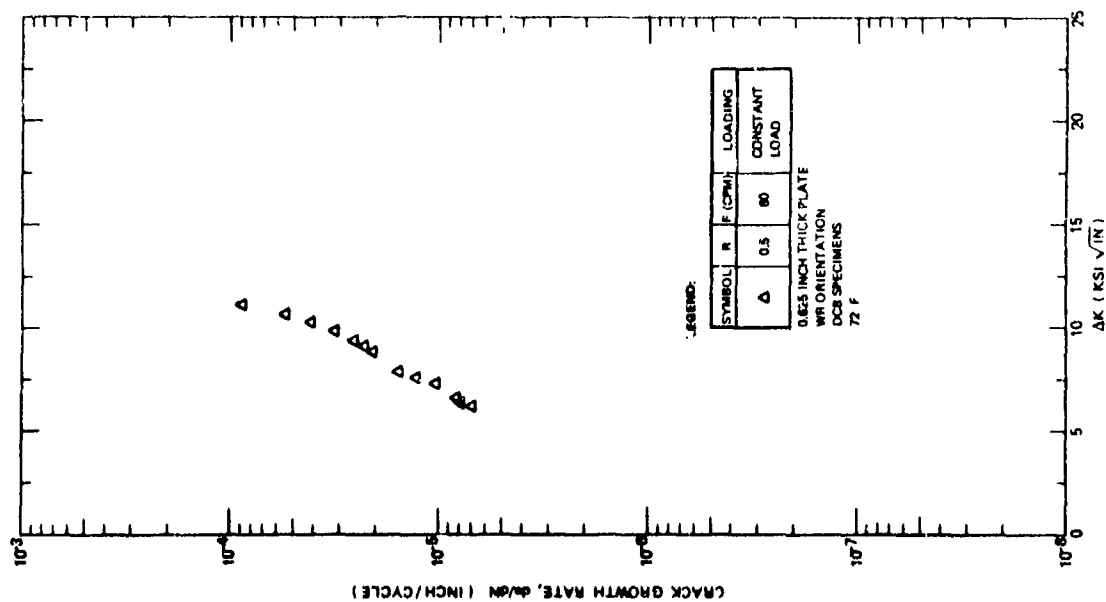


Figure A3: Fatigue Crack Growth Rates For 7075-T651 Aluminum Alloy in Distilled Water, Crack Surface Sprayed With LPS-3 and Dried For 3.0 Hours Prior to Immersion in Test Media

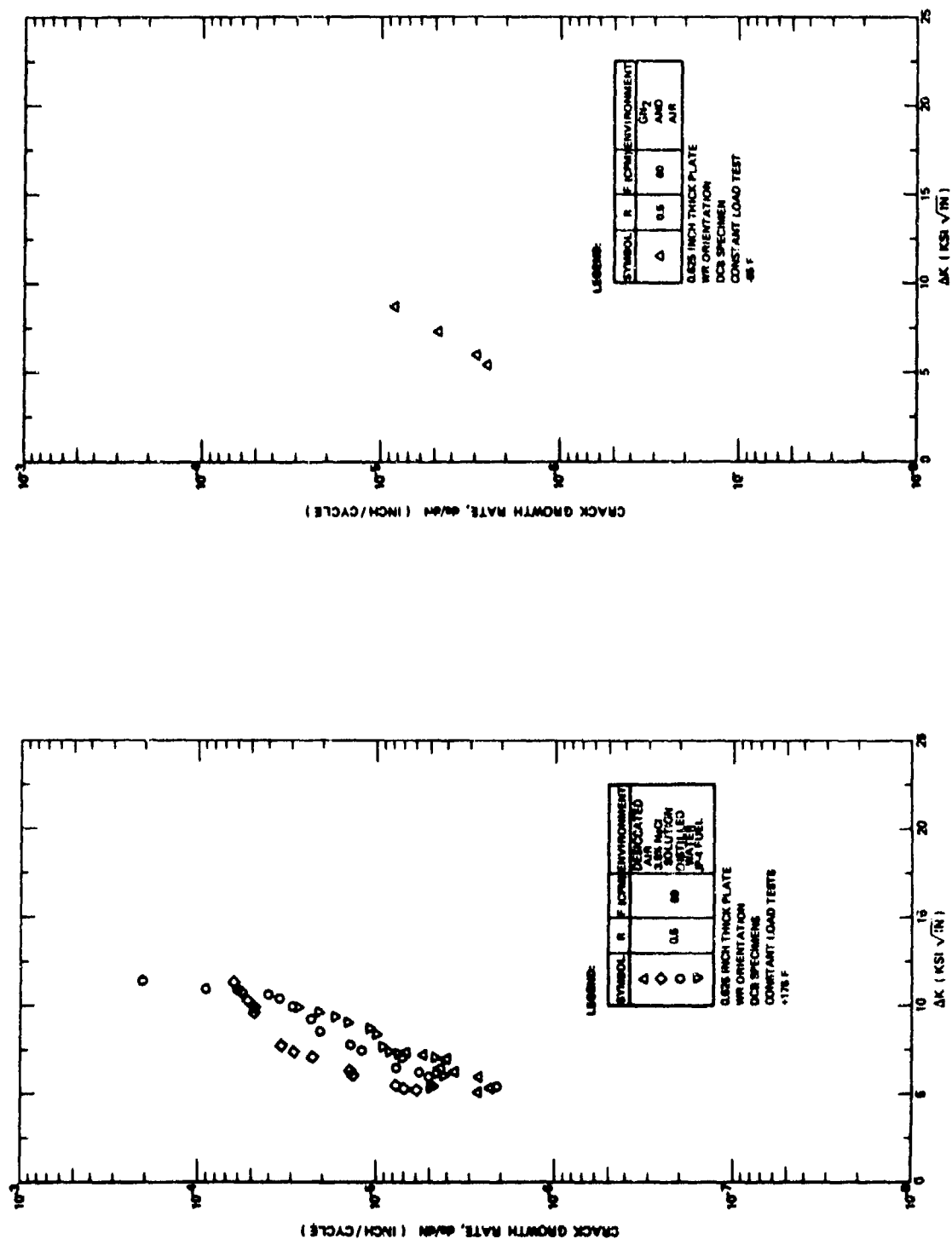


Figure A9: Fatigue Crack Growth Rates For 7075-T651 Aluminum Alloy in Various Environments at +175F and -65F

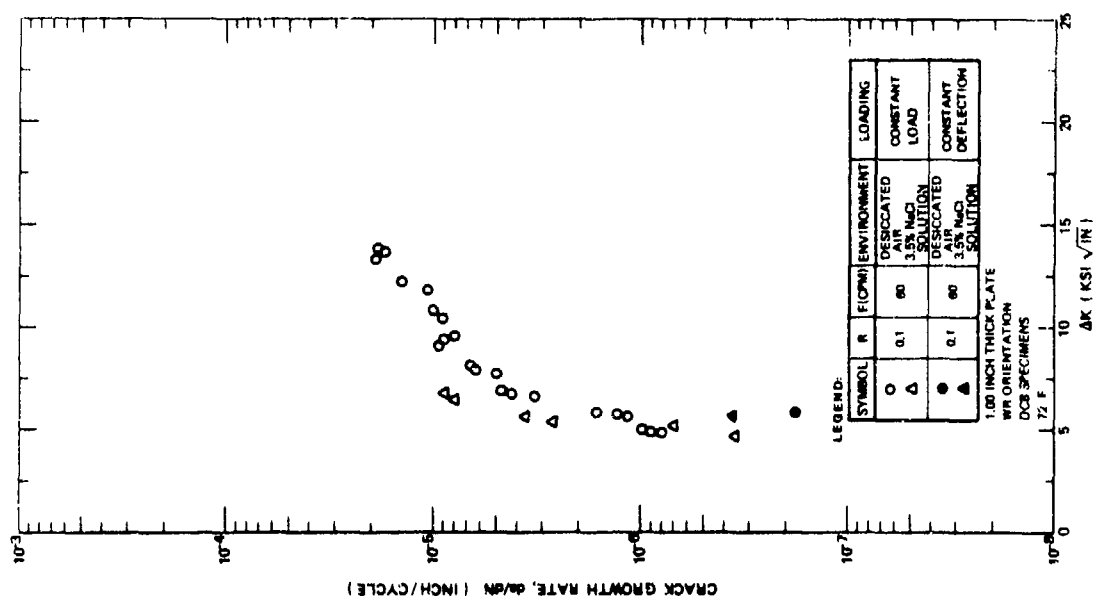


Figure A10: Fatigue Crack Growth Rates For 7475-T651 Aluminum Alloy in 3.5% NaCl Solution and Desiccated Air

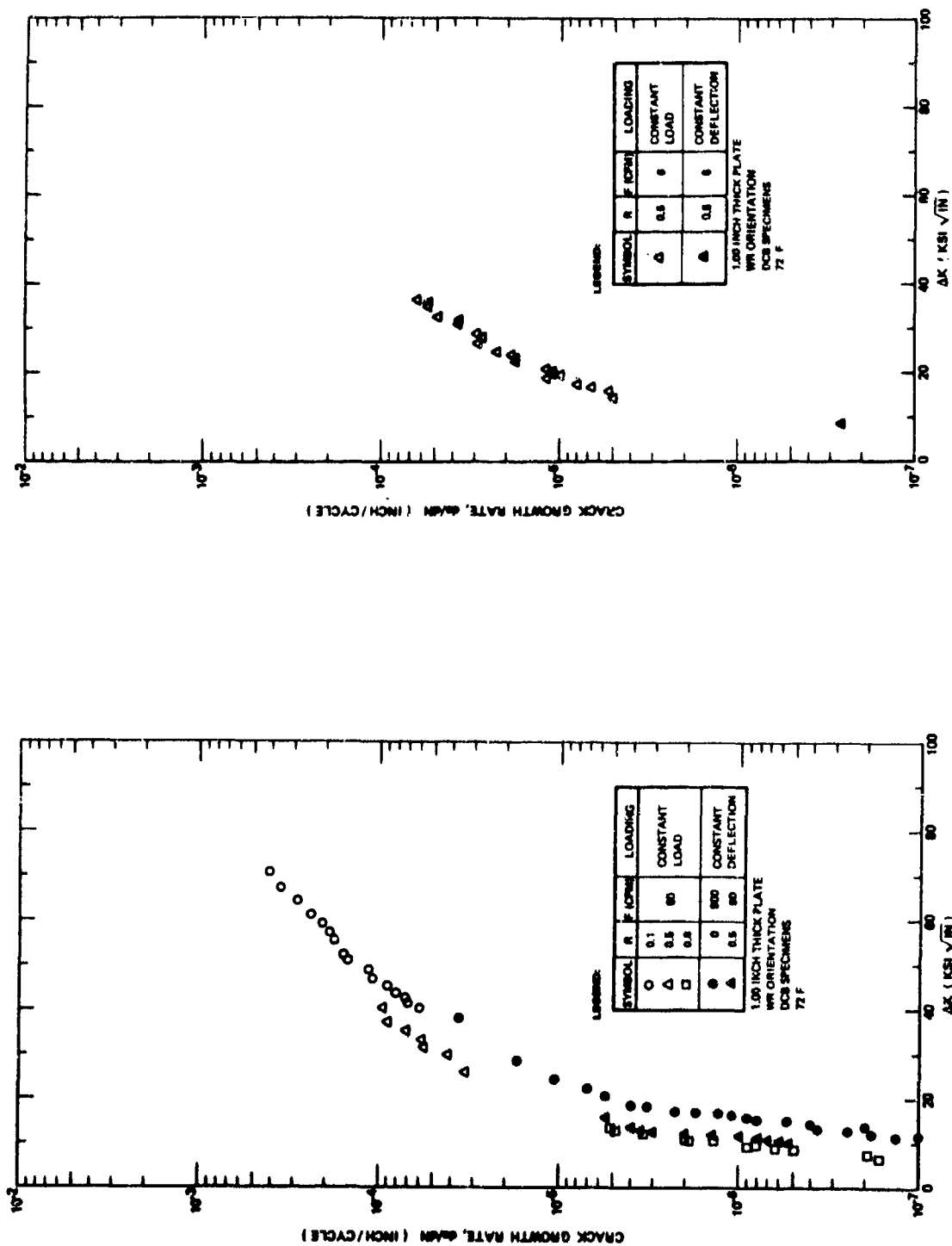


Figure A11: Fatigue Crack Growth Rates For 6Al-4V Standard ELI Beta Annealed Titanium Alloy in Desiccated Air

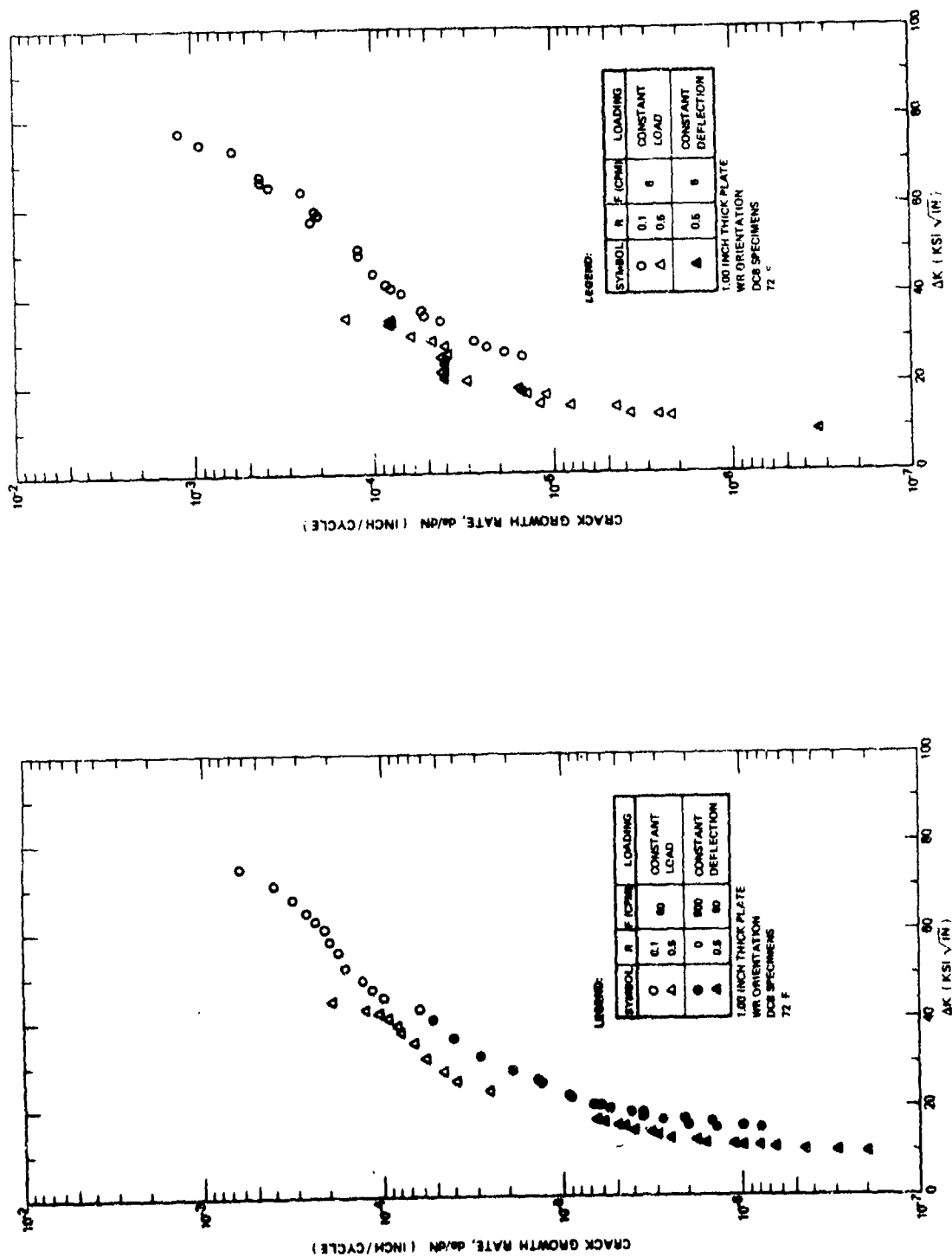


Figure A12: Fatigue Crack Growth Rates For 6Al-4V Standard ELI Beta Annealed Titanium Alloy in Distilled Water

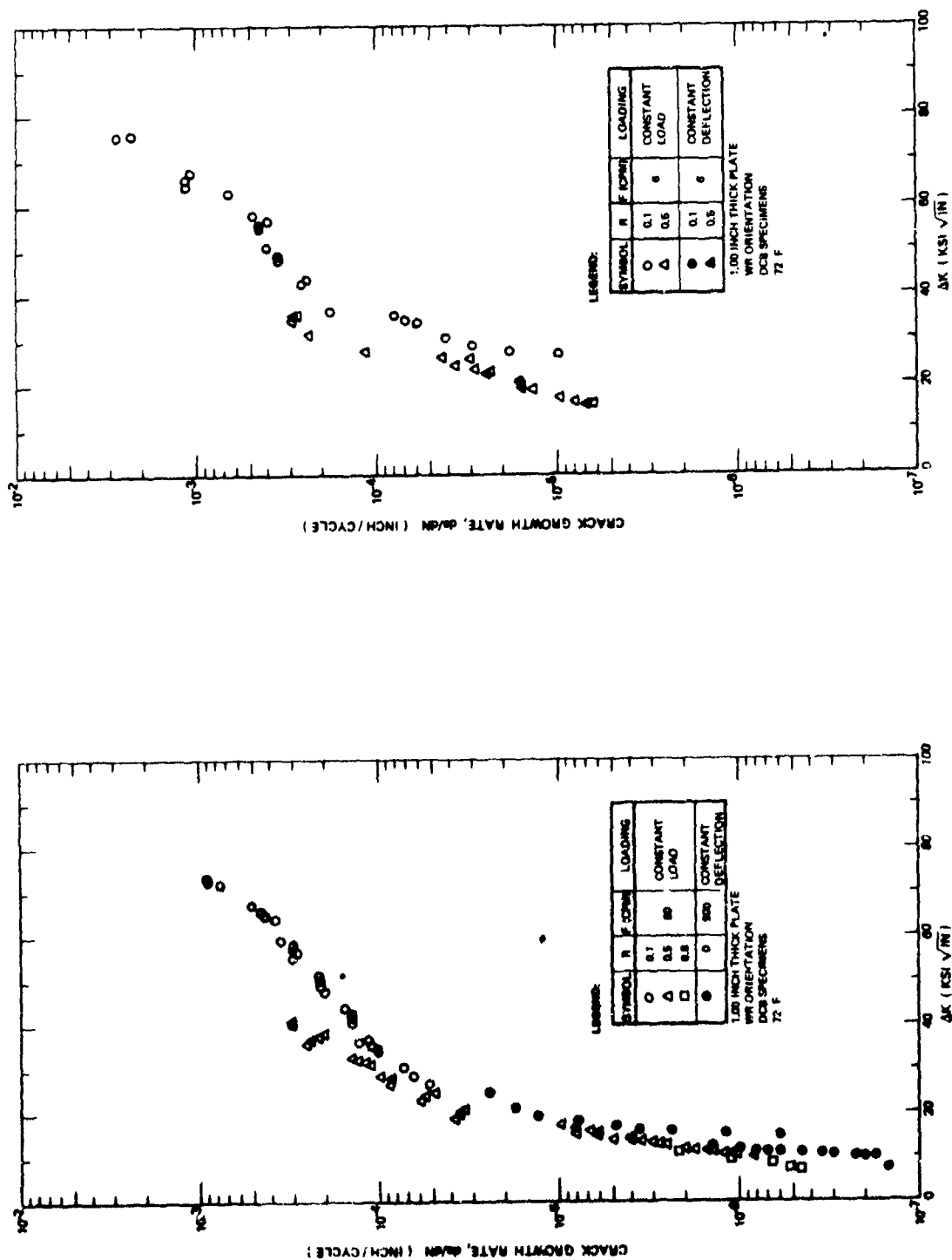


Figure A13: Fatigue Crack Growth Rates For 6Al-4V Standard ELI Beta Annealed Titanium Alloy in 3.5% NaCl Solution

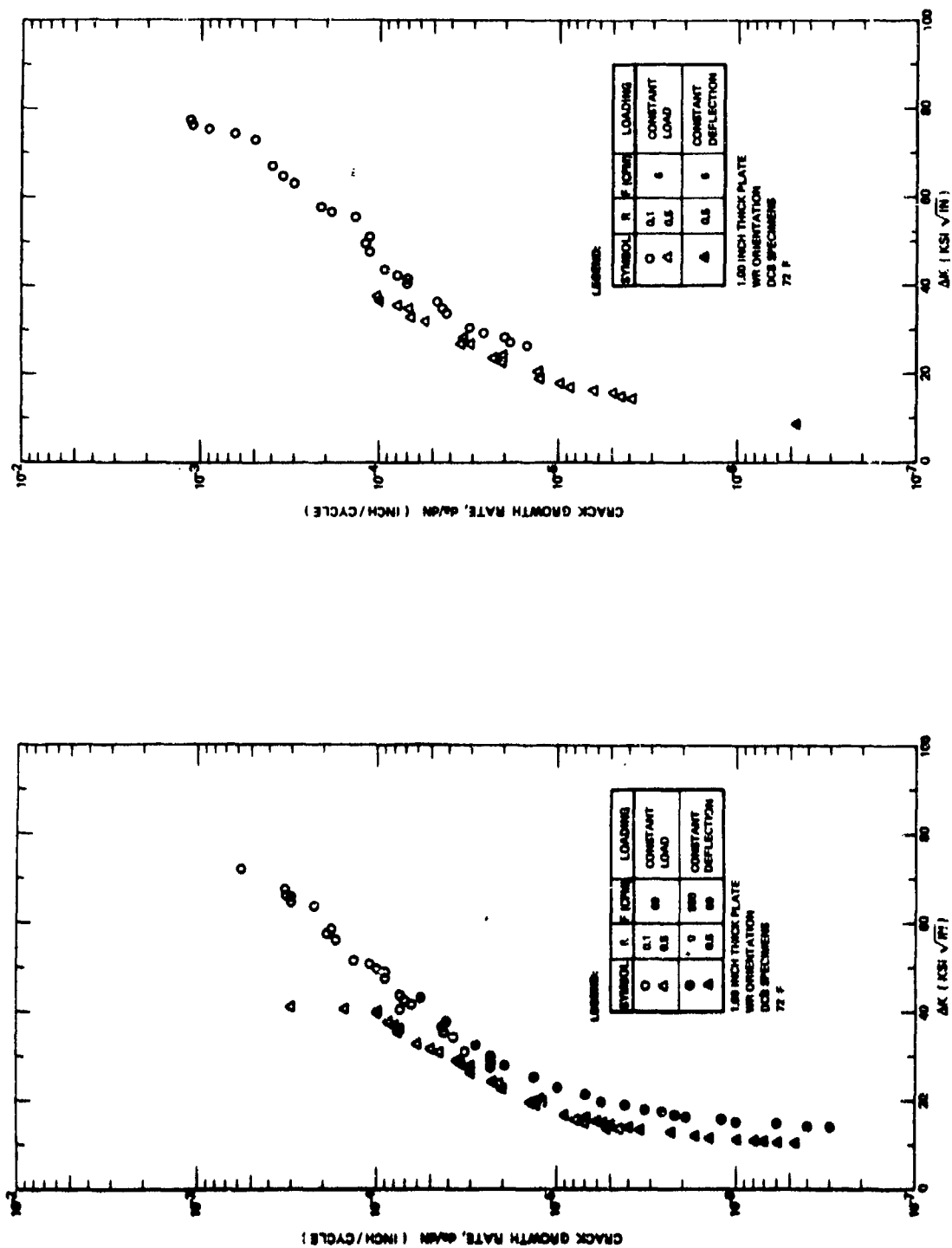


Figure A14: Fatigue Crack Growth Rates F-76 Al-4V Standard ELI Beta Annealed Titanium Alloy in Water Saturated JP-4 Fuel

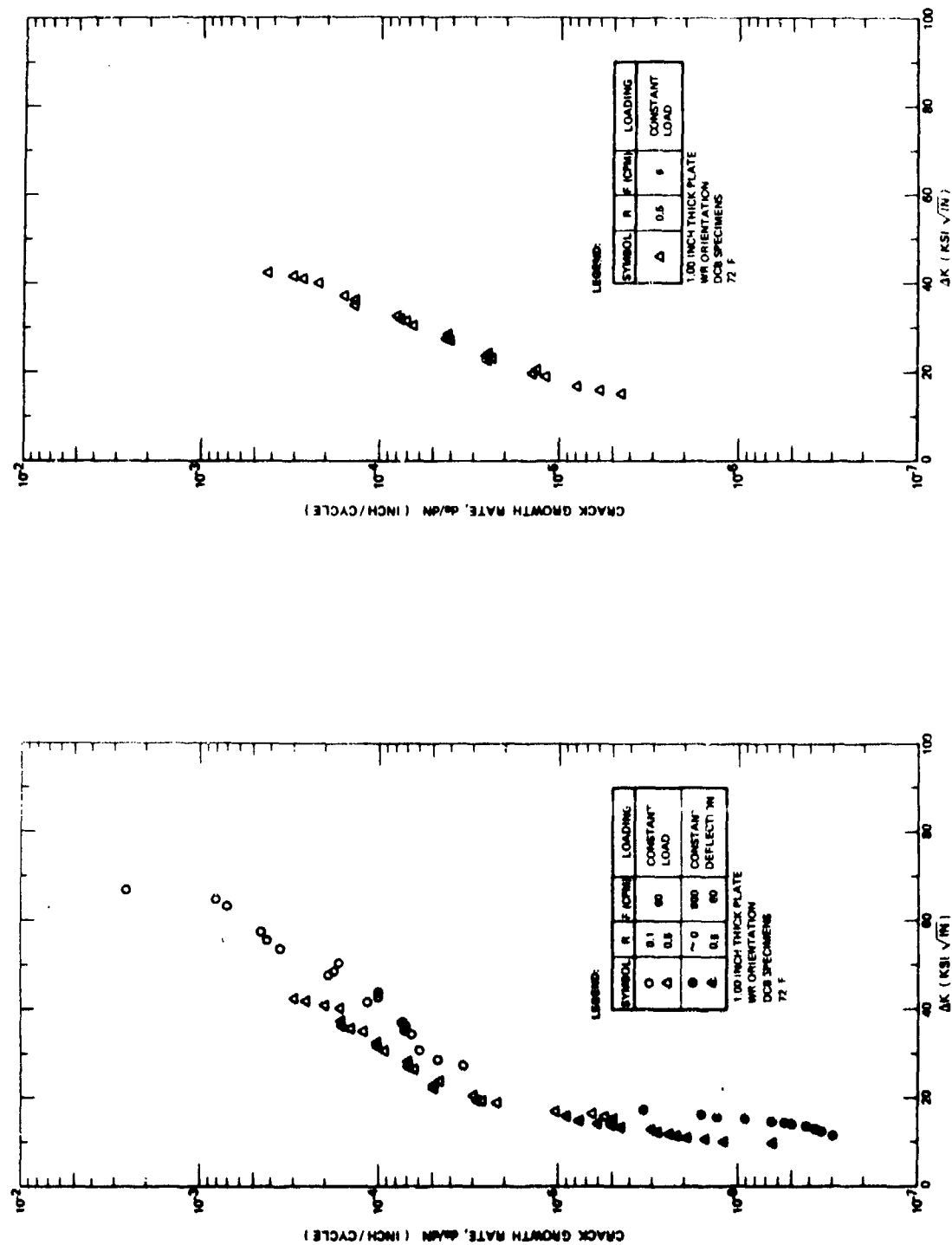


Figure A15: Fatigue Crack Growth Rates For 6Al-4V Standard ELI Beta Annealed Titanium Alloy in Sump Tank Water

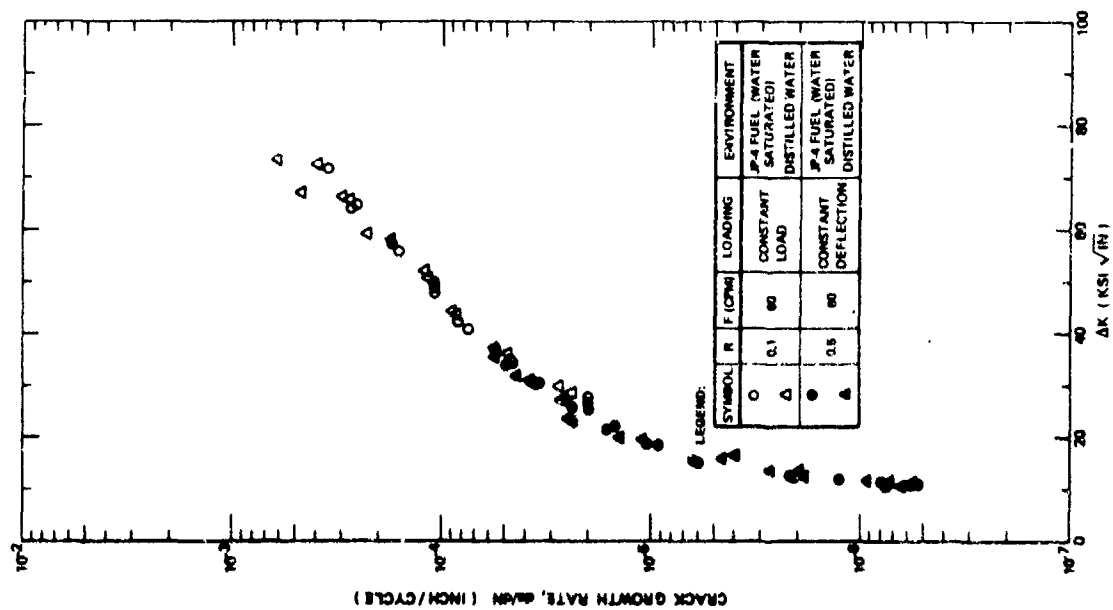


Figure A16: Fatigue Crack Growth Rates For 6Al-4V Standard ELI Beta Annealed Titanium Alloy in Alternating JP-4 Fuel and Distilled Water

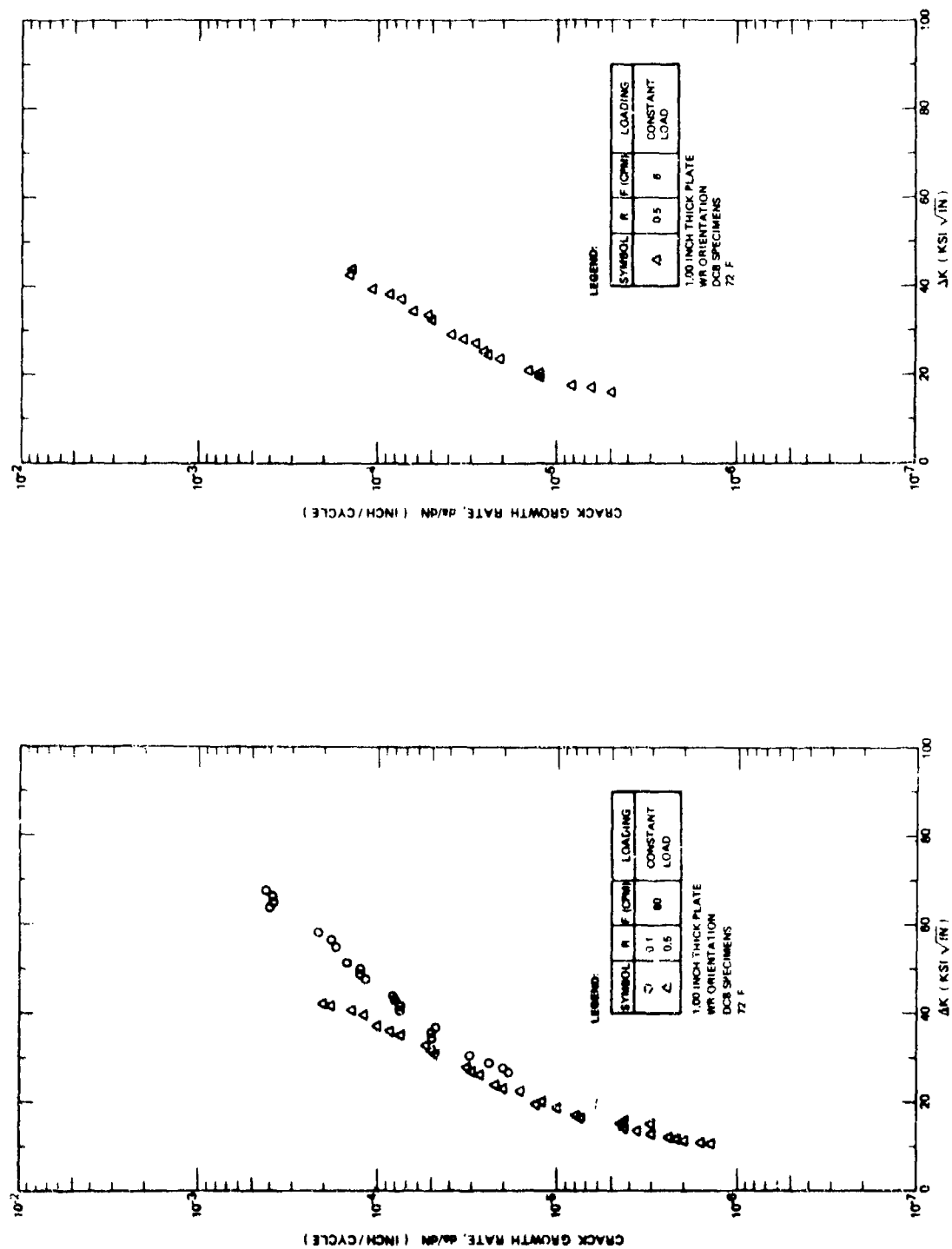


Figure A17: Fatigue Crack Growth Rates For 6Al-4V Standard ELI Beta Annealed Titanium Alloy Plate in Dye Penetrant (Type ZL-2A)

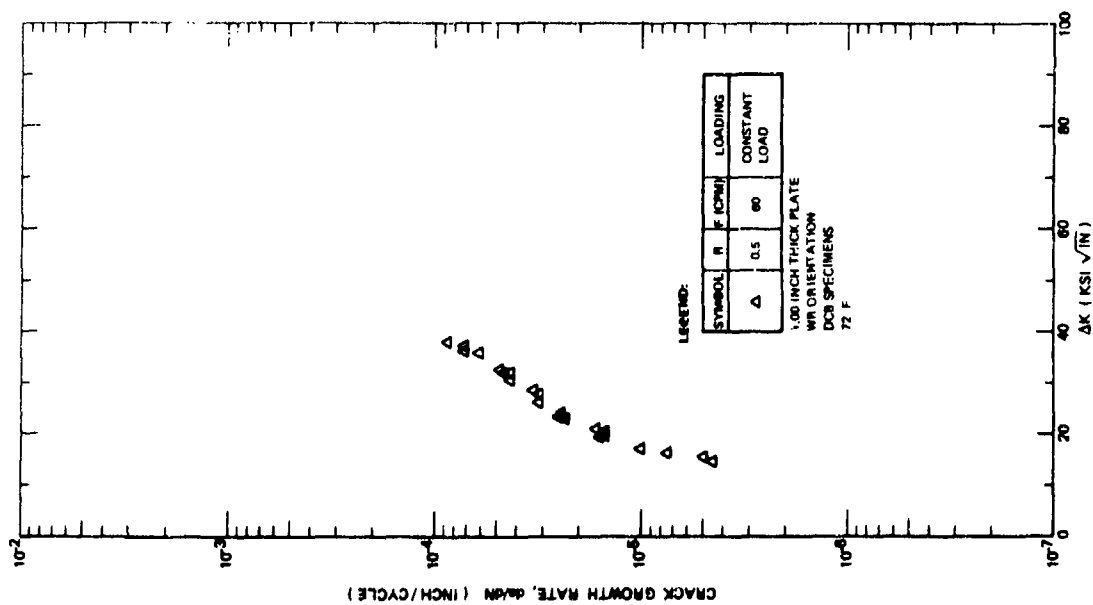


Figure A18: Fatigue Crack Growth Rates For 6Al-4V Standard ELI Beta Annealed Titanium Alloy in Distilled Water, Crack Surface Sprayed With LPS-3 and Dried For 3.0 Hours Prior to Immersion in Test Media

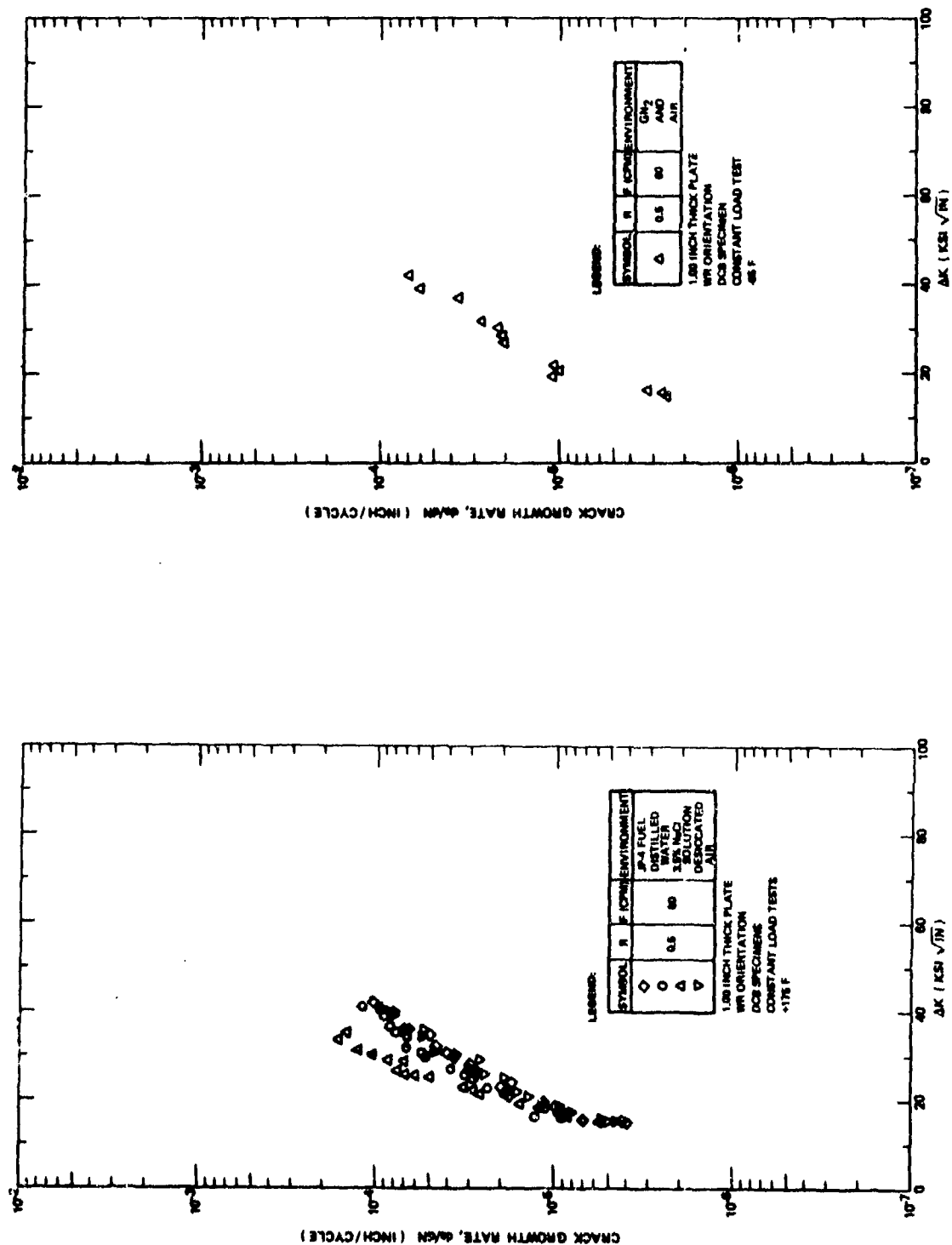


Figure A19: Fatigue Crack Growth Rates For 6Al-4V Standard ELI Beta Annealed Titanium Alloy in Various Environments at +175F and -65F

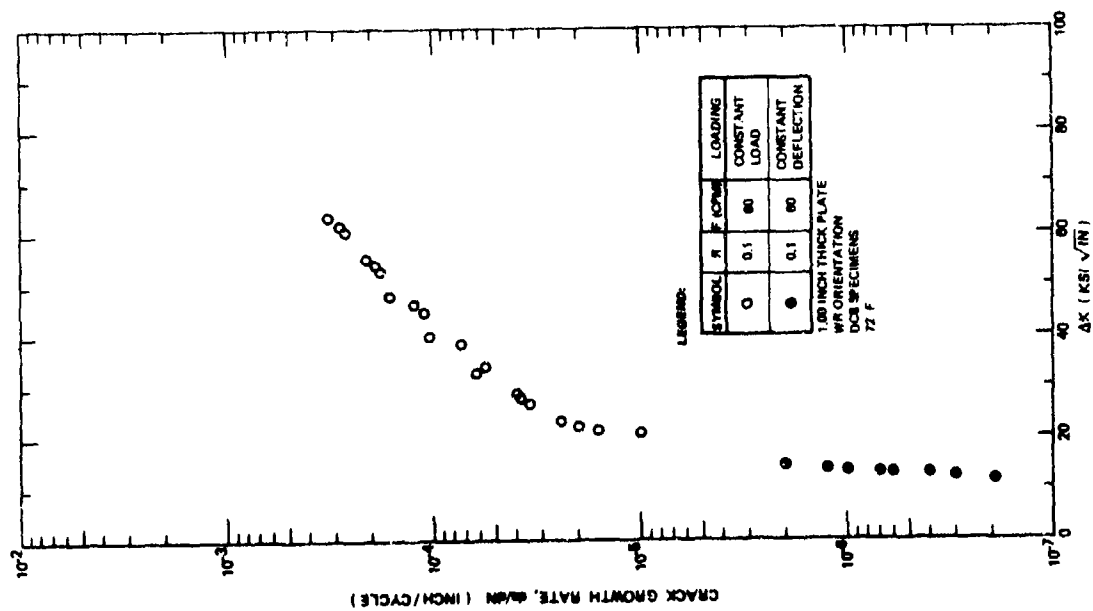


Figure A20: Fatigue Crack Growth Rates For 6Al-4V "Super ELI" (0.06 O₂ Content) Beta Annealed Titanium Alloy in 3.5% NaCl Solution

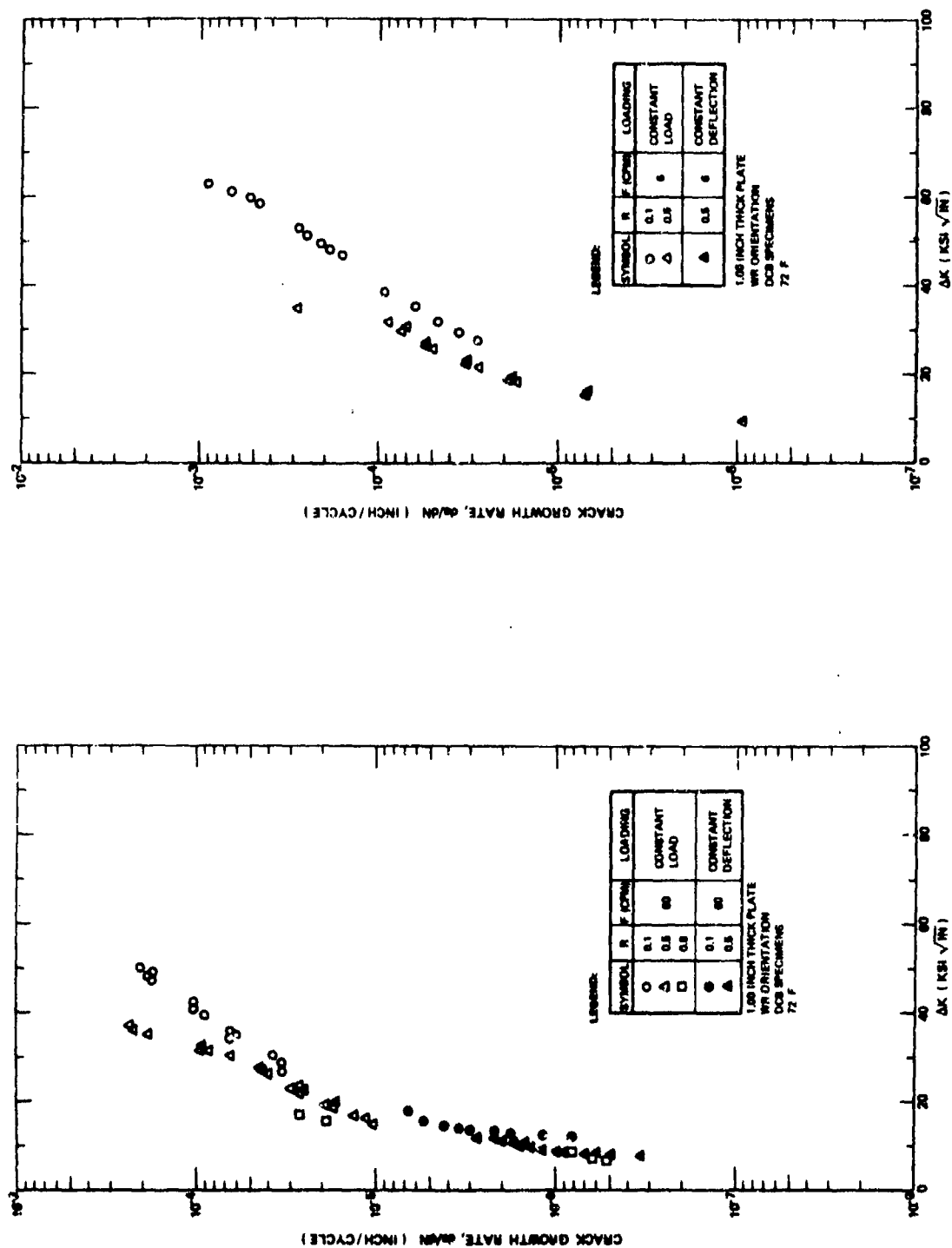


Figure A21: Fatigue Crack Growth Rates For 6Al-4V Recrystallized Annealed Titanium Alloy in Desiccated Air

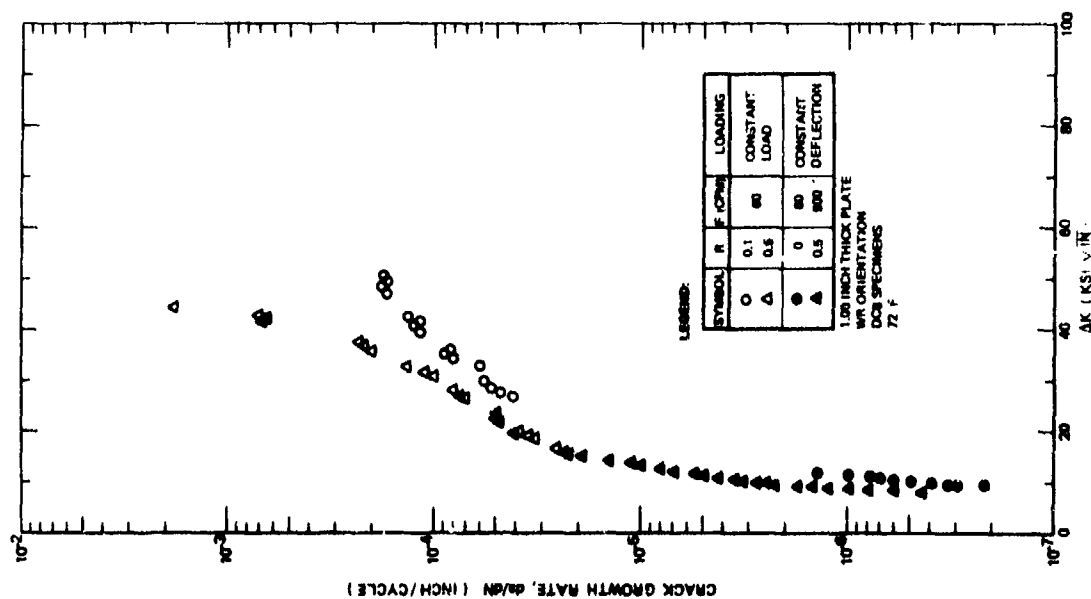
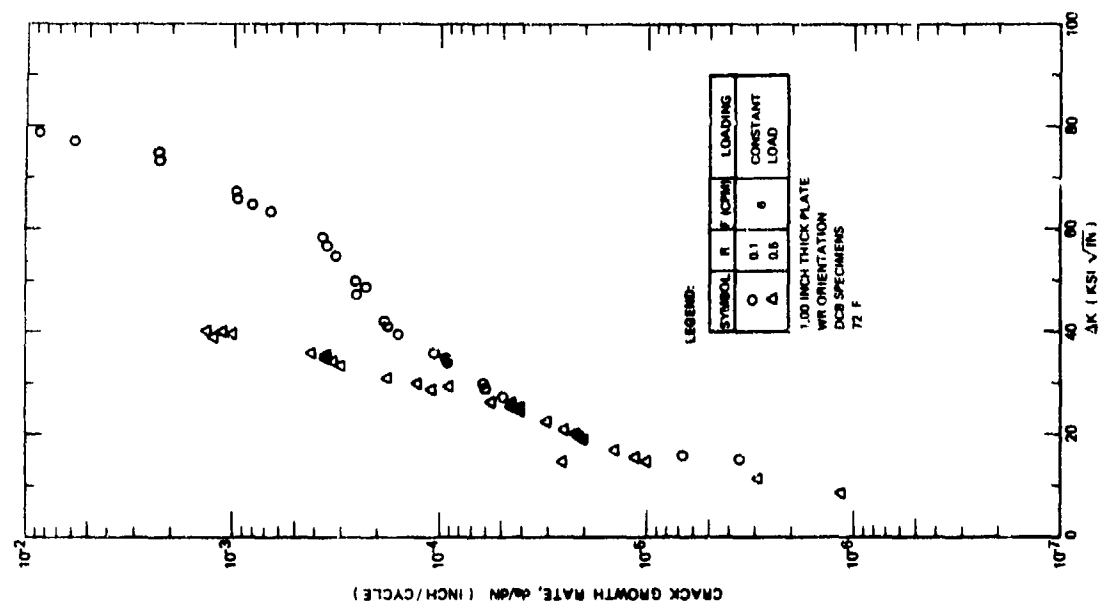


Figure A22: Fatigue Crack Growth Rates For 6Al-4V Recrystallized Annealed Titanium Alloy in Distilled Water

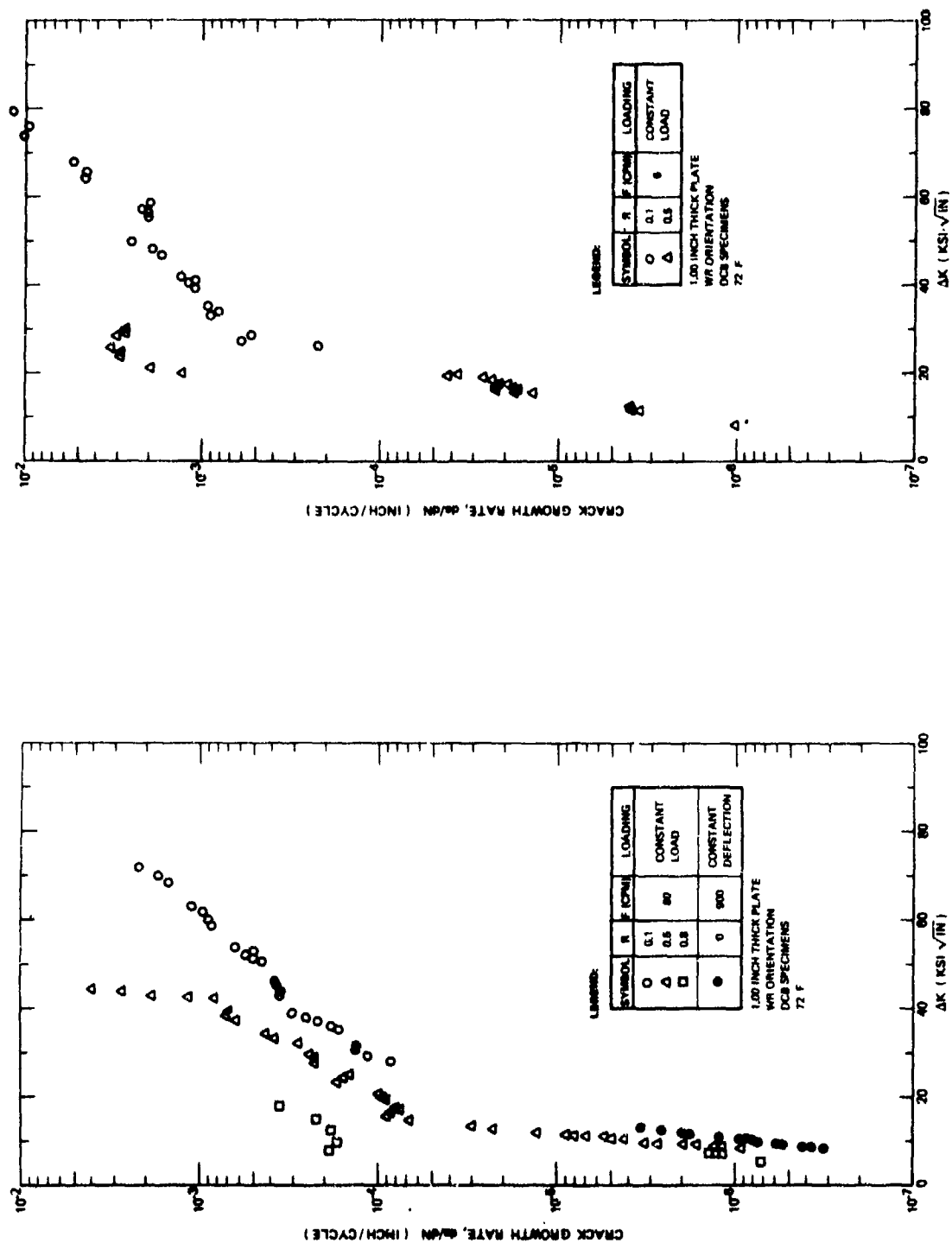


Figure A23: Fatigue Crack Growth Rates For 6Al-4V Recrystallized Annealed Titanium Alloy in 3.5% NaCl Solution

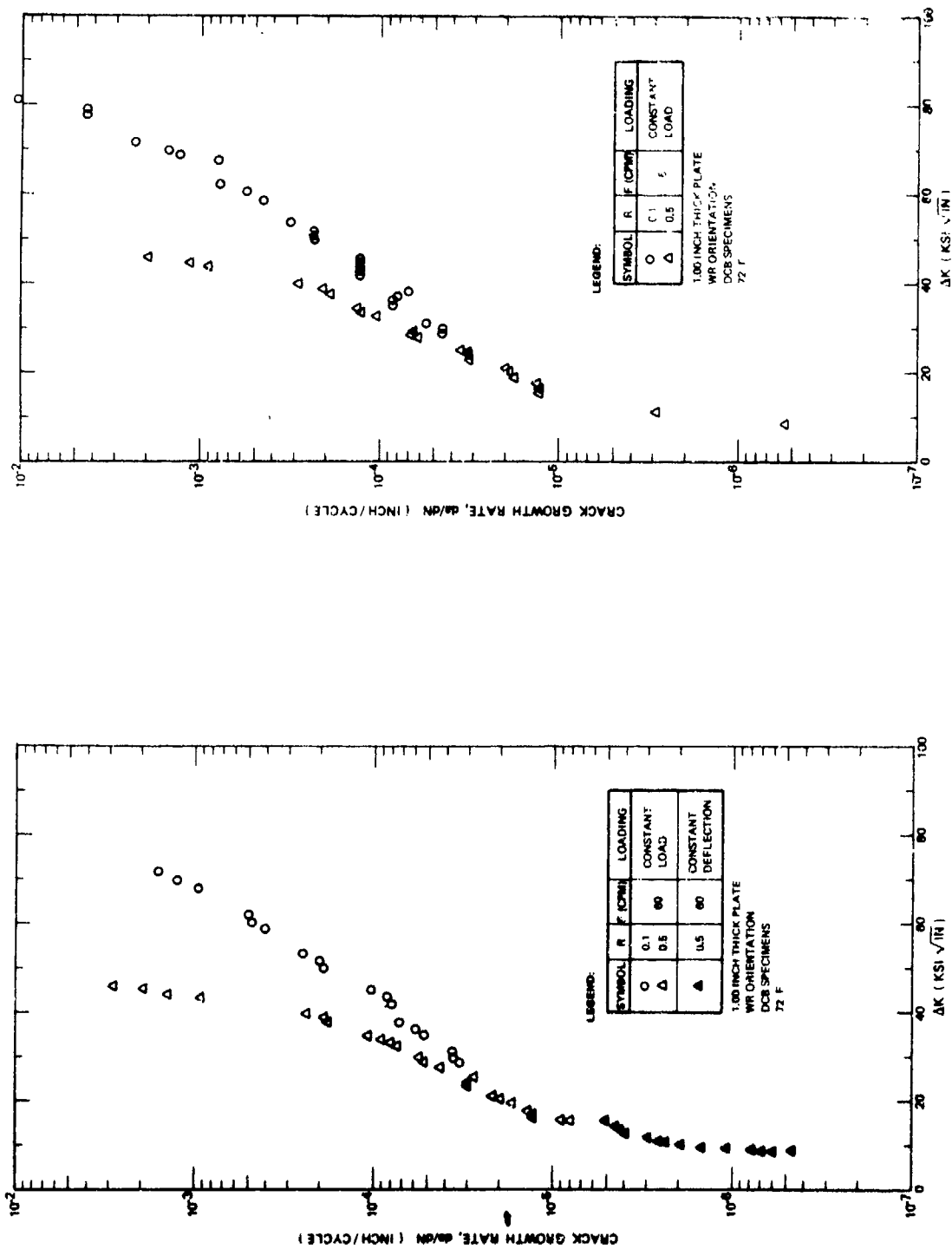


Figure A24: Fatigue Crack Growth Rates For 6Al-4V Recrystallized Annealed Titanium Alloy in Water Saturated JP-4 Fuel

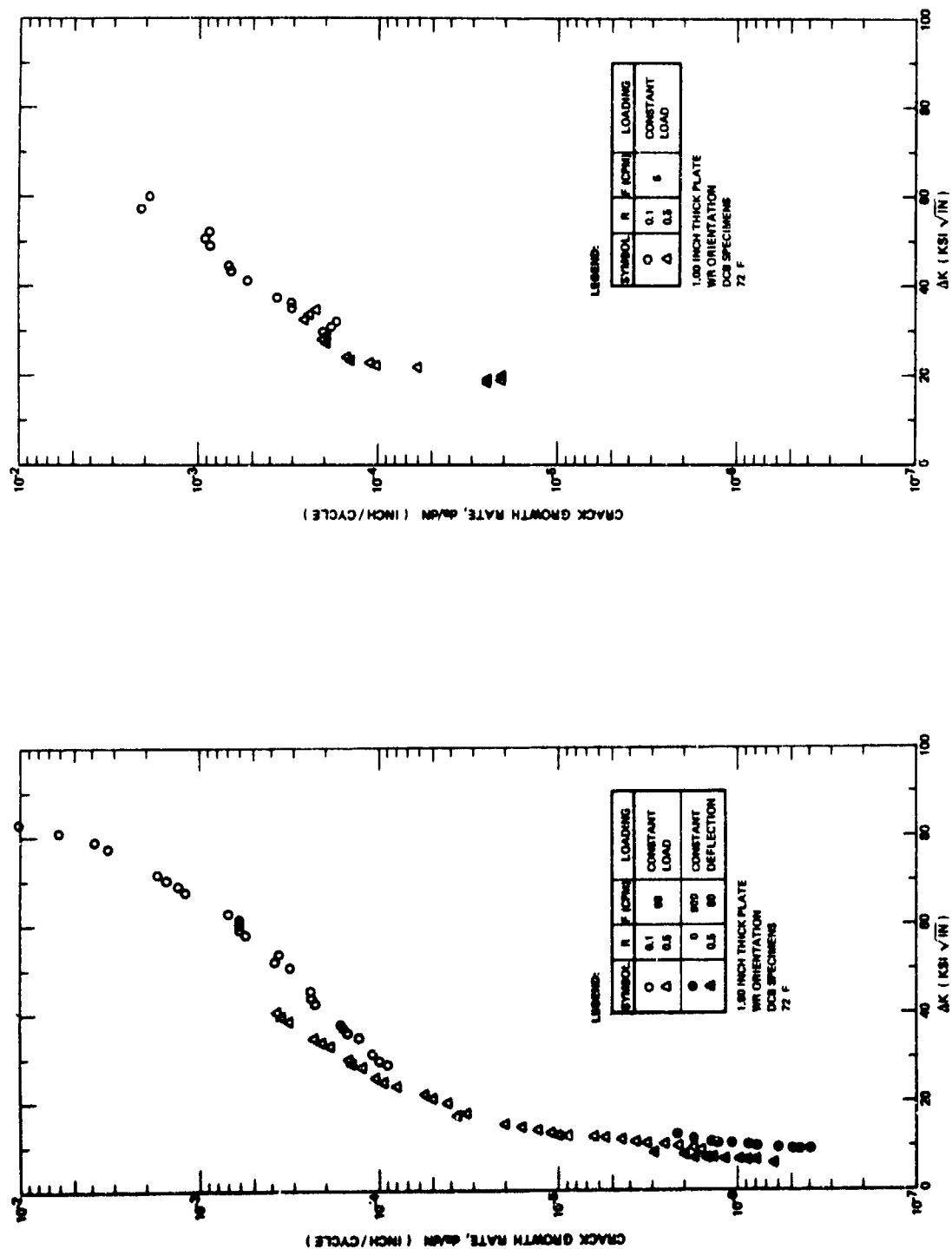


Figure A25: Fatigue Crack Growth Rates For 6Al-4V Recrystallized Annealed Titanium Alloy in Sump Tank Water

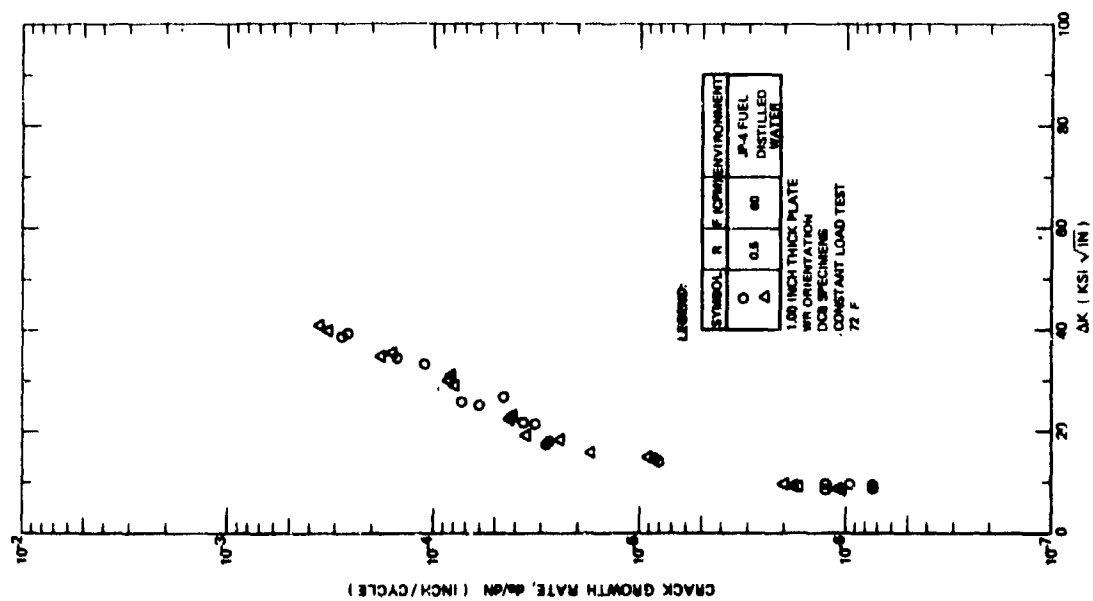


Figure A26: Fatigue Crack Growth Rates For 6Al-4V Recrystallized Annealed Titanium Alloy in Alternating JP-4 Fuel and Distilled Water

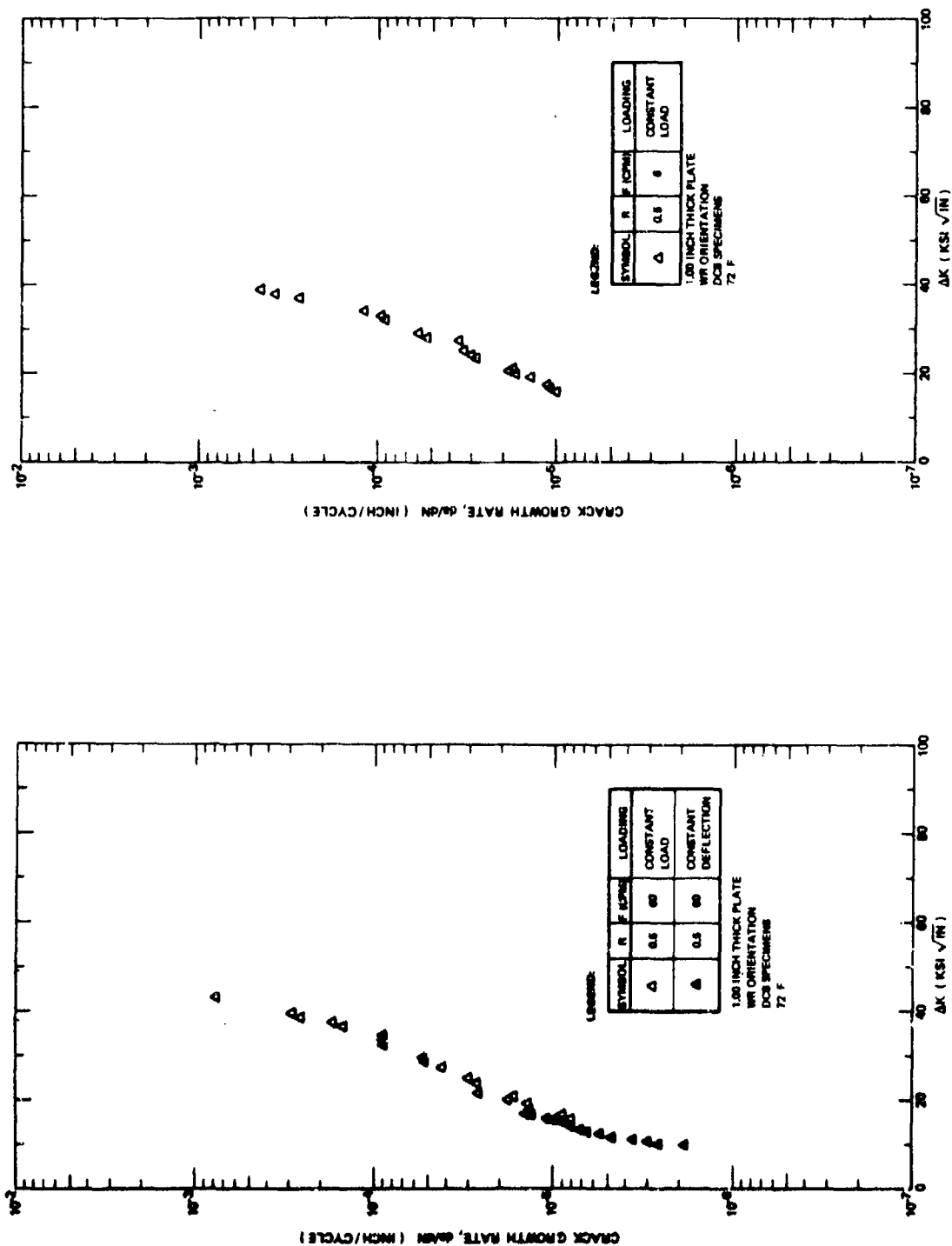


Figure A27: Fatigue Crack Growth Rates For 6Al-4V Recrystallized Annealed Titanium Alloy in Dye Penetrant (Type ZL-2A)

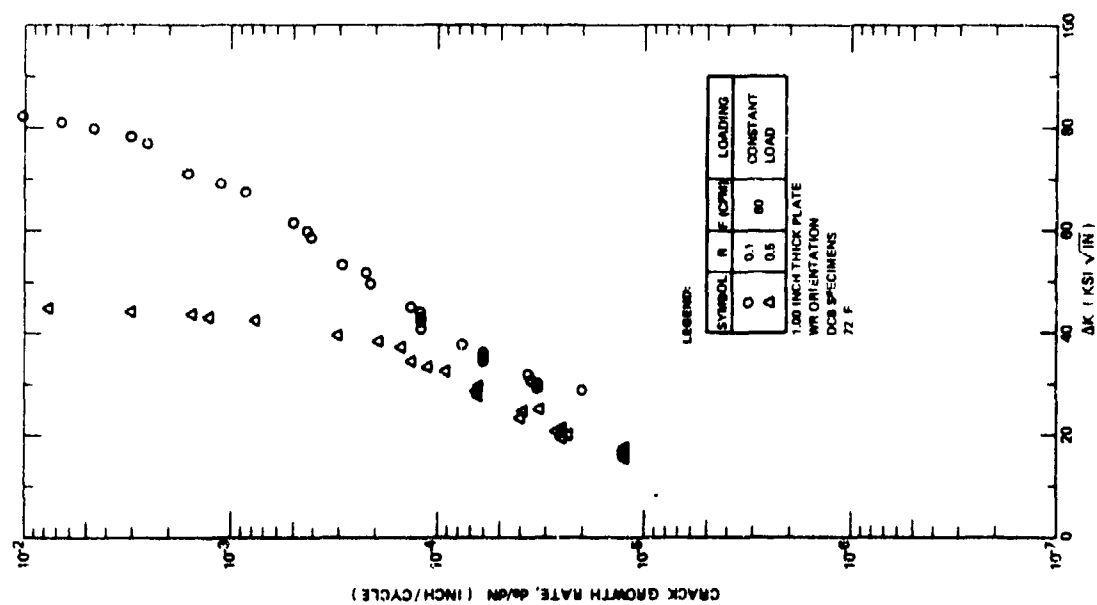


Figure A28: Fatigue Crack Growth Rates For 6Al-4V Recrystallized Annealed Titanium Alloy in Distilled Water, Crack Surface Sprayed With LPS-3 and Dried For 3.0 Hours Prior to Immersion in Test Media

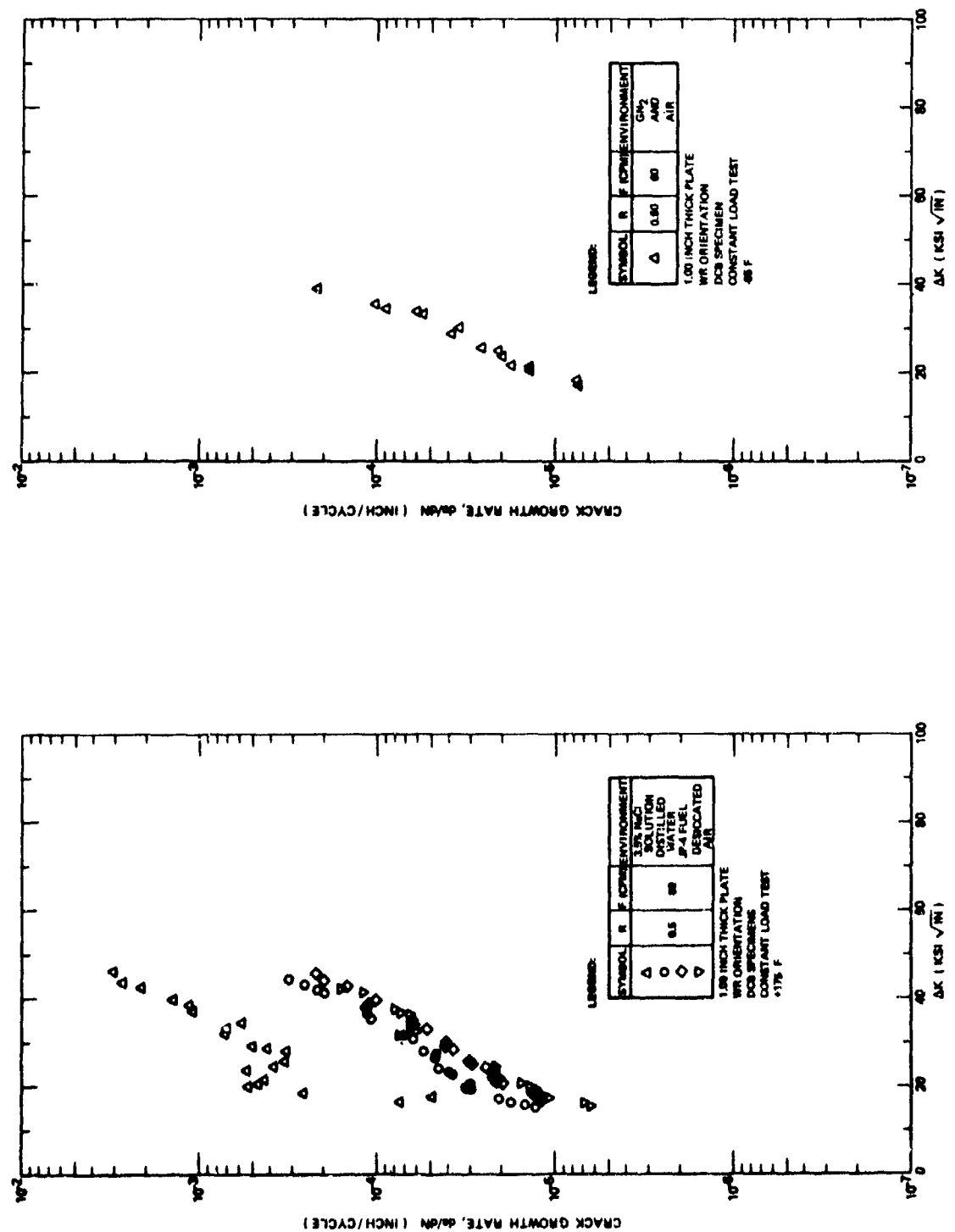


Figure A29: Fatigue Crack Growth Rates For 6Al-4V Recrystallized Annealed Titanium Alloy in Various Environments at +175F and -65F

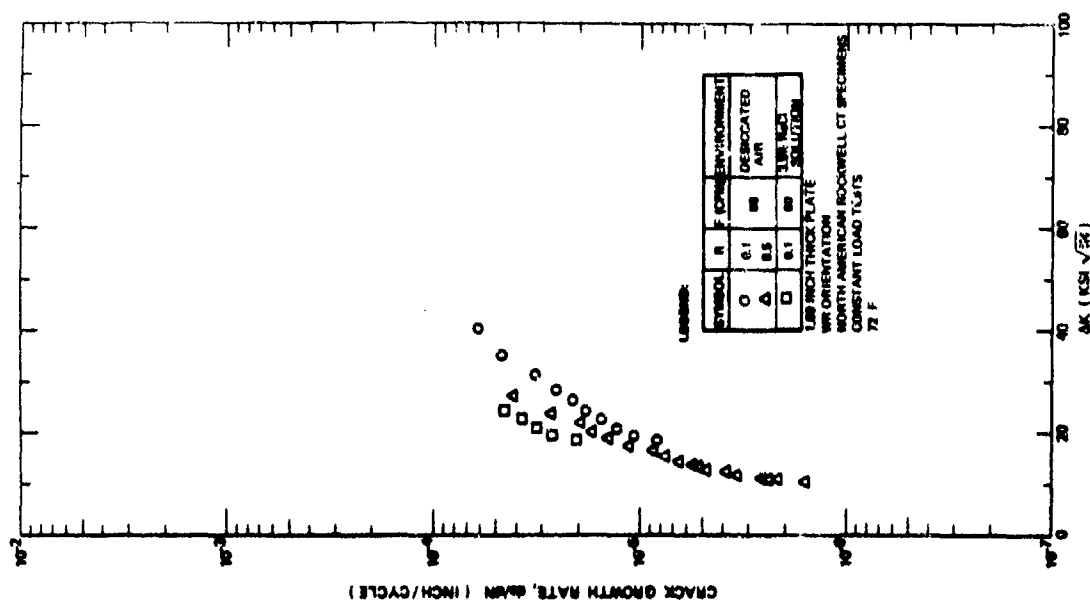


Figure A30: Fatigue Crack Growth Rates For 6Al-4V Recrystallized Titanium Alloy in 3.5% NaCl Solution and Desiccated Air

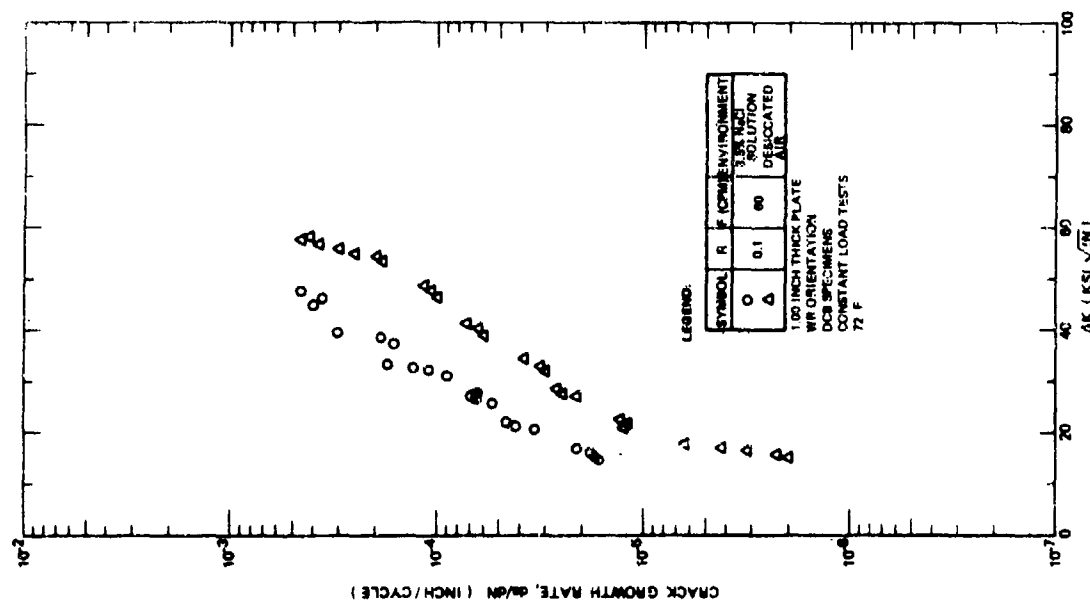


Figure A31: Fatigue Crack Growth Rates For 6Al-4V (Fast Cooled) Recrystallized Annealed Titanium Alloy in 3.5% NaCl Solution and Desiccated Air

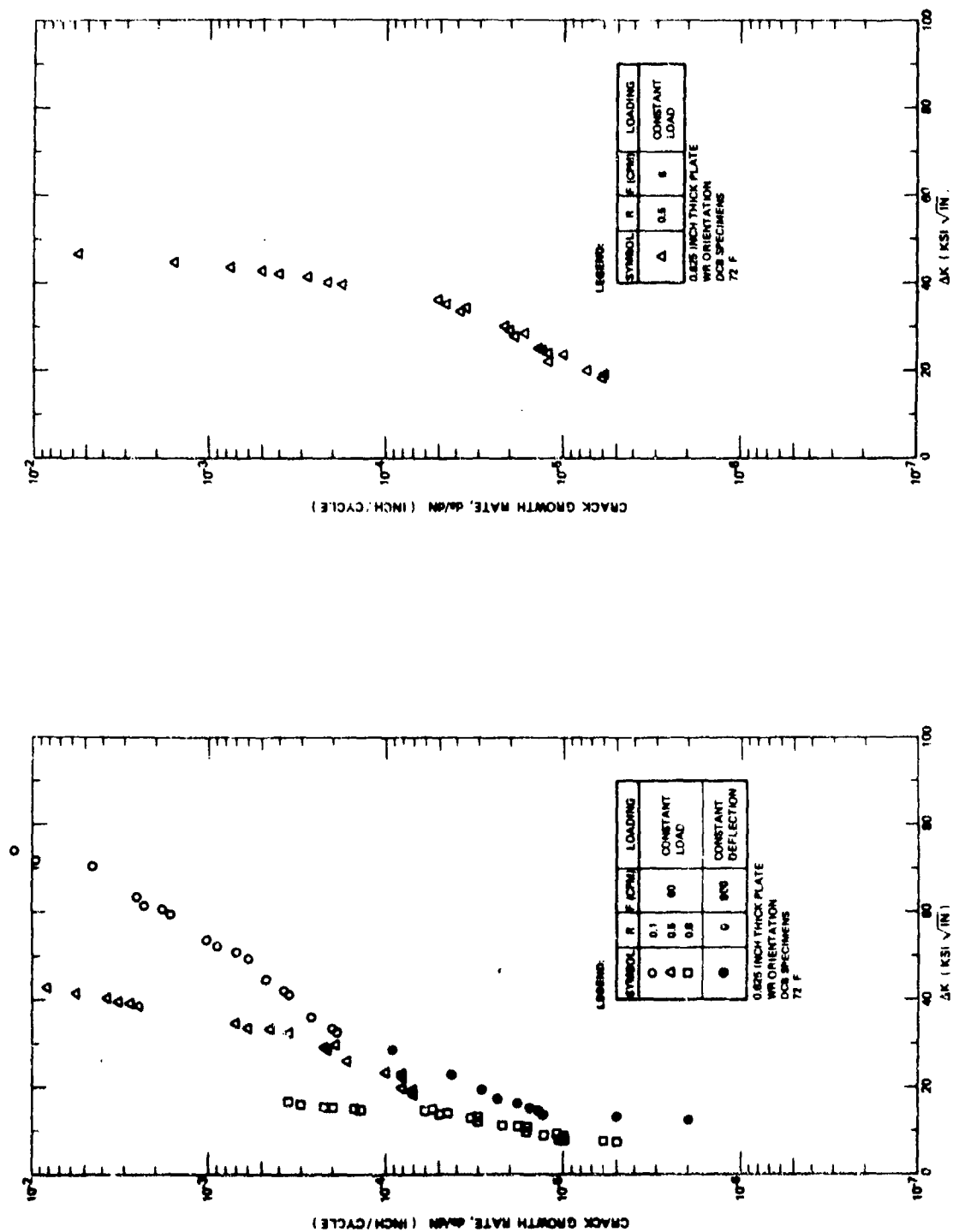


Figure A32: Fatigue Crack Growth Rates For 9Ni-4Co-0.3C Steel Alloy in Desiccated Air

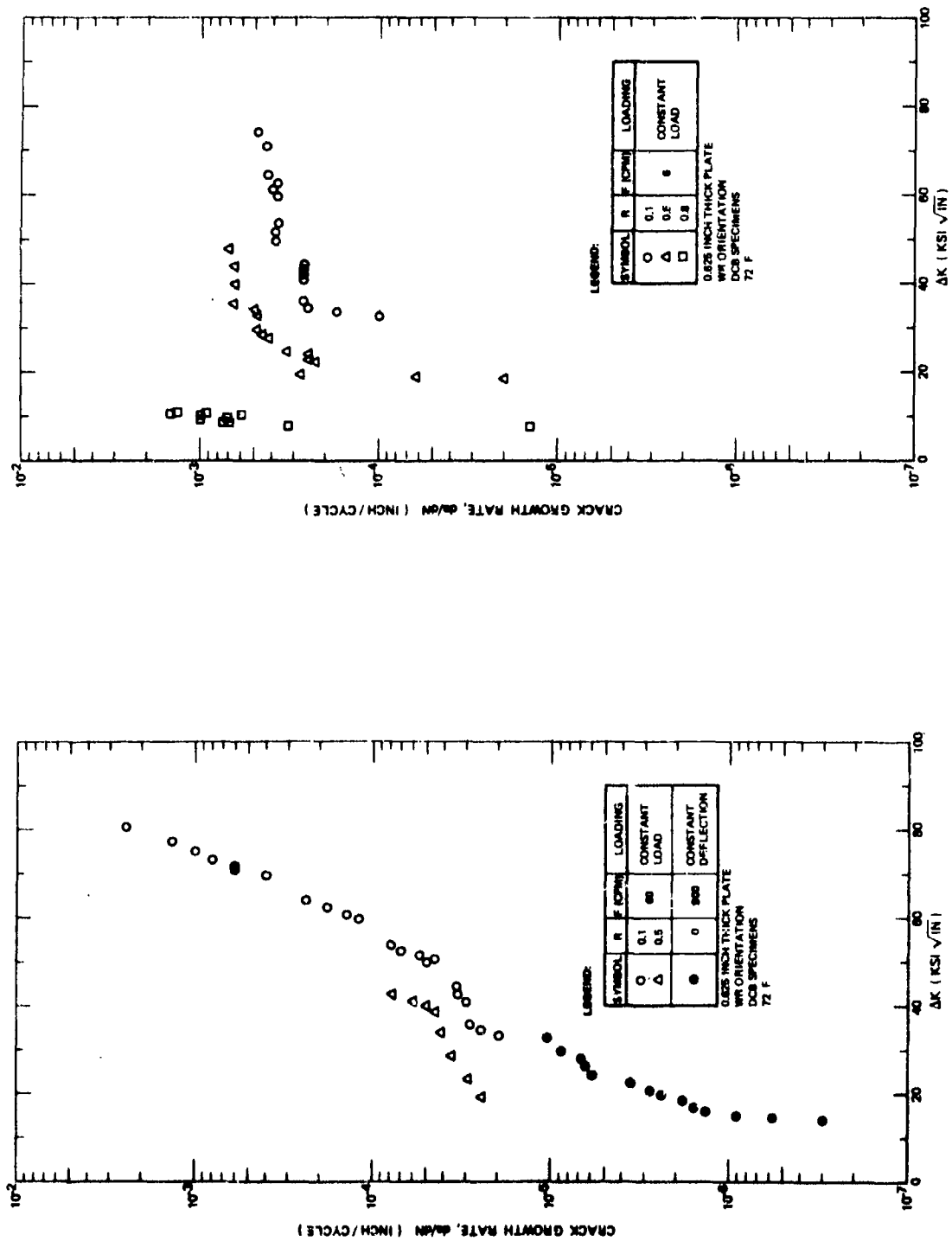


Figure A33: Fatigue Crack Growth Rates For 9Ni-4Co-0.3C Steel Alloy in Distilled Water

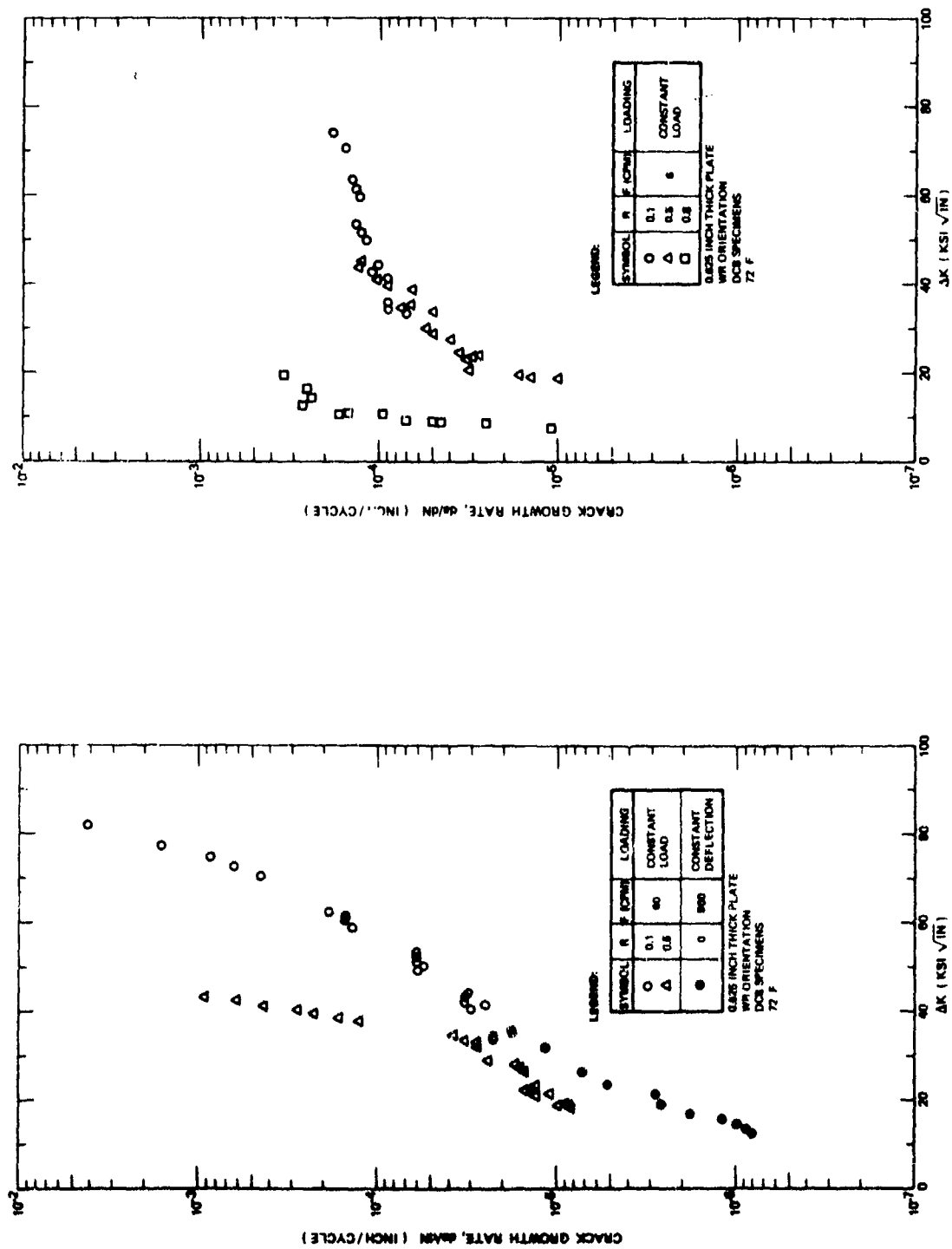


Figure A34: Fatigue Crack Growth Rates For 9Ni-4Co-0.3C Steel Alloy in 3.5% NaCl Solution

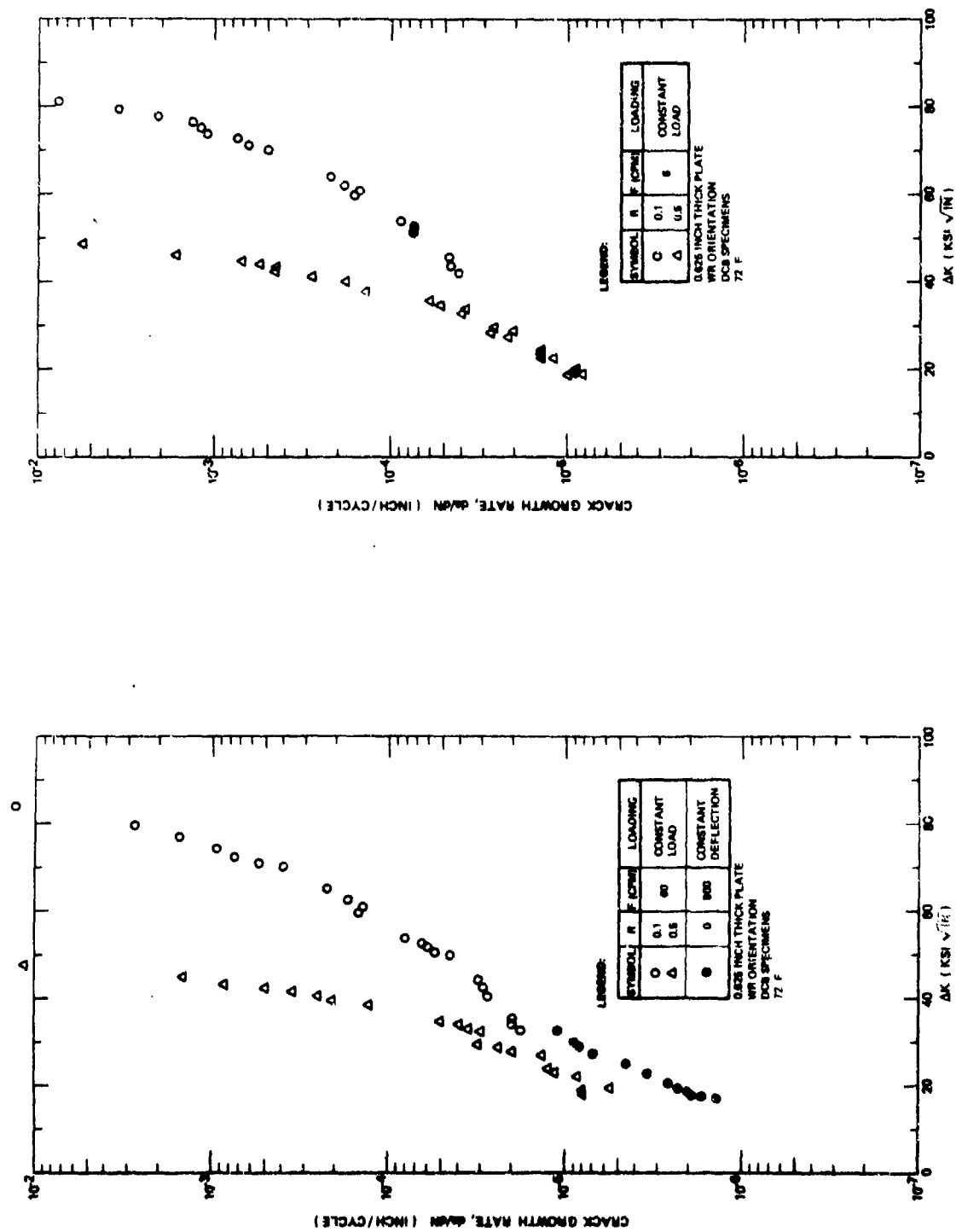


Figure A35: Fatigue Crack Growth Rates For 9Ni-4Co-0.3C Steel Alloy in Water Saturated JP-4 Fuel

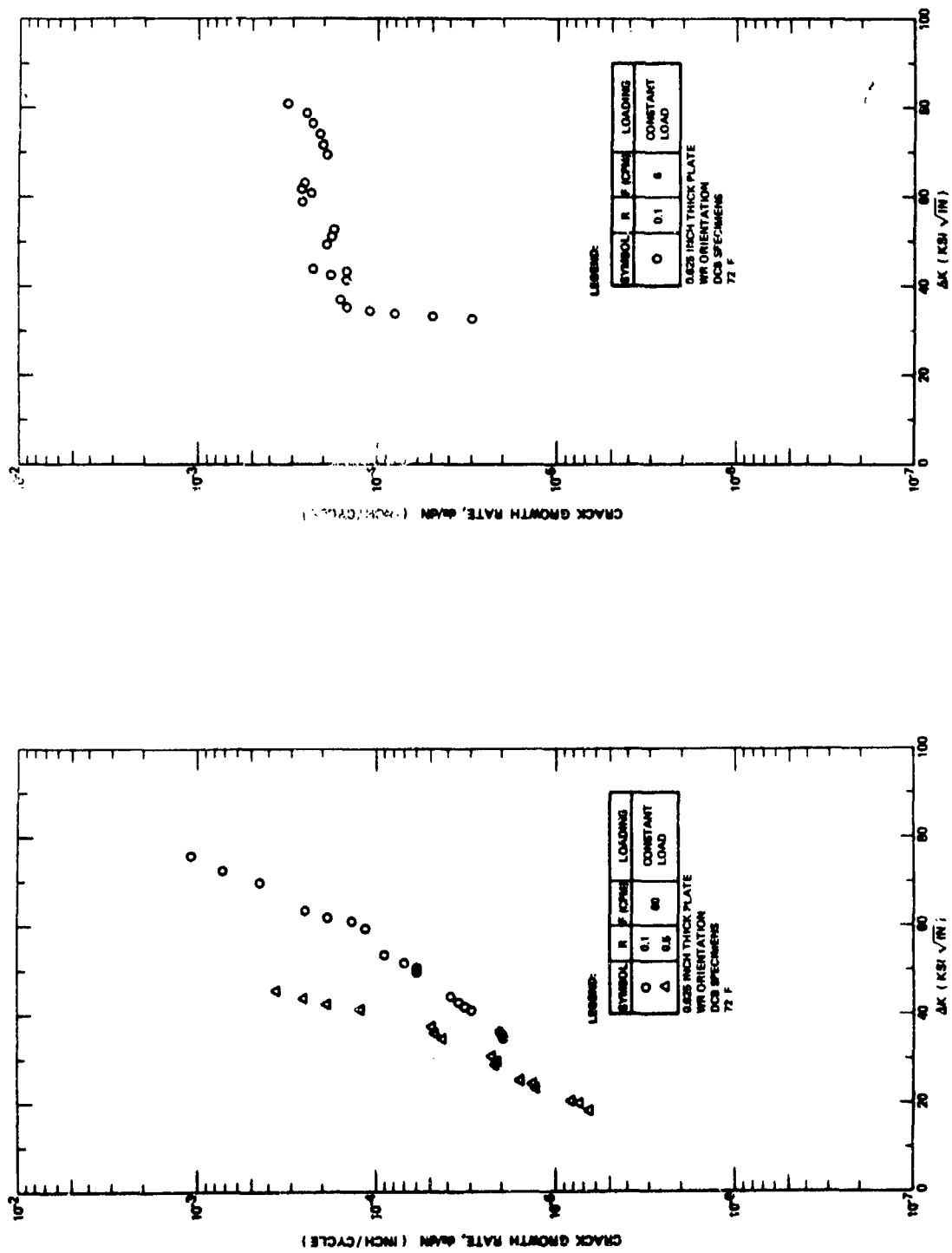


Figure A36: Fatigue Crack Growth Rates For 9Ni-4Co-0.3C Steel Alloy in Sump Tank Water

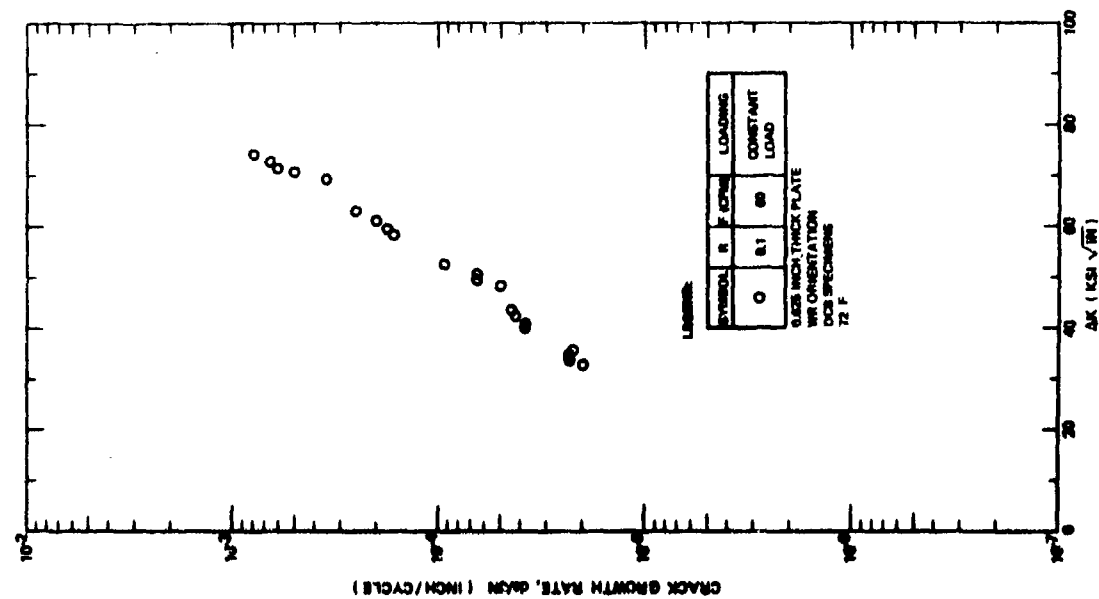
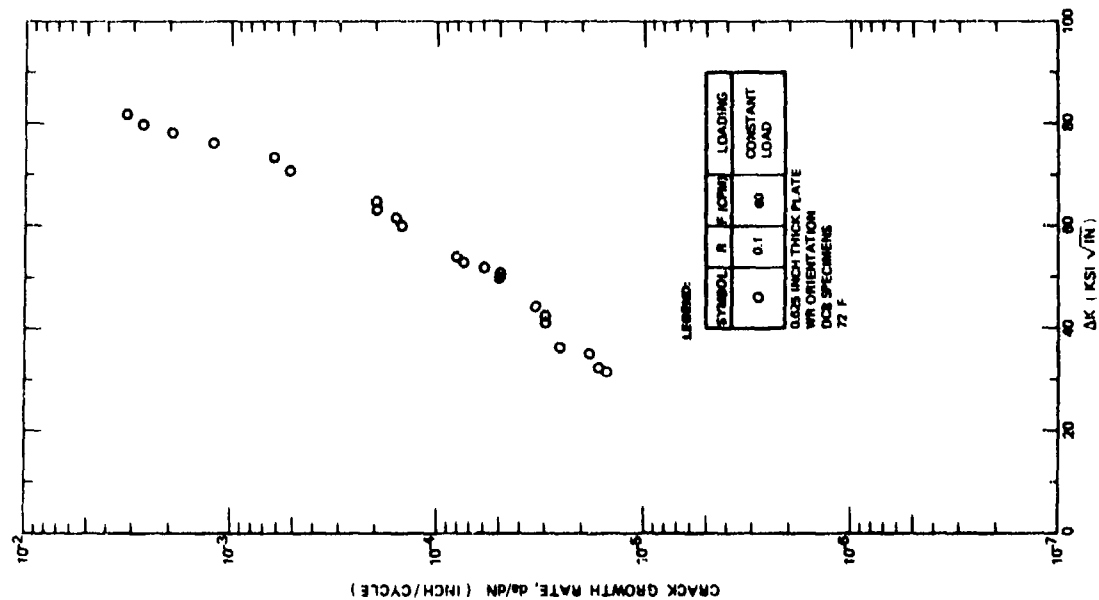


Figure A37: Fatigue Crack Growth Rates For 9Ni-4Co-0.3C Steel Alloy in Alternating JP-4 Fuel and Distilled Water

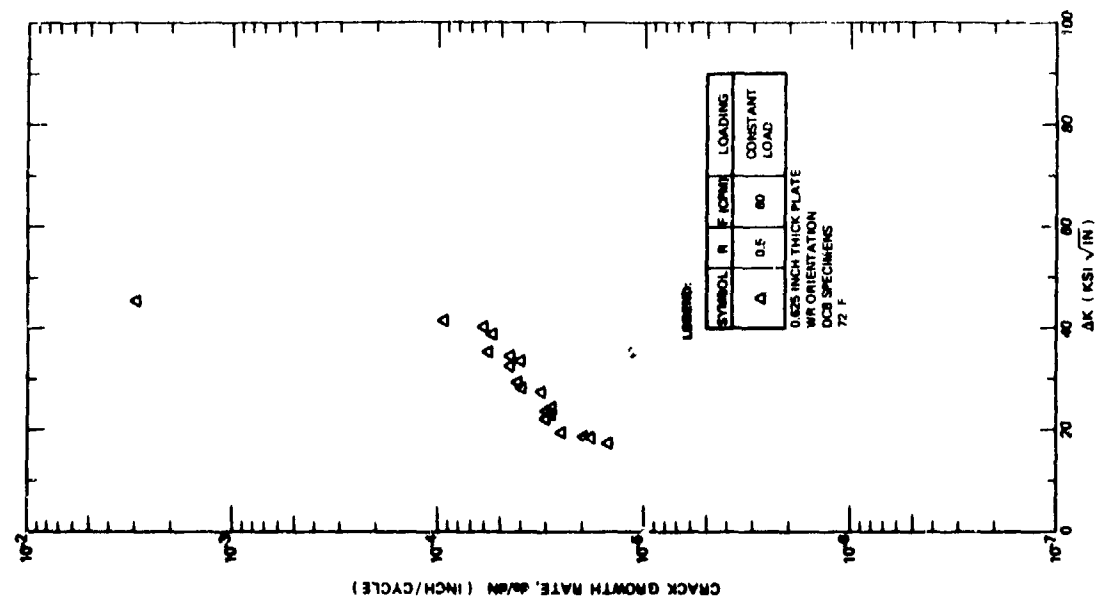


Figure A38: Fatigue Crack Growth Rates For 9Ni-4Co-0.3C Steel Alloy in Distilled Water, Crack Surface Sprayed With LPS-3 and Dried For 3.0 Hours Prior to Immersion in Test Media

APPENDIX B TEST SPECIMENS

Thirteen different specimen configurations were used to conduct the tests described in the body of this report. The thirteen configurations are detailed in Figures B1 through B13. A summary identifying the particular specimen configuration used for each alloy and test type is presented in Table B1.

PRECEDING PAGE BLANK-NOT FILMED

Table B1: Summary of Specimen Configurations Used For Each Type of Test

TEST TYPE	ALLOY	CYCLIC FREQUENCY	SPECIMEN TYPE	CONFIGURATION (Figure No.)
Mechanical Property	All Alloys	—	Tensile	B1
Fracture Toughness	All Alloys	—	CT	B2
	Aluminum	—	SF	B3
	Steel } Titanium }	—	SF	B4
Stress Corrosion Cracking	All Alloys } TR Direction }	—	DCB	B5
	Aluminum } Steel }	—	DCB	B6
	Titanium	—	DCB	B7
	Aluminum	—	SF	B8
	Titanium	—	SF	B4
Corrosion Fatigue Tests	All Alloys	6, 60	DCB	B9
	All Alloys	900	DCB	B10
	Aluminum	60	SF	B8
	Titanium	60	SF	B11
	Titanium	60	CT	B12
Overload	Aluminum Titanium	60	TDCB	B13

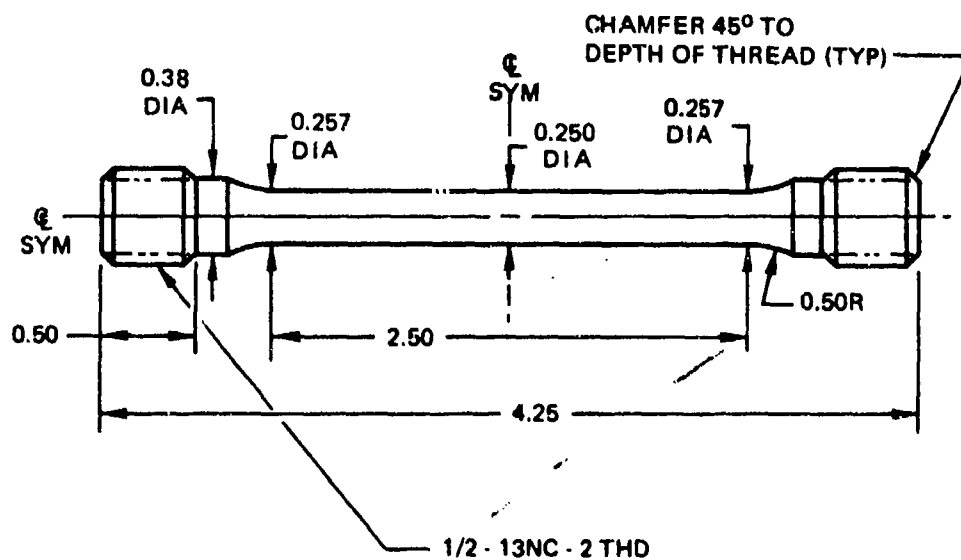


Figure B1: Tensile Specimen For Mechanical Property Measurements

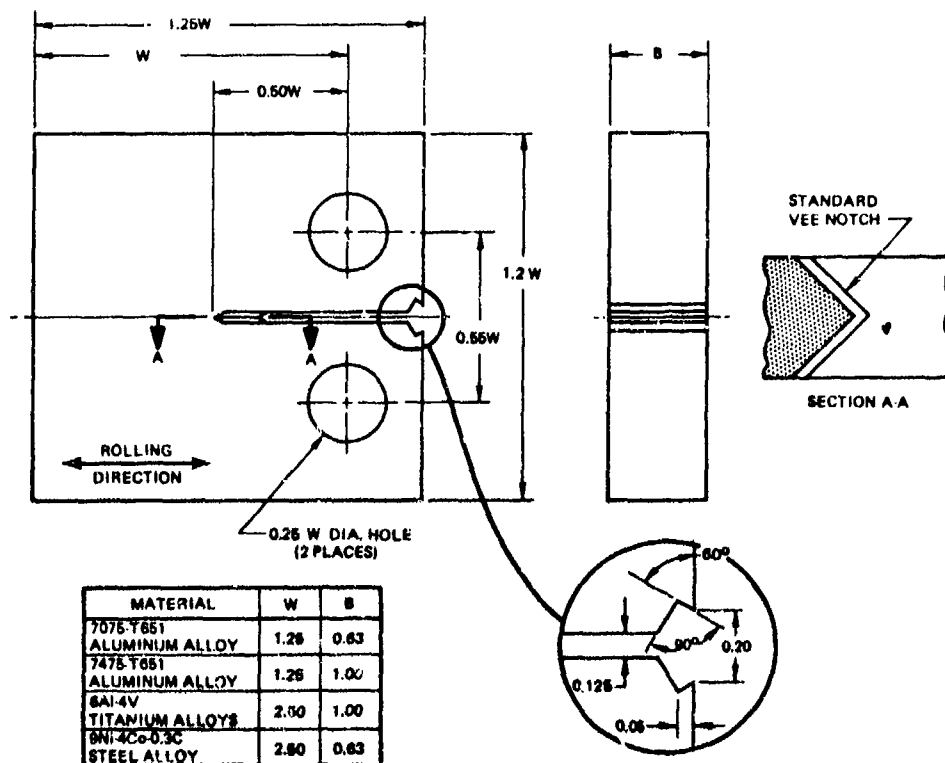


Figure B2: Compact Tension Specimen Configuration Used For Static Fracture Testing

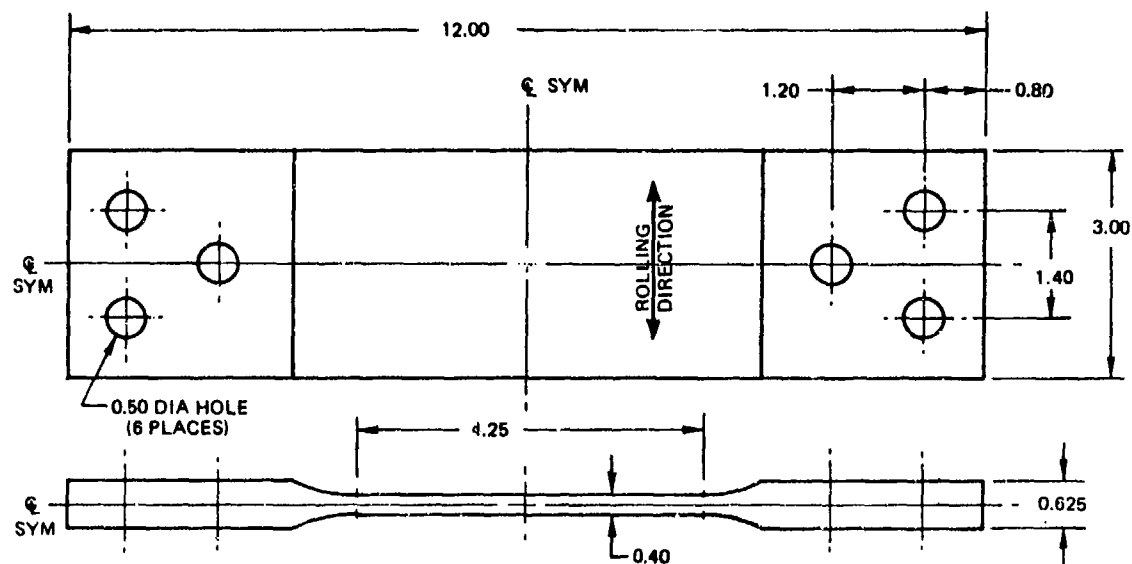
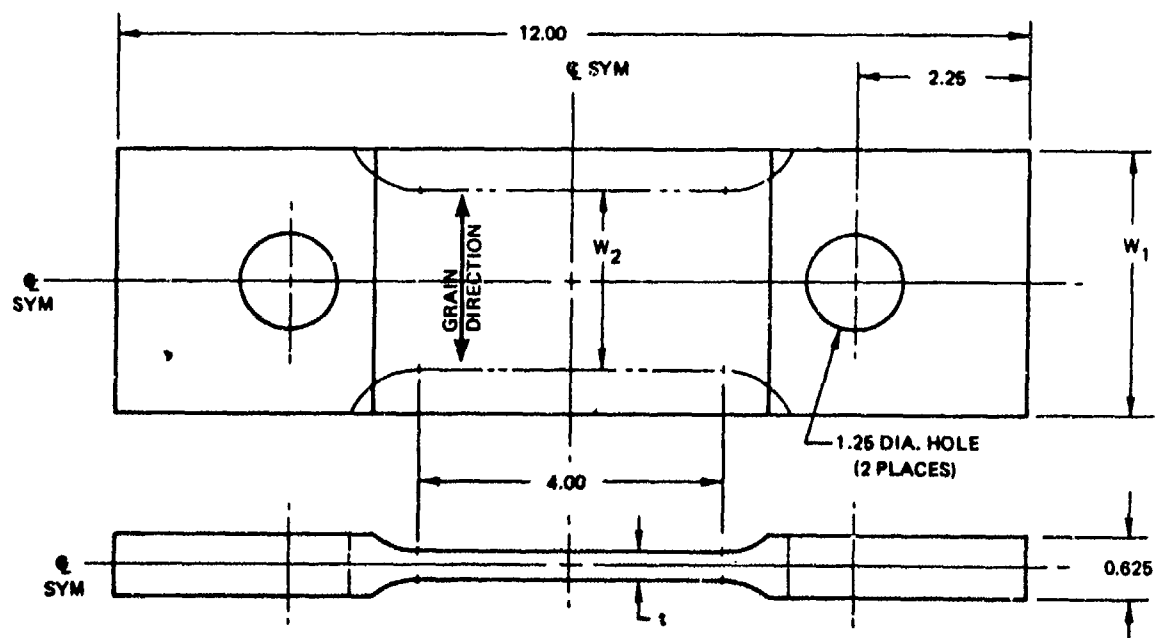


Figure B3: Surface Flawed Specimen Configuration For 7075-T651
Aluminum Alloy Plate Static Fracture Testing



MATERIAL	W_1	W_2	t
9NI-4Co-0.3C STEEL ALLOY	3.00	2.25	0.400
8Al-4V TITANIUM ALLOYS	3.50	3.50	0.325

Figure B4: Surface-Flawed Specimen Configuration

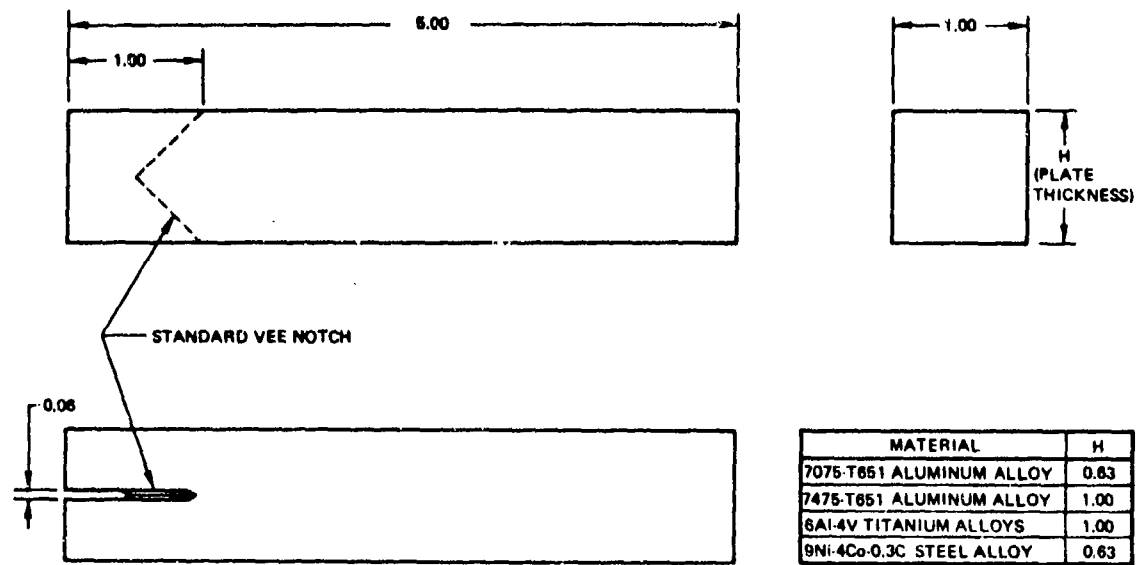


Figure B5: Short Transverse DCB Specimen Configuration Used For Stress Corrosion Testing

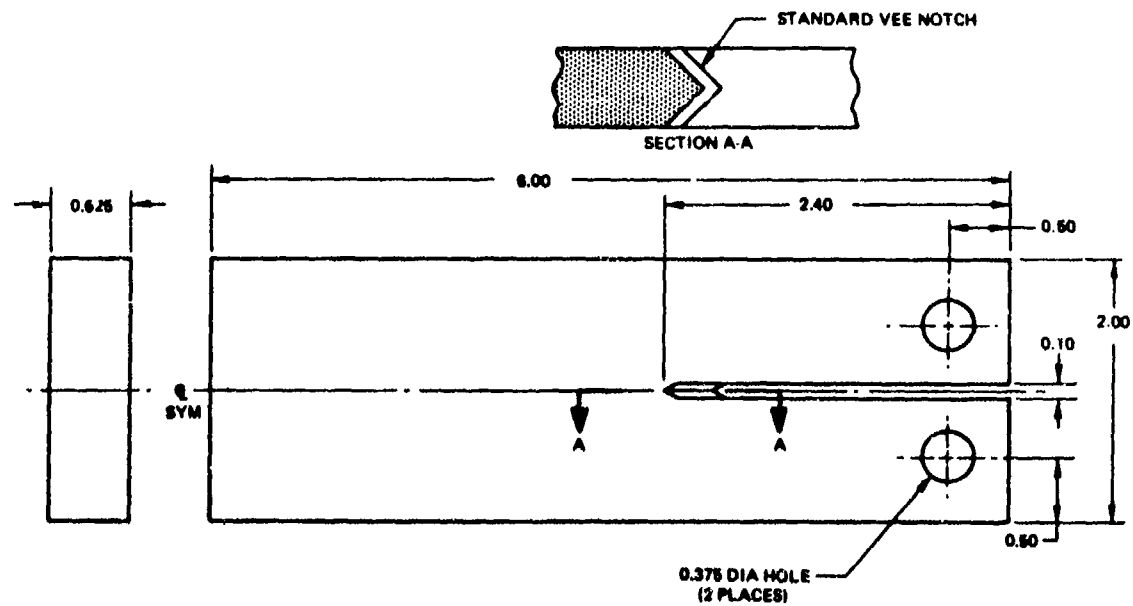


Figure B6: DCB Specimen Configuration Used For Stress Corrosion Testing
(7075-T651 Aluminum and 9Ni - 4Co - 0.3C Steel Alloys)

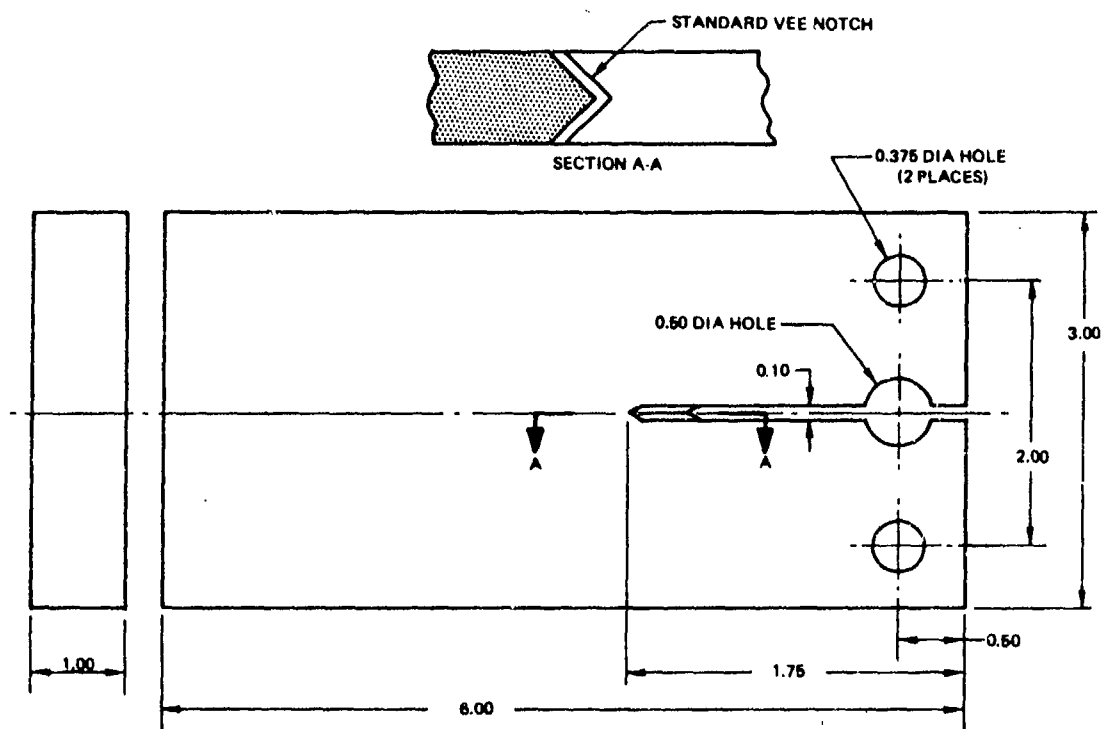


Figure B7: DCB Specimen Configuration Used For Stress Corrosion Testing (Titanium Alloys)

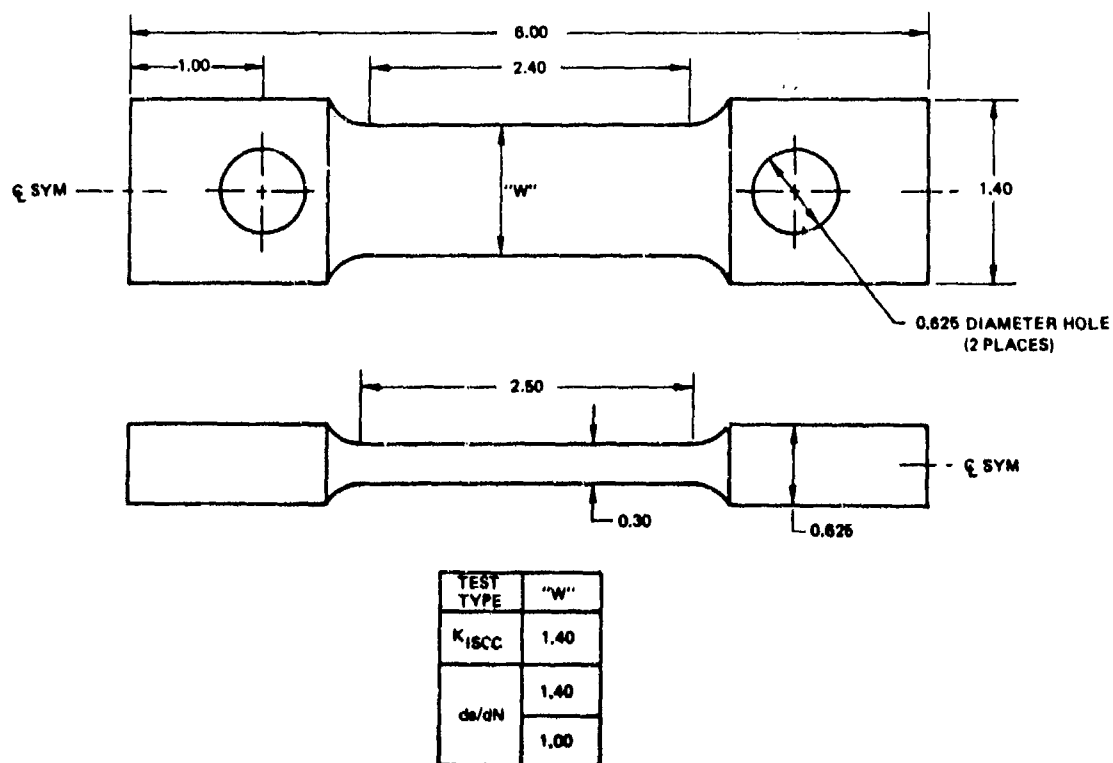


Figure B8: Surface-Flawed Specimen Configuration for 7075-T651 Aluminum Alloy K_{ISCC} and da/dN Testing

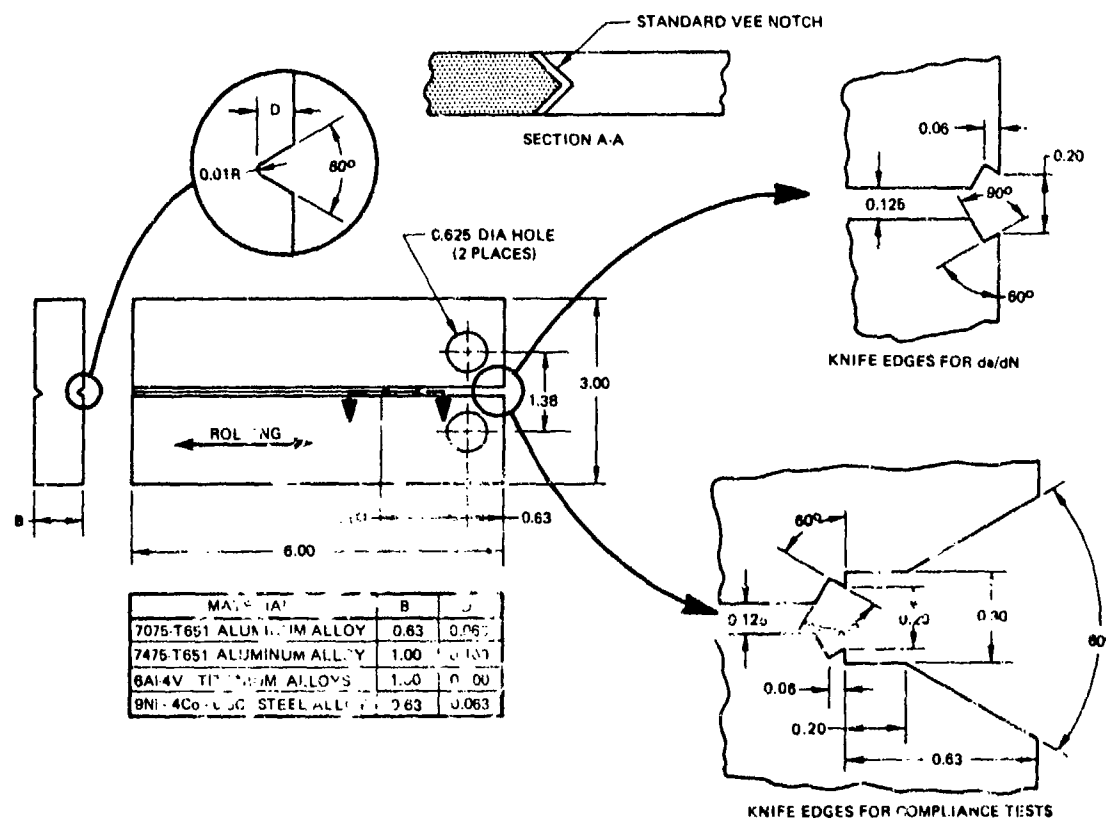


Figure B9: DCB Specimen Configuration Used For da/dN and Compliance Testing

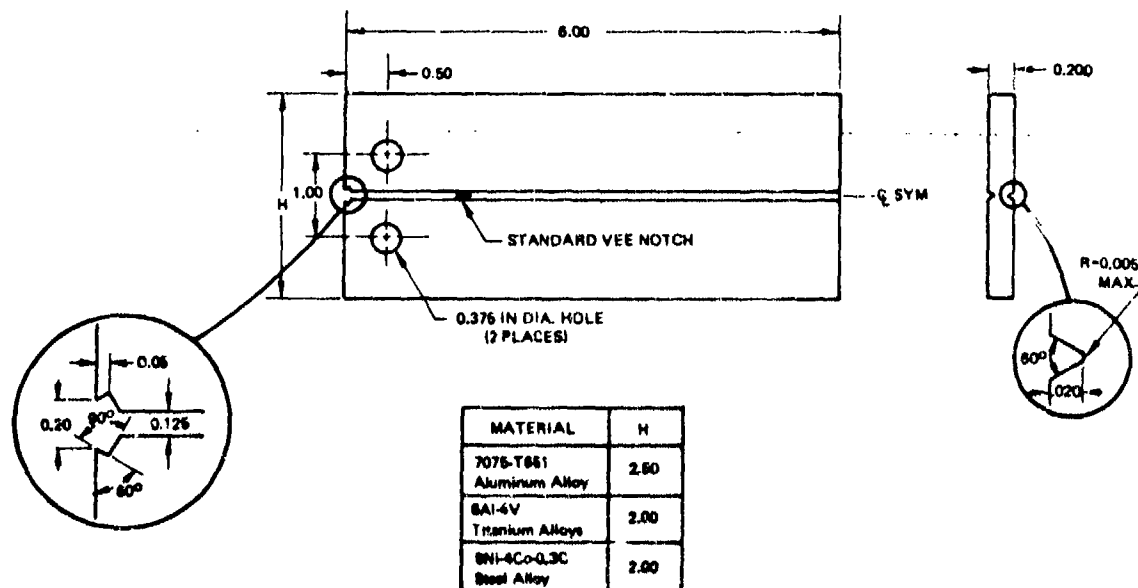


Figure B10: Specimen Configuration Used for da/dN Testing (900 CPM)

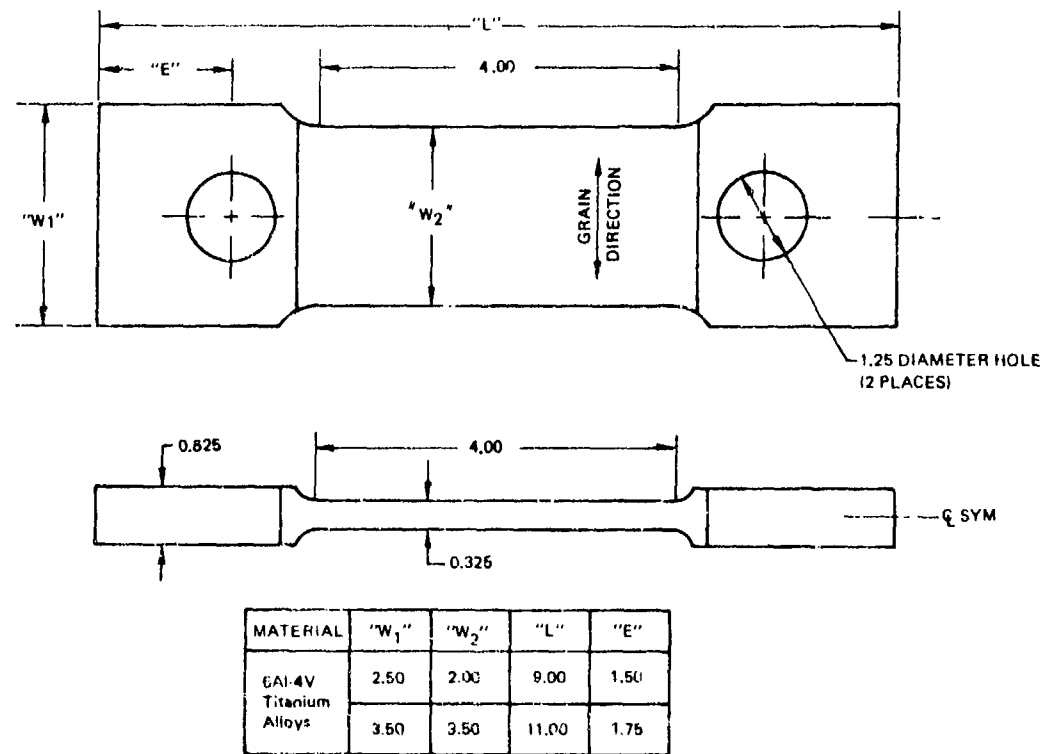


Figure B11: Surface-Flawed Specimen Configuration Used For Titanium Alloys da/dN Testing

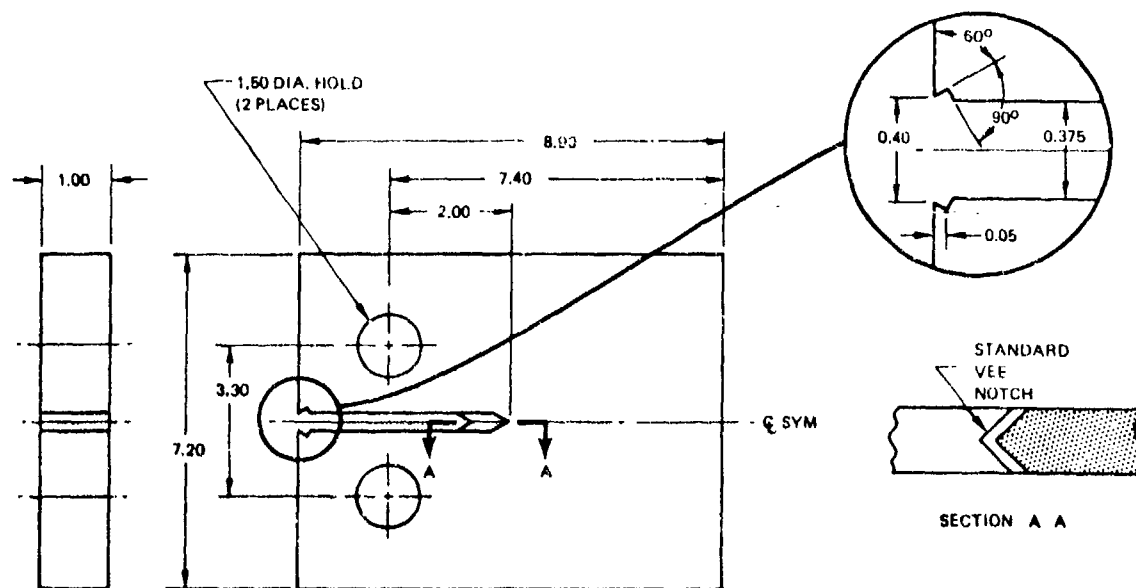


Figure B12: NAR Compact Tension Specimen Configuration

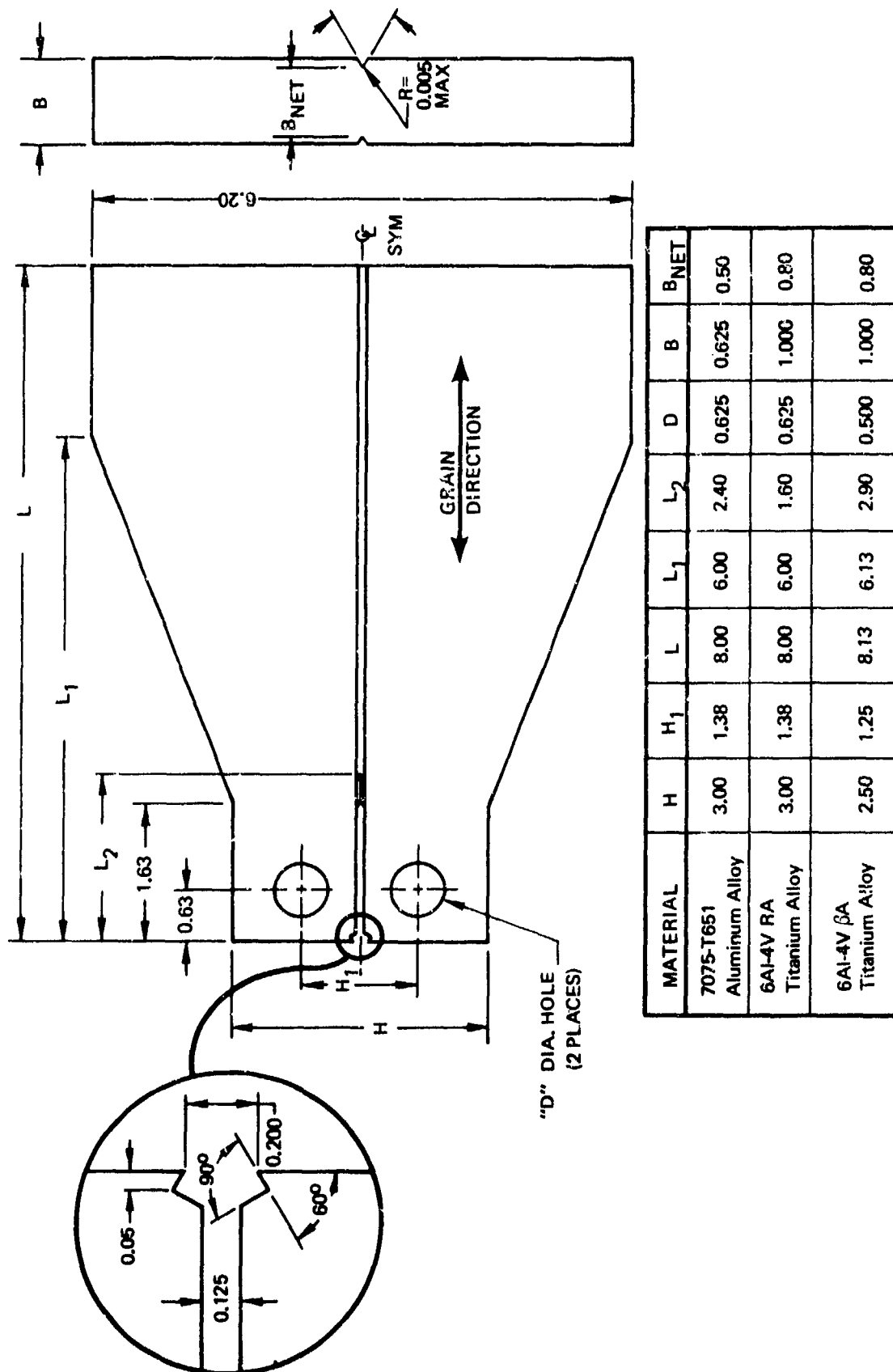


Figure B13: TDCB Specimen Configuration Used For Overload Testing

APPENDIX C
COMPLIANCE MEASUREMENTS FOR DOUBLE
CANTILEVER BEAM SPECIMENS

Results of tests undertaken to measure specimen compliance as a function of crack length for the 7075-T651 aluminum, 9Ni-4Co-0.3C steel and 6Al-4V beta annealed and recrystallized annealed titanium alloys are described in this appendix. Values of specimen compliance were determined for both the uniform height Double Cantilever Beam (DCB) and Tapered Double Cantilever Beam (TDCB) specimens for the aluminum and titanium alloys, and for DCB specimens for the steel alloy. Values of specimen compliance were used in crack length calculations for the DCB corrosion fatigue tests, and stress intensity factor calculations for the TDCB specimen tests.

Procedures

Compliance values were determined using the slopes of load displacement plots obtained when specimens were loaded in tensile test machines. Displacements were measured using clip gages spring loaded against integrally machined knife edges. Both clip gage and load cell were connected to an X-Y recorder to obtain the load-displacement graphs. For the 7075-T651 aluminum and 6Al-4V β A alloy DCB specimens, knife edges were located both at the end of the specimen and at the load line as shown in Figure B10. For all other specimens, knife edges were located only at the end of the specimens. When knife edges were located at the end of the specimen, load line displacements were calculated by multiplying end displacements by the ratio $a/(a+l)$ where "a" is crack length and "l" is the distance from the load line to the end of the specimen. Load line displacements were divided by the corresponding load to calculate compliance values. Crack lengths were visually measured.

Results

Compliance measurements for the uniform height DCB specimens are plotted in Figures C1 and C2, and for the TDCB specimens in Figure C3. For the DCB specimens compliance values determined using deflections measured at the end of the specimen and the load line agreed very well. Furthermore, compliance values for the crack lengths less than 3.5 inches agreed with values calculated using

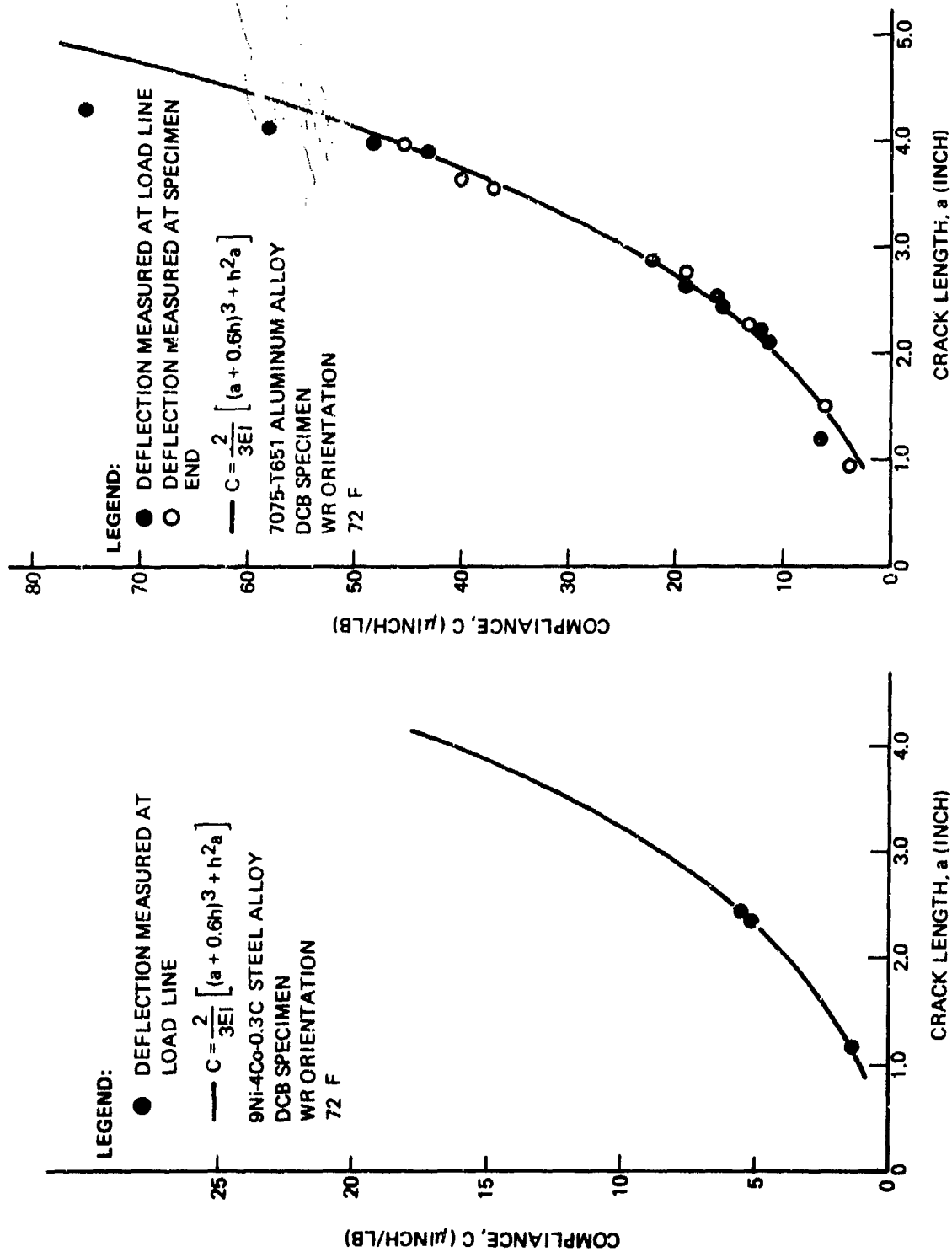


Figure C1: Compliance Values for 7075-T651 Aluminum and 9Ni-4Co-0.3C Steel Alloy
Double Cantilever Beam Specimens

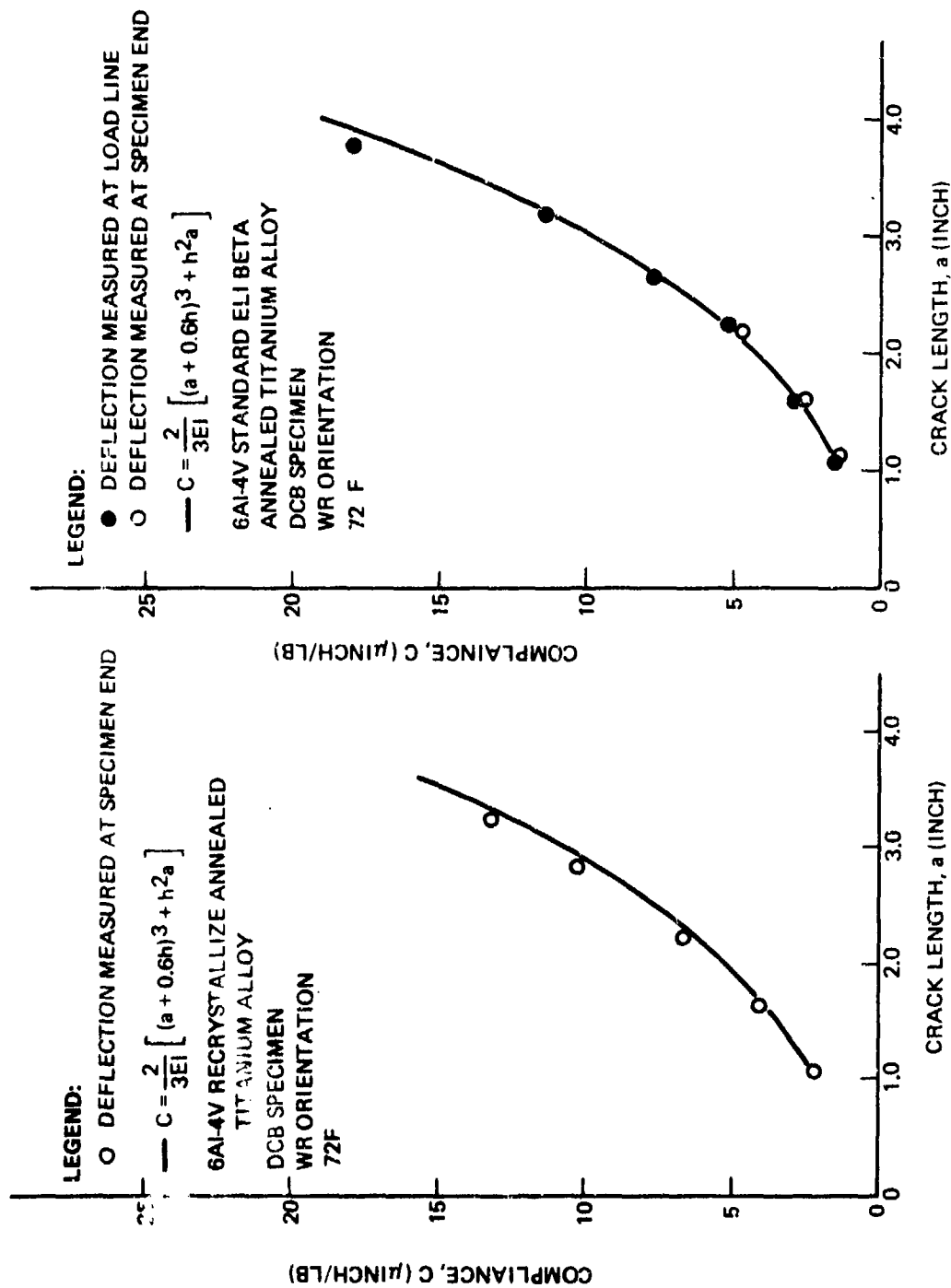


Figure C2: Compliance Values for 6Al-4V Standard ELI Beta Annealed and Recrystallized Titanium Alloys, Double Cantilever Beam Specimens

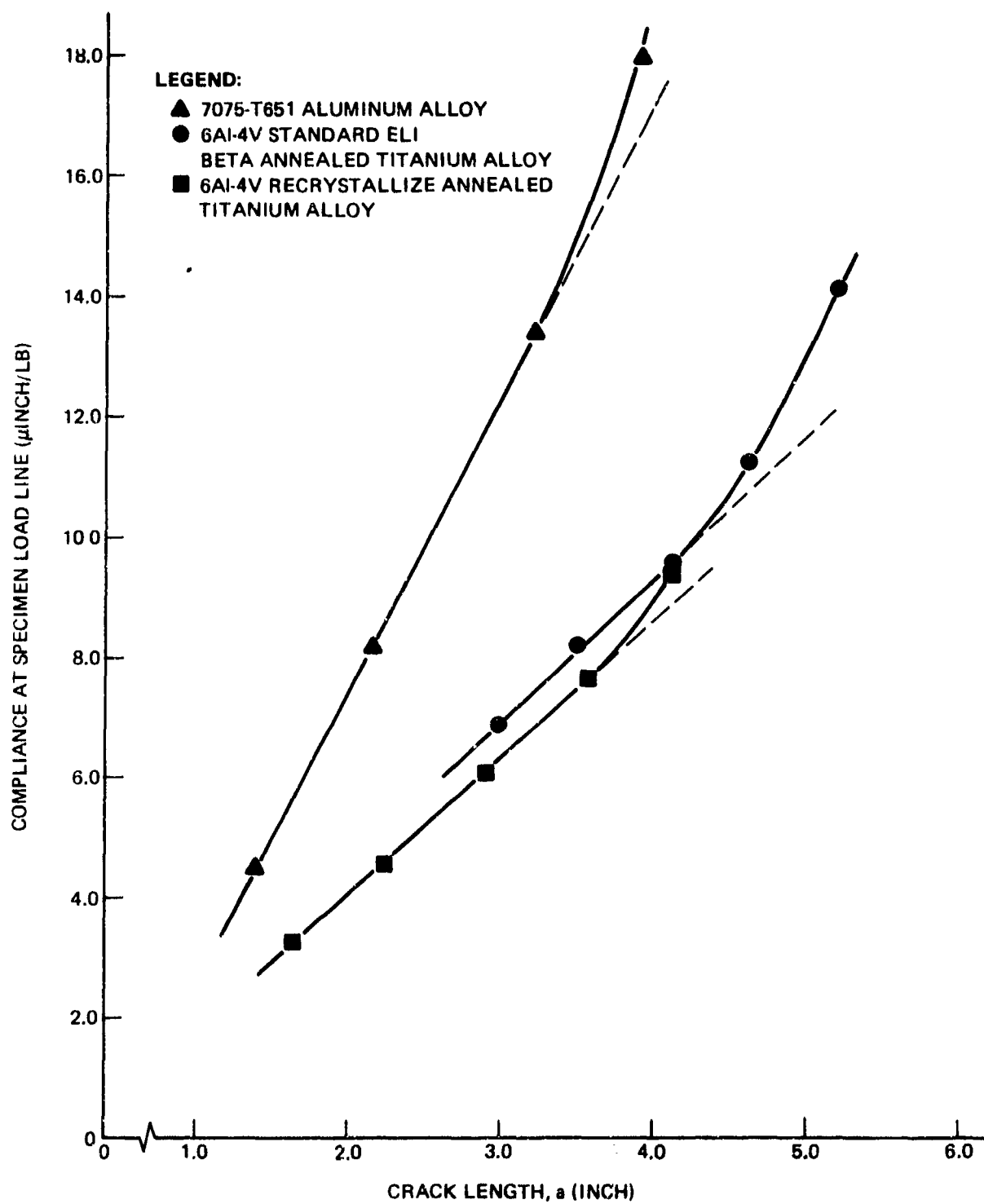


Figure C3: Compliance Values for 7075-T651 Aluminum, 6Al-4V Standard ELI Beta Annealed and Recrystallized Annealed Titanium Alloys, Taper Double Cantilever Beam Specimens

the semi-empirical relationship (1)*

$$C = \frac{2}{3El} \left[(a + 0.6h)^3 + h^2a \right] \quad (C1)$$

where: C is specimen compliance, E is modulus of elasticity, I is moment of inertia of one of the specimen arms, a is crack length, and h is one half the specimen height. For crack lengths in excess of 3.5 inches, specimen compliance increased over those given by Equation C1 due to interaction effects between the crack and back specimen face.

Reference

1. S. Mostovoy, P. B. Crosley, and E. J. Ripling, "Use of Crack-Line-Loaded Specimens for Measuring Plane Strain Fracture Toughness", Journal of Materials, Vol. 2, No. 3, September 1967.

* Numbers in parentheses refer to references at end of Appendix.

APPENDIX D
CRYSTALLOGRAPHIC TEXTURE MEASURED
BY X-RAY POLE FIGURES

Background

Each grain in a polycrystalline aggregate normally has a crystallographic orientation different from that of its neighbors (1)*. The orientations of all the grains may be randomly distributed in relation to some selected frame of reference, or they may tend to cluster, about some particular orientation or orientations. Any aggregate characterized by the latter condition is said to have a preferred orientation, or texture. Since most single crystals are anisotropic, i.e., have different properties in different directions, it follows that an aggregate of crystals having preferred orientation must also have directional properties.

Preferred orientation is best described by means of a pole figure. This is a stereographic projection which shows the variations in pole intensity with pole orientation for a selected set of crystal planes. Poles are the projection points onto a sphere of the normal to the crystallographic plane. The pole figure is a contour map of pole intensities plotted on polar coordinates showing the alignment of the selected set of planes as schematically shown in Figure D1.

A significant metallurgical technique developed for titanium characterization by Boeing was a quantitative, computerized pole figure analysis for determining the preferred orientation in titanium alloys. The technique was developed and modified over 4 years by Olsen (Ref. 2), and the following provides a brief description of the procedure. X-ray diffraction data are obtained using a modified Siemens texture goniometer, which is precisely aligned. Approximately 700 data points are taken. A computer program analyzes the data, subtracting for background and correcting for defocusing, and then plots a pole figure. The pole figure gives the iso-intensity lines of poles for a given crystallographic plane in terms of "times random intensity". This random intensity can be likened to taking all the data from a preferred titanium sample and spreading the data evenly over the entire pole figure, resulting in an average or a

* Numbers in parentheses refer to references at end of Appendix.

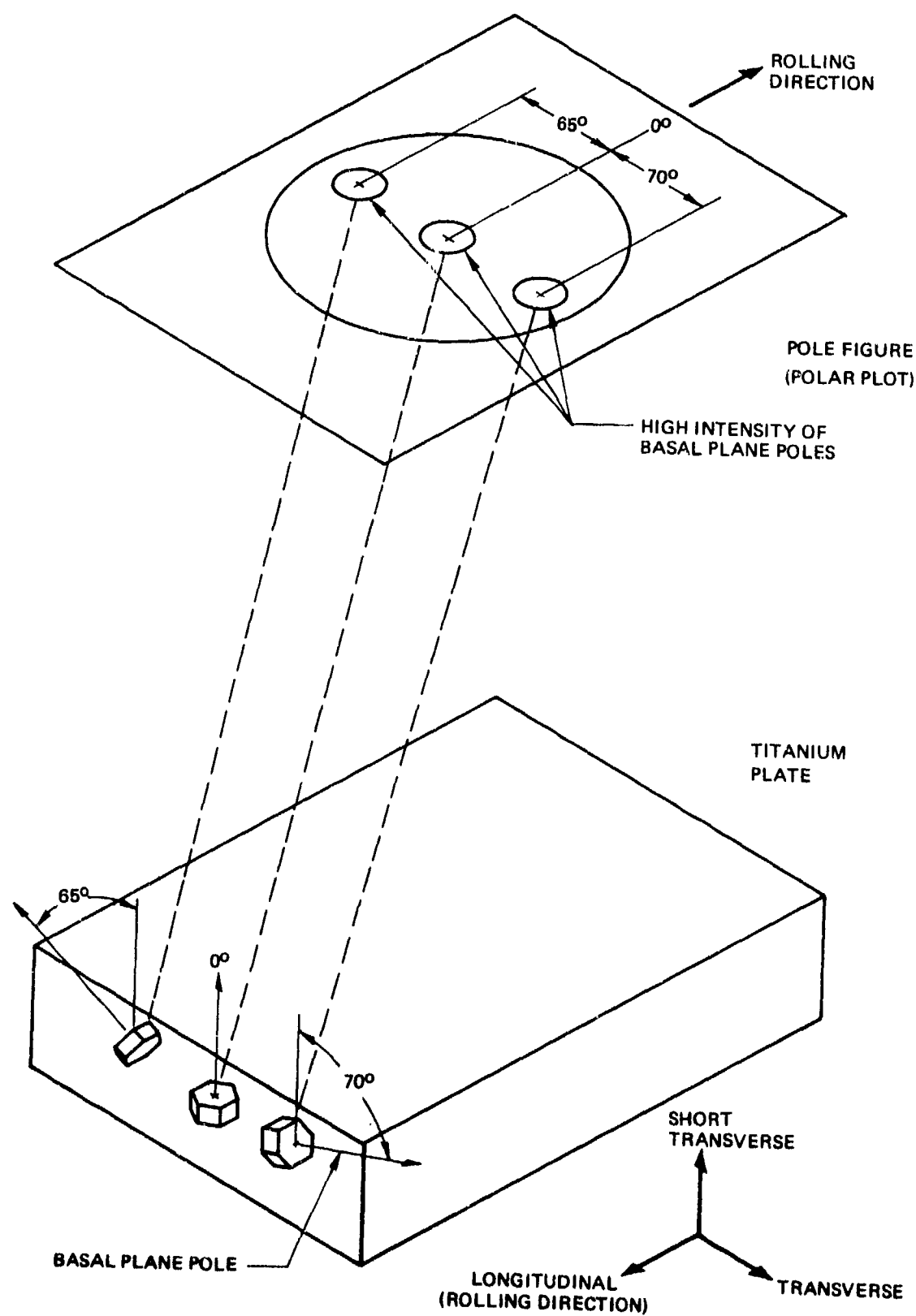


Figure D1: Relationship of Basal Plane Poles in Titanium Plate and Resulting Pole Figure

"random" intensity. Most of the data obtained were for the basal (0002) plane, although some data were also obtained for the prismatic (1010) plane for the alpha phase in Ti-6Al-4V. Some data were also obtained for the (110) plane of the retained beta phase in Ti-6Al-4V.

Procedure

Using the complex 45° cut to form the specimen, data points are taken on a spiral with θ changing 5° for every 360° change in α (See Figure D2). A total of 698 data points are recorded for each pole figure. Loss in intensity due to defocusing and absorption during tilting of the specimen is corrected by use of a random standard specimen.

After correction for absorption and defocusing, each data point is ratioed to the reading from a random sample. A code is then given to different intensity values in "times random" intensity (i.e., 1 = 0.5 times random, 2 = 1.0 times random, etc.). This code is reported immediately below the pole figure. Identical consecutive numbers are then connected to form contour lines on the pole figure via a plot program and an SC 4020 plotter. A typical pole figure is shown in Figure D3 with the polar coordinates superimposed over the pole figure.

The X-ray data used to plot the pole figure is also used to calculate elastic modulus for various directions and the percentage of plane intensity oriented in the longitudinal, transverse and short transverse directions. The percentages ($\%I_L$, $\%I_T$ & $\%I_{ST}$). These percentages provide quantitative values for the differences in plane orientation as related to the three primary directions.

References

1. Cullity, B. D., Elements of X-Ray Diffraction, Addison-Wesley Publishing Company, Inc. (1957)
2. Olson, R. H. "Computer Plotting Pole Figure", Metallography 5, 369-371 (1972)

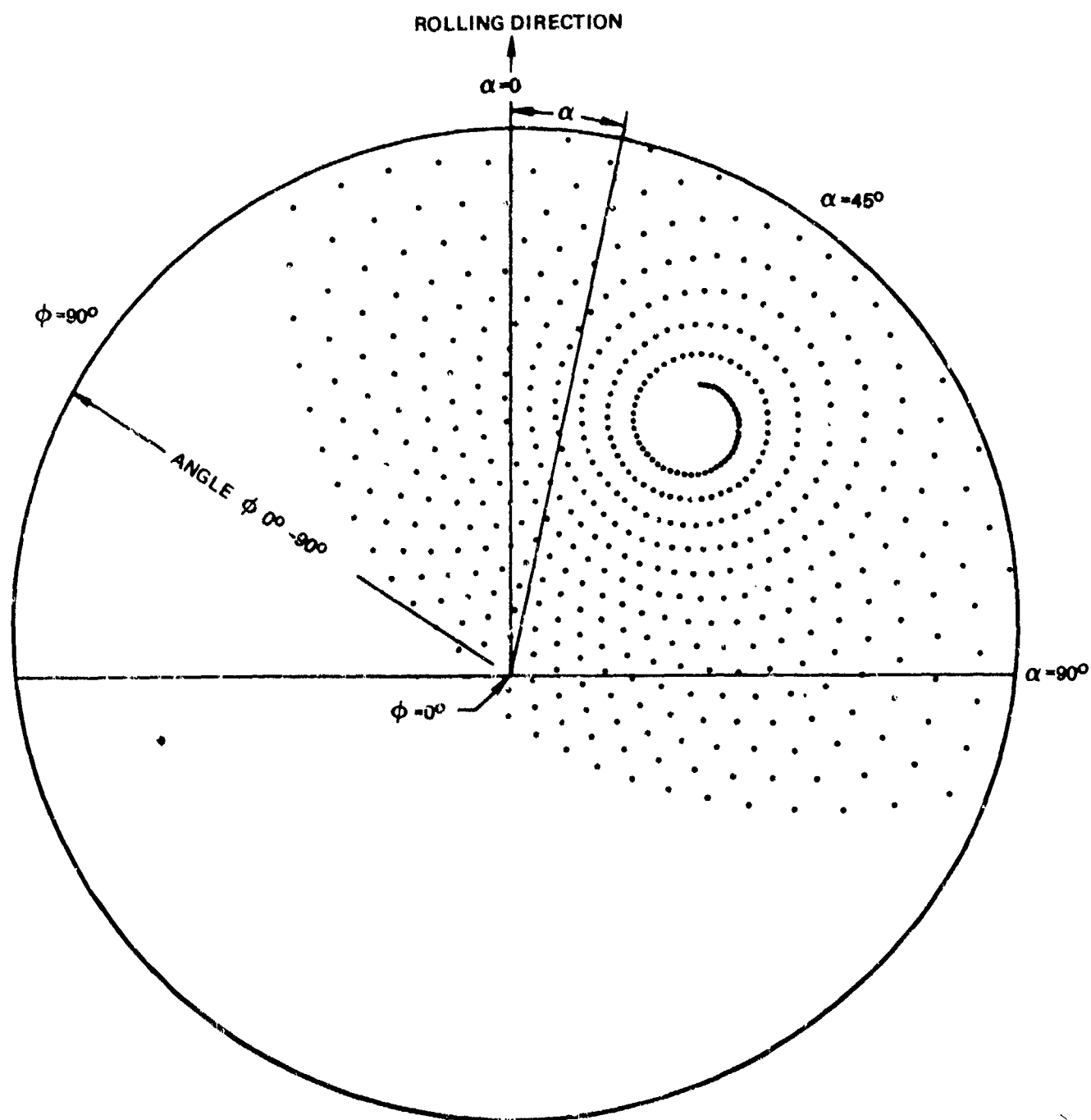
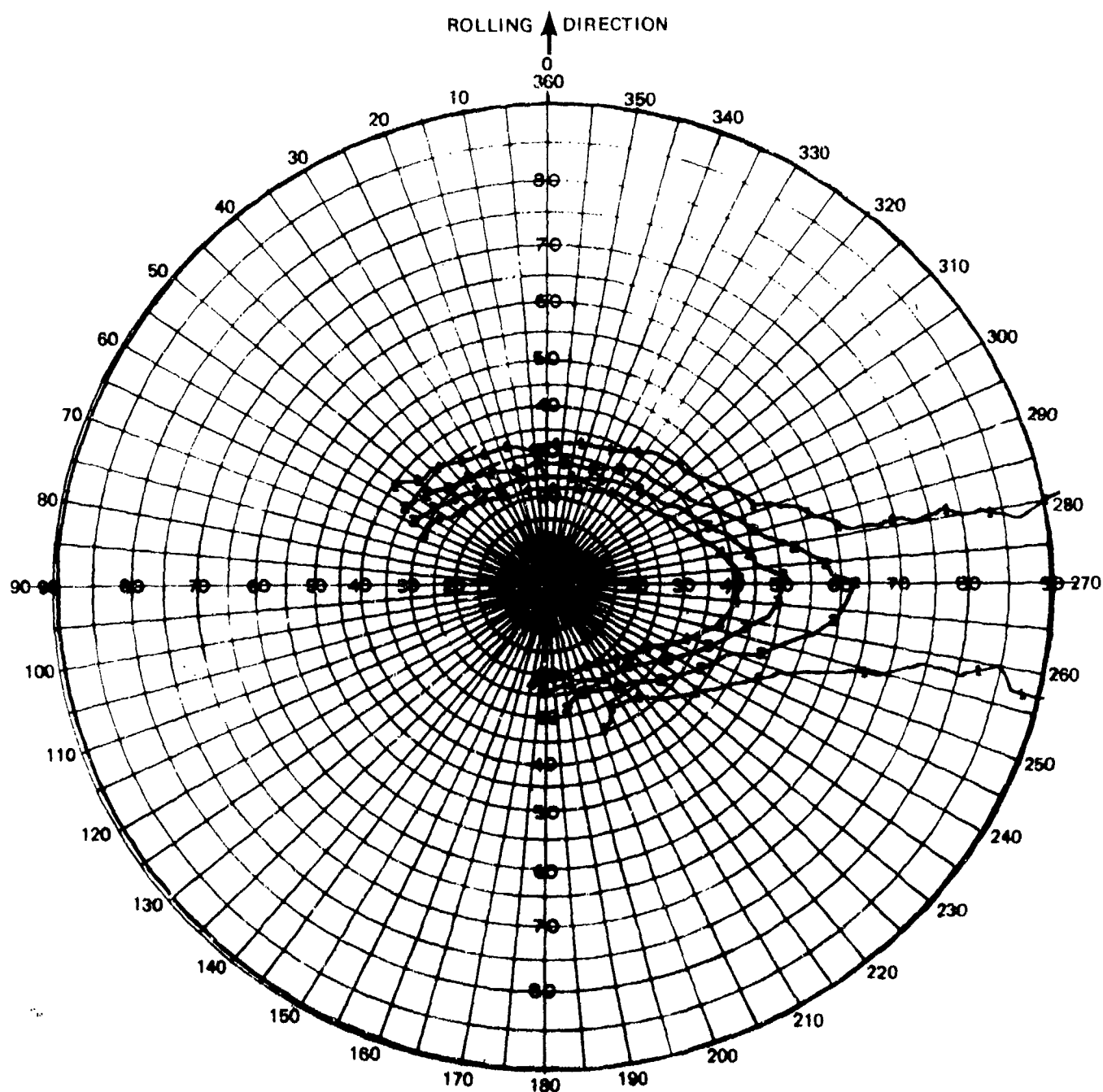


Figure D2: Method of Collecting Pole Figure Data



CONTOUR LINES	1	2	3	4	5	6	7	8	9	0
TIMES RADIATION INTENSITY	0.5	1.0	1.5	2.0	4.0	8.0	14.0	20.0	25.0	30.0

Figure D3: Example of a Basal Plane Pole Figure for Titanium With Polar Coordinates Superimposed